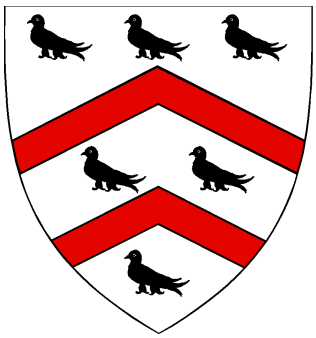
Silicon isotopes and the development of the Earth

by

Paul Simon Savage





Thesis submitted for the Degree of Doctor of Philosophy, University of Oxford

Department of Earth Sciences

&

Worcester College

Trinity Term 2011

Supervisors: A.N. Halliday, R.B.Georg & H.M. Williams



Silicon isotope ratios show little variation in igneous rocks and minerals; hence, they have little import for studies of igneous rocks.

C.B. Douthitt, 1982

Picture: (from L to R) the author, Dr. I. Parkinson, Dr. J. Prytulak and Dr. C. Pearce heading toward the summit of Mt. Hekla, Iceland, on a sampling trip. Photograph taken by R. Armytage

Silicon isotopes and the development of the Earth

Paul Simon Savage

The Department of Earth Sciences & Worcester College, University of Oxford

Trinity Term 2011

ABSTRACT

Silicon (Si) isotopes have been extensively studied in low temperature environments but the science of Si isotopes in igneous material has been comparatively ignored. This is because the degree of isotopic fractionation at high temperatures is relatively small, making the accurate measurement of these variations extremely challenging. Using state-of-the-art analytical techniques and instrumentation, which deliver high levels of precision, the objective of this research is to rectify this omission. Specifically, this study aims to investigate whether there are systematic Si isotope variations within, and provide robust Si isotopic compositions for, the major silicate reservoirs on Earth. To this end, a broad range of mantle and crustal lithologies, sourced globally and from various tectonic regimes, have been analysed using high resolution MC-ICP-MS.

Analyses indicate that the Si isotopic compositions of mantle-derived mafic and ultramafic material are extremely homogeneous. These data are used to calculate a Bulk Silicate Earth (BSE) average of $\delta^{30}Si = -0.29 \pm 0.08$ ‰ (2 s.d.). The degree of Si isotopic fractionation as a result of magmatic differentiation has also been assessed, and found to be small but resolvable between basalt and rhyolitic end-members. Finally, this research shows that, although igneous rocks and sediments derived from the continental crust can be relatively heterogeneous with respect to Si isotopes, bulk averages calculated for the upper, middle and lower continental crust are all very similar to that of BSE. Providing robust estimates for these reservoirs has greatly improved our knowledge of the behaviour of Si isotopes in silicate lithologies and provides a framework for further Si isotopic investigations of such material.

Silicon isotopes and the development of the Earth

Paul Simon Savage

The Department of Earth Sciences & Worcester College, University of Oxford

Trinity Term 2011

EXTENDED ABSTRACT

This study is a reassessment of the silicon (Si) stable isotope compositions of high temperature silicate rocks and their associated sources. Using state-of-the-art analytical techniques that provide pre-eminent levels of analytical precision, this research aims to investigate whether there are systematic Si isotope variations within, and provide robust Si isotopic compositions for, the major silicate reservoirs on Earth. Chapter 1 provides a brief review of the study of Si isotopes in the current scientific literature and, also, theory of stable isotope fractionation. Chapter 2 describes the novel sample processing methods as well as the high-resolution Multi-Collector Inductively-Coupled-Plasma Mass Spectrometer (MC-ICP-MS) used in the analysis of Si isotopes in this work. The research then begins by studying the behaviour and composition of Si isotopes in the mantle and ends in the continental crust, investigating as it does such processes as magmatic differentiation and granite formation (Chapters 3 to 7).

Silicon has three stable isotopes, ^{28}Si, ^{29}Si and ^{30}Si and is a key component in many and varied geo- and biochemical cycles on Earth. Resolvably large degrees of isotopic fractionation take place at low temperatures, and particular attention has been paid to Si isotope behaviour in the hydrological and biological cycles, i.e. weathering processes (e.g. Ziegler et al., 2005a&b) or uptake by vegetation (e.g. Opfergelt et al., 2008) and silica-utilising marine organisms (e.g. De La Rocha, 2006). Despite the large relative mass difference between the isotopes (~7% between ^{30}Si and ^{28}Si), the relative degree of fractionation is much smaller in high temperature systems. This is because Si has only one valence state (Si^{4+}) and does not form volatile compounds readily; in silicates it is almost always in tetrahedral coordination with four oxygen atoms. As such, variations in igneous rocks tend to be very limited ($\delta^{30}Si \pm < 0.20$ ‰). Because analysing Si isotopes to these levels of precision is not trivial, until recently very little research effort has been invested into this field. However, using modern analytical techniques, accurate and precise

Si isotope measurement is now routine, and a reappraisal of the isotopic composition of the largest Si reservoirs on Earth, the mantle and lithosphere, is timely.

All samples and standards were processed for Si isotope analysis following the HF-free alkali fusion technique described in Georg et al. (2006b). The use of HF was avoided for two reasons. Firstly, although Si does not volatilise easily, it can form gaseous SiF_4 on reaction with HF, which could cause sample loss and introduce artificial isotopic fractionation. Secondly, fluorine acts to reduce mass spectrometer sensitivity because of its high ionisation potential, which suppresses the ionisation efficiency of the plasma. Alkali fusion of a sample powder was performed in a silver crucible, using a NaOH flux. The crucible was heated to 720ºC for 12 minutes, before being transferred into solution (MQ-e water acidified with HNO_3). Sample purification for MC-ICP-MS analysis was performed using a single-pass column technique with BioRAD AG50W X12 200-400 mesh cation resin.

Silicon isotope measurements were made using a Nu Instruments Nu Plasma HR High Resolution Multi-Collector Inductively-Coupled-Plasma Mass Spectrometer (HR-MC-ICP-MS). The analysis of Si isotopes is hampered on low resolution instruments because of significant poly-atomic interferences on the minor isotope beams (particularly ^{30}Si). The capability of the Nu Plasma HR to run at “medium” and “high” resolution means that the analyte and interference beams can be resolved, making accurate Si isotopic analysis using MC-ICP-MS possible. Typically, the instrument was operated at “medium” resolution (resolving power $m/\Delta m \sim 3300$, where Δm is defined at 5% and 95% for peak height; Weyer and Schweiters, 2003), which resulted in a ~ 85% reduction of instrument sensitivity and a total analyte signal of 1×10^{-10}A (at 750 ppb Si). Isotopic analyses were corrected for instrumental mass bias using the standard-sample bracketing protocol normalising against the NBS28 silica sand standard. Variations in Si isotopes are represented by the delta notation, as $\delta^{30}Si$, in per mil (‰).

To begin with, thirty five mafic and ultramafic samples, sourced globally, have been analysed with an aim of providing a robust estimate for the average Si isotope composition of Bulk Silicate Earth (BSE). The sample set define a very limited range of isotopic values, which include basalts from mid-ocean ridge, island arc and ocean island tectonic settings, as well as mantle xenoliths. As such, the BSE is regarded as homogeneous with respect to Si isotopes, with an average value of $\delta^{30}Si = -0.29 \pm 0.08$ ‰ (2 s.d.).

To study the effect of magmatic differentiation on Si isotopes, a suite of igneous rocks from the volcano of Hekla, Iceland, have been studied. Hekla is particularly suitable for such a study because it produces eruptive material with a wide range of silica-contents from a cogenetic source. Also, previous research suggests that petrogenesis at Hekla involves only igneous processes (e.g. Sigmarsson et al., 1992; Schuessler et al., 2009). The Si isotope data from these samples display a strong, positive, linear relationship with proxies for differentiation (i.e. SiO_2 content, Ba content), and a range of ~ 0.20 ‰ between basaltic and rhyolitic samples. This variation can only be the result of magmatic differentiation. To compliment the Hekla suite, a range of extrusive igneous rocks (from the Afar Rift Zone, Ethiopia, UGSG standards and elsewhere on Iceland) have also been analysed. These data fall on the same array as the Hekla samples. Therefore, it appears that Si isotopes behave predictably during magmatic differentiation and, as such, an empirical "igneous array" can be established:

$$\delta^{30}Si\ (‰) = 0.0056 \times SiO_2 - 0.567\ (\pm\ 0.05\ ‰;\ 2\ s.e.).$$

Assuming an "andesitic" composition (SiO_2 = 60.6 wt.%; Rudnick and Gao, 2003) and the above expression, an "igneous" Si isotopic composition for the upper continental crust of $\delta^{30}Si$ = -0.23 ± 0.05 ‰ can be calculated. This value is used for comparison in later studies.

Because ~ 50% of the Upper Continental Crust (UCC; Wedepohl, 1995) is comprised of felsic intrusive material, the Si isotopic composition of granitoid rocks has been investigated, using a suite of samples from Australia and South-west England. As an added motivation, there was also the potential that Si isotopes could potentially discriminate between granites of different crustal affinities. The data show that granites define a wider range of $\delta^{30}Si$ values than their extrusive counterparts (rhyolites and dacites), and that S-type granites (granites with a sedimentary affinity) have, on average, lighter Si isotope compositions. S-type granites should be isotopically lighter than granites with an igneous affinity (I-type granites) because their sedimentary source is typically isotopically light (see Basile-Doelsch, 2006, and references therein). However, the data show a large degree of overlap, and it appears that other geochemical proxies are much more effective at distinguishing between granites "types". The average Si isotopic composition of granites is $\delta^{30}Si$ = -0.23 ± 0.15 ‰ (2 s.d.), which is identical to that calculated by the "igneous array".

To provide a more robust estimate for the Si isotope composition of the UCC, a selection

of loess and shale samples, sourced globally, have been analysed. The loess and shale data define significantly different isotopic ranges, which reflect the contrasting petrogenetic histories of the two lithologies. The Si isotopic composition of loess is very similar to igneous rocks, and the data define a very narrow range ($\delta^{30}Si$ = -0.28 to -0.15 ‰). This is most likely because loess is predominantly derived as a result of mechanical erosion processes. This is further confirmed by the average loess value ($\delta^{30}Si$ = -0.22 ± 0.07 ‰; 2 s.d.), which is almost identical to the granite average and the calculated "igneous array" value (see above). In comparison, the Si isotopic composition of shales are much more variable ($\delta^{30}Si$ = -0.82 to +0.00 ‰), a result of their more complicated petrogenesis, which can involve both chemical and mechanical weathering, as well as metamorphism and diagenesis. The Si isotopic composition of shales appears to be a function of the proportions of detrital quartz and secondary phases. Also, these secondary phases may record variably light Si isotope compositions, depending on the degree of weathering a sample has experienced (e.g. Georg et al., 2009a). Using the granite, loess and shale data, a weighted average UCC composition of $\delta^{30}Si$ = -0.25 ± 0.16 ‰ (2 s.d.) has been calculated.

The final research chapter investigates the Si isotopic composition of the deep continental crust, using a suite of granulite facies xenoliths. These have a similar range of compositions to those of igneous rocks from elsewhere in the crust and mantle ($\delta^{30}Si$ = -0.43 to -0.15 ‰). Two different controls over Si isotopic composition have been identified using these samples. The first is magmatic differentiation, akin to that investigated in Chapter 4 (see above). The second is mineralogical, and is displayed by xenoliths that have a cumulate igneous protolith. Weighted average compositions for the middle and lower crust have been calculated using these data. These are $\delta^{30}Si$ = -0.29 ± 0.04 ‰ (95% s.e.) for the lower crust, and $\delta^{30}Si$ = -0.23 ± 0.04 ‰ (95% s.e.) for the middle crust.

This thesis has greatly improved our knowledge of the behaviour of Si isotopes in endogenous rocks but, in many ways, it has merely confirmed what was previously assumed. For instance, the BSE has, for a long time, been inferred as homogeneous (Douthitt, 1982; Ding et al., 1996) but now we can say just *how* homogeneous it is. Also, the theory that increasing polymerisation should cause Si isotopic fractionation (Grant, 1954) had never been explicitly tested until the work on magmatic differentiation (Chapter 4). Until then, it was simply a vague

trend of high-silica rocks having, on average, heavier isotopic compositions (Douthitt, 1982; Ding et al., 1996). Finally, the similarity of the $\delta^{30}Si$ values for BSE, UCC and the deep crust are testament to the ubiquity of Si in silicate rocks. Even though highly fractionated sediments may be present in substantial proportions in these reservoirs, they do not affect bulk composition to any great degree. The provision of robust compositional estimates for these reservoirs, and studies into how Si isotopes react to igneous processes are necessary. They provide a framework for further Si isotopic investigations, where igneous rocks play a significant role.

ACKNOWLEDGEMENTS

To begin with, I would like to acknowledge my supervisors, Alex Halliday, Bastian Georg and Helen Williams. Firstly, Alex deserves a massive thank-you for putting his faith in me as a student, and for always finding time to offer support, experience and guidance. Helen was, as always, equally approachable and insightful. Bastian was a fantastic teacher, and this research would have been much more arduous without his instruction in chemical techniques and mass spectrometer operation and theory, as well as his comprehensive knowledge of Si isotopes. Finally, Tim Elliott had the onerous task of supervising my Masters project at the University of Bristol, but his enthusiasm for isotope geochemistry and sage advice are the main reasons I remained in academia.

Next, I would like to extend my thanks to all the geochemists at Oxford. Kevin Burton was always eminently helpful and is still a formidable table football opponent. Julie Prytulak, Chris Siebert, Sophie Opfergelt, Kate Hendry and Dave Cook all offered research suggestions, help in the laboratory and general advice throughout, not to mention evenings in the Lamb and Flag. Also, Kevin, Chris and Sophie were kind enough to allow me to accompany them on fieldwork to Iceland (with the proviso that I dug soil pits); otherwise, the Hekla study would not have been possible. As an aside, I would like to express my gratitude to all the staff at the Institute of Earth Sciences, Iceland, and particularly Karl Grönvold, who advised us on sample location and accessibility for the Hekla suite. Finally, I could not go without acknowledging the constant support and friendship of Ros Armytage, who has been there from the start and with whom I have experienced the ups and downs of Si isotope research.

As well as the fine tutelage provided by Bastian, my time running the MC-ICP-MS at Oxford was made easier by the support of Teo Krastev and Nick Belshaw. Also, many thanks to all the laboratory support staff at Oxford, but especially to Steve Wyatt, who was always accommodating when I needed to use the furnace or rock crushing facilities. I would also like to express my gratitude to John Watson at the Open University, who not only supervised the processing of all my Hekla samples, but also kindly provided the XRF analyses.

This project would not have been possible without the kind donation of samples from many parties. In particular, most of the mafic and ultramafic samples analysed in Chapter 3 were from the collections of Charlie Langmuir, Bill White, Barry Dawson and Cassi Paslick. Dave

Waters and Monica Price were instrumental in organising access to Laurence Wager's Skaergaard suite. Dave Ferguson did all the hard work collecting and characterising the Afar samples. All the shales, loess and granulite xenoliths were graciously supplied by Roberta Rudnick and Scott McLennan. I am indebted to Bruce Chappell, who not only gave a large and representative suite of granites for analysis, but who also took the time out to visit the department and discuss them. Other granitoid samples were generously provided by Simon Turner and the British Geological Survey. Lastly, I would like to thank Richard Scrivener, who acted as a fantastically knowledgeable and erudite guide to the igneous geology of SW-England.

Because I am terrified of missing somebody off this list, I would like to acknowledge the whole post-graduate student body of the Department of Earth Sciences at Oxford; one couldn't ask for a nicer bunch of co-workers. However, there are those who merit special mention: Mark Bourne for putting up with my clutter, and also for being a fastidious proof-reader; Giovanni Fontana for the cups of tea/coffee and movie trivia; the Oxford Earth Sciences Football Team for being so inclusive even when faced with such a terrible sportsman as I; Marcus Bell, Phil Renforth and Rich Walker for making a fellow northerner feel less out of his depth, and; last but not least, everyone who I shared a drink with at Happy Hour and beyond. Cheers!

Finally, this thesis is dedicated to my family and Emily, whose patience and support over the last four years has kept me going through the good times and the bad. Thank you all.

CONTENTS

Abstract i
Extended Abstract iii
Acknowledgements ix
Contents xi
List of Figures xv
List of Tables xvii

1 INTRODUCTION 1
1.1 The global silicon cycle 2
1.2 The study of silicon isotopes 2
1.2.1 Weathering and biogenic silica – the "secondary" silicon isotope cycle 4
1.2.2 Extra-terrestrial samples 5
1.3 Stable isotope theory and its application to silicon isotopes 6
1.3.1 Mass dependent fractionation 8
1.4 Objectives of this study 9

2 METHODS AND TECHNIQUES FOR THE ANALYSIS OF SILICON ISOTOPES 13
2.1 Introduction 14
2.1.1 Historical analysis of Si isotopes 14
2.1.2 The application of MC-ICP-MS to silicon isotope analysis 15
2.2 Samples and reagents 16
2.3 Sample processing – alkali fusion 17
2.4 Sample processing – column chemistry 19
2.5 Mass Spectrometry 21
2.5.1 General theory 21
2.5.2 Sample introduction 22
2.5.3 Sample ionisation and acceleration into the mass spectrometer 23
2.5.4 The mass analyser 25
2.5.5 Detectors 26
2.5.6 High resolution MC-ICP-MS 27
2.5.7 Running silicon isotopes on a Nu Plasma HR-MC-ICP-MS 29
2.6 In-situ silicon isotope analysis 30

3 THE SILICON ISOTOPIC COMPOSITION OF BULK SILICATE EARTH 31
Abstract 32
3.1 Introduction 32
3.2 Samples 34
3.2.1 Standards 34
3.2.2 Ultramafic rocks 34
3.2.3 Mid-Ocean Ridge Basalts (MORB) 35
3.2.4 Island-arc Basalts (IAB) 35
3.3 Methods 36
3.3.1 Fusion 36
3.3.2 Mass spectrometry 36
3.4 Results 37
3.4.1 Data accuracy and reproducibility 37
3.4.2 Sample data 38
3.5 Discussion 40

3.5.1 The bulk composition of the BSE 40
3.5.2 Assessing the possible causes of sample irreproducibility 42
3.5.3 Is the Earth's mantle heterogeneous with respect to silicon isotopes? 44
3.6 Conclusions 46
Acknowledgements 47

4 SILICON ISOTOPE FRACTIONATION DURING MAGMATIC DIFFERENTIATION 49
Abstract 50
4.1 Introduction 50
4.2 Geological Background 53
4.2.1 The volcano of Hekla 53
4.2.2 Magma differentiation on Hekla 54
4.3 Samples and analytical techniques 55
4.3.1 Iceland 55
4.3.2 Additional samples 57
4.3.3 Alkali fusion 58
4.3.4 Mass spectrometry 59
4.4 Results 60
4.4.1 External standards 60
4.4.2 Sample data 62
4.5 Discussion 65
4.5.1 Silicon isotope fractionation in the Hekla volcanic suite 65
4.5.2 The igneous array for silicon isotopes 70
4.5.3 Modelling silicon isotope variation during magmatic differentiation 71
4.5.4 Modelling silicon isotope fractionation as a result of fractional crystallisation 72
4.5.5 The silicon isotopic composition of the continental crust 74
4.6 Conclusions 74
Acknowledgements 75

5 THE SILICON ISOTOPIC COMPOSITION OF GRANITOID ROCKS 77
Abstract 78
5.1 Introduction 78
5.2 Samples 82
5.2.1 I- and S-type granites from SE Australia 82
5.2.2 New England Batholith 85
5.2.3 A-type granites from SE Australia 85
5.2.4 Aplites and pegmatites from South-west England 86
5.3 Methods 87
5.3.1 Alkali fusion 88
5.3.2 Mass spectrometry 88
5.4 Results 89
5.4.1 External standards 89
5.4.2 Whole-rock sample data 90
5.4.3 Aplites and pegmatite mineral separates 93
5.5 Discussion 95
5.5.1 Silicon isotope variation in granitoid rocks 95
5.5.2 Silicon isotope variations in granites as a function of source heterogeneity 100
5.5.3 The silicon isotopic composition of the upper continental crust 104
5.6 Conclusions 105

6 THE SILICON ISOTOPIC COMPOSITION OF THE UPPER CONTINENTAL CRUST 107
6.1 Introduction 108
6.2 Samples 109
6.2.1 Loess 109
6.2.2 Shales 110
6.3 Methods 112
6.4 Results 113
6.4.1 External standards 113
6.4.2 Sample data 113
6.5 Discussion 118
6.5.1 Loess as a proxy for the composition of the upper continental crust 118
6.5.2 The composition of Archaean continental crust 120
6.5.3 The formation of shales 121
6.5.4 Evolution of shale silicon isotope composition over time 125
6.5.5 The silicon isotope composition of the upper continental crust 127
6.6 Conclusions 130

7 THE SILICON ISOTOPIC COMPOSITION OF THE DEEP CONTINENTAL CRUST 133
7.1 Introduction 134
7.2 Sample descriptions 134
7.2.1 McBride xenolith suite, Queensland, Australia 135
7.2.2 Chudleigh xenolith suite, Queensland, Australia 136
7.3 Methods 137
7.4 Results 138
7.4.1 External standards 138
7.4.2 Granulite facies xenoliths 138
7.5 Discussion 140
7.5.1 Silicon behaviour during high-grade metamorphism 140
7.5.2 Silicon isotope heterogeneity in the deep crust 142
7.5.3 Silicon isotopic variation in the McBride xenolith suite 142
7.5.4 Silicon isotopic variation in the Chudleigh xenolith suite 144
7.5.5 Silicon isotope composition of the lower and middle crust 147
7.6 Conclusions 149

8 SUMMARY AND OUTLOOK 151

REFERENCES 157

APPENDIX 1: Hekla samples - major and trace elements 173

FIGURE LIST

1.1	Range of $\delta^{30}Si$ values in terrestrial and extraterrestrial environments	3
1.2	Three isotope plot with terrestrial mass fractionation lines	9
2.1	Schematic diagram of a Nu Instruments Nu Plasma MC-ICP-MS	22
2.2	Low, pseudo-high (medium) and "true" high mass resolution on a MC-ICP-MS instrument.	28
3.1	Sample reproducibility over the course of sample analysis	38
3.2	Three isotope plots of mafic and ultramafic sample Si isotope data	41
3.3	Plot of $\delta^{30}Si$ vs. Fe content	42
3.4	Plot of $\delta^{30}Si$ vs. SiO_2 and Al_2O_3 contents	45
3.5	Plot of $\delta^{30}Si$ vs. NBO/T	46
4.1	Histogram of igneous rock data from Douthitt (1982)	52
4.2	Simplified map of Iceland showing the location of Hekla	54
4.3	Sketch map of Hekla volcano, Iceland, showing sample localities	56
4.4	Total alkali–silica (TAS) diagram	58
4.5	Graphs of $\delta^{30}Si$ vs. SiO_2 and Ba of the Icelandic, Afar and USGS samples	64
4.6	Rayleigh fractionation models of Si isotope evolution in a magma chamber	71
4.7	Silicon isotope evolution models showing the effects of varying fractionating phases	73
5.1	Plot of $\delta^{30}Si$ vs. SiO_2 displaying the "igneous array" for Si isotopes	80
5.2	Selection of clay mineral and whole rock $\delta^{30}Si$ data	81
5.3	Silicon isotope data for whole-rock granite samples	96
5.4	Silicon isotope data for the aplite and pegmatite mineral separate samples	97
5.5	Plot of $\delta^{30}Si$ vs. SiO_2 for contrasting granite types	98
5.6	Silicon isotope data plotted against proxies of granite source affinity	101
5.7	Isotope mixing models for granite petrogenesis ($\delta^{30}Si$ vs. $^{87}Sr/^{86}Sr_{(i)}$)	103
6.1	Plot of $\delta^{30}Si$ values for the loess and shale samples	117
6.2	Plot of $\delta^{30}Si$ against SiO_2 for all loess and shale samples	118
6.3	Plot of $\delta^{30}Si$ against CIA value for all loess and shale samples	119
6.4	Plot of $\delta^{30}Si$ against $\delta^{26}Mg$ and $\delta^{7}Li$ for all loess and shale samples	120
6.5	Plot of $\delta^{30}Si$ against Nb contents for all loess and shale samples	124

6.6 Graph of $\delta^{30}Si$ against deposition age for the PAAS and Pilbara shales, Australia 127

6.7 Histogram of $\delta^{30}Si$ values for upper crustal lithologies 128

7.1 Plot of $\delta^{30}Si$ against SiO_2 for granulite facies xenolith samples 140

7.2 Plot of $\delta^{30}Si$ against $^{87}Sr/^{86}Sr$ and $\delta^{18}O$ for granulite facies xenolith samples 144

7.3 Plot of $\delta^{30}Si$ against Mg# and Eu/Eu* for the granulite facies xenolith samples 145

8.1 Summary of Si isotope data analysed in this thesis 156

TABLE LIST

2.1	Ion chromatography resin pre-cleaning and cleaning procedures	19
2.2	Example column recipe	21
2.3	Nu Plasma HR-MC-ICP-MS example running conditions	21
3.1	External standard data	38
3.2	Silicon isotope data for mafic and ultramafic samples	39
4.1	External standard data	61
4.2	Silicon isotope data for Hekla, Afar and Skaergaard mineral separate samples	63
5.1	External standard data	91
5.2	Whole rock Si isotope data for Australian granites	92
5.3	Silicon isotope data for aplite and pegmatite samples	95
6.1	External standard data	114
6.2	Silicon isotope data for loess	115
6.3	Silicon isotope data for shales	116
6.4	Silicon isotope composition of the upper continental crust	130
7.1	Silicon isotope data for external standards and granulite facies xenoliths	139
7.2	Silicon isotope composition of the deep continental crust	148

Chapter 1: Introduction

1.1 THE GLOBAL SILICON CYCLE

Silicon (Si, atomic weight = 28.08553) is a ubiquitous element, the third-most abundant on Earth (10.68% Si; Palme and Jones, 2003). Although it is likely present in a few weight percent in the Earth's core (Wade and Wood, 2005; Georg et al., 2007; Armytage et al., 2011), it is *the* major cation in the Earth's mantle and lithosphere. The mantle is composed of ~ 21.5 wt.% Si and, because Si behaves slightly incompatibly during partial melting, the Earth's crust is more Si-rich than the mantle (~ 24 wt.% Si; Hofmann, 1988). Continental crust contains, on average, ~ 28 wt.% Si (Rudnick and Gao, 2003) but is compositionally zoned, such that the upper continental crust, i.e. that which interacts with the hydrosphere and biosphere, is more evolved (more Si-rich), with an average Si content of 31 wt.%.

Silicon is a key component in many and varied geo- and biochemical cycles: for instance, dissolved silica in the oceans is a major nutrient for marine organisms such as diatoms and radiolaria (Tréguer et al., 1995), whose productivity in the oceans mediates atmospheric CO_2. Also, weathering of primary silicates in the continental crust removes CO_2 from the atmosphere (Berner, 1997). Because of its importance in these processes and its intrinsic link to the global carbon cycle, the study of Si isotopes in the "secondary" Si pool (that is, any Si that is not contained in igneous material; Basile-Doelsch, 2006) is now well established (see later). However, due to the small and apparently non-systematic variations noted in the Si isotopic compositions of igneous rocks in previous low precision research (Fig. 1.1; e.g. Douthitt, 1982; Ding et al., 1996), this area has been somewhat ignored in the literature. Using modern analytical methods and state-of-the-art equipment, this research aims to investigate whether or not there are systematic Si isotope variations within the igneous realm, whilst providing robust Si isotopic compositions for the major silicate reservoirs on Earth and, hopefully, identifying further uses for this sometimes overlooked isotopic system.

1.2 THE STUDY OF SILICON ISOTOPES

The study of Si isotopes is not a novel subject, and research into this topic began in the 1950's. The studies of Reynolds and Verhoogen (1953) and Allenby (1954) used Gas Source Mass Spectrometry (GS-MS), with an analytical precision of $\delta^{30}Si \sim \pm 0.4$ ‰ (where the $\delta^{30}Si$ is defined as a sample's isotopic ratio relative to a global reference standard, see Section 1.3), to analyse a variety of natural samples. These studies demonstrated that natural Si isotopic

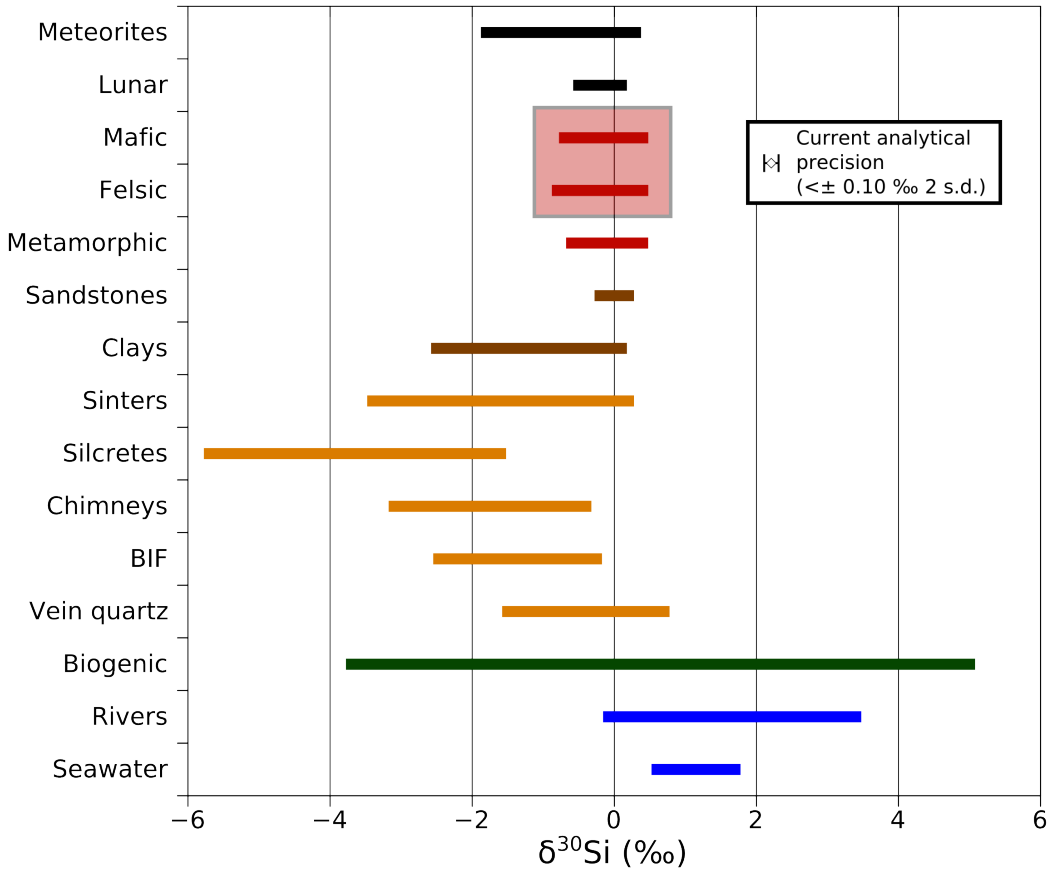


Fig. 1.1 Range of $\delta^{30}Si$ values in terrestrial and extraterrestrial environments, showing the relatively limited isotopic range defined by igneous rocks (red box). The current analytical precision is also illustrated. This plot shows that clays and secondary silica are, on average, lighter than igneous rocks, and a corresponding enrichment is recorded by river and seawater samples. Data taken from Douthitt (1982), Molini-Velsko et al (1986), Ding et al. (1996), De la Rocha et al. (2000), De la Rocha (2003), Ding et al. (2004), Basile-Doelsch et al. (2005), Ziegler et al. (2005a,b), André et al. (2006), Robert and Chaussidon (2006) and Georg et al. (2007).

variations were measurable but limited compared to the variations being measured in other systems at the time, i.e. oxygen. At the same time, Grant (1954) calculated that, on a theoretical basis, equilibrium fractionation between igneous mineral phases would result in Si isotopic fractionation on the order of $\Delta^{30}Si \sim 1.0$ to 5.0 ‰, with the heavier isotopes being concentrated in the more polymerised phase. This concept is still broadly accepted, although with major caveats and much smaller degrees of fractionation (e.g. Méheut et al., 2009).

More research into Si isotopes followed in the 1960's (Tilles, 1961a, b). These studies were made at higher precision (± 0.2 ‰) than previous reported, and were the first to infer that more primitive igneous materials have, in general, lighter Si isotopic compositions than their evolved counterparts, in line with the predictions of Grant (1954). Although there was a brief renaissance of Si isotope research using lunar samples (Epstein and Taylor, 1970, 1973; Taylor and Epstein, 1970, 1973), it was not until the extensive studies of terrestrial material by Douthitt

(1982) and Ding et al. (1996) and extra-terrestrial material by Molini-Velsko et al. (1986) appeared, that research into Si isotopes began to gather momentum.

Douthitt's (1982) and Ding et al.'s (1996) large compilations of Si data were, until recently, the most detailed studies of igneous rocks in the literature and both are still widely cited (Fig. 1.1). The analyses of Douthitt (1982) define an igneous isotopic range of $\delta^{30}Si$ = -0.8 to +0.3 ‰, with an average mafic and ultramafic (i.e. Bulk Silicate Earth; BSE) value of $\delta^{30}Si$ = -0.4 ± 0.2 ‰. Unfortunately, these data were not normalised using the current standard isotope ratio (NBS28) and, as such, direct comparisons are difficult to make.

Ding et al. (1996), using NBS28 as their standard, define the range of mafic and ultramafic material as between $\delta^{30}Si$ = -1.0 to +0.4 ‰ with a lighter mean of -0.63 ‰. This average is probably biased towards lighter values because they used the data of Douthitt (1982), recalculated using a measured (negative) offset between the two bracketing standards that each study used. This offset has since been measured as virtually zero (Georg et al., 2007). In both studies, it was noted that felsic igneous rocks have on average heavier $\delta^{30}Si$ values than mafic, again confirming the sense, but not the magnitude, of fractionation as predicted by Grant (1954).

Since the study of Ding et al. (1996), very little research has been invested into the Si isotope composition of igneous rocks, and the reappraisal planned by this study is extremely timely. Current analytical precision now allows Si isotopic measurements to be made accurately at the sub-per mil level and, if the data ranges defined by the two studies described above are real, then these could be recording small but systematic isotopic variations. Also, new-found interest in the Si isotopic variation between BSE and chondritic meteorites (e.g. Georg et al., 2007; see later) means that robust and well-constrained estimates of the Si composition of igneous rocks are necessary.

1.2.1 Weathering and biogenic silica – the "secondary" silicon isotope cycle

As mentioned above, Si isotope behaviour in the "secondary" Si pool has been the subject of much research interest, due to its link with atmospheric carbon and its palaeo-environmental significance. Also, the degree of Si isotopic fractionation at low temperatures is much larger, meaning that analysis of resolvable isotopic variations is less challenging (Fig. 1.1). For instance, the effect of weathering on Si isotopes is now well established by studies of natural soil and clay formation (Ziegler et al., 2005a&b; Georg et al., 2009a; Bern et al., 2010;

Opfergelt et al., 2008, 2009, 2010, 2011; Steinhoefel et al., 2011), experimental work (Ziegler et al, 2005a; Delstanche et al., 2009) as well as studies of riverine Si and associated bedrock (De la Rocha et al., 2000; Ding et al., 2004, Georg et al., 2006a, 2009b; Cardinal et al., 2010; Engström et al., 2010). This large body of work broadly indicates that precipitation of Si from solution enriches the product in the lighter isotopes, whether this be as a weathering product (clay mineral) or as chemically precipitated silica (e.g. Basile-Doelsch et al., 2005), leaving an isotopically heavy fluid. Because ~85% of dissolved Si in the ocean is derived from the continents (Tréguer et al., 1995), this has imbued the oceans with a heavy Si isotopic composition (De la Rocha et al., 2000; Varela et al., 2004).

Biogenic silica records the largest range of $\delta^{30}Si$ values in the terrestrial realm and have been used to infer nutrient utilisation in past oceans (e.g. De La Rocha, 2006). Diatoms have $\delta^{30}Si$ = -1.3 to +1.4 ‰, radiolaria are more limited ($\delta^{30}Si$ = +0.2 to +0.3‰), sponges are more negative with $\delta^{30}Si$ = -3.7 to +0.9 ‰, whereas stromatolites are more positive viz. $\delta^{30}Si$ = +2.4 to +3.4‰ (Ding et al., 1996; Hendry et al., 2010, Wille et al., 2010). Siliceous sediments derived from such materials reflect the composition of their sources (i.e. Ding et al., 1996; De la Rocha 2002; Robert and Chaussidon 2006).

1.2.2 Extra-terrestrial samples

Although the study of Molini-Velsko et al. (1986) presented a large compilation of meteorite Si isotope data, it was the work of Georg et al. (2007) that sparked current interest in the Si isotopic composition of extra-terrestrial material. Using a novel sample preparation technique and cutting edge instrumentation (Georg et al., 2006b), this study was able to observe resolvable isotopic variations between Bulk Silicate Earth (BSE) and meteorites. This was interpreted as evidence that Si entered the core during formation (Allègre et al., 1995; Wade and Wood, 2005), and that partitioning of Si between metal and silicate phases sequestered the lighter isotopes into the core. This important result generated a great deal of further research, and was a major impetus for this thesis. Such work included constraining the Si isotopic composition of BSE (Chapter 3, Zambardi et al., 2009) and more extra-terrestrial samples (Fitoussi et al., 2009; Armytage et al., 2011) with the aim of better refining the offset between the two groups, and also quantifying metal-silicate isotope fractionation factors (Shahar et al., 2009; Ziegler et al., 2010). Even still, the picture is not clear, as a recent paper by Chakrabarti

and Jacobsen (2010) claims that there is no difference between BSE and meteorites.

1.3 STABLE ISOTOPE THEORY AND ITS APPLICATION TO SILICON

Silicon has three stable isotopes: ^{28}Si (atomic mass = 27.97693, abundance = 92.22 %); ^{29}Si (atomic mass = 28.97649, abundance = 4.69 %) and; ^{30}Si (atomic mass = 29.97377, abundance = 3.09 %). As with the vast majority of stable isotope systems, Si isotope variations are reported using "delta notation", defined as the deviation of a sample's isotopic ratio from that of a standard isotopic ratio (in per mil, ‰), as such:

$$\delta^{i} D_{X} = \left(\frac{R_{X}^{i/j}}{R_{STD}^{i/j}} - 1 \right) \times 1000$$

where R represents the ratio of isotopes i and j of element D, in the sample (X) and a standard (STD). Typically, the heaviest isotope is used as the numerator in ratio R, so that positive values of $\delta^{i}D$ indicate that such a sample is enriched in isotope i and has a "heavy" isotopic composition relative to the standard. For Si isotopes, two delta values can be defined (δ^{30}Si and δ^{29}Si):

$$\delta^{30} Si_{X} = \left(\frac{^{30}Si/^{28}Si_{X}}{^{30}Si/^{28}Si_{NBS28}} - 1 \right) \times 1000 \qquad \delta^{29} Si_{X} = \left(\frac{^{29}Si/^{28}Si_{X}}{^{29}Si/^{28}Si_{NBS28}} - 1 \right) \times 1000$$

Silicon isotopic data is commonly represented using δ^{30}Si values, which are approximately twice the magnitude of δ^{29}Si values, assuming mass dependent fractionation (see later). The standard reference used for reporting Si isotopic data is the silica sand reference material RM 8546, distributed by the National Institute of Standards and Technology (NIST). Due to historical reasons, the equivalent name used by most of the literature for this standard is NBS28; this practice is continued throughout this research. Before NBS28 was established, the Caltech Rose Quartz Standard (RQS) was used as a reference standard (e.g. Douthitt, 1982). Unfortunately, the isotopic composition of RQS is poorly constrained against NBS28 and so direct comparison of older data is not possible, although the most recent estimate indicates that both standards have approximately equal isotopic compositions (Georg et al., 2007).

Reactions governing stable isotope fractionation can be split into two groups,

equilibrium and kinetic. During equilibrium fractionation, the reactants and products are able to react with each other continuously, e.g. condensation of a liquid from a gas. Kinetic reactions are one-way, in which the product is prevented from re-equilibrating with the reactant, e.g. evaporation of a gas from a liquid. The only chemical or physical difference between isotopes of an element is mass; therefore, isotopic fractionation is a function of kinetic and thermodynamic discrimination, during these reactions, by mass.

Isotopic fractionation results from the reduction in the zero-point energy when a heavier isotope is substituted for a lighter one (e.g. Schauble, 2004). This leads to higher concentrations of the heavier isotopes in substances where the vibrational energy in a system is lowest, i.e. in a solid or liquid compared to a gas, or, in the case of O or Si isotopes, in a more polymerised phase compared to a less polymerised phase (Grant, 1954, Garlick, 1966). The degree of isotopic fractionation between two phases depends on a number of physical properties, which include reaction temperature and rate, relative mass difference, bonding environment and oxidation state (O'Neil, 1986; Schauble, 2004). Although the relative mass difference between its isotopes is large (^{30}Si - ^{28}Si ~ 7 %), Si isotope fractionation is limited in the igneous realm because of a) the high temperatures associated with this environment (the degree of isotopic fractionation decreases as temperature increases, following the relationship: ln α ✪ $1/T^2$); b) the constancy of the bonding environment of Si in silicates, wherein it is almost always tetrahedrally coordinated with oxygen, and; c) the single oxidation state of Si (4+). Silicon isotopic variations on the order of < 0.1 ‰ are typical at high temperatures.

The degree of isotopic fractionation between two phases, A and B, is described using the fractionation factor, α, as follows:

$$\alpha_{A-B} = \frac{^{30}Si/^{28}Si_A}{^{30}Si/^{28}Si_B} = \frac{1000+\delta^{30}Si_A}{1000+\delta^{30}Si_B}$$

which is simply the ratio of the isotopic ratios of the two phases. It can be written in terms of delta values, also defined above. An α value > 1 indicates that phase A is enriched in the heavier isotopes relative to phase B. Because of the small magnitudes associated with stable isotope fractionation, α values are always very close to 1.

The isotopic difference between two phases is often expressed in terms of the difference in their delta values (i.e. $\delta^{30}Si_A$ and $\delta^{30}Si_B$) as a Δ ("Big Delta") value, and can be linked to the fractionation factor by a simple (and very useful) approximation, as such:

$$\Delta^{30}Si_{A-B} = \delta^{30}Si_A - \delta^{30}Si_B \approx 10^3 \ln \alpha_{A-B}$$

1.3.1 Mass dependent fractionation

Isotopic fractionation is a mass-dependent process. For a system such as Si that has three stable isotopes, the extent of fractionation of the $^{30}Si/^{28}Si$ ratio will be greater than that of the $^{29}Si/^{28}Si$ as a function of the mass difference of the ratios. As shown by Young et al. (2002), this mass dependence can be described in terms of the fractionation factors:

$$\alpha_{29/28} = (\alpha_{30/28})^{\beta}$$

The exponent β is defined differently for kinetic and equilibrium fractionation, in terms of the atomic masses m_x of each of the isotopes. For silicon, these exponents are calculated as follows:

$$\beta_{kin} = \frac{\ln\left(\frac{m_{28}}{m_{29}}\right)}{\ln\left(\frac{m_{28}}{m_{30}}\right)} = 0.5092 \qquad \beta_{eq} = \frac{\left(\frac{1}{m_{28}} - \frac{1}{m_{29}}\right)}{\left(\frac{1}{m_{28}} - \frac{1}{m_{30}}\right)} = 0.5178$$

On a three isotope plot (a plot of $\delta^{30}Si$ vs. $\delta^{29}Si$), mass dependent isotopic data falls on a straight line with a slope of β_{eq} or β_{kin}, depending on how the isotopes were fractionated. In theory, this should allow us to differentiate between kinetic and equilibrium isotopic processes; however, for Si these slopes are extremely similar at low degrees of fractionation and analytical precision is not good enough to distinguish between the two lines (an example is shown in Fig. 1.2). In practise, this relationship is used as an indicator of data quality. If unresolved interferences are affecting an ion beam in the mass spectrometer (see Chapter 2), this may artificially alter one of

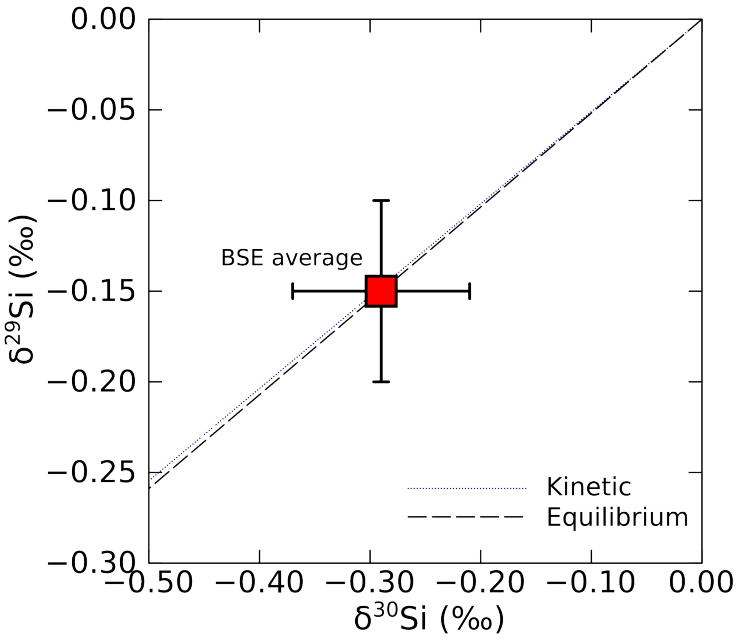


Fig. 1.2 Three isotope plot with the terrestrial mass fractionation lines for kinetic and equilibrium fractionation. These two lines are indistinguishable at low degrees of fractionation at current analytical precision. As an example and for comparison, the average $\delta^{30}Si$ value for Bulk Silicate Earth (Chapter 3) with error bars of 2 standard deviations is plotted.

the isotope ratios, which will displace the data point away from the mass fractionation line. Therefore, all data is checked for mass dependence before it is utilised further.

All of this, of course, assumes mass dependence of Si isotopes during isotopic fractionation. For terrestrial samples, this is a valid assumption; none of the three stable isotopes has a radiogenic component, nor does Si take part in any photochemical or spin-forbidden reactions (e.g. Thiemens, 2006; Bergquist and Blum, 2007). Mass-independent Si isotopic values have been measured from silicon carbide (SiC) grains in enstatite and carbonaceous chondrites ($\delta^{29}Si$ = -20.0 to +124.2‰, Stone et al. 1991) and are attributed to mixing between material inherited from a previous generation of stars and heavy isotopic material produced by neutron capture; no mass-independent Si isotope variations have been measured in terrestrial samples.

1.4 OBJECTIVES OF THIS STUDY

The major aim of this study was to reappraise the Si isotope composition (and any isotopic variations therein) of the major silicate reservoirs of the Earth using the methods for precise Si isotope analysis as detailed by Georg et al. (2006b). The analyses of Georg et al. (2006a, 2007) were made on a large geometry mass spectrometer (the Nu 1700) at ETH Zürich, Switzerland, which has a better intrinsic mass resolving power. As such, the first aim of this study was to establish that accurate, precise and routine Si isotope analysis was possible on the

small geometry Nu Plasma High Resolution MC-ICP-MS instruments at Oxford. This was done by repeat analysis of the external standards Diatomite, IRMM-018 and Big Batch, all of which have been the subject of a round robin Si isotope standard assessment by Reynolds et al. (2007) and also, the USGS rock standards BHVO-1 and BHVO-2 (Abraham et al., 2008). These latter samples have igneous chemical matrices that, if not quantitatively removed before analysis, could cause matrix effects in the mass spectrometer that perturb the true isotopic composition. Silicon isotope analyses using two Nu Plasma HR instruments at Oxford revealed extremely good agreement with the reference values. These standard data are listed in Chapter 3 (Table 3.1 and Fig. 3.1) and the methods and techniques used in preparing and running samples for Si isotope analysis, as well as a detailed description of the Nu Plasma HR MC-ICP-MS are provided in Chapter 2.

After it was established that Si isotope analysis of igneous materials at Oxford was robust, the major research aim (see above) was tackled through a number of smaller studies, which comprise Chapters 3 to 7 of this thesis. These are described in brief below.

Chapter 3: The research covered in Chapter 3 aims to provide an accurate and robust Si isotopic composition for Bulk Silicate Earth (BSE) and, also, investigate any small isotopic variations that could be present. Thirty five mafic and ultramafic samples were analysed and it is shown that the BSE is relatively homogeneous as regards Si isotopes. The average BSE δ^{30}Si value was found to be -0.29 ± 0.08 ‰ (2 s.d.). This research has been published in *Earth and Planetary Science Letters* (Savage et al., 2010).

Chapter 4: The behaviour of Si isotopes during magmatic differentiation was studied using a set of samples taken from the volcano of Hekla, Iceland, and also the Afar Rift Zone, Ethiopia. Analyses display a strong linear relationship between SiO_2 and δ^{30}Si, which can only be a result of magmatic differentiation. All data fall on the same array, with the more evolved (Si-rich) samples showing enrichment in the heavier Si isotopes. The magnitude of isotopic fractionation between basaltic and rhyolitic end-members is ~ 0.20 ‰. This research has been published in *Geochimica et Cosmochimica Acta* (Savage et al., 2011).

Chapter 5: The Si isotopic compositions of a selection of granitoid rocks (predominantly from the Lachlan Fold Belt) were analysed to investigate: a) the behavior of Si isotopes during granite petrogenesis; b) if Si isotopes could be used to distinguish between granites with igneous or sedimentary affinities, and; c) to provide an average igneous composition of the upper

continental crust. Whole-rock granite data fall between $\delta^{30}Si$ = -0.40 and -0.11 ‰ (average $\delta^{30}Si$ = -0.23 ± 0.15 ‰) but, although S-type granites are on average lighter than I- and A-type granites there is considerable overlap between groups. It is the author's intention to submit this chapter for publication, with minor modifications, to *Geochimica et Cosmochimica Acta*.

Chapter 6: A selection of loess and shales, sourced globally, were analysed to finalise the study of the Si isotopic composition of the upper continental crust. These samples also allowed for an investigation of Si isotopic fractionation during different weathering regimes, and also, the evolution of Si isotopes in the upper continental crust over time. Data suggest that the upper continental crust is heterogeneous with respect to Si isotopes ($\delta^{30}Si$ = -0.82 to +0.00 ‰) and has a weighted average composition of $\delta^{30}Si$ = -0.25 ± 0.16 ‰ (2 s.d.).

Chapter 7: The Si isotopic composition of the deep continental crust was investigated by analysis of a selection of well-characterised granulite facies xenoliths from the McBride and Chudleigh volcanic provinces, Australia. In the absence of metasomatism, Si isotopes appear to be robust during granulite facies metamorphism. The data show that the deep continental crust is isotopically heterogeneous compared to BSE, but that it has a similar bulk $\delta^{30}Si$ average. Chapters 6 and 7 will be submitted together as a paper defining the Si isotopic composition of the continental crust, most likely to *Chemical Geology*.

Chapter 2: Methods and techniques for the analysis of silicon isotopes

2.1 INTRODUCTION

The purpose of this chapter is to provide the reader with a comprehensive overview of the techniques used to analyse Si isotopes throughout the work covered in this thesis. Other analytical techniques, such as X-ray Fluorescence (XRF), have also been employed during this research to generate additional data. These methods are well-established and specific references are provided detailing such techniques where relevant.

Dissolution and purification of Si for isotopic analysis was made following the methods of Georg et al. (2006b) and little was modified from their original description. Any variations in technique or additional tests made to confirm the robustness of the method will be clearly identified.

2.1.1 Historical analysis of silicon isotopes

The isotopic analysis of Si is not a novel area of research and a few pioneering studies were made as early as the 1950's (c.f. Reynolds and Verhoogen, 1953; Allenby, 1954). These studies utilised Gas Source Mass Spectrometry (GS-MS), which requires that the Si be introduced into the mass spectrometer in the form of the volatile SiF_3^+ species. This was done either by in-line direct fluorination of SiO_2 by reaction with BrF_5 (Allenby, 1954) or by conversion to, and subsequent thermal decomposition of Ba_2SiF_2 (Reynolds and Verhoogen, 1953). Up until the end of the 20th century, analysis by GS-MS techniques generated most of the Si isotope data, from the lunar studies in the 1970's (e.g. Taylor and Epstein, 1970) to the biogenic silica studies of De La Rocha et al. (1997), including three of the most cited works in the field (Douthitt, 1982; Moline-Velsko et al, 1986; Ding et al., 1996).

It became clear, in both the aforementioned papers and in many others, that the natural variation of Si isotopes is limited, especially in the realms of high temperature geochemistry and cosmochemistry. Although constant refinements to the GS-MS methods and setup over the years strove to improve these techniques, workers could not achieve precision below ~ ± 0.1 ‰ (Ding et al., 1996), not sufficient to resolve any sub per mil variations that might exist. Also, GS-MS analysis is not ideal, as it requires relatively large sample quantities and the use of extremely hazardous, fluoride-based, chemicals. The advent of the Multi-Collector Inductively Coupled Plasma Mass Spectrometer (MC-ICP-MS) in the late 1990's introduced a new tool for isotopic analysis (Belshaw et al., 1998). The application of this instrument to the Si isotope system

means that, nowadays, the analysis of Si isotopes is routine and can be made at much improved degrees of precision.

2.1.2 The application of MC-ICP-MS to silicon isotope analysis

The application of MC-ICP-MS to any isotope system is not without its caveats and analytical pitfalls, and Si was no exception. Firstly, a plasma ion-source is indiscriminate with regards to what elements it ionises and most elements in a sample will therefore get transferred into the mass analyser. Each element will behave differently during ionisation and such effects can change the behaviour of the plasma, altering the ionisation efficiency of the element of study. These so-called "matrix effects" are unpredictable but normally result in the instrument producing incorrect or biased data, depending on the chemically composition of the sample. It is necessary, therefore, to have a method which quantitatively purifies the sample, in many cases through ion chromatography (see later), before it can be confidently and accurately analysed. To avoid artificially induced isotope fractionation during ion chromatography, it is also necessary to achieve quantitative recovery of the element of interest (yields as close to 100% as possible) from the column chemistry (e.g. Roe et al., 2003).

Another problem associated with application of MC-ICP-MS to many isotope systems, not least Si, is that of polyatomic interferences. Even though each sample is purified before analysis, elements present in the ambient atmosphere and the sample solution become ionised and combine in the plasma to form molecules that are, nominally, the same mass as the elements of interest. These molecules are affected by the mass analyser as if they were the ion(s) of interest and are therefore measured as such, resulting in an overestimation of the concentration of certain isotopes. In the case of Si, the interfering molecules are SiH^+, CO^+, N_2^+ and NO^+. In particular, the interference of $^{14}N^{16}O^+$ on $^{30}Si^+$ meant that early MC-ICP-MS studies only measured the $^{29}Si/^{28}Si$ ratio (i.e. Cardinal et al., 2003). This problem was solved by the introduction of "high-" and "medium-" resolution instruments, such as the Nu Instruments Nu-Plasma HR, which can resolve polyatomic interferences from the Si mass spectrum by physically narrowing the ion beam. A more comprehensive description of this process can be found in the *Mass Spectrometry* section of this chapter.

Finally, a problem that is specific to the analysis of Si isotopes is the use of HF in sample preparation. HF is a common reagent during silicate dissolution, but the presence of fluorine (F)

has a detrimental effect on the plasma. Fluorine has a very high 1st ionisation potential – 17.42 eV – higher even than argon (Ar – 15.76 eV) from which the plasma is generated, which will suppress the ionisation efficiency and reduce instrument sensitivity. More importantly for the analysis of Si isotopes, F can form volatile compounds with Si. These could induce artificial isotopic fractionation in the sample at any time during dissolution, transfer to and analysis in the mass spectrometer (Georg et al., 2006b). Therefore, an alternative method was sought. Use of HF can be avoided during sample processing by dissolving the sample in a strong alkaline solution. In particular, this research uses an alkali-fusion technique as established by Georg et al. (2006b) and is described in detail below. Most Si isotope studies utilise alkali-attack to avoid the use of HF; Fitoussi et al. (2009), Armytage et al. (2011) and Zambardi and Poitrasson (2011) all use the methods of Georg et al. (2006b); Abraham et al. (2008) use a similar method but use different flux material and Si purification techniques; finally, van den Boorn et al. (2006, 2007 and 2009) and Chakrabarti and Jacobsen (2010) both use a method that involves alkali digestion in Parr bombs.

2.2 SAMPLES AND REAGENTS

Only rock samples were used in this research, i.e. no biogenic, soil or water samples have been analysed. Samples were received as either whole rocks, crushates or powders. In order to ensure complete dissolution during fusion, all samples needed to be in powder form. Crushates were powdered using an alumina pestle and mortar to avoid the use of agate; however, many of the samples received in powder form had been processed in agate, and the use of agate swing mills was required to process large whole rocks samples, i.e. the Hekla suite (Chapter 4). This should not cause any isotopic bias as a result of silica contamination. Considering the mass balance, even if a silica-poor sample contained 5% agate after milling, this would only shift the sample's $\delta^{30}Si$ value by ~0.015‰ (undetectable at current method precision). This was tested (Chapter 4) by powdering the same sample in both agate and steel mills; no resolvable isotopic offset was detected between the two aliquots. A similar test made by Zambardi and Poitrasson (2011) confirms these findings.

Samples and standards were processed using identical techniques throughout this research. The widely-accepted standard NBS28 (also called NIST RM8546; hereafter just referred to as NBS28), a sample of quartz sand distributed by National Bureau of Standards of

the United States (now National Institute of Standards and Technology) was used as a bracketing standard. The external standards BHVO-1, BHVO-2, Diatomite, Big Batch and IRMM-018 have all been used throughout this research to monitor data accuracy and check for instrumental mass-bias. In particular, BHVO-2 and Diatomite have been routinely analysed during each measurement session. The external standards that have been employed will be listed in each research chapter along with the data and associated external reproducibility. Furthermore, also included in the research chapters are details, where applicable, of replicate analyses (where a new dissolution of the sample was analysed to test for method robustness) and analysis on different MC-ICP-MS instruments (to check for any instrumental variations).

As a major element, blank problems are not a major worry during chemistry. However, as with any analytical method, the aim is to keep method-introduced Si to extremely low levels, as follows. All acids used in this research were at least quartz-distilled, and acids used for the acidification of samples after alkali fusion and liquid chromatography were purified further by sub-boiling in PTFE elbows. The water used in this study was deionised using a MilliQ-element (MQ-e) water polisher, providing high purity water with a resistivity of 18.2 MΩ cm^{-1}. Samples were stored in pre-cleaned PTFE or PP bottles. Fusions were made in silver crucibles, made in-house using 99.99% pure Ag sheet. The flux used was analytical grade NaOH (in pellet form; Merck), which has a Si blank of around 5ppm. To clean the crucibles, they were first leached in weak, quartz-distilled HCl (Merck) overnight. Following this, a blank fusion using an excess of NaOH was made in each crucible, after which the crucibles were rinsed in MQ-e and left overnight in another HCl leach.

A total procedural blank registered no Si concentrations above background, when measured on the MC-ICP-MS – for a typical running solution Si concentration of 1 ppm, this equates to no more than 5 ppb background.

2.3 SAMPLE PROCESSING - ALKALI FUSION

Alkali fusion is not a novel technique for processing silicate samples and the theory is outlined in Potts' Handbook of Silicate Rock Analysis (Potts, 1987). The sample and alkali flux are placed in a crucible at a high heat at which point the flux melts to produce a strong hyper-alkaline liquid that completely dissolves silicate material. When this cools, it forms a water-soluble meta-stable silicate called a "fusion cake", which can then be dissolved in a weakly

acidic solution. Because the Si in the fusion cake is metastable, it will dissociate completely upon acidification.

In the method used in this research (Georg et al., 2006b), around 10 mg of sample is weighed into a silver crucible. This amount is adjusted roughly, taking into account sample composition and dilution strength to yield a final solution concentration of between 10 and 20 ppm Si. Around 200 mg of NaOH flux, in pellet form, is then added to the crucible; one pellet weighs roughly 200mg. NaOH flux is used as it recovers >95% of the sample during fusion and the chemical composition of NaOH is comparatively simple and, upon dissolution with HNO_3, adds only Na cations to the sample. Hence, the amount of cations artificially added to the sample is kept at a minimum, which makes chemical separation via ion-chromatography relatively simple. Alternative flux reagents are available and used in various alkali fusion techniques (i.e. $LiBO_4$; Abraham et al., 2008) but NaOH is preferred, given the reasons above. The choice of flux also dictates the material of which the crucibles are made, with Ag being most resistant to NaOH attack.

The crucible containing the sample and flux is placed in a muffle furnace (preheated to 720°C) for 12 minutes, which allows enough time for complete fusion to take place. After removal from the furnace, the crucible is left to cool slightly for 30 seconds and then carefully transferred into 20 ml MQ-e water in a 30 ml PTFE vial, capped and left to react for approximately 24 hours.

Before transferring the sample into solution, the capped PTFE vial is placed in an ultrasonic bath heated at ~ 60ºC (heating the sample is a recent addition to the method, as suggested by Zambardi and Poitrasson, 2011) to agitate the fusion cake. The sample is transferred into solution by 5 ml pipette into pre-cleaned PTFE or PP bottles – the crucible is rinsed a number of times in MQ-e to ensure all sample is transferred. The solution is then acidified to 1% HNO_3 v/v and left overnight to stabilise. HCl can also be used to acidify the sample solution and some research groups prefer this, due to the possibility that it may reduce the $^{14}N^{16}O^+$ interference on the $^{30}Si^+$ beam (although most of the N and O is introduced into the instrument from the ambient environment). However, use of HCl could cause a drop in machine sensitivity, due to chlorine's high 1st ionisation potential (12.97 eV). In either case, work by Armytage et al. (2011) shows that there is no isotopic bias introduced by storing samples in either HNO_3 or HCl; our choice of HNO_3 is merely historical.

The Si concentration in each solution is checked on a Hach-Lange DR 2700 portable photospectrometer using the "Heteropoly-Blue" method – typical Si fusion yields are between 95 and 100%; average sample yield for each set of samples is provided in the corresponding research chapters. A quantitative transferral of the fusion cake can sometimes be difficult and, in some cases, small amounts may remain adhered to the crucible surface. In these cases recoveries are under 100%. However, since this represents a physical loss of sample material, no isotopic effects are observed, even if recovery during the fusion was not 100%.

2.4 SAMPLE PROCESSING - COLUMN CHEMISTRY

To purify samples for Si isotope analysis, this method employs a one-step column procedure using BioRad AG50 X-12 (200-400 mesh) cation exchange resin. The resin is pre-cleaned in a PTFE container before it is loaded, using the method given in Table 2.1. Standard BioRad Poly-Prep columns with a 2 ml bed volume and 10 ml reservoir volume are used, which have been cleaned in 1% HNO_3 v/v. A resin bed volume of 1.8 ml is packed into each column and the resin is then further cleaned using the method described in Table 2.1. Before any sample is loaded, the resin is cleaned twice and between samples it is cleaned once. The resin is robust enough to continue performing after 4–5 sets of samples and cleaning acids have passed through the column.

Such a simple exchange method is possible because, between pH2 - pH8, Si is in the form $Si(OH)_4$ in equilibrium with the anionic species $H_3SiO_4^-$ (the prevailing anionic species in dissolved silicate samples). Most matrix elements are cationic and are quantitatively retained by

Table 2.1. Ion chromatography resin pre-cleaning and cleaning procedures

	Resin pre-clean procedure			*Resin cleaning procedure*	
	Wash liquid	**Notes**		**Wash liquid**	**Notes**
2x	MQ-e		*6ml*	3N HNO3	
1x	6N HNO3		*6ml*	6N HNO3	
1x	MQ-e		*5ml*	Conc. HCl	
1x	6N HNO3		*3ml*	6N HNO3	
1x	MQ-e		*3ml*	3N HNO3	
1x	50% HNO3	*wait 30 minutes*	*10ml*	MQ-e	*to top of column*
2x	MQ-e		*3ml*	MQ-e	
1x	50% HNO3	*wait 30 minutes*	*3ml*	MQ-e	
2x	MQ-e				
1x	6N HNO3	*leave overnight*			

the resin as the sample passes through the column. For this type of resin, the equilibrium coefficients of the cationic species in water are all greater than 1, which means that cationic species will remain on the resin exchange sites, thus being immobilised, whereas the anionic silicic acid is not retained and Si is quantitatively eluted with H_2O. Column calibration curves show that only anionic species such as SO_4^{2-} and NO_3^- are present in the elute (Georg et al., 2006b). Before any analyses were made at Oxford, this was checked by analysing a solution of BHVO-1 before and after column chemistry – as was expected, only Si, S and N were present in detectable quantities after one column pass (even the large amount of Na, introduced by the fusion procedure, was quantitatively stripped from solution).

In their method paper, Georg et al. (2006b) investigated whether the remaining anionic species in a sample solution could cause matrix effects during analysis. As such, they doped an NBS28 solution to a SO_4^{2-}/Si ratio of ~14 and measured it against an undoped solution – no isotopic deviation or decrease in precision was detected. They repeated the experiment with a NO_3^- dopant, with similar results. Such large SO_4^{2-}/Si and NO_3^-/Si ratios are unlikely to exist in natural lithogenic material, and so it is assumed that the presence of these species will not affect the measured isotopic ratios. This assumption is corroborated by the extremely good levels of reproducibility and precision exhibited by repeat analysis of the external standards. However, Van den Boorn et al. (2009) demonstrated that removal of sulphur by ignition at 1350ºC from a sample before digestion improved their Si isotope reproducibility. A key difference is that their digestion step takes place at 200ºC, which is below the boiling point of sulphur ($T_{boiling}$ =444.72 °C). In our method the fusion step takes place at 720ºC and, as such, it is expected that most of the sulphur will be volatilised and removed prior to column chemistry.

Fitoussi et al. (2009) noted an effect of pH during column chemistry, namely that, at low pH, Si can sorb on to iron hydroxides and be retained by the resin, causing artificial isotopic fractionation. However, this effect has not been replicated by Zambardi and Poitrasson (2011) and Armytage et al. (2011) who found no evidence for pH-induced fractionation (see Chapter 3).

Sample solutions are loaded directly on to the column and are collected immediately in 7 ml PTFE vials. Depending on the current instrumental sensitivity, between 3.0 and 6.0 µg of Si is loaded on to the column, which will result in final Si running concentrations of between 500 ppb to 1.0 ppm. The Si is then eluted in MQ-e, the volume of which is at least twice the resin volume, i.e. 5 ml. An example column recipe is given in Table 2.2.

Table 2.2. Example column recipe

Example conditions	
Concentration required	750 ppb Si
Solution concentration	20 ppm Si
Final sample volume	6 ml
Column recipe	
Sample solution	0.225 ml
MQ-e	5 ml
MQ-e added to elute	0.775 ml

2.5 MASS SPECTROMETRY

2.5.1 General Theory

Throughout this research, we have used two separate Nu Instruments Nu Plasma High Resolution Multi-Collector Inductively Coupled Plasma Mass Spectrometer (HR-MC-ICP-MS; Fig. 2.1.). The multi-collector system means that multiple ion beams can be measured simultaneously, which means that isotopic measurements are more accurate and fluctuations in beam strength are cancelled out when isotope ratios are taken. Although this instrument has a number of additional features that allow it to operate at "high resolution", it shares common components with all MC-ICP-MS instruments. These are illustrated in Figure 2.1. and described below, along with more specific details about the equipment we use to measure Si in our analysis. An overview of the running conditions for a typical Si isotope analysis session is given in Table 2.3.

Table 2.3. Nu Plasma HR-MC-ICP-MS example running conditions

Parameter	
RF Power	1300 W
1st acceleration potential	6 kV
Sampler cone	Nickel, 'B'-type
Sampler cone	Nickel, 'B'-type
Coolant flow rate	13 l/min
Auxiliary gas flow rate	0.9-1.1 l/min
Nebuliser	6mm microflow PFA Savillex
Nebuliser flow rate	50 µl/min
Mass resolution	~ 3300
Cup configuration	L5 (^{28}Si), H1 (^{29}Si), H5 (^{30}Si)
Desolvating device	Cetac Aridus II

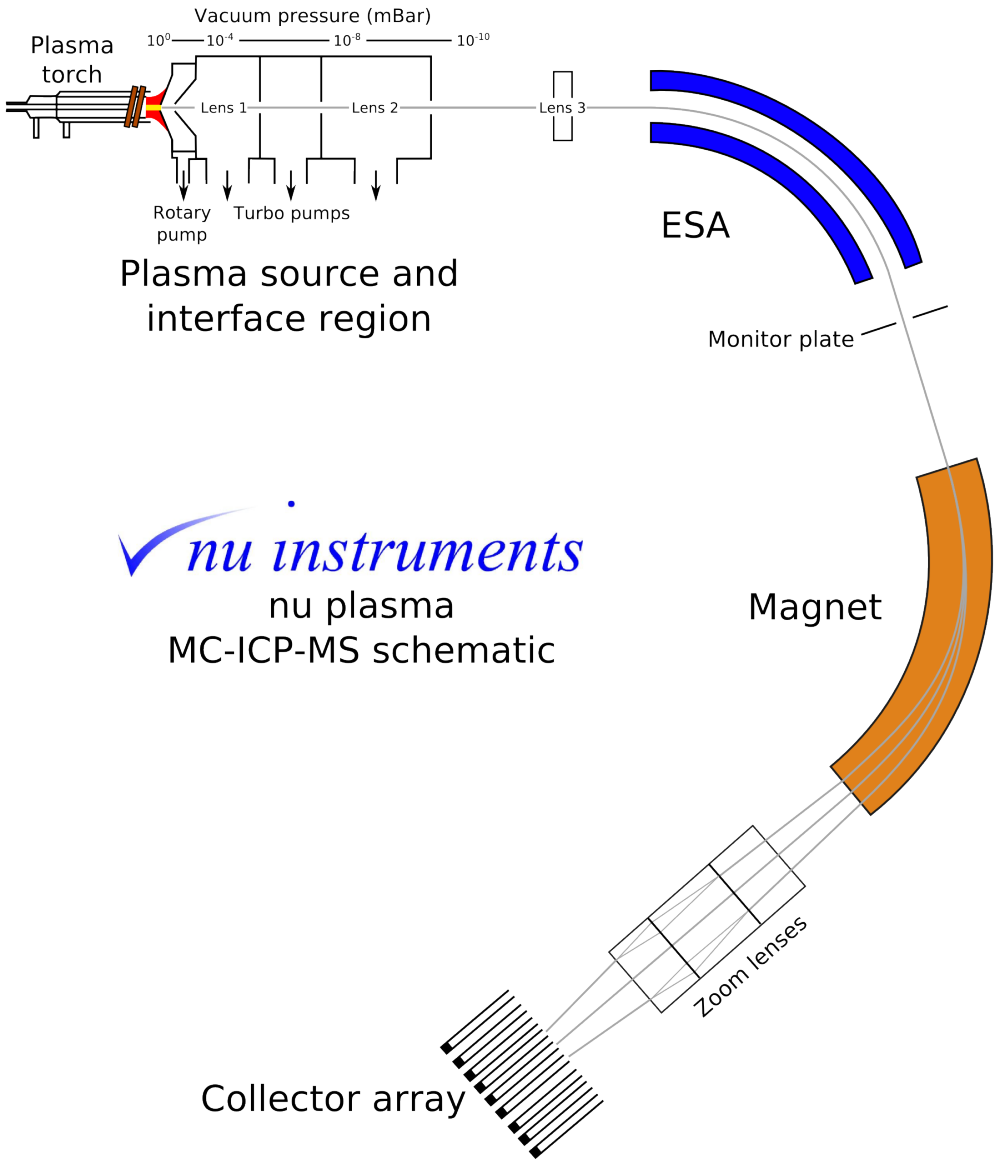


Figure 2.1. Schematic diagram of a Nu Instruments Nu Plasma MC-ICP-MS, showing the plasma source and interface region, mass analyser (ESA and magnet) and collector array.

2.5.2 Sample introduction

To be quantitatively ionised in the plasma, samples need to be introduced into the instrument in the form of a fine aerosol. This is achieved by using a nebuliser in conjunction with a spray chamber. Most nebulisers work by using a fast flow of argon (Ar) gas to create a low-pressure environment at the end of a narrow capillary tube. The sample is drawn up the capillary and converted to a fine aerosol when it reaches the low-pressure region. A number of 6mm microflow PFA nebulisers made by ESI and Savillex were utilised during this research. The uptake rate of the nebulisers can vary and, for Si isotope analysis, rates of between 60 and

80 μl min^{-1} provided the best balance between stability and signal strength.

Plasma stability is also affected by aerosol droplet size and size distribution. For efficient ionisation, a steady flow of fine aerosol particles with a narrow size distribution is ideal. To achieve this, a spray chamber is typically employed. In its simplest form, a spray chamber uses gravity separation to discriminate against larger droplet sizes – the geometry and gas flow strength in the chamber ensure only the fine droplets make it to the plasma, at a constant rate.

In the absence of further processing, the sample that enters the plasma from the spray chamber will be a mixture of analyte and solvent which, in the case of Si isotopic analysis, will be MQ-e water acidified with 1% HNO_3 (v/v). High solvent to analyte ratios have been found to reduce instrument sensitivity for a given analyte concentration and increase oxide formation in the plasma. Reducing oxide formation reduces polybaric interferences on the analyte masses; this is especially important to the analysis of Si, where $^{14}N^{16}O^+$ acts as a considerable interference on the ^{30}Si beam. We use a membrane desolvation device, the Cetac Aridus II, to achieve this; as such we are using a "dry" plasma. Without the Aridus, desolvation would occur during sample ionisation; this is called a "wet" plasma. In the Aridus II desolvator, a spray chamber made from PFA is housed within the device and is heated to 110°C. The heating step evaporates the solvent, which further reduces droplet size and separates the solvent from the analyte. Both analyte and solvent then pass along a heated (160°C), semi-permeable, hydrophobic PTFE membrane. The gaseous solvent can pass through the membrane and is removed by a flow of Ar gas (the sweep gas) whereas the analyte, in particulate form, stays within the membrane and continues on into the plasma. Sample desolvation can reduce the amount of solvent reaching the plasma by up to 99%. Note that Si isotopic analysis have been made successfully using a wet plasma, in conjunction with a Mg-doping technique (Zambardi and Poitrasson, 2011), the caveat being that larger quantities of sample are required to generate comparable sensitivities.

2.5.3 Sample ionisation and acceleration into the mass spectrometer

In the case of an MC-ICP-MS the sample ionisation takes place in an Ar plasma operating at temperatures over 5000 K. There are three key components to the generation of the plasma: the plasma torch, the radio frequency (RF) coil and the RF generator.

The plasma torch is usually made of quartz, and consists of three concentric tubes. Argon

gas, used to feed the plasma, passes between the outer and middle tube with a flow rate of ~ 15 $lmin^{-1}$. Another flow of Ar (~1 $lmin^{-1}$) between the middle and outer tubes controls the position of the plasma within the torch (the auxiliary gas). The central tube is used to inject the sample into the plasma. This is located so that the analyte stream will enter into the core of the plasma. The torch is mounted horizontally with the end inside the RF coil and 10-20 mm from the interface with the mass spectrometer. As a sample passes through different regions of the plasma it undergoes phase changes that convert it from droplets to ions. At the end of the torch the analyte enters the mass spectrometer through the sample interface.

In an attempt to keep Si blanks as low as possible, a semi-demountable sapphire sample injector was tested. However, comparisons with running Si with a regular fixed quartz torch did not show any large improvements in blank intensities. Furthermore, lighting the plasma was often troublesome with the demountable injector, so now a standard fixed torch is used.

To light the plasma, firstly the Ar gas flows are initialised, such that the Ar flows down the torch toward the RF coil and interface region. The RF generator supplies power (1300 W) and induces a high frequency (27 MHz) alternating current to the RF coil; this in turn generates a strong electromagnetic field at the end of the plasma torch. When a high voltage spark is applied to the plasma, electrons are stripped off the Ar gas. The free electrons are accelerated in the electromagnetic field induced by the RF-coil and collide with more Ar atoms which, in turn, strip off more free electrons. This cascading ionisation effect is known as an inductively coupled plasma discharge and will continue (i.e. the plasma will be maintained) as long as the RF coil is active. The ionisation energy of Ar atoms (15.8 eV) is high enough that most other elements will be ionised upon entering the plasma.

The interface region is designed to introduce the analyte ion beam into the mass analyser at a constant rate. Samples enter the instrument through apertures at the centre of two nickel cones, the “sampler” and “skimmer”. A negative pressure gradient between the end of the plasma torch (atmospheric) and the mass spectrometer (~ 10^{-9} bar; see Fig. 2.1.) acts to introduce the analyte through the interface region. Even so, around 99% of the material entering the plasma will not make it into the mass analyser. Once through the interface region, a potential difference between the interface and the back end of the mass spectrometer accelerates the ion beam. On the Nu Plasma HR-MC-ICP-MS a series of high voltage and electrostatic lenses focus the ion beam into the mass analyser; the first accelerating potential is held at 6 kV.

2.5.4 Mass analyser

The mass analyser is used to create the "mass spectrum" by splitting a single ion beam into discrete beams of separate masses. To achieve high precision isotopic measurements, a standard Nier-Johnson double-focusing magnetic sector mass analyser is employed on the Nu Plasma. This setup consists of an electromagnet and an electrostatic analyser (ESA) working in series, and can (in conjunction with additional hardware; see later) provide a mass resolving power of $m/\Delta m > 5000$ (where Δm is defined at 5% and 95% of peak height; Weyer and Schwieters, 2003). This is in contrast to quadrupole mass analysers that have a maximum resolving power of $m/\Delta m \sim 300$, and are more suited for multi-element analysis (in addition, a quadrupole setup does not allow for simultaneous multi-ionbeam detection, as it only permits one nominal mass to pass at any time).

Magnetic beam separation works as such: at constant magnetic field strength, the electromagnet imparts a force upon the ion beam, orthogonal to direction of travel, which causes the beam to curve in the magnetic field (a Lorentz force). The magnet is a momentum analyser, i.e. the amount of deflection of a single ion is proportional to the mass to charge ratio (m/z) and the kinetic engery (E_{kin}) of that ion. A heavier ion has more momentum and so will experience less force than a lighter one, so the beam of heavier ions will experience less deflection (it will have a wider curvature). Each ionic mass will travel along a discreet path so that, at the focal length of the mass spectrometer, a mass spectrum is created. The strength of the magnet can then be altered to direct the beam(s) of interest into the detector array.

However, this principle will only hold if the kinetic energy of the ions entering the magnet are the same. If two ions of equal m/z, one travelling faster than the other, enter the magnetic field, the faster ion will have more momentum and will travel along a wider trajectory than the slower ion, leading to an inaccurate mass spectrum. This is an inherent difficulty with using a plasma as an ion source; the plasma produces ions with a large spread of kinetic energies. To correct for this energy spread, an Electro-Static Analyser (ESA) is used in tandem with the electromagnet; hence a double-focusing mass spectrometer.

The ESA focuses ions in terms of their kinetic energies *only*, and is independent of the mass/charge ratio of an ion. Simply, it is a curved tube with two electrically charged plates with the inner plate negatively charged and the outer, positive. A carefully chosen set of magnet and ESA work as follows: the focusing of the magnet (ϑ_{MAG}) is dependent on mass/charge ratio

(m/z) and kinetic energy (E_{kin}) whereas focusing by ESA (ϑ_{ESA}) depends on only the kinetic energy. The ESA and magnet are chosen to have the exact same magnitude but opposite sense of energy focus. Simplistically, one might consider the following condition for the overall focusing through the ICP-MS ($\vartheta_{ICP\text{-}MS}$), so that

$$\vartheta_{ICP\text{-}MS} = \vartheta_{ESA} + \vartheta_{MAG}$$

Substituting $-E_{kin}$ for ϑ_{ESA} and E_{kin} + m/z for ϑ_{MAG} gives:

$$\vartheta_{ICP\text{-}MS} = -E_{kin} + E_{kin} + \text{m/z}$$

in which the term for kinetic energy cancels out so that $\vartheta_{ICP\text{-}MS}$ = m/z. The double-focusing system means that beams of identical m/z ratios and varying kinetic energies can be focussed into a single collector.

In a Nu Instruments Nu Plasma MC-ICP-MS the ESA is situated before the electromagnet, which is called forward geometry (Fig. 2.1.). Reverse geometry configurations (magnet before ESA), do also exist, but are only suitable for instruments with a single collector configuration and not for multiple collector arrays.

2.5.5 Detectors

The Nu Instruments Nu Plasma HR-MC-ICP-MS fixed collector array is fitted with two types of detectors: 12 Faraday cups and 3 discreet dynode electron multiplier ion counters.

Ion counters are designed to detect single ions and as such are very sensitive to low analyte concentrations; however, due to this sensitivity they saturate when the count rate reaches the 10^5 counts s^{-1} range. Faraday cups are more suited to higher analyte concentrations, but have an intrinsic noise that means that below a current of 3×10^{-16} A (comparable to a count rate of 10^4 counts s^{-1}) the detector becomes unusable. They are also limited to slow scan rates and as such are normally only used as detectors in multi-collector systems.

The Faraday cup is a thin bucket, at the base of which is an electrode held at ground potential and a low-noise resistor. When an ion beam impinges on the electrode it generates a negative current through the resistor to balance the positive charge of the ions, which increases

linearly with the strength of the ion beam (i.e. the concentration of the analyte). The flow of electrons generates a voltage that can be calibrated to give an isotope concentration. Typically, a 10^{11} Ω resistor is fitted to the Faraday cup, which will convert a typical current of 10^{-12} A to a measurable voltage of ~ 100 mV.

Because of the large mass difference between the three Si isotopes, Si isotope analysis requires almost the whole width of the detector array. On a standard Nu Plasma HR-MC-ICP-MS collector array, the Faraday cups used for Si isotope analysis are L5 (^{28}Si), H1 (^{29}Si) and H5 (^{30}Si) where H = heavy and L = light, centred around the axial cup (Ax).

2.5.6 High Resolution MC-ICP-MS

As has already been mentioned, the high ionisation potential of an Ar plasma means that most elements introduced to the plasma make it into the mass analyser. Although this is useful for elements with high ionisation potentials (such as Fe) it also means that sample matrix elements and solute material can act as polyatomic interferences on the masses of interest, thus affecting isotopic measurement.

Such procedures as quantitatively purifying the element of interest in the sample via ion chromatography, and the use of a desolvating membrane ("dry plasma") and collision cell technology have gone some way to reducing interferences, but elements in the sample medium or any Ar-based compounds are almost impossible to completely avoid. Accurate analysis of Si isotopes is not routine as each isotope of interest can be affected by such polyatomic interferences from SiH^+, CO^+, N_2^+ and NO^+. The least abundant isotope, ^{30}Si (~3% by mass), especially requires that the instrument be able to resolve the large interference generated by $^{14}N^{16}O^+$.

Despite being notionally similar in mass, polyatomic interferences are almost always slightly heavier than the isotope of interest. Therefore, with increasing mass resolution, that is, increasing the ability of the instrument to resolve two beams of increasingly smaller mass difference, such interferences can be resolved. With a fixed collector array at low resolution, the Nu Instruments Nu Plasma MC-ICP-MS has a mass resolution of about $m/\Delta m \sim 400$ (see above) which is not good enough to resolve the polyatomic interferences on the ^{30}Si isotope beam (see setup 'i' in Fig. 2.2a). Therefore, to accurately analyse Si isotopes, the instrument needs to be operating at a "medium-" or "high-resolution" mode.

One way of increasing the mass resolution of a MC-ICP-MS is to increase the geometry of the instrument. By doubling length of a flight tube, the separation of two beams can be essentially doubled. This has been successfully implemented in the Nu Instruments Nu1700. This machine has minimum mass resolution of $m/\Delta m \sim 1000$ (which is then further improved by altering the beam, see later).

Greater mass resolution can also be achieved by optically separating the beams. By narrowing a source slit before the mass analyser the beam can be narrowed enough that, at the focal plane of the mass spectrometer two previously interfering beams can be separated (Fig.2.2a). However, narrowing the beam reduces the sensitivity of the instrument so a compromise must be reached between mass resolution and sensitivity.

At this point a distinction should be made between so-called “pseudo” and “true” high resolution. At pseudo high resolution (also called “medium” resolution), narrowing the beam will completely resolve interferences at the focal plane. However, the orifice of the collector is wide enough that both beams enter the collector (setup 'ii' in Fig. 2.2a). In this case, a mass scan

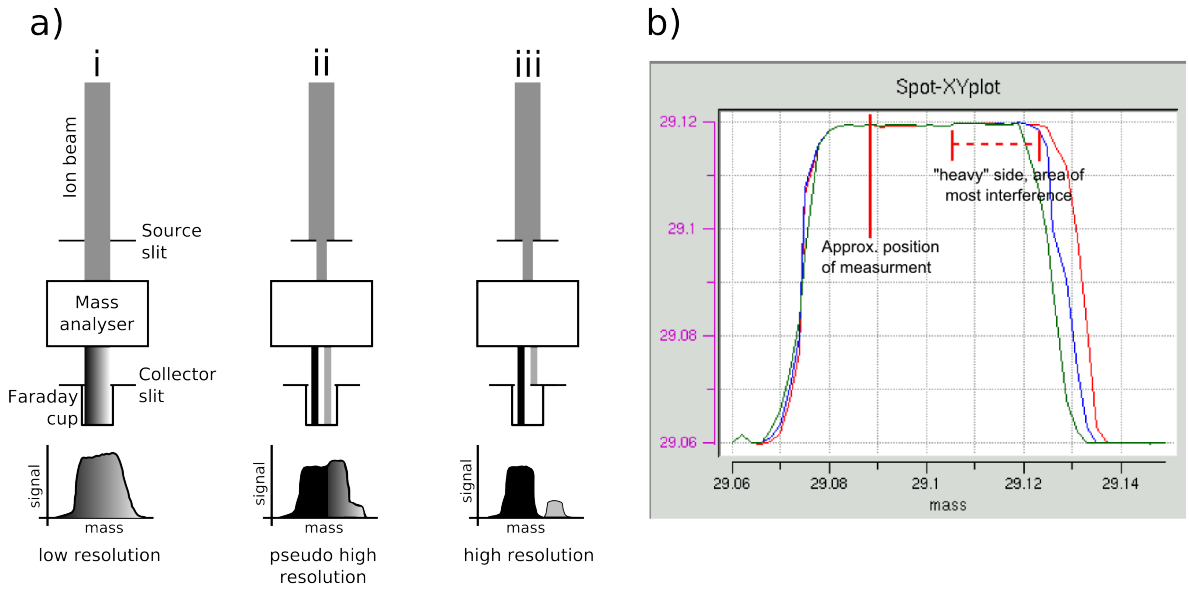


Figure 2.2. a) Schematic diagram of low, pseudo-high (medium) and “true” high mass resolution on a MC-ICP-MS instrument. In setup 'i', the analyte (black) and interference (grey) beams are too wide to be resolved by the mass analyser and so the collector detects one beam, with poor peak flatness. In setup 'ii' the source slit is narrowed so two separate beams exit the mass analyser and enter the collector. Because both beams can enter the collector entrance, a mass scan shows the two peaks overlapping,with two plateaus. The instrument can then be set to make isotopic measurements on the analyte plateau. In setup 'iii', the collector slit is closed to cut out the interference beam and a mass scan displays two separate peaks; this is “true” high resolution. b) Typical “psuedo-high” resolution mass scan from the Nu Instruments Nu Plasma HR-MC-ICP-MS at Oxford, showing the two plateaus and position of interference. Based on a figure from Georg (2006).

over the beam will reveal three plateaus. From low to high mass the first plateau will be the lighter beam, normally the isotope of interest; the second plateau will be combination of the analyte beam and the interference beam; the third plateau, normally much less intense than the first and second, is interference beam (Fig. 2.2a). In this case the instrument can be set to take measurements from the first plateau, which should be free of interference. Silicon isotope analysis on the Nu Plasma HR at Oxford is made at medium resolution ($m/\Delta m \sim 3500$); a typical Si mass scan showing position of measurement and interference peak are shown in Figure 2.2b.

True high resolution requires even further alteration of the beam. The most common way to accomplish this is to prevent the interference beam from entering the detector at the focal plane. Slits on the collector orifices can be closed towards the heavy mass side, making the entrance to the detector smaller. This prevents the inference from entering the cup at the same time as the isotope of interest. Such a scenario is shown in Figure 2.2a (setup 'iii'). True high resolution is only accomplished when the the collector entrance is narrower than the distance between adjacent beams, and so a mass scan displays these beams as two separate peaks.

Today most multi-collector mass spectrometer operators strive to achieve flat-topped peaks; these are only attained when an ion beam is narrower than the collector entrance. This means that all of the analyte isotope is being detected, so isotopic measurements are more robust. Because the mass spectrometer is measuring multiple beams, it must be arranged so that all masses of interest enter the collectors at the same position. To accomplish this, a series of quadrupole “zoom” lenses act on all the beams to align the peaks (see Fig. 2.1.). On a mass scan all the peaks should be superimposed on one another (e.g. Fig 2.2b).

2.5.7 Running silicon sotopes on a Nu Plasma HR-MC-ICP-MS

A typical sample run consists of 2 external standards, 4-6 samples and the bracketing standard, all of which have undergone identical chemical preparation. The external standards are used to assess data accuracy as other correction techniques are not applicable to Si isotopes (see above).

Running the instrument at medium resolution for Si isotope analysis requires narrowing the beam width from 0.3 mm to 0.05 mm, and closing the “Alpha” slits (to correct for beam aberrations), which reduces the sensitivity by ~ 85%. At standard operating conditions, sample

concentrations of 750 ppb Si yield a typical beam intensity of ~ 1 x 10^{-10}A.

Isotope measurements are calculated using the standard-sample-standard protocol to correct for instrumental mass bias, using NBS28 silica sand as the bracketing standard. Instrument background is measured at the beginning of each analysis by deflecting the ESA for 20 s. Typical background intensity for Si is in the order of ~ 2 x 10^{-13} A, giving a signal to background ratio of ~ 500 using 10^{11} Ω resistors. Each isotope measurement consists of between 6-8 sample analyses resulting in an average of 11-15 values. Each analysis is comprised of 20-25 cycles, with each cycle being integrated for 8s. Variations in Si isotopes are reported by the delta notation as δ^{30}Si or δ^{29}Si, defined in this study as the deviation in per mil (‰) of a sample's ratio of ^{x}Si/^{28}Si from the standard (NBS28), as defined in Chapter 1.

2.6 IN-SITU SILICON ISOTOPE ANALYSIS

Analysis of Si isotopes is also possible using in-situ techniques. The first studies utilised Secondary Ion Mass Spectrometry (SIMS; Alexandre et al., 1997; Robert and Chaussidon, 2006; Heck et al., 2011), but more recently Laser Ablation-MC-ICP-MS has been applied to Si isotope analysis (Shahar and Young, 2007; Chmeleff et al., 2008; Ziegler et al, 2010; Steinhoefel et al., 2011). An advantage of using such techniques is that they allow investigation of Si isotope variations at high spatial resolution, for instance in finely laminated siliceous sediments such as cherts (Robert and Chaussidon, 2006) or banded iron formations (Steinhoefel et al., 2009; Heck et al., 2011). They also provide a means of analysing small disseminated phases such as metal and silicate phases in enstatite meteorites (Ziegler et al., 2010). In all these cases, the degree of Si isotopic fractionation under analysis is relatively large (variations greater than 0.50 ‰). The drawback with both SIMS and LA-MC-ICP-MS methods is that their associated precisions have generally been too poor (± 0.20 to 0.30 ‰; 2 s.d.) to investigate the small, sub per mil variations that are present in high temperature systems. As such, in the following research, they were overlooked in favour of solution MC-ICP-MS as described above. However, recent improvements in laser technology has increased precision on Si isotopic measurements, which are now approaching those attainable by solution MC-ICP-MS (Schuessler and von Blanckenburg, 2011).

Chapter 3: The silicon isotopic composition of the Bulk Silicate Earth

Published as

Silicon isotope homogeneity in the mantle

P.S. Savage, R.B. Georg, R.M.G. Armytage, H.M. Williams, A.N. Halliday

2010 *Earth and Planetary Science Letters*, **295**, 139-146

ABSTRACT

Thirty-five mafic and ultramafic rocks have been analysed for their silicon isotopic composition to very high precision with the aim of providing a robust average value for the silicate earth. This is of importance to studies using the difference between meteorite and terrestrial isotope composition to quantify silicon sequestration during core formation and, also, for understanding crustal processes. The δ^{30}Si values of the samples are more limited than previously reported, ranging between just −0.39 and −0.23 ‰ despite significant variations in chemical and other isotopic compositions. A hint of a trend exists between δ^{30}Si and both SiO_2 and Al_2O_3, which can be explained by concentration of the heavier isotopes in the melt as a function of silica polymerisation. Our best estimate for the δ^{30}Si of the bulk silicate earth (BSE) is −0.29 ± 0.08 ‰ (2 s.d.).

3.1 INTRODUCTION

Silicon (Si) is the third most abundant element on Earth and has three stable isotopes, ^{28}Si, ^{29}Si and ^{30}Si. Despite its abundance and geological importance in diverse geochemical reservoirs, isotopic fractionation in the terrestrial realm is limited because silicon has one valence state (Si^{4+}) and does not form volatile compounds readily. Since the early 1950s there has been a limited amount of research into Si isotopes (e.g. Reynolds and Verhoogen, 1953; Allenby, 1954; Epstein and Taylor, 1970; Molini-Velsko et al., 1986; Douthitt, 1982; Ding et al., 1996). These early studies utilised gas-source mass spectrometry (GS-MS) and were insufficiently precise to reliably resolve any small (sub per mil) variations. This was not a problem for low temperature geochemistry because relatively substantial Si isotopic fractionation takes place during formation of clays during chemical weathering (Ziegler et al., 2005a,b; Georg et al., 2006a, 2009a; Delstanche et al., 2009), silcrete from groundwater (Basile-Doelsch et al., 2005; van den Boorn et al., 2007), diatoms and other silica-utilising organisms (e.g. De La Rocha et al., 1998) and banded iron formations (André et al., 2006). However, the smaller isotopic variations that must be present at some level in high temperature processes are only just being explored. The advent of multiple collector inductively coupled plasma mass spectrometry (MC-ICPMS) together with novel sample digestion and purification techniques has improved precision and sensitivity greatly, allowing the possible resolution of differences between reservoirs that, in the past, would have been considered identical.

Georg et al. (2007) used such methods to demonstrate that the Si isotope composition of meteorites was isotopically different to that of bulk silicate earth (BSE). The authors proposed that this difference was best explained by Si isotope fractionation during core formation. The high Mg/Si of the BSE has been explained by loss of a significant amount of Si early in Earth history (e.g. Jagoutz et al., 1979; Ringwood, 1989); a common explanation is that Si was sequestered into the metal phase during core segregation (Allègre et al., 1995; Wade and Wood, 2005).

More recently, Fitoussi et al. (2009), Armytage et al. (2009), and Zambardi et al. (2009) have presented studies on Si isotopes in extraterrestrial rocks confirming that there does indeed exist a resolvable difference between meteorites and the BSE, as proposed by Georg et al. (2007). This is a major step forward in our understanding of the composition of the Earth's core, and also the conditions of the early mantle during core accretion. However, the exact magnitude of the difference ($\Delta^{30}Si_{core-mantle}$) is unclear because it is close to the analytical reproducibility (in the range of 0.1–0.2 ‰). It is critical to determine the composition of the BSE and chondrites more precisely in order to model this difference effectively and use it to constrain the conditions under which the core formed.

This paper is focused on determining an accurate Si isotopic composition for the BSE. Douthitt (1982) gives a mean for the BSE of $\delta^{30}Si \sim -0.4 \pm 0.2$‰ (2 s.d.) based on mafic and ultramafic rocks. Georg et al. (2007) give a more precise value of $\delta^{30}Si = -0.38 \pm 0.12$ ‰ (2 s.d.), based on 3 mid-ocean ridge basalts, 5 ocean island basalts and 4 ultramafic mineral separates. Although the averages are similar, the individual MORB and OIB data in Georg et al. (2007) show some scatter that could be real or could be an analytical artefact induced by, for instance, sample solution instability. Differences also exist between the published data for the USGS Hawaiian BHVO standards (Abraham et al., 2008) and other Hawaiian basalts analysed by Ziegler et al. (2005a). More recently, Fitoussi et al. (2009) analysed nine mafic and ultramafic samples and calculated an average for BSE of $\delta^{30}Si = -0.28 \pm 0.06$ ‰ (2 s.d.). Other recent estimates (e.g. Zambardi et al., 2009) support this value. This is ~0.1 ‰ heavier than, although within error of, the earlier studies of Douthitt (1982) and Georg et al. (2007).

This study aims to determine a more precise and reliable value. We also aim to investigate whether some of the lighter data reported by Georg et al. (2007) are (a) caused by real isotopic variation in the mantle not captured by other studies or (b) reflect inaccuracies in

the data leading to a shift to a lighter average reported by Georg et al. (2007).

Considering the limited high temperature isotopic fractionation and large budget of the mantle Si reservoir it might seem unlikely that there could exist any significant isotopic variability, particularly given the long history of convective mixing. Nevertheless, a recent study has proposed that reflectors in the deep mantle may be the remnants of ancient subducted banded iron formations (Dobson and Brodholt, 2005). Such rocks are extremely fractionated in Si isotopic composition with δ^{30}Si ranging from −2.80 ‰ to +0.68 ‰ (André et al., 2006). Large scale preservation of these domains in the deep mantle could, in principle, have a small effect on Si isotope homogeneity.

In this paper we report Si isotope data for 35 mafic and ultramafic rocks to provide an accurate value for the silicon isotope composition of BSE. By analysing a large number of already well-characterised samples we also hope to assess the possibility that there is some heterogeneity in the mantle and, if so, what this stems from.

3.2 SAMPLES

We analysed 35 samples sourced globally (see Table 3.2 for locations) with compositions ranging from ultramafic to basaltic andesite. Brief descriptions of each sample group are given below.

3.2.1 Standards

Over the course of the study we routinely analysed a number of silicon standards to assess external reproducibility. These include the Diatomite and IRMM018 standards, already well-characterised for Si isotopes in an inter-laboratory study by Reynolds et al. (2007). We also analysed 3 basaltic standards, BHVO-1, BHVO-2 and BCR-1, as these are more representative of the elemental matrix of our samples; we have also used these data in our overall value for the BSE. The Si isotopic compositions of the BHVO standards were published by Abraham et al. (2008) and they are becoming widely-used as Si isotope external standards (i.e. Georg et al., 2009a).

3.2.2 Ultramafic rocks

Eleven ultramafic xenoliths were analysed, representing a range of compositions,

geographical localities and ages (rock types are listed in Table 2). These comprise 5 samples from the East African Rift (Dawson et al., 1970; Paslick et al., 1995), 1 sample from the Cameroon Line (Lee et al., 1996), 3 samples from Kohistan (Williams et al., 2005) and 2 regularly used ultramafic standards from the USA, San Carlos Bulk and Kilbourne Hole.

3.2.3 Mid-Ocean Ridge Basalts (MORB)

Ultramafic rocks are subject to the possibility of being unrepresentative. For this reason we analysed several MORBs as these are formed by relatively large degrees of partial melting and sample large volumes of the upper mantle. Also, there is the possibility of melt-induced isotopic fractionation to consider. To assess any bias in Si isotope composition as a result of mantle heterogeneities, our 18 samples were taken from the Atlantic (Langmuir et al., 1993), the East Pacific Rise (Batiza and Niu, 1992; Reynolds et al., 1992), the Indian Ocean (Hamelin and Allègre, 1985; Schiano et al., 1997) and the Australian–Antarctic Discontinuity (AAD, Klein et al., 1991). All samples were already well characterised for major and trace elements.

3.2.4 Island-Arc Basalts (IAB)

Given that some arc basalts show the geochemical effects of input from a sedimentary source, we analysed 3 samples from the Marianas arc. Compared to mantle rocks, sedimentary material is more likely to exhibit a relatively extreme isotopic signature (i.e. Ziegler et al., 2005a,b) and its incorporation into sub-arc mantle could alter the isotopic composition of subsequent eruption products. The Marianas arc is ideally suited, as the geochemical composition of the eruptive products varies along the arc, from sediment-dominated to fluid-dominated (Elliott et al., 1997). One basalt and two basaltic andesites were taken from both geochemical “ends” and from the “middle” of the arc, to reflect a range of putative sedimentary contamination.

In addition, we analysed a basalt from the South Sandwich arc. The predominant rock type being subducted there is siliceous ooze (Plank and Langmuir, 1998), which can accumulate from material that has relatively extreme isotopic values of between -3.70 ‰ $< \delta^{30}Si < +2.60$ ‰ (Douthitt, 1982; De La Rocha et al., 1998; Varela et al., 2004). Depending on the exact composition, incorporation of > 5% of subducted sediment could significantly alter the Si isotopic composition of the sub-arc mantle.

3.3 METHODS

The sample material was received either as glass chips, a crushate or as pre-crushed powder. Glass chips and crushate were powdered under ethanol in an alumina pestle and mortar. Some of the samples received as powders were processed in agate mills; although this is a possible source of silica contamination, even if the powder contained 5% agate after milling, this would only shift the $\delta^{30}Si$ by ~0.015 ‰, an inconsequential amount even at this high precision.

3.3.1 Fusion

Samples were dissolved using the HF-free alkali fusion technique described by Georg et al. (2006b). Between 10 and 20 mg of sample powder was measured into a silver crucible, into which ~250 mg of flux (analytical grade NaOH in pellet form) was added. After heating in a muffle furnace for 12 min, the resultant fusion cake was then transferred into solution and acidified with HNO_3.

The samples were purified before mass spectrometry using a single column pass through BioRad columns filled with 1.8 ml of DOWEX 50W-X12 (200–400 mesh) cation exchange resin. Under acidic pH conditions, Si in solution is in the form of non-ionic monosilicic acid $Si(OH)_4$ or the anionic species $H_3SiO_4^-$ and so will not be retained by the resin.

3.3.2 Mass spectrometry

Silicon isotope compositions were determined using a Nu Plasma HR-MC-ICP-MS (Nu Instruments, Wrexham, UK) at the Department of Earth Sciences, University of Oxford during 2008–2009; this instrumentation is described further by Georg et al. (2006b). This machine is capable of operating at a pseudo-high ("medium") resolution mode ($M/\Delta M \sim 3500$, where ΔM is measured at 5% and 95% of peak height), which allows us to avoid all polyatomic interferences on the silicon isotope ion beams. Samples were introduced into the mass spectrometer using a 6 mm concentric micro-flow PFA nebuliser (ESI) with an uptake rate of ~75 μl min^{-1}. Samples were de-solvated in a Cetac Aridus II and introduced to the plasma by means of a semi-demountable sapphire injector (ESI). Setting the machine to medium resolution requires narrowing the source slit from 0.3 to 0.05 mm and also closing the alpha slits to correct for beam aberrations. This reduced sensitivity by ~85–90% and, at concentrations of 750 ppb Si, a

total Si beam intensity of $\sim 1\times10^{-10}$ A was typical. Samples were corrected for instrumental mass bias using a standard-sample-standard bracketing protocol, using NBS28 silica sand as the standard. Instrument background was measured by deflecting the ESA for 20 s; typical background intensity was $\sim 2\times10^{-13}$ A, which corresponds to a signal to background ratio of $\sim$500, using 10^{11} Ω resistors. Each sample was run 8–12 times, depending on the uptake rate; each run consisted of 20 cycles and each cycle was integrated for 8 s.

Variations in Si isotopes are represented by the delta notation as $\delta^{30}Si$ or $\delta^{29}Si$, defined in this study as the deviation in per mil (‰) of a sample's ratio of $^{x}Si/^{28}Si$ from the international standard NBS28:

$$\delta^{30}Si = [\ (^{30}Si/^{28}Si_{sample})/(^{30}Si/^{28}Si_{standard}) - 1\ ] \times 1000;$$

$$\delta^{29}Si = [\ (^{29}Si/^{28}Si_{sample})/(^{29}Si/^{28}Si_{standard}) - 1\ ] \times 1000.$$

3.4 RESULTS

3.4.1 Data accuracy and reproducibility

The data for the external Si standards Diatomite, IRMM018, BHVO-1 and BHVO-2 facilitate an assessment of data accuracy and reproducibility (Table 3.1, Fig. 3.1). Our values of $\delta^{30}Si = 1.26 \pm 0.08$ ‰ for Diatomite, $\delta^{30}Si = -1.61 \pm 0.11$ ‰ for IRMM018 and $\delta^{30}Si = -0.27 \pm 0.10$ ‰ for BHVO (all errors are 2 s.d.) all agree well with the literature data (Reynolds et al., 2007; Abraham et al., 2008). These standards were analysed alongside samples over a period of about 12 months; Figure 3.1 shows the data for each standard arranged in chronological order. Any data associated with poorly replicated external standards were discarded. We used two Nu-Plasma HR mass spectrometers to collect our data; the averages for the standards are based on runs from both machines and there are no systematic differences in the standard data between instruments.

Our averages for BHVO-1 and BHVO-2 are identical and in agreement with the values quoted by Abraham et al. (2008), van den Boorn et al. (2009), Georg et al. (2009a), Zambardi et al. (2009) and Fitoussi et al. (2009). These standards are “matrix-matched” in that they both are basaltic and therefore their chemical composition is similar to that of our samples. The reproducibility of these standard data provides evidence that there are no matrix effects compromising the accuracy of the method.

Table 3.1 – External standard data

Sample		δ^{30}Si (‰)	2 s.d. *(2 s.e.)*	δ^{29}Si (‰)	2 s.d. *(2 s.e.)*	*n*
Pure silicate standards						
NBS28	This study	− 0.01	0.03	0.01	0.03	26
Diatomite	This study	1.25	0.08	0.65	0.05	229
	Reynolds et al. (2007)	1.26	0.20	0.64	0.14	
IRMM018	This study	− 1.61	0.11	− 0.82	0.07	90
	Reynolds et al. (2007)	− 1.65	0.22	− 0.85	0.14	
Big Batch	This study	− 10.65	0.32	− 5.47	0.10	11
	Reynolds et al. (2007)	− 10.48	0.54	− 5.35	0.30	
Basaltic standards						
BHVO-1	This study	− 0.27	0.09	− 0.15	0.04	192
	Abraham et al. (2008)	− 0.33	0.05	− 0.17	0.03	
BHVO-2	This study	− 0.27	0.10	− 0.14	0.05	59
	Abraham et al. (2008)	− 0.29	0.11	− 0.17	0.04	
	van den Boorn et al. (2009)	− 0.27	0.22	–	–	
	Zambardi et al. (2009)	− 0.27	0.08	–	–	
BCR-1	This study	− 0.28	*0.07*	− 0.13	*0.03*	14

This average standard data is taken from repeat analysis of the standard over a period of ~12 months. For Diatomite, BHVO-1 and BHVO-2 separate cuts were analysed over the year to detect any inhomogeneity or chemistry-induced bias. All standards were run at "medium" resolution on a Nu Plasma high resolution-multi collector-ICP-MS in Oxford. The number of measurements (n) denotes the number of times a sample was analysed, although the 2 s.d. is based on an average of the different aliquots of the sample (each aliquot n~14).

3.4.2 Sample data

Sample data are given in Table 3.2 and Figure 3.2. All errors in the table are 2 standard deviations (2 s.d.) unless in italic; these values are twice the standard error of the mean (2 s.e.), and are given if only one aliquot of the sample was analysed. All the data fall on or near to the mass-dependent terrestrial fractionation lines describing either kinetic or equilibrium fractionation (Fig. 3.2), which are indistinguishable at such low degrees of fractionation.

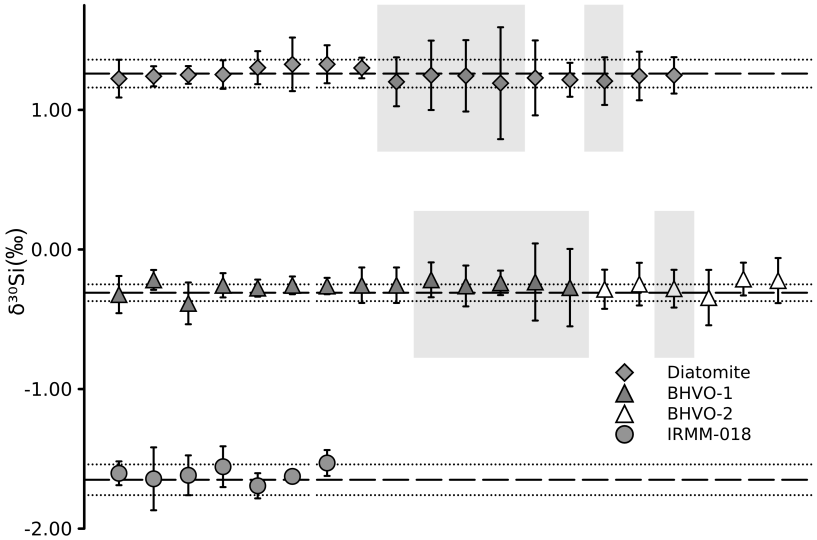


Fig. 3.1 Sample reproducibility over the course of sample analysis, data points are plotted in chronological order. Dashed lines indicate the published value for the standards and dotted lines indicate the associated error; published values and references are as follows: Diatomite δ^{30}Si = 1.26 ± 0.10 ‰ (1 s.d.) (Reynolds et al., 2007); BHVO δ^{30}Si = −0.31 ± 0.06 ‰ (2 s.e.) (Abraham et al., 2008); and IRMM-018 δ^{30}Si = −1.65 ± 0.11 ‰ (1 s.d.) (Reynolds et al., 2007). Grey boxes indicate those data collected on a separate Nu Plasma MC-ICP-MS.

Table 3.2 – Silicon isotope data for mafic and ultramafic samples

Sample		δ^{30}Si (‰)	2 s.d. *(2 s.e.)*	δ^{29}Si (‰)	2 s.d. *(2 s.e.)*	*n*	SiO2 (wt.%)	NBO/T	Latitude	Longitude
Basaltic standards										
BHVO-1	Basalt	−0.27	0.09	−0.15	0.04	192	49.9	1.046	19.4081°N,	155.2826°W
BHVO-2	Basalt	−0.27	0.10	−0.14	0.05	59	49.9	1.046	19.4081°N,	155.2826°W
BCR-1	Basalt	−0.28	*0.07*	−0.13	*0.03*	14	54.1	0.726	45.5523°N,	122.1918°W
Mid-ocean ridge basalt glasses										
Atlantic										
D1-5	Basalt	−0.30	0.09	−0.16	0.04	25	50.3	1.054	33.1738°N,	39.2478°W
D5-5	Basalt	−0.24	0.01	−0.12	0.03	28	49.6	1.053	33.1738°N,	37.7117°W
D15-1	Basalt	−0.26	0.05	−0.13	0.02	28	51.4	1.009	33.1738°N,	32.2825°W
D22-5	Basalt	−0.23	0.07	−0.13	0.06	41	51.9	0.840	33.1738°N,	30.025°W
D26-5	Basalt	−0.27	0.03	−0.13	0.01	25	51.4	0.989	33.1738°N,	29.6722°W
D27-5	Basalt	−0.29	*0.05*	−0.16	*0.02*	14	51.5	0.970	33.1738°N,	29.7378°W
Group average		−0.27	0.06	−0.14	0.04			0.985		
Pacific										
R82-1	Basalt	−0.25	0.02	−0.12	0.06	26	49.3	1.062	11.505°N,	103.603°W
R94-2	Basalt	−0.25	0.02	−0.13	0.03	28	51.0	1.009	12.34°N,	103.715°W
VE23-5	Basalt	−0.33	0.04	−0.17	0.04	26	49.4	0.925	12.0678°N,	103.7833°W
VE32-3	Basalt	−0.25	*0.03*	−0.15	*0.02*	14	51.1	0.938	15.52°N,	105.38°W
Group average		−0.27	0.07	−0.14	0.05			0.983		
Indian										
MD57 D13-7	Basalt	−0.28	0.02	−0.14	0.01	24	51.1	0.957	1.47°S,	67.64°E
MD34 D4	Basalt	−0.30	0.07	−0.18	0.06	26	49.4	0.955	40.98°S,	43.7°E
MD57 D10-4	Basalt	−0.30	*0.02*	−0.15	*0.01*	15	51.9	0.970	6.22°S,	68.25°E
MD34 D6	Basalt	−0.24	*0.03*	−0.12	*0.01*	15	50.8	0.974	44.18°S,	38.795°E
MD57 D10-1	Basalt	−0.28	*0.03*	−0.14	*0.02*	13	50.7	0.932	6.22°S,	68.25°E
Group average		−0.28	0.05	−0.15	0.04			0.958		
Australian–Antarctic discontinuity										
D04-54	Basalt	−0.23	*0.05*	−0.13	*0.02*	15	49.7	1.090	50.215°S,	137.555°E
D10-10	Basalt	−0.28	*0.04*	−0.14	*0.02*	14	50.9	0.988	49.917°S,	115.375°E
Group average		−0.25	0.08	−0.14	0.01			1.039		
MORB	average	−0.27	0.06	−0.14	0.04					
Island arc glasses										
Marianas										
URA6	Basaltic andesite	−0.25	*0.03*	−0.13	*0.02*	80	59.9	0.253	20.54°N,	145.87°E
GUG13	Basalt	−0.27	*0.04*	−0.14	*0.02*	51	51.8	0.219	17.32°N,	145.84°N
ALAM5	Basaltic andesite	−0.32	*0.05*	−0.16	*0.02*	64	53.4	0.379	17.59°N,	145.83°N
Group average		−0.28	0.07	−0.15	0.03					
South Sandwich										
SS15.1	Basalt	−0.28	*0.05*	−0.15	*0.05*	15	53.7	0.749	*59.0471°S,*	*26.5699°W*
IAB average		−0.28	0.06	−0.15	0.02					
Ultramafic xenoliths										
Kilbourne Hole	Spinel peridotite	−0.29	0.08	−0.13	0.04	42	44.5	4.175	*32.00°N,*	*107.00°W*
San Carlos	Spinel lherzolite	−0.31	0.07	−0.16	0.06	129	45.6	3.829	*33.37°N,*	*110.48°W*
Group average		−0.30	0.04	−0.15	0.04					
Cameroon Line										
C235A	Spinel lherzolite	−0.29	0.14	−0.16	0.05	40	43.2	4.211	*4.2067°N,*	*9.1689°E*
East African Rift										
H93 X1	Garnet lherzolite	−0.33	0.06	−0.17	0.04	34	43.3		4.5692°S,	35.4339°E
H93 X8	Spinel lherzolite	−0.35	0.06	−0.17	0.03	16	43.3		4.5692°S,	35.4339°E
BD730	Garnet lherzolite	−0.34	0.16	−0.18	0.08	48	44.4	4.499	*3.3667°S,*	*36.4333°E*
BD744	Alkali pyroxenite	−0.30	*0.07*	−0.16	*0.04*	14	44.0		*3.3667°S,*	*36.4333°E*
BD1542	Chromite harz.	−0.37	*0.05*	−0.20	*0.03*	12	40.0		*3.3667°S,*	*36.4333°E*
Group average		−0.34	0.05	−0.18	0.03					
Kohistan										
J25	Garnet pyroxenite	−0.29	0.06	−0.16	0.06	30	44.5	1.837	35.0736°N,	72.9569°E
J27	Websterite	−0.39	0.10	−0.21	0.02	29	49.1	3.347	35.0947°N,	72.9158°E
J30	Dunite	−0.39	0.11	−0.21	0.03	30	36.8	5.890	35.0817°N,	72.9211°E
Group average		−0.35	0.12	−0.19	0.06					
Ultramafic average		−0.33	0.08	−0.17	0.05					
BSE average		−0.29	0.08	−0.15	0.05	35				

The $\delta^{30}Si$ of the sample data ranges from −0.39 to −0.23 ‰. The average Si isotope composition of the three geological settings analysed in this study are strikingly similar to each other, viz. $\delta^{30}Si_{MORB} = -0.27 \pm 0.06$ ‰, $\delta^{30}Si_{IAB} = -0.28 \pm 0.06$ ‰ and $\delta^{30}Si_{ultramafic} = -0.33 \pm 0.08$ ‰ (2 s.d.). There are no significant differences in Si isotope composition between magmatic or geographical settings and the range of values is small, only 0.16‰. There are no significant correlations ($R^2 > 0.5$) between $\delta^{30}Si$ and any other element or isotopic system (i.e. SiO_2, MgO, $^{208}Pb/^{204}Pb$, $^{206}Pb/^{204}Pb$, $^{87}Sr/^{86}Sr$). The $\delta^{30}Si$ average of all the samples is −0.29 ± 0.08 ‰ (2 s.d.).

3.5 DISCUSSION

3.5.1 The bulk composition of the BSE

When choosing samples for this study, we avoided the use of evolved crustal material as this has been shown to have a heavier $\delta^{30}Si$ when compared to mafic and ultramafic rocks (see Douthitt, 1982; Ding et al., 1996), which could be due to a combination of endogenous and surficial processes. It could then be argued that we should have limited our sample set to ultramafic samples only; however, this paper is concerned with variations in the mantle and so a large suite of mantle-derived rocks is critical to answering that question. Given the limited range of values found in this study, BSE averages calculated using a) only the ultramafic samples, b) all our samples and c) a weighted average (by mass) do not give statistically different results. Those values are a) $\delta^{30}Si_{ultramafic} = -0.33 \pm 0.08$ ‰; b) $\delta^{30}Si_{all} = -0.29 \pm 0.08$ ‰; c) $\delta^{30}Si_{weighted} = -0.33 \pm 0.08$ ‰ (all 2 s.d.). We would recommend using the value calculated for $\delta^{30}Si_{all}$ because it is not clear how representative the ultramafic samples, i.e. some samples do not represent equilibrium melt assemblages, and there may be a component of metamorphism or metasomatism to take into account. In any case, all three values are statistically indistinguishable.

The results reported here are consistent with previous work, which show that mafic and

Table 3.2 (previous page) All sample data from this study, analysed at "medium" resolution on a Nu Plasma HR MC-ICP-MS in Oxford. The aim was to run more than one aliquot of each sample; in this case the errors published are 2 s.d. If only one aliquot was successfully analysed the errors given are 2 standard error of the mean; those numbers are in italics. Si isotope data is plotted in Fig. 3.2, see text for more details. The NBO/T values were calculated using the theory given in Mysen (1983) and using the assumption that all Fe_2O_3 is in VI-fold co-ordination, which will overestimate (in most cases) the final NBO/T value. However, this assumption does not affect the general trend, and the relationship still exists if we assume the opposite, i.e. complete IV-fold co-ordination for Fe_2O_3. Sample localities are given as co-ordinates; those in italics are estimates based on the locality name and are not exact.

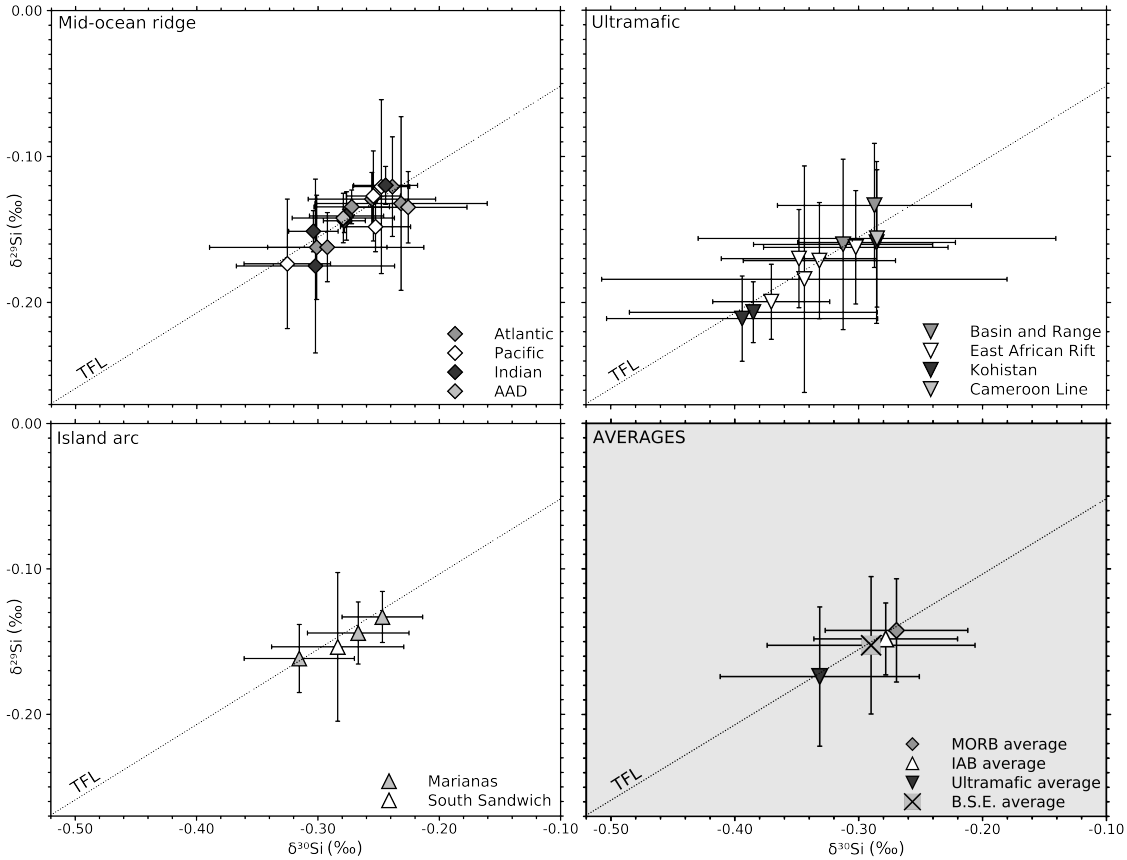


Fig. 3.2 3-isotope plots showing all the data from this study. The dotted line in each graph plots along the equilibrium terrestrial fractionation line (TFL, slope=0.5178); the kinetic fractionation line is almost identical in the range plotted and for clarity the line is omitted. Error bars are predominately 2 standard deviations, but may be 2 standard error of the mean if only one aliquot was analysed; Table 2 gives more detail. In each graph the data cluster about one point and there is no detectable fractionation outside of analytical error. The averages of each group are plotted the bottom right graph, again there are no detectable heterogeneities outside analytical error; however the ultramafic average still plots slightly lighter than the two basaltic averages; see text for discussion. The average for all data in this study $\delta^{30}Si = -0.29 \pm 0.08$ ‰ (2 s.d.), i.e. the bulk silicate earth average, is also plotted.

ultramafic rocks have Si isotope compositions in the range $\delta^{30}Si = -0.5$ to -0.2‰ (Douthitt, 1982; Ding et al., 1996; Ziegler et al., 2005a; Georg et al., 2007). Our data also agree well with the study of Fitoussi et al. (2009), who give a more restricted value for BSE of $\delta^{30}Si_{BSE} = -0.28 \pm 0.06$ ‰ (2 s.d.), albeit on the basis of fewer samples. Our data are also consistent with other recent studies (e.g. Armytage et al., 2009; Zambardi et al., 2009), which all suggest that the $\delta^{30}Si_{BSE}$ value is close to −0.3 ‰.

When considering those earlier studies, the range of data can be explained by the method and associated precision; both Douthitt (1982) and Ding et al. (1996) had errors of up to ± 0.3 ‰ (2 s.d.). However, the ~ 0.1 ‰ offset between our average for BSE and that given in Georg et al. (2007) is less easy to explain, considering we used essentially the same methods and similar instrumentation. For instance, the data for MORB given by Georg et al. (2007) are

noticeably lighter ($\delta^{30}Si$ = −0.51 to −0.35 ‰) than ours ($\delta^{30}Si$ = −0.33 to −0.23 ‰), the possible reasons for which are assessed below.

3.5.2 Assessing the possible causes of sample irreproducibility

Determining Si isotopic compositions to extremely high precision is difficult given the lack of opportunity for double spiking. Here we consider various artefacts that have been proposed and assess the degree to which our data or those of Georg et al. (2007) could be affected.

3.5.2.1 Iron hydroxide formation

Fitoussi et al. (2009) suggest that the some of the lighter $\delta^{30}Si$ values generated by Georg et al. (2007) can be explained by instability of the sample solution at low pH, at which the Si can sorb on to iron hydroxide particles. This is an unlikely scenario as all the iron was in solution in the samples; i.e. no particulates were noted. However, if this were the case, more extreme isotopic values may be related to higher Fe content. In Figure 3.3 we have plotted $\delta^{30}Si$ data from Georg et al. (2007) and this study against Fe_{total} wt.%. Our data do not show any relationship between Fe_{total} and $\delta^{30}Si$ (R^2 = 0.06), largely due to the limited variations in both quantities. With regards to data of Georg et al. (2007), although the samples with the lightest $\delta^{30}Si$ do have the most Fe, this trend does not continue; sample groups with broadly similar Fe contents have markedly different $\delta^{30}Si$ compositions (e.g. lunar vs. martian/eucrite/diogenite samples). Also, many of the terrestrial samples analysed by Georg et al. (2007) have very

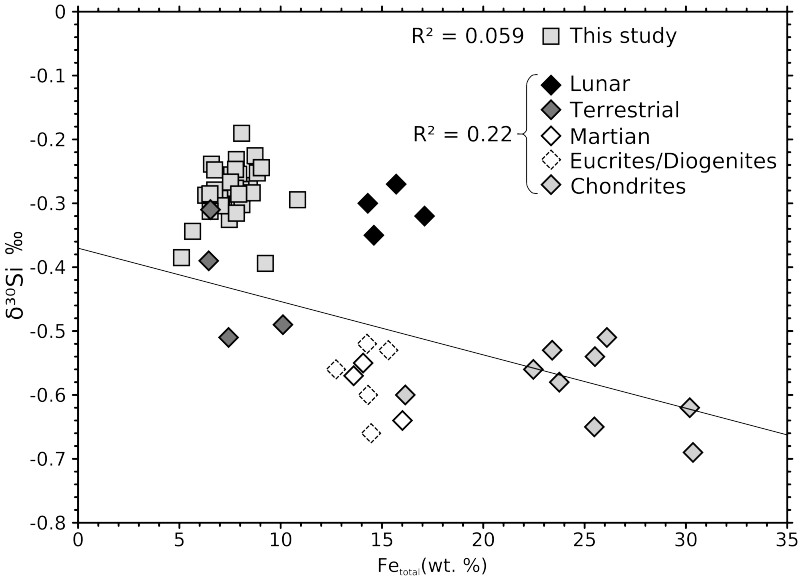


Fig. 3.3 Plot of $\delta^{30}Si$ vs. Fe content in the samples from this study (grey squares) and those from Georg et al. (2007, diamonds). The trend line is for the data from Georg et al. only; the spread of data from our study is too small for any meaningful correlation to be described. This plot does not support the idea that sorbtion of Si on to FeOOH particles in solution is responsible for the light values observed by Georg et al. (2007), as samples with similar Fe contents have markedly different $\delta^{30}Si$ values.

similar Fe_{total} to our samples but are isotopically lighter. Therefore the disparity between our terrestrial average and the value quoted by Georg et al. is likely unrelated to sample instability caused by iron oxyhydroxide formation.

3.5.2.2 Suppressed sample ionisation by sulphur

Van den Boorn et al. (2009) suggest that anionic species such as sulphates can affect the ionisation of the sample in the mass spectrometer and thus the final isotopic value; however, our column calibrations show that Si is the only element present in resolvable quantities. Also, our ability to reproduce the basaltic BHVO standards without any further sample processing suggests our chemistry is adequately removing all matrix-related interferences. Van den Boorn et al. (2009) suggest removal of the sulphur by ignition of the sample at 1350 °C before digestion, at 200 °C. Because our digestion (alkali fusion) step takes place at 720 °C, we expect that most of the sulphur ($T_{boiling}$=444.72 °C) in our sample will be volatilised and removed prior to ion-exchange chemistry.

3.5.2.3 Sample instability during column chemistry due to pH

On the basis of tests made using standards of varying acidity, Fitoussi et al. (2009) suggest that Si isotope fractionation can occur during column chemistry if the pH of the solution is 1<pH<2, as a function of the speciation of the Si in solution. As the pH of our solutions is <1, it is unlikely that our data has not been compromised in this way. In any case, when the sample is eluted in MQ-e, the pH of the sample will be raised to near neutral.

3.5.2.4 Isotopic variation related to sample alteration

Low temperature alteration products are typically concentrated in the lighter isotopes of Si, for instance in clay minerals (Opfergelt et al., 2010) or iron oxides (Delstanche et al., 2009). However, all our samples were specifically chosen for their freshness and so the risk of any data being compromised by alteration products is extremely low. There is little possibility, given the mass balance, that alteration products have affected our data and, moreover, the fact that ultramafic and basalt glass samples give very similar average compositions would then be fortuitous.

Given the above arguments, coupled with our ability to reproduce external, matrix-

matched standards, the data appear to record the real Si isotope composition of the BSE. Considering that our shared methodology appears robust, it is unclear as to whether the data of Georg et al. (2007) show a systematic offset or merely reflect stochastic analytical artefacts. Certainly, a repeat of sample D5-5 in this study does not replicate the value published in their paper; our value is ~0.1‰ heavier, a difference that is reflected in the $\delta^{30}Si_{BSE}$ average offset between our two papers and with other authors. Also, as mentioned above, the range of our MORB data is not coincident and is isotopically heavier than those of Georg et al. (2007). Given the smaller range and greater number of values analysed in our study, the lighter BSE $\delta^{30}Si$ estimate provided by Georg et al. (2007) are, most likely, a reflection of data inaccuracies rather than real mantle heterogeneities that only they have sampled. The differences between our averages, however, are still at the limits of analytical uncertainty and so it is not appropriate to describe the study of Georg et al. (2007) as inaccurate, rather that their BSE estimate is in broad agreement with ours.

3.5.3 Is the Earth's mantle heterogeneous with respect to silicon isotopes?

The spread of data provided in this study is too small to be reliably resolved given the reproducibility of the method (± 0.10 ‰ at 2 s.d.) and Earth's mantle therefore appears to be homogeneous with respect to Si isotopes, within achievable uncertainty.

It is worth noting that there could be a small difference between basalts and ultramafic rocks. The $\delta^{30}Si$ of MORB and IAB range from −0.33 to −0.23 ‰ and −0.32 to −0.25 ‰ respectively, whereas the ultramafic rocks are on average slightly lighter, varying between −0.39 and −0.29 ‰. With the present data set it is hard to be certain whether this effect is real.

In a similar manner, the limited spread in $\delta^{30}Si$ means that any strong relationships with major and trace elements or other isotopic tracers cannot be demonstrated. There are, however, possible relationships between $\delta^{30}Si$ and both SiO_2 and Al_2O_3 contents (Fig. 3.4). Systematic variations between SiO_2 content and Si isotope composition have been recorded before (Douthitt, 1982; Ding et al., 1996) and our data support this trend: the most silica-poor sample J30, a dunite from Kohistan, also displays the lightest Si isotope composition in our dataset ($\delta^{30}Si$ = −0.39 ‰). Correspondingly, the most Si-rich sample URA6, a basaltic andesite from the Marianas ($\delta^{30}Si$ = −0.25 ‰), does have a relatively heavy Si isotope composition. Sample J30 also has an isotopically light Fe composition ($\delta^{56}Fe$ = −0.3 ‰ relative to $\delta^{56}Fe_{MORB}$= +0.1 ‰;

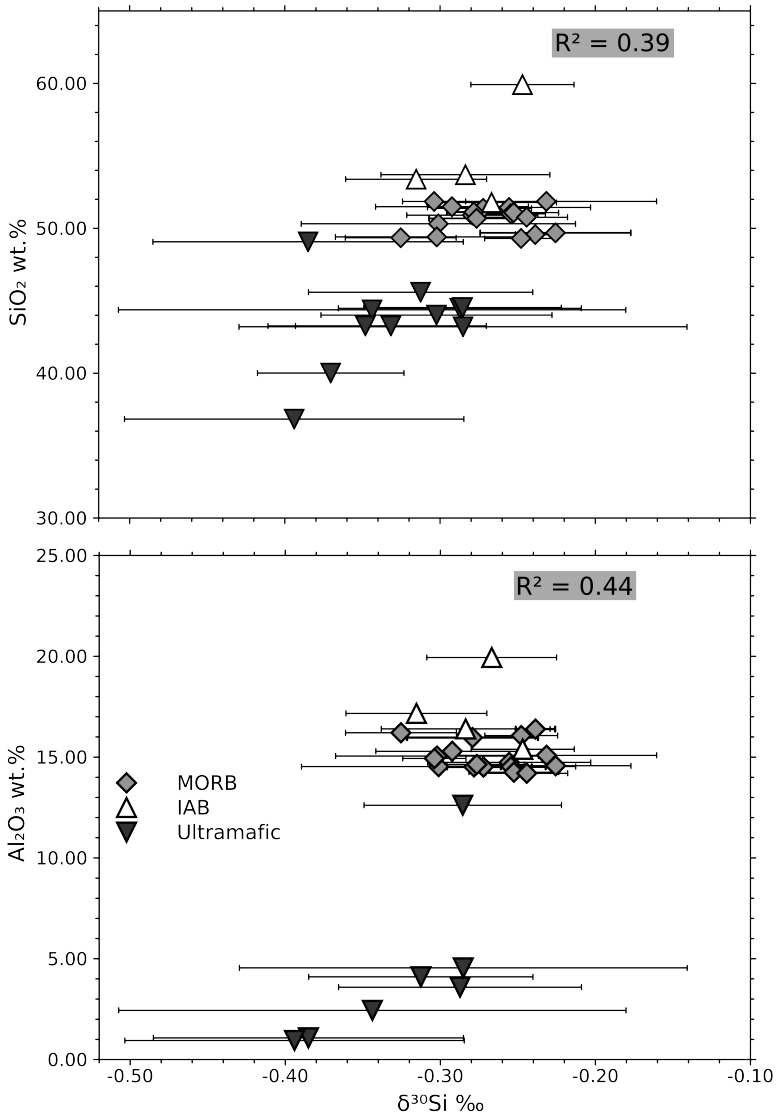


Fig. 3.4. Plot of $\delta^{30}Si$ vs. a) SiO_2 and b) Al_2O_3 using all the data in this study, where available. Error bars are normally 2 s.d., but may be 2 standard error of the mean if only one aliquot was analysed. See text for discussion.

Williams et al., 2005); this was related to melt extraction. The process of melt extraction agrees with our favoured explanation for the variation of Si isotopes with SiO_2 content; this is discussed below.

The weak correlation with Al_2O_3 could be evidence of a mineral fractionation effect. During crystallisation of basaltic magma the most obvious fractionating phase is feldspar. However there is no correlation with Sr or any other tracer for feldspar fractionation. There is also no co-variation between Ni contents and $\delta^{30}Si$, which could indicate that olivine formation was affecting Si isotope composition. Al_2O_3 variations could also be related to the presence of garnet in the mantle source region. The garnet-bearing ultramafic rocks analysed in bulk in this study do not show any trend towards lighter $\delta^{30}Si$ but this bulk feature does not preclude inter-mineral fractionation. Garnet-related Si isotope fractionation was noted by Georg (2006) and

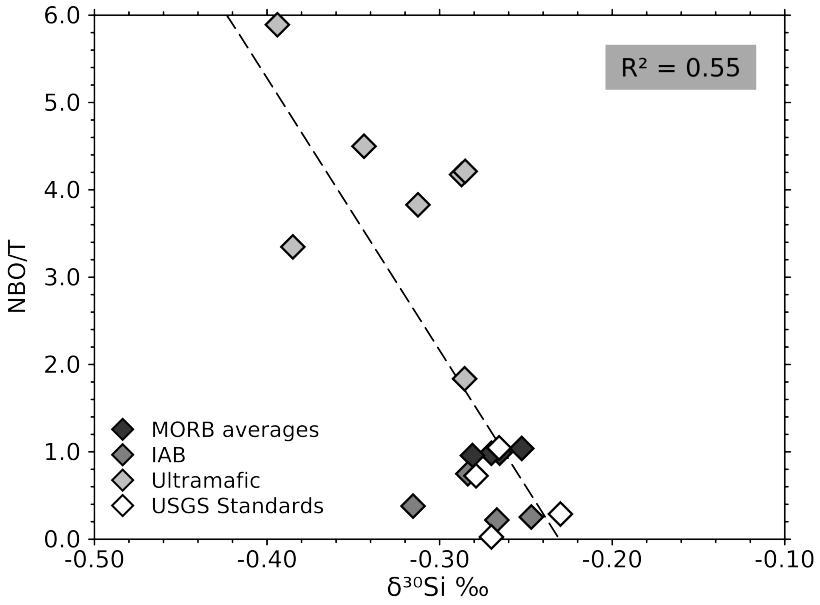


Fig. 3.5. Plot of $\delta^{30}Si$ vs. the calculated ratio NBO/T (Mysen, 1983). The line of best fit through all the data is shown as well as the R^2 value. The negative trend suggests that the more tetrahedrally co-ordinated oxygen in a system, the heavier its silicon isotope composition should be. The MORB values for NBO/T have been averaged for each ocean basin as otherwise they dominate the correlation — however, the trend still exists if all data is plotted but the R^2 value is reduced to <0.5.

André et al. (2006), with garnet tending to be lighter. Research is on-going to further investigate high temperature mineral fractionation of Si isotopes.

A relationship between SiO_2 content and Si isotope composition was predicted theoretically by Grant (1954); specifically that equilibrium fractionation of Si isotopes would occur as a function of silicon polymerisation and that the heavier isotopes would favour the phase(s) with a greater degree of polymerisation. Although Grant predicted fractionation magnitudes that overestimate those seen in nature, a more recent paper by Méheut et al. (2009) uses density function theory to support this relationship. Critically, it is also predicted that the presence of other network forming cations (the authors specifically mention aluminium) can have an effect on the degree of fractionation. This should be seen on a plot of NBO/T vs. $\delta^{30}Si$ (Fig. 3.5). The NBO/T value of a sample (Mysen, 1983) is a ratio of the non-bridging oxygen anions over the oxygen ions bonded in tetrahedral co-ordination, i.e. it describes the polymerisation degree of a melt by taking into account all network-forming cations. A negative trend exists between NBO/T and $\delta^{30}Si$, although it is not a particularly strong relationship. Considering the small range of isotope data and that silicon is such a major element, it is our opinion that degree of polymerisation could be the dominant control over Si isotope composition.

3.6 CONCLUSIONS

We have analysed a sample set of 35 well-characterised terrestrial mafic and ultramafic

samples in an attempt to investigate the Si isotope composition of the mantle and thus the bulk silicate earth (BSE). We find that there are no significant relationships between δ^{30}Si and locality, age and chemistry and thus conclude that the BSE is homogeneous with respect to Si isotopes. The average BSE δ^{30}Si value found by this study is −0.29 ± 0.08 ‰ (2 s.d.).

At current analytical precision, the variations presented in this study are too small to confidently resolve any fractionation outside of analytical uncertainty. However, a vague negative correlation exists between δ^{30}Si and the parameter NBO/T (Mysen, 1983) that we infer could be related to increase of the heavier isotopes of Si as a function of melt polymerisation (Grant, 1954; Méheut et al., 2009). Although our data are not inconsistent with this sense of variation, the spread of data presented here is not sufficient to confirm any trends. The effect of melting of Si isotope composition is an important issue to understand and one that we hope to address in the future.

ACKNOWLEDGEMENTS

We are extremely grateful to Charlie Langmuir, Bill White and others who provided the MORB samples that were analysed in this study. We thank Tim Elliott for the Marianas and South Sandwich samples. The xenoliths from East Africa were collected by Barry Dawson and Cassi Paslick. We are also indebted to Kevin Burton (who also contributed the San Carlos and Kilbourne Hole samples) and Julie Prytulak who have both contributed helpful discussion and useful suggestions along the way. The authors would also like to thank Nick Belshaw and Teodor Krastev for invaluable technical support. Finally, we would like to thank the two anonymous reviewers and Rick Carlson for helpful and insightful comments, which have greatly improved this manuscript. This work was funded by a NERC CASE studentship supported by Nu Instruments.

Chapter 4: Silicon isotope fractionation during magmatic differentiation

Published as

Silicon isotope fractionation during magmatic differentiation

P.S. Savage, R.B. Georg, H.M. Williams, K.W. Burton, A.N. Halliday

2011 *Geochimica et Cosmochimica Acta*, **75**, 6124-6139

ABSTRACT

The Si isotopic composition of Earth's mantle is thought to be homogeneous ($\delta^{30}Si$ = -0.29 ± 0.08 ‰, 2 s.d.) and not greatly affected by partial melting and recycling. Previous analyses of evolved igneous material indicate that such rocks are isotopically heavy relative to the mantle. To understand this variation, it is necessary to investigate the degree of Si isotopic fractionation that takes place during magmatic differentiation. Here we report Si isotopic compositions of lavas from Hekla volcano, Iceland, which has formed in a region devoid of old, geochemically diverse crust. We show that Si isotopic composition varies linearly as a function of silica content, with more differentiated rocks possessing heavier isotopic compositions. Data for samples from the Afar Rift Zone, as well as various igneous USGS standards are collinear with the Hekla trend, providing evidence of a fundamental relationship between magmatic differentiation and Si isotopes. The effect of fractionation has been tested by studying cumulates from the Skaergaard Complex, which show that olivine and pyroxene are isotopically light, and plagioclase heavy, relative to the Si isotopic composition of the Earth's mantle. Therefore, Si isotopes can be utilised to model the competing effects of mafic and felsic mineral fractionation in evolving silicate liquids and cumulates.

At an average SiO_2 content of ~ 60 wt.%, the predicted $\delta^{30}Si$ value of the continental crust that should result from magmatic fractionation alone is -0.23 ± 0.05 ‰ (2 s.e.), barely heavier than the mantle. This is, at most, a maximum estimate, as this does not take into account weathered material whose formation drives the products toward lighter $\delta^{30}Si$ values. Mass balance calculations suggest that removal of continental crust of this composition from the upper mantle will not affect the Si isotopic composition of the mantle.

4.1 INTRODUCTION

Silicon (Si) is the third-most abundant element on Earth and is critical to many varied geochemical and biochemical processes. Despite its ubiquity and the large relative mass difference between its three stable isotopes (^{28}Si, ^{29}Si and ^{30}Si), high temperature isotope fractionation is limited, at least in the terrestrial realm. This is due in part to Si having only one valence state (Si^{4+}) and, also, because Si does not form volatile compounds readily. In the past decade, analytical techniques have improved sufficiently that small but significant high temperature isotopic variations are now resolvable (e.g. Georg et al., 2007).

Silicon isotopes are widely utilised in low temperature geochemistry, where isotopic variation is generally larger. Fractionation has been demonstrated during growth of diatoms, sponges and other silica-utilising organisms (e.g. De La Rocha et al., 1998; Hendry et al., 2010), formation of clays during chemical weathering (Ziegler et al., 2005a,b; Georg et al., 2006a, 2009a; Delstanche et al., 2009), silcrete and other groundwater precipitates (Basile-Doelsch et al., 2005; van den Boorn et al., 2007), and banded iron formations (André et al., 2006).

Interest in applying Si isotopes to high temperature geological processes increased after Georg et al. (2007) observed resolvable isotopic variations between Bulk Silicate Earth (BSE) and meteorites. They interpreted this as evidence that Si was one of the light elements that entered the core (Allègre et al., 1995; Wade and Wood, 2005), and that the isotopic offset was generated by the partitioning of Si between metal and silicate phases. Such an important result generated a great deal of further research, ranging from refining the Si isotopic signature of BSE (e.g. Zambardi et al., 2009; Savage et al., 2010), quantifying the amount of Si isotope fractionation between metal and silicate (Shahar et al., 2009; Ziegler et al., 2010) and analysing more meteorite groups with the hope of better refining the offset between the two groups (e.g. Fitoussi et al., 2009; Armytage et al., 2011). Even still, the picture is not completely clear, as a recent paper by Chakrabarti and Jacobsen (2010) claims that there is no difference between BSE and meteorites.

Considering the amount of research effort invested into the Si isotope composition of the mantle, very little progress has been made in understanding what happens to mantle products that evolve toward more Si-rich compositions; to our knowledge, as yet there are no studies that specifically address this issue. Defining how igneous processes affect Si isotopes is important for two main reasons: firstly, the continental crust is a major source in the Si weathering cycle and a proper understanding of the isotopic composition of this source is an important issue; secondly, if fractionation is taking place, identifying the cause of fractionation is fundamental and Si isotopes could provide new constraints on crystal fractionation and melt generation processes.

There is already some evidence to suggest that magmatic differentiation affects Si isotopes. In their widely cited studies, both Douthitt (1982) and Ding et al. (1996) find an enrichment of the heavier Si isotopes in the more evolved, Si-rich rocks that they analysed (Fig. 4.1). However, the spread of isotopic compositions reported in both studies is large and the

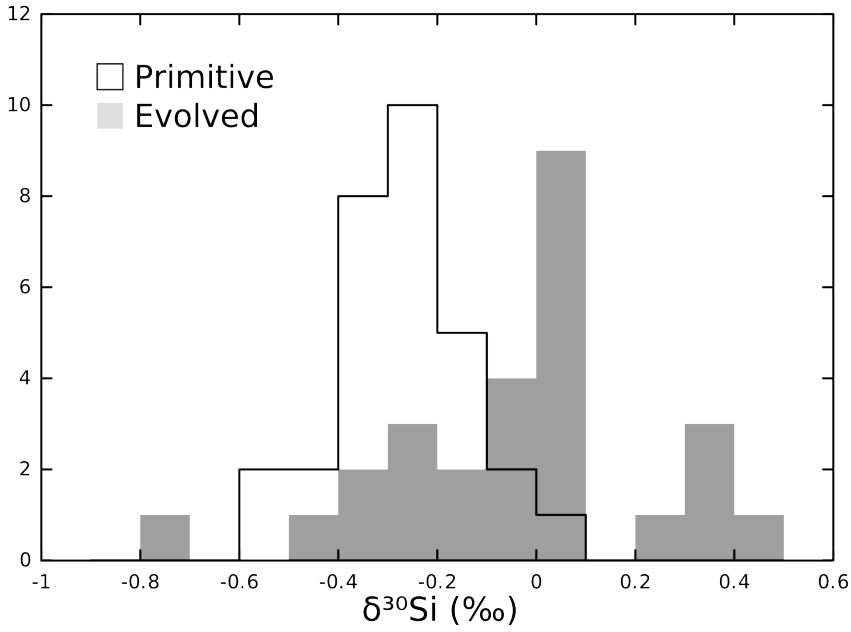


Fig. 4.1 Histogram of igneous rock data from Douthitt (1982) showing that, in general, evolved samples appear to be more enriched in the heavier Si isotopes than primitive rocks. This phenomenon has been noted in other work, i.e. Ding et al. (1996).

analytical precision too poor to attribute these observations to any specific process. Also, both studies use, in their sample sets, a number of granitic rocks where sedimentary anatexis, fluid alteration or crystal aggregation could complicate interpretation. Douthitt (1982) concluded, "silicon isotopes show little variation in igneous rocks and minerals; hence, they have little import for studies of igneous rocks".

Grant (1954) calculated, from first principles, that equilibrium isotopic fractionation of Si isotopes is a function of the internal vibrational frequencies of the Si–O bonds in the equilibrating phases. A major control over this is Si polymerisation, and Grant (1954) calculated that heavier isotopes would favour the phase(s) with a greater degree of polymerisation. This agrees with the general trend of Si-rich samples displaying heavier Si isotopic compositions (see above; Fig. 4.1). However, the calculated magnitude of fractionation (variations on the order of 1–5 ‰ at mantle conditions) is much greater than any measured isotopic data has demonstrated.

In a more recent paper, Méheut et al. (2009) use density functional theory to show that this relationship is not as simple as suggested by Grant (1954), i.e. the more polymerised phase will not necessarily be more enriched in the heavier isotopes. They suggest that other network forming cations, e.g. aluminium, can alter the vibrational frequencies associated with crystallographic sites, which will alter bond strength and ultimately affect the degree of fractionation. It is evident that isotopic measurements of natural samples could help explain what effect polymerisation has on fractionation.

This study aims to quantify the amount of Si isotope fractionation that takes place as a result of igneous processes that occur during magmatic differentiation. Given the limited Si isotopic fractionation noted in previous studies (e.g. Savage et al., 2010), a large range of silica contents should be necessary to detect any resolvable isotopic effects. Also, as mentioned above, relatively large low temperature isotopic effects have been documented in sedimentary rocks. Therefore, we have selected the volcano of Hekla, Iceland, as a study area, which erupts material with a wide range of SiO_2 contents, and where there is evidence that petrogenesis has been unaffected by sedimentary, metasedimentary or hydrothermally altered components (see below).

4.2.GEOLOGICAL BACKGROUND

4.2.1 The volcano of Hekla

Hekla is an active fissure volcano located in the South Iceland Volcanic Zone, at the intersection with the South Iceland Fracture Zone (Figs. 4.2 and 4.3). It is, historically, one of the most active volcanoes on Iceland and is unusual in that it emits a wide range of volcanic products (basalts, basaltic andesites, andesites, dacites and rhyolites) from a cogenetic source.

There have been 18 historic eruptions since 1104 A.D. (Thorarinsson, 1967), and the volcano last erupted in 2000 A.D. (Höskuldsson et al., 2007) – the current eruptive periodicity is ~10 years. Eruptions typically begin with an explosive Plinian stage, which may last minutes to days. This is followed by a more effusive stage, when most of the eruptive material is emplaced. Eruption products evolve from more differentiated (SiO_2-rich) to more primitive (SiO_2-poor) over the course of an eruption, ranging from basaltic andesites to rhyolites. Basalt does not erupt on the main edifice; instead it is erupted from vents on the flanks of Hekla. The degree of SiO_2-enrichment in the initial explosive stage is related to the dormancy interval, with longer periods of quiescence corresponding to more evolved initial compositions (Thorarinsson, 1967).

Five prehistoric eruptions have been identified (Larsen and Thorarinsson, 1977), the most recent of which (1104 A.D.) marks the beginning of historic eruptions (Thorarinsson, 1967). These were violent events, emitting large (>10 km^3) volumes of silicic tephra, the composition of which ranged from 70% to 74% SiO_2 at the onset to ~57% SiO_2 in the final eruptive products. No lava flows have been linked to these eruptions.

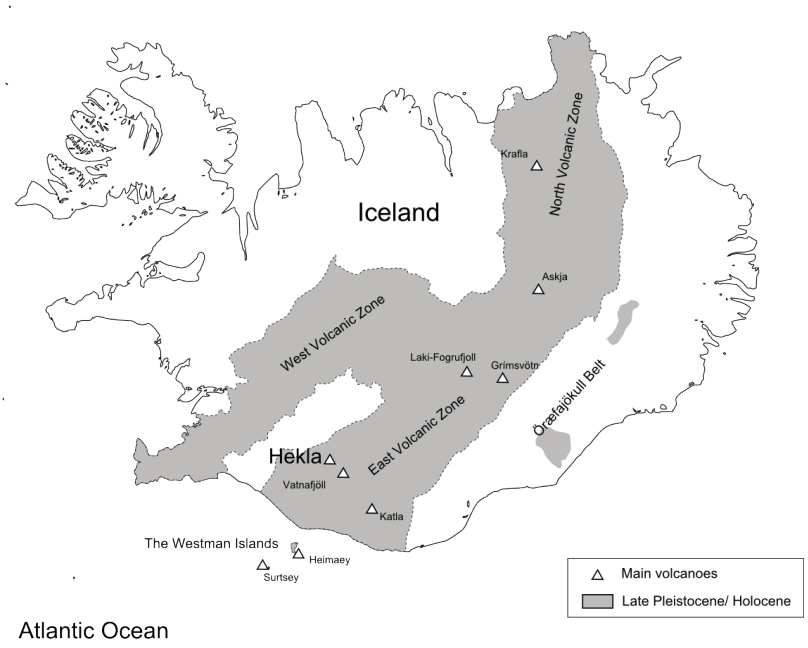


Fig. 4.2 Simplified map of Iceland showing the location of Hekla volcano, as well as other major centres of volcanic activity.

4.2.2 Magma differentiation on Hekla

The major element characteristics of Hekla lavas appear to indicate a simple differentiation sequence in the magma chamber – i.e. all samples from Hekla plot on a single liquid line of descent, suggesting that the range of Si content can be explained by fractional crystallisation. However, using Th, Sr and O isotopes, Sigmarsson et al. (1992) demonstrated that this is not the case. They proposed a three stage model to generate the wide range of silica contents:

1. Basaltic magma rises and ponds at the base of a shallow (8–15 km depth) magma chamber. This material undergoes fractional crystallisation to form basaltic andesite.
2. The same basaltic magma also causes partial melting of crustal metabasalt and metagabbro. This results in the formation of a dacitic magma, which can mix with the melt of basaltic andesite composition, to form andesitic material.
3. Further fractional crystallisation of the dacitic melt generates rhyolitic compositions.

The model of Sigmarsson et al. (1992) has been brought into question recently by Chekol et al. (2011) who cite the lack of seismological evidence for a shallow long-lived magma chamber (Soosalu and Einarsson, 2004). Instead, they suggest that a layer of magma at the base of the Moho continuously intrudes smaller lenses of magma into the crust, which then differentiate through AFC (assimilation and fractional crystallisation; DePaolo, 1981) processes. However, as far as magmatic differentiation is related to Si isotopes, this model is not

fundamentally different to that of Sigmarsson et al. (1992).

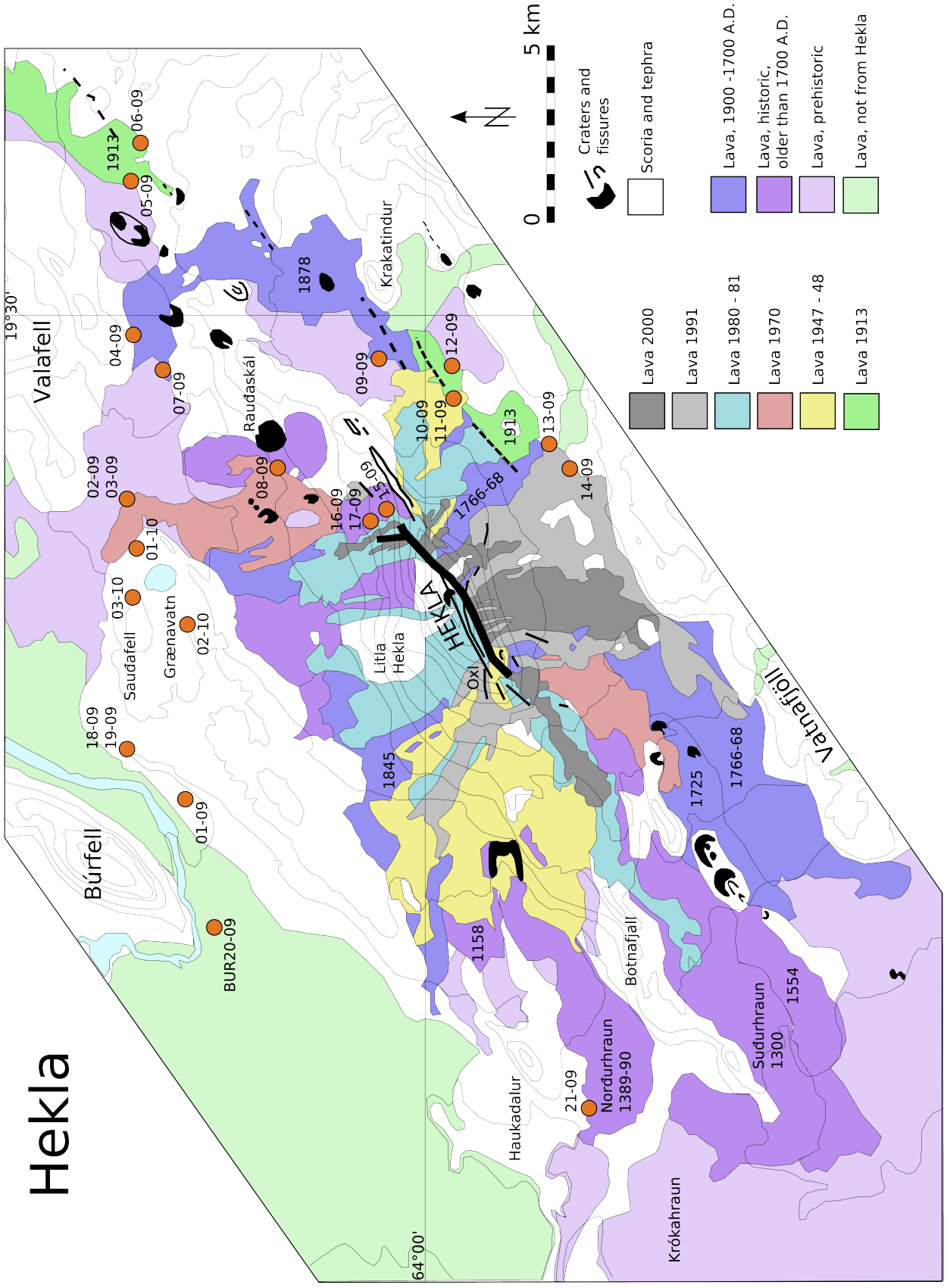
Hekla has already been exploited as a natural laboratory for studying differentiation by Schuessler et al. (2009) who measured stable Fe and Li isotopes in the same samples as Sigmarsson et al. (1992). They report a variation in $\delta^{56}Fe$ between basaltic and rhyolitic end-members of ~ 0.1 ‰, with the more evolved material enriched in isotopically heavy Fe (i.e. in $\delta^{56}Fe$). Crucially, $\delta^{56}Fe$ only starts to vary between 65% and 72% SiO_2, i.e. during stage 3 of the magma differentiation model of Sigmarsson et al. (1992 – see above). This variation is attributed to the formation of isotopically light titanomagnetite in the magma chamber, an effect that becomes exacerbated at lower Fe concentrations (at more rhyolitic compositions). Similar increases in $\delta^{56}Fe$ in high silica magmas have also been noted in studies by Poitrasson and Freydier (2005), Schoenberg and von Blanckenburg (2006) and Teng et al. (2008).

In contrast to Fe isotopes, Schuessler et al. (2009) found no variation of stable Li isotopes away from mantle values on Hekla, which suggests that there has been no fluid alteration (via degassing or metasomatism) in the magmatic system. This is important, as far as our research is concerned, because secondary processes such as dissolution and reprecipitation of silica in hydrothermal fluids (van den Boorn et al., 2007) could potentially result in much larger degrees of Si isotopic fractionation, which may otherwise mask the effect of magmatic differentiation on the Si isotope composition of igneous rocks (discussed further in Section 4.5.1.1).

4.3 SAMPLES AND ANALYTICAL TECHNIQUES

4.3.1 Iceland

Between September 2009 and July 2010, we collected 24 rock samples from Hekla and a further three unrelated Icelandic volcanic samples. The samples are aphyric, with phenocryst contents generally below 5%. We aimed to collect material that was as fresh as possible from flow cores, from most of the historic eruptions. We also collected tephra from some prehistoric eruptions (ages are given in Table 4.2, sample sites are shown in Fig. 4.3). All samples were washed to remove organic material and/or soil, crushed in a jaw crusher and powdered in an agate TEMA mill at the Open University, Milton Keynes. To assess any Si contamination from the agate, repeat samples were crushed using a steel mill; no resolvable difference in SiO_2 was measured. Furthermore, repeat isotopic analyses of the same sample show no difference


Hekla
Valafell
Búrfell
Saudafell
Grænavatn
Litla Hekla
HEKLA
Oxi
Rauðaskál
Krakatindur
Vatnafjöll
Botnafjall
Haukadalur
Krókahraun
Nordurhraun 1389-90
Suðurhraun 1300
1554
1158
1845
1766-68
1725
1878
1913
19°30'
64°00'
N
0
5 km
Craters and fissures
Scoria and tephra
Lava, 1900 -1700 A.D.
Lava, historic, older than 1700 A.D.
Lava, prehistoric
Lava, not from Hekla
Lava 2000
Lava 1991
Lava 1980 - 81
Lava 1970
Lava 1947 - 48
Lava 1913

between the material crushed in the agate (HEK07-09 $\delta^{30}Si$ = -0.34 ± 0.08 ‰; 2 s.d.) and steel mills (HEK07-09c $\delta^{30}Si$ = -0.36 ± 0.09 ‰; 2 s.d.).

Major and selected trace elements were measured by the XRF facility at the Open University, Milton Keynes (Ramsey et al., 1995; Watson, 1996; Table 4.2, Appendix 1). The average relative precision values, using this method, are ~0.23 % for major elements and ~1.5 % for trace elements (Ramsey et al., 1995; individual element precision values are listed in Appendix 1). The SiO_2 content of our samples ranges from 46 % to 72 %, encompassing the range of compositions recorded in Hekla rocks from previous studies (e.g. Sigmarsson et al., 1992). On a total alkali–silica (TAS) plot (Le Bas et al., 1986), the samples plot as a transitional alkali series (Fig. 4.4), also consistent with other studies of Hekla. Thin sections of a selection of the samples show that olivine, clinopyroxene and plagioclase feldspar are the major crystal phases forming, along with accessory apatite, magnetite and minor zircon.

4.3.2 Additional samples

To broaden our sample set, we analysed 6 samples from the Afar rift zone, Ethiopia. The Afar rift zone produces both basaltic and rhyolitic material, characteristic of bimodal volcanism in a rift zone setting (e.g. Courtillot, 1982). The samples we analysed are from a number of localities along the Dabbahu – Manda Hararo rift zone (Barberi et al., 1970; Lahitte et al., 2003; Ferguson et al., 2010), not restricted to one volcanic source as in the Hekla samples. In this setting, basalts are normally erupted in extensive flow fields, whereas the rhyolitic material is erupted from on axis volcanic centres. Samples are both aphyric and fresh with eruption ages ranging from 300 k.a. to recent. All samples were provided as glass chips, which were then powdered in an alumina pestle and mortar – see Table 4.2 for sample ages and localities.

As well as using the USGS standard BHVO-2 as an additional basaltic sample, we also analysed the andesite standard AGV-2 and the granodiorite standard GSP-2 (both USGS).

Lastly, to investigate the effect that crystal formation might have on Si isotopes during magma differentiation, we hand-picked and analysed mineral separates of the major crystal phases forming in the Hekla magma chamber (see above). Specifically, two samples of cumulate material from the Skaergaard intrusion (rocks 2307 and 5181; described as “average rock” and

Fig. 4.3 Sketch map of Hekla volcano, Iceland, showing the localities of samples collected for this study, as well as the major lava flows, ages and vent locations. This map is based on one provided by Höskuldsson et al. (2007). Samples collected in 2009 are suffixed -09, samples collected in 2010 are suffixed -10.

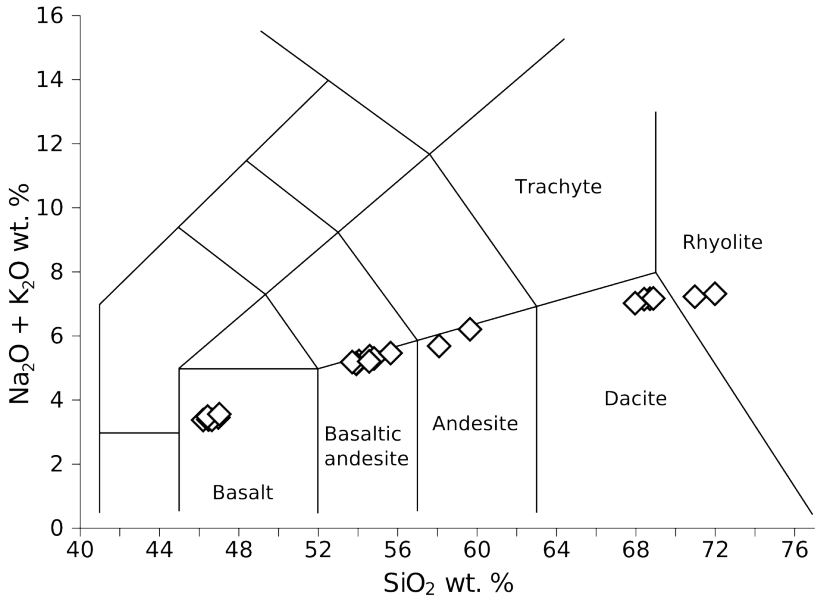


Fig. 4.4 Total alkali – silica (TAS) diagram demonstrating the transitional alkali nature of Hekla volcanics, as well as the range of compositions analysed in this study (TAS diagram as defined in Le Bas et al., 1986). Major and trace element analyses are provided in Appendix 1.

"ferrogabbro" by Wager, 1960) were picked for olivine, clinopyroxene and plagioclase under a binocular microscope, which were then powdered as for the Afar samples. The Skaergaard suite is especially suitable for this study, because the intrusion formed from a single (prolonged) pulse of magma (McBirney, 1996) and evidence from Sr and Nd isotopes suggests minimal (~4 %) magma contamination by crustal sources (Stewart and DePaolo, 1990; McBirney and Creaser, 2003). Variable, low $\delta^{18}O$ values from a number of Skaergaard samples indicate that pervasive low temperature alteration by meteoric waters has occurred throughout the intrusion (Taylor and Forester, 1979) and so we have chosen samples from localities where the $\delta^{18}O$ values reflect a primary mantle signature. Both samples are from the layered zone, which formed from material crystallising from the base of the intrusion upwards; sample 5181 is from the Upper Layered zone (UZa) and has a $\delta^{18}O_{plagioclase}$ value of +6.4 ± 0.7 ‰; sample 2307 is from the Lower Layered zone (LZc) and, although there is no $\delta^{18}O$ data for this sample, it is taken from an area (Kraemers Island) where a primary O isotope signature dominates ($\delta^{18}O$ ~6 ‰; Fig. 15 in Taylor and Forester, 1979).

4.3.3 Alkali fusion

All samples and standards were dissolved using the HF-free alkali fusion technique described by Georg et al. (2006b). Between 5 and 10 mg of sample powder was measured into a silver crucible, into which ~200 mg of NaOH flux was added. After heating at 720ºC in a muffle

furnace for 12 min, the resultant fusion cake was then transferred into solution with MQ-e water (18.2 MΩ) and acidified with triple-distilled HNO_3 (1% v/v). Silicon concentrations and yields were checked after the alkali fusion stage using the "molybdenum-blue" method on a Hach Lange DR 2800 photospectrometer; the average yield of the Hekla samples was 100 ± 2 % (1 s.d.).

Both samples and standards (including the bracketing standard) were purified before mass spectrometry using a single column pass, in BioRad (Hercules, CA, USA) Poly- Prep 10 ml columns filled with 1.8 ml DOWEX 50W-X12 (200–400 mesh) cation exchange resin. At low pH, Si in solution is in the form of non-ionic monosilicic acid $Si(OH)_4$ or the anionic species $H_3SiO_4^-$ and so will not be retained by the resin. The samples were eluted in MQ-e water and, after purification, each sample was acidifed to 1% HNO_3 v/v (again with triple-distilled HNO_3). Silicon recovery is quantitative, as shown by Georg et al. (2006b) wherein elution profiles give a measured sample Si recovery of 100.1 ± 1.6% and show no detectable concentrations of the major cations and trace metals in the eluate. Column calibrations made in-house confirm these results. Further tests and evidence for the robustness of this method are provided in Chapter 3, Zambardi and Poitrasson (2011) and Armytage et al.(2011).

The presence of anionic species (such as SO_4^{2-}, NO_3^- or PO_4^{3-}) in the eluate do not appear to cause any matrix effects, as our external standard data demonstrate (see later). This is expected, as [Si]/[anionic species] ratios are generally large in most silicate rocks, and the dilution factors integral to the methods work to further reduce anionic concentrations. Nevertheless, Georg et al. (2006b) tested this possibility by doping solutions of NBS28 with relatively large quantities of anionic species and measuring them against undoped solutions; no resolvable offset was recorded.

4.3.4 Mass spectrometry

Silicon isotopes were measured on a Nu Plasma High Resolution Multiple Collector ICP-MS (Nu Instruments, Wrexham, UK) in the Department of Earth Sciences, Oxford. The instrument and running conditions for Si isotope measurement are described in detail by Georg et al. (2006b). We ran a "dry" plasma; samples were introduced by means of a Savillex C-Flow 6 mm concentric nebuliser with an uptake rate of ~50 µl min^{-1} and desolvated using an Aridus II (CETAC, NE, USA). To avoid polyatomic interferences on the silicon beams, we ran the

instrument at "medium" resolution (mass resolving power M/ΔM ~ 3300, where ΔM is defined at 5% and 95% of peak height). This entails narrowing the beam from 0.3 mm to 0.05 mm, and closing the "Alpha" slits, which reduces the sensitivity by ~85 %. At standard operating conditions, sample concentrations of 750 ppb Si yielded a typical beam intensity of ~1×10^{-10} A.

Isotope measurements were calculated using the standard- sample bracketing protocol to correct for instrumental mass bias, using NBS28 (silica sand) as the bracketing standard. Instrument background was measured at the beginning of each analysis by deflecting the ESA for 20 s, and the subsequent measured ratios were corrected using this value. Typical background intensity was in the order of ~2×10^{-13} A, giving a signal to background ratio of ~500 (using 10^{11} Ω resistors). Each isotope measurement consisted of 5–6 sample analyses resulting in an average of 11 values – each analysis comprised 20 cycles and each cycle was integrated for 8 s.

Variations in Si isotopes are represented by the delta notation as $\delta^{30}Si$ or $\delta^{29}Si$, defined in this study as the deviation in per mil (‰) of a sample's ratio of $^{x}Si/^{28}Si$ from the standard (NBS28), as such:

$$\delta^{30}Si = [\ (^{30}Si/^{28}Si_{sample})/(^{30}Si/^{28}Si_{standard}) - 1\ ] \times 1000;$$

$$\delta^{29}Si = [\ (^{29}Si/^{28}Si_{sample})/(^{29}Si/^{28}Si_{standard}) - 1\ ] \times 1000.$$

In the following, we discuss our Si isotopic data using $\delta^{30}Si$ values, which are approxiamately twice the magnitude of $\delta^{29}Si$ values. This is assuming mass dependence, which for terrestrial samples is a valid assumption – indeed, this relationship was used as an extra test for data quality and any data that did not display mass dependence were discarded.

4.4 RESULTS

4.4.1 External standards

To assess the accuracy and reproducibility of the data, the external Si standards Diatomite and BHVO-2 were included routinely between samples during analysis (Table 4.1).

Diatomite is a well characterised, natural, pure silica standard, (Reynolds et al., 2007; Georg et al., 2009a; Ziegler et al., 2010; Chakrabarti and Jacobsen, 2010) and BHVO-2 is a USGS basaltic standard that is quickly becoming established as a "real" rock standard in Si isotope studies, particularly where mantle rocks are being analysed (Abraham et al., 2008; van

den Boorn et al., 2009; Zambardi and Poitrasson, 2011). Our values of $\delta^{30}Si = 1.23 \pm 0.10$ ‰ (2 s.d., n = 177) for Diatomite and $\delta^{30}Si = -0.29 \pm 0.09$ ‰ (2 s.d., n = 188) for BHVO-2 agree well with literature data and demonstrate the extremely good levels of precision and reproducibility that the method can achieve. In this study, the typical 2 s.d. (the mean of the 2 s.d. values of every sample analysed) is 0.09 ‰, which is identical to the those given by analysis of external standards, suggesting that 0.09 ‰ is a good estimate of the current reproducibility (cf. Zambardi and Poitrasson, 2011). Because all standards and samples were processed through identical chemistry, the errors associated with the data are a combination of both the "chemical" and "mass spectrometric" reproducibility.

The chemical composition of BHVO-2 is similar to that of primitive samples and as such is suitable as a "matrix-matched" standard. Therefore, the reproducibility of BHVO-2 confirms that the analyses are unlikely to have experienced matrix effects. Unfortunately, there is no high-Si counterpart to BHVO-2 available to assess matrix-related issues in the more evolved samples. However, the value for the USGS andesite standard AGV-2 ($\delta^{30}Si = -0.21 \pm 0.07$ ‰, 2 s.d.) agrees with that given in a recent method and standard assessment by Zambardi and Poitrasson (2011; $\delta^{30}Si = -0.15 \pm 0.06$ ‰, 2 s.d.).

Table 4.1 – Silicon isotope data for external standards analysed in this study

Sample		$\delta^{30}Si$ (‰)	2 s.d.	$\delta^{29}Si$ (‰)	2 s.d.	n
BHVO-2	This study	–0.29	0.09	–0.15	0.08	188
	Savage et al. (2010)	–0.27	0.10	–0.14	0.05	
	Abraham et al. (2008)	–0.29	0.11	–0.17	0.04	
	van den Boorn et al. (2009)	–0.27	0.22	–	–	
	Zambardi and Poitrasson (2011)	–0.27	0.08	–0.14	0.05	
Diatomite	This study	1.23	0.10	0.64	0.08	177
	Savage et al. (2010)	1.25	0.08	0.65	0.05	
	Reynolds et al. (2007)	1.26	0.20	0.64	0.14	
	Georg et al. (2009a)	1.23	0.16	0.62	0.11	
	Ziegler et al. (2010)	1.22	0.18	0.63	0.01	
	Chakrabarti and Jacobsen (2010)	1.23	*0.03*	0.61	*0.02*	

Silicon isotope data (relative to NBS28) for external standards analysed in this study, as well as reference values for said standards. Errors are twice the standard deviation from the mean, unless in italics – these are twice the standard error (2 s.e. = 2 s.d./$n^{½}$).

4.4.2 Sample data

4.4.2.1 Whole rock data

All data are given in Table 4.2. To represent analytical uncertainty, both the two standard deviation (2 s.d.) and standard error of the mean at the 95% confidence level (95% s.e.) values are given (95% s.e. = t × s.d./$(n)^{1/2}$, where t = inverse survival function of the Student's t-test at the 95% significance level and (n - 1) degrees of freedom). All samples fall on or are within error of the terrestrial mass fractionation lines for equilibrium and kinetic fractionation, whose slopes are analytically identical at low degrees of fractionation.

The $\delta^{30}Si$ data for Hekla samples range from -0.34 to -0.14 ‰; a relatively large spread of data in the realm of high temperature Si isotopes. Figures 4.5a and b show a strong, positive, linear functional relationship between Si isotopic values and both SiO_2 and Ba content (both good indicators of magmatic differentiation, assuming Ba is behaving incompatibly). Even though there is overlap between adjacent rock types, the average isotopic value for each group becomes heavier as the samples become more evolved, as follows: $\delta^{30}Si_{basalt}$ = -0.31 ± 0.05 ‰; $\delta^{30}Si_{basaltic\ andesite}$ = -0.27 ± 0.05 ‰; $\delta^{30}Si_{andesite}$ = -0.23 ± 0.03 ‰; $\delta^{30}Si_{dacite}$ = -0.19 ± 0.04 ‰; $\delta^{30}Si_{rhyolite}$ = -0.16 ± 0.04 ‰ (all errors 2 s.d.).

The data from Afar range from $\delta^{30}Si$ = -0.31 to -0.28 ‰ in the basalts and from $\delta^{30}Si$ = -0.19 to -0.12 ‰ in the rhyolites (Table 4.2 and Fig. 4.5c). There is a resolvable difference between primitive and evolved samples, comparable to that seen for Hekla. Three samples that we collected from Iceland (two basalts and a dacite) that are genetically unrelated to each other and to Hekla range from $\delta^{30}Si$ = -0.33 to -0.20 ‰ (Fig. 4.5c), and also fit the trend described above. The three USGS standards (BHVO-2, AGV-2 and GSP-2) display the same relationship (Table 4.2 and Fig. 4.5c).

4.4.2.2 Skaergaard mineral separates

Silicon isotope data for the mineral separates from two Skaergaard Intrusion samples (Wager, 1960) are as follows: sample 2307: $\delta^{30}Si_{olivine}$ = -0.42 ± 0.08 ‰, $\delta^{30}Si_{clinopyroxene}$ = -0.50 ± 0.16 ‰ and $\delta^{30}Si_{plagioclase}$ = -0.15 ± 0.08 ‰; sample 5181: $\delta^{30}Si_{olivine}$ = -0.45 ± 0.08 ‰ and $\delta^{30}Si_{plagioclase}$ = -0.21 ± 0.09 ‰ (Table 4.2). The similarity and magnitude of the isotopic compositions and the differences between equivalent minerals in the two samples is striking.

The higher $\delta^{30}Si$ values of feldspar compared to both olivine and clinopyroxene is

Table 4.2 Sample silicon isotope data.

Sample	Eruption date	Rock type	SiO_2 (wt.%)	Ba (ppm)	$\delta^{30}Si$ (‰)	2 s.d.	95% s.e.	$\delta^{29}Si$ (‰)	2 s.d.	95% s.e.	*n*
Hekla lavas											
HEK06-09	1913 A.D.	Basalt	46.20	169	–0.31	0.09	0.03	–0.16	0.05	0.02	11
HEK05-09	1913 A.D.	Basalt	46.47	180	–0.32	0.12	0.04	–0.19	0.11	0.04	11
HEK04-09	1878 A.D.	Basalt	46.97	181	–0.31	0.06	0.02	–0.16	0.05	0.02	11
HEK07-09	1878 A.D.	Basalt	46.64	177	–0.34	0.08	0.03	–0.19	0.06	0.02	11
HEK07-09c			46.47	193	–0.36	0.09	0.04	–0.18	0.06	0.02	10
HEK12-09	1913 A.D.	Basalt	46.42	185	–0.29	0.10	0.03	–0.17	0.05	0.02	10
HEK09-09	1878 A.D.	Basalt	47.01	190	–0.28	0.06	0.01	–0.12	0.02	0.01	22
HEK02-09	1970 A.D.	Basaltic andesite	53.92	328	–0.25	0.06	0.02	–0.13	0.05	0.02	11
HEK03-09	1970 A.D.	Basaltic andesite	54.05	337	–0.22	0.10	0.02	–0.13	0.01	0.01	22
HEK08-09	1970 A.D.	Basaltic andesite	54.59	328	–0.29	0.07	0.02	–0.13	0.06	0.02	11
HEK13-09	1991 A.D	Basaltic andesite	53.90	319	–0.29	0.05	0.02	–0.18	0.04	0.01	11
HEK16-09	1980 A.D.	Basaltic andesite	54.81	343	–0.27	0.07	0.02	–0.12	0.05	0.02	11
HEK14-09	1991 A.D.	Basaltic andesite	53.71	329	–0.26	0.06	0.02	–0.16	0.05	0.02	7
HEK17-09	1980 A.D.	Basaltic andesite	54.57	338	–0.25	0.18	0.04	–0.16	0.04	0.01	20
HEK21-09	1390 A.D.	Basaltic andesite	55.64	351	–0.29	0.15	0.05	–0.12	0.07	0.02	11
HEK10-09	1947 A.D.	Andesite	57.67	372	–0.25	0.10	0.03	–0.13	0.10	0.03	11
HEK11-09	1947 A.D.	Andesite	58.09	386	–0.23	0.07	0.02	–0.12	0.04	0.01	22
HEK15-09	1980 A.D.	Andesite	59.64	443	–0.22	0.03	0.01	–0.13	0.03	0.01	22
HEK01-09	2800 B.P.	Dacite (tephra)	68.71	616	–0.18	0.03	0.01	–0.07	0.03	0.01	22
HEK18-09	2800 B.P.	Dacite (tephra)	68.41	619	–0.17	0.10	0.04	–0.10	0.06	0.02	11
HEK19-09	2800 B.P.	Dacite (tephra)	68.88	618	–0.21	0.06	0.01	–0.11	0.01	0.01	21
HEK02-10	2800 B.P.	Dacite (tephra)	68.00	600	–0.21	0.17	0.06	–0.12	0.07	0.03	10
HEK01-10	6600 B.P.	Rhyolite (tephra)	72.00	679	–0.14	0.16	0.05	–0.08	0.08	0.03	11
HEK03-10	4000 B.P.	Rhyolite (tephra)	71.00	659	–0.17	0.11	0.04	–0.09	0.07	0.02	11
Other Icelandic											
BUR20-09	~ 1700 A.D.	Basalt	49.05	40	–0.31	0.13	0.04	–0.17	0.11	0.04	11
SIB	Postglacial	Basalt	49.52	115	–0.33	0.08	0.03	–0.19	0.06	0.02	11
RHY01-09	Postglacial	Dacite	68.53	463	–0.20	0.10	0.02	–0.11	0.11	0.02	20
Afar											
DF28-08	~300 k.a.	Rhyolite	75.05		–0.19	0.05	0.02	–0.08	0.02	0.01	22
DF29-07	~300 k.a.	Rhyolite	74.72		–0.16	0.03	0.03	–0.09	0.03	0.01	41
DAB05-02	2005 A.D.	Rhyolite	73.20		–0.12	0.10	0.03	–0.07	0.05	0.01	15
DF28-05	29.6 ± 5.3 k.a.	Basalt	46.64		–0.29	0.15	0.05	–0.16	0.07	0.03	11
Badi 05	25.4 ± 9.4 k.a.	Basalt	48.80		–0.28	0.05	0.01	–0.13	0.02	0.01	22
DFMH-07	2007 A.D.	Basalt	48.34		–0.31	0.05	0.01	–0.17	0.06	0.01	22
Skaergaard mineral separates											
2307		Olivine	36.28		–0.42	0.08	0.01	–0.23	0.04	0.01	30
5181		Olivine	33.20		–0.45	0.06	0.01	–0.22	0.02	0.01	31
2307		Clinopyroxene	52.00		–0.50	0.16	0.04	–0.25	0.06	0.01	21
2307		Plagioclase	55.78		–0.15	0.08	0.02	–0.07	0.02	0.01	22
5181		Plagioclase	58.08		–0.21	0.07	0.03	–0.11	0.01	0.01	20
USGS standards											
BHVO-2		Basalt	49.90		–0.29	0.09	0.01	–0.14	0.08	0.01	188
AGV-2		Andesite	59.30		–0.21	0.07	0.02	–0.10	0.03	0.01	11
GSP-2		Granodiorite	66.60		–0.19	0.10	0.03	–0.11	0.03	0.01	11

Silicon isotope data for all samples used in this study. SiO_2 (wt.%) and Ba (ppm) are also provided, as these are referred to in this text. Other elemental data for the Hekla samples is available in the Electronic annex EA-1. The ages for the Hekla samples were established using sample localities from Sigmarsson et al. (1992); although historic flows were easy to locate, the tephra samples were less so and, as such, the ages should be regarded as estimations. Repeat sample HEK07-09c was powdered in a steel mill, providing an assessment of possible sample contamination from the standard agate milling process.

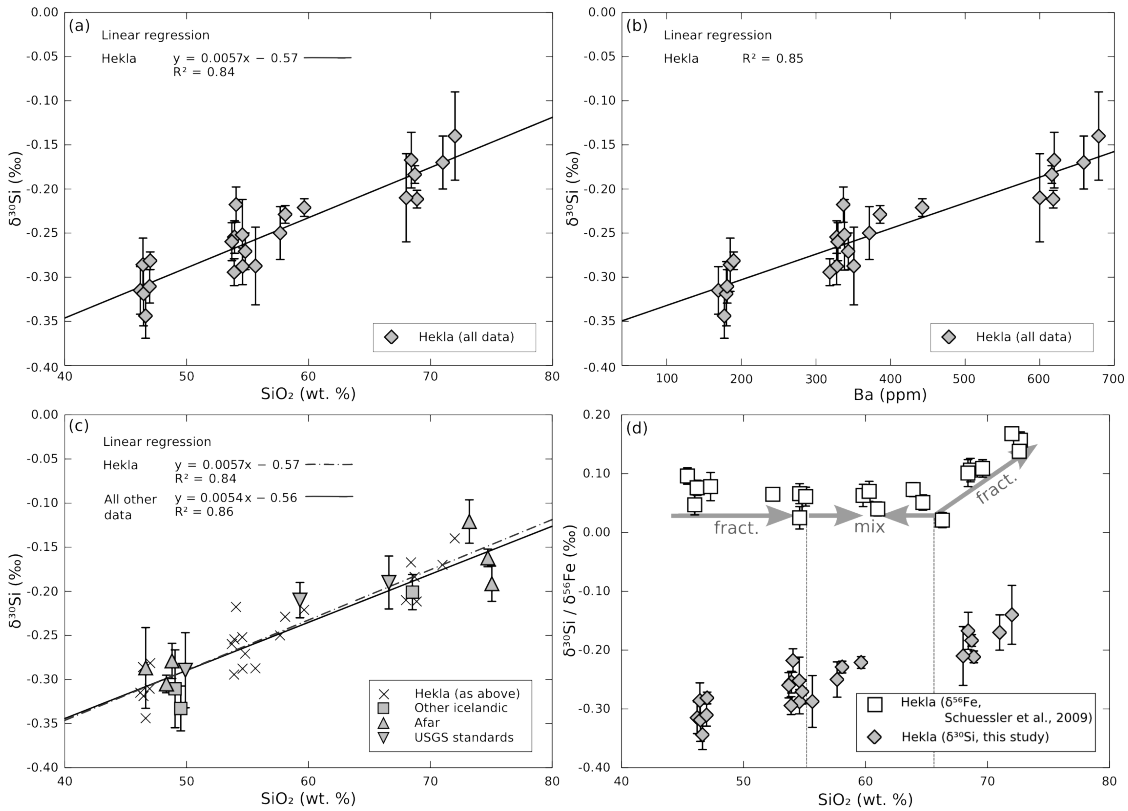


Fig. 4.5 (a and b) Graphs of $\delta^{30}Si$ vs. SiO_2 and Ba of the Hekla samples analysed in this study, showing a strong positive relationship between Si isotopes and proxies for magmatic differentiation, with more evolved samples displaying heavier isotopic compositions. (c) Graph of $\delta^{30}Si$ vs. SiO_2 of the Afar, USGS standards and other Icelandic samples used in this study. The range and trend of the data are extremely similar to that described by the Hekla data (shown for comparison). (d) Graph as in Fig. 5a, with $\delta^{56}Fe$ data for Hekla also plotted (Schuessler et al., 2009). The Fe data show fractionation at the most evolved end of the array (ascribed to fractional crystallisation) whereas the Si isotope data exhibit a continuous gradual enrichment of the heavier isotopes, through both fractional crystallisation and mixing regimes. Error bars are 95% s.e., linear regression statistics were calculated using Gnumeric (http://projects.gnome.org/gnumeric/).

consistent with heavier Si isotopes favouring the more polymerised phase, as theorised by Grant (1954). Assuming that plagioclase will have a similar isotopic composition to quartz (given their respective degrees of polymerisation and corroborated by analyses by Georg, 2006), our data agree well with the fractionation factors calculated by Méheut et al. (2009) for quartz-enstatite and quartz-forsterite (viz. ~0.3 ‰ at ~1000ºC).

Méheut et al. (2009) also predict that enstatite should be isotopically lighter than forsterite, by a small degree. Similarly, Georg et al. (2007) measured small variations between olivine and clinopyroxene, on the order of $\Delta^{30}Si_{CPX\text{-}OL}$ = -0.06 to -0.11 ± 0.05 ‰ (2 s.e.). The negative offset in $\delta^{30}Si$ that we observe between olivine and clinopyroxene agrees with both of these studies.

The possible effects of fractional crystallisation on the Si isotope composition of a

coexisting magma (taking into account the above results) will be considered further in the discussion.

4.5 DISCUSSION

4.5.1 Silicon isotope fractionation in the Hekla volcanic suite

The average values for the basalts and basaltic andesites from Hekla are close to the Si isotopic composition of BSE reported in previous research ($\delta^{30}Si_{BSE}$ = -0.29 ± 0.08 ‰, Chapter 3). The evolution to heavier isotopic values to reach a "rhyolitic" Si isotopic composition that is resolvably different to that of BSE demonstrates that there is some process or combination of processes that are fractionating Si isotopes during the magmatic differentiation in the Hekla magma chamber. Given such strong linear relationships between $\delta^{30}Si$ and SiO_2 (Fig. 4.5a and c), as well as other proxies for magmatic differentiation, for example Ba (Fig. 5b) and Mg# (not shown), we explore the extent to which the observed range in Si isotopes in the Hekla volcanic suite can be explained in terms of magmatic differentiation processes, as discussed in detail below.

4.5.1.1 Ruling out non-magmatic causes of silicon isotope fractionation

The magnitude of Si isotope fractionation is much larger during low-temperature processes than at mantle temperatures, so it is prudent to assess what contribution these processes might make to the isotopic trend seen on Hekla. The large number of previous studies can help place constraints on the types of secondary processes that may have affected Si isotope compositions during magmatic differentiation at Hekla.

Very little deviation from typical mantle values are seen in Sr and Nd isotopes at Hekla (Sigmarsson et al., 1992), suggesting that even after assimilation of crustal metabasalt or metagabbro, alteration was either limited or recent enough so as not to perturb the radiogenic isotopic values. In particular, $^{87}Sr/^{86}Sr$ ratios in geothermal fluids and hydrothermally altered rocks are much higher than in pristine mantle rocks (Elderfield and Greaves, 1981) – the similarity between Hekla $^{87}Sr/^{86}Sr$ data with other pristine Icelandic basalts argues against any large scale contamination by such enriched material.

Also in Sigmarsson et al. (1992), stable oxygen isotope data from Hekla are shown to be remarkably constant, with $\delta^{18}O$ between +4.5 and +5.3 ‰. These are slightly lower than mantle

values ($\delta^{18}O$ = +5.5 ± 0.7 ‰; Mattey et al., 1994), which could suggest contamination by a source affected by hydrothermal alteration (Hemond et al., 1993). However, low-$\delta^{18}O$ lavas are a common feature on Iceland, and the lack of other geochemical evidence to support an altered component in many pristine samples has led some authors to suggest that low-$\delta^{18}O$ is a characteristic feature of the Icelandic plume (Thirlwall et al., 2006). Although they cannot rule it out, Thirlwall et al. (2006) note that the constancy of the Hekla $\delta^{18}O$ values over time is unlikely to be generated by contamination from the lower crust. Sigmarsson et al. (1992) also report a general enrichment of the heavier isotopes of oxygen with increasing SiO_2 content, which is more consistent with equilibrium fractionation as a result of fractional crystallisation.

Although there is no hydrothermal system associated with volcanic activity at Hekla, exsolution of fluids from the melt could affect the Si isotopic composition during magmatic differentiation, as there is evidence that such processes can fractionate Fe isotopes (Heimann et al., 2008). In their stable isotope study of Hekla, Schuessler et al. (2009) addressed this possibility using Li concentrations and isotopic analyses. Lithium is a moderately incompatible, fluid-mobile element ($D_{fluid/melt}$ >>1), so fluid exsolution would be recorded by a drop in Li concentrations over the differentiation sequence. In their Hekla samples, Li content increases linearly with increasing SiO_2, which is consistent with Li behaving incompatibly during magmatic differentiation, without loss due to fluid segregation.

In addition, the Li isotopic values from the complete sequence of Hekla rocks are remarkably constant, displaying similar isotopic values to other Icelandic rocks (Jeffcoate et al., 2007) and also the upper mantle $\delta^{7}Li$ value (e.g. Tomascak et al., 2008). Both experimental results and fluid inclusion analyses indicate that Li isotopes undergo resolvable fractionation between silicate melts and supercritical fluids at magma chamber conditions (Teng et al., 2006; Wunder et al., 2006, 2007; Schuessler et al., 2009). Given the susceptibility of Li isotopes to high temperature fluid interaction, as well as hydrothermal alteration (Chan et al., 2002), diffusion (Lundstrom et al., 2005) and/or assimilation of metasomatised material (Rudnick and Ionov, 2007), the constancy of the values from Hekla are good evidence that such processes can only have played minor roles in the volcanic system.

Lastly, a qualitative assessment can be made from the positive correlation between $\delta^{30}Si$ values and SiO_2 content. Secondary mineral formation typically enriches the product in the lighter isotopes of Si (e.g. Ziegler et al., 2005a,b) – therefore, assimilation of such material

would drive the isotopic composition of the final rock towards lighter values. The isotopic trend we see recorded at Hekla is toward heavier values as SiO_2 increases, even over the "mixing" regime (Fig. 4.5d), where assimilation of altered country rock might generate unpredictable $\delta^{30}Si$ values, and would not provide such a systematic trend as we see. Therefore, it does not seem likely that secondary mineral formation has not affected Si isotopes on Hekla.

Although it is noted above that Si does not readily form volatile compounds, it can react with HF to form the gaseous (at standard temperature and pressure) compound SiF_4, via the reaction:

$$SiO_2 + 4HF = SiF_4 + 2H_2O$$

Poor precision Si isotopic measurements for samples digested in HF have been attributed to volatile loss of SiF_4 during sample introduction to the mass spectrometer (Georg et al., 2006b), and so it is possible that removal of Si from volcanic systems via this process might lead to kinetic fractionation of Si isotopes. Here we assess this possibility.

The stability of SiF_4 (expressed as the ratio of the partial pressures of HF and SiF_4: P_{HF}/P_{SiF4}) in volcanic gas budgets is controlled by overall pressure, temperature and partial pressure of HF (Rosenberg, 1973). At the conditions present in the Hekla magma chamber, $P_{HF}/P_{SiF4} \sim 10{,}000$, i.e. the total amount of SiF_4 is not significant (de Hoog et al., 2005). Because the stability of SiF_4 is inversely related to temperature, large amounts of the gas are generally only detected at volcanoes where long-lived fumarolic activity is ongoing, and gas temperatures are <400ºC (Francis et al., 1996). Although Hekla lavas are known to have high concentrations of fluorine, there is a distinct absence of fumarolic activity on the volcano.

Moune et al. (2007) show that the Hekla magma is not F-saturated and that exsolution of F from the magma does not occur, even as melt inclusions begin to form. Assuming that exsolution of F and consequent reaction with Si is necessary for any isotopic fractionation to occur, we conclude that it is unlikely that formation of SiF_4 has affected the Si isotopic compositions of our Hekla samples. It is possible that this process is detectable from the Si isotopes compositions of samples from localities associated with significant SiF_4 output, such as Vulcano, Italy (Francis et al., 1996) and this merits further investigation.

4.5.1.2 Silicon isotope fractionation from igneous processes

From the above arguments, we conclude that only high temperature, igneous processes involved in magmatic differentiation can explain the range in Si isotope compositions of the Hekla magmas. The question then is whether the degree of fractionation can be attributed to equilibrium processes, such as fractional crystallisation, or diffusion-related kinetic processes. The magnitude of equilibrium isotopic fractionation decreases with increasing temperature and many stable isotope systems, such as Li (Tomascak et al., 1999) and Mg (Teng et al., 2007), do not show any isotopic variation related to magmatic differentiation, whereas there is experimental evidence that kinetic isotope fractionation can occur at mantle temperatures (cf. Richter et al., 2009a). Because the mass-dependent slopes for kinetic and equilibrium Si isotope fractionation are so similar at low fractionation degree, we cannot use this parameter to assess fractionation behaviour and so these various processes and evidence for or against them are discussed below.

Isotopic fractionation driven by chemical diffusion (that is, chemical flux over a compositional gradient) has been demonstrated in a number of isotope systems, such as Li, Mg and Ca (Richter et al., 2003; Watkins et al., 2011). Evidence for a zoned magma chamber (Sigmarsson et al., 1992) implies that such a process could take place at Hekla. However, there is no evidence that Si isotopes can be fractionated by chemical diffusion – Richter et al. (1999), using GeO_2 as a proxy for SiO_2, found no resolvable isotopic fractionation in chemical diffusion experiments. They also note that, even if their proxy underestimated the susceptibility of Si isotopes to chemical diffusion, SiO_2 gradients large enough to encourage isotope fractionation in this way rarely exist in natural systems. Finally, the constancy of Li isotopes across the differentiation sequence on Hekla (see above) preclude the possibility of kinetic isotope fractionation due to chemical diffusion.

Thermal (Soret) diffusion (driven by a temperature gradient) is another means to generate kinetic isotope effects (e.g. Huang et al., 2010) and there is evidence to suggest that Si isotopes can be fractionated by this process (Richter et al., 2009b). So far, in all experiments and all multi-isotopic systems, the heavier isotopes are consistently enriched toward the cold end of the system. The Si isotope trend seen on Hekla could therefore be consistent with thermal diffusion-controlled isotopic fractionation, whereby $\delta^{30}Si$ increases with decreasing depth, with the colder, more felsic material at the top of the magma chamber displaying the heaviest Si

isotope signatures. However, there are a number of arguments that rule out this process.

Firstly, of the major stable isotope systems to be affected by thermal diffusion, Si shows the lowest magnitude of fractionation, with Fe and O displaying, respectively, two and three times larger effects (Richter et al., 2009b). The small variations noted in both O and Fe isotopes on Hekla suggest that any fractionation as a result of thermal diffusion is minor for Si isotopes. Also, in thermal diffusion experiments, the magnitudes of fractionation between two isotopic systems are linearly correlated (Fig. 6 in Richter et al., 2009b); this is not the case between Si isotopes and other isotopic systems on Hekla. It is also unclear how these experiments can be applied to a magma chamber, as they were made on a homogeneous material, which was not affected by fractional crystallisation, assimilation or chemical diffusion, that would otherwise perturb the mass flux generated by a thermal gradient.

Secondly, the time scale necessary to generate thermal diffusion isotopic fractionation in a large magma chamber is probably on the scale of millions of years (Lundstrom, 2009) whereas eruptions producing isotopically fractionated material from Hekla have occurred at a rate of between tens (recent) and thousands (prehistoric) of years. This also assumes that the magma chamber model is correct for Hekla; if instead, as Chekol et al. (2011) suggest, magma differentiation occurs in small, discreet pods at varying crustal depths, then large temperature variations (>100ºC) may not be present to drive kinetic isotope fractionation.

We conclude then, that kinetic effects are unlikely to be controlling the Si isotopic composition of the Hekla volcanic suite, and so equilibrium processes are the predominant cause of isotopic fractionation. This is in agreement with other studies of stable isotopic variations on Hekla, which attribute isotopic variations to fractional crystallisation (see above; Sigmarsson et al., 1992; Schuessler et al., 2009). However, in contrast to the $\delta^{18}O$ and $\delta^{56}Fe$ data, the Si isotopic compositions of the Hekla lavas become gradually heavier over the whole range of SiO_2. In Figure 4.5d, we can see that this occurs in both the proposed fractional crystallisation and mixing regimes, i.e. a simple relationship between SiO_2 and $\delta^{30}Si$ is preserved during both the removal of solids and the partial melting of country rock followed by mixing between basaltic andesite and dacite. This assumes that the zoned magma chamber model of Sigmarsson et al. (1992) is correct although, even if magma differentiation on Hekla occurs in smaller "pods" (Chekol et al., 2011), assimilation and fractional crystallisation are still the major controls upon magma composition. We conclude that a fundamental property of the system is

controlling the Si isotope composition, and that we cannot assign the cause of isotopic fractionation to any singular cause.

Given the theoretical evidence that equilibrium Si isotope fractionation can result as a function of relative bond strengths and internal vibrational frequencies of the Si–O bonds in coexisting phases (Grant, 1954), we infer that this is the predominant control over Si isotope fractionation due to magmatic differentiation. This is because, during fractional crystallisation and/or partial melting there will almost always be differences in such properties between the solid(s) and melt phases, due to polymerisation degree, presence of other network-forming cations, etc. (Méheut et al., 2009). This discriminating factor is therefore fundamental to the Si isotopic system and, without this, it is difficult to identify what else may be the mechanism behind igneous Si isotope fractionation on Hekla.

4.5.2 The igneous array for silicon isotopes

If the relationship between SiO_2 and $\delta^{30}Si$ is fundamental to igneous rocks, then it should be apparent in other, unrelated, igneous systems, which appears to be the case. If we plot our $\delta^{30}Si$ data from the Afar rift zone, elsewhere on Iceland, and USGS standards against SiO_2, we see that they plot on an identical array to that of Hekla, with similar regression statistics (Fig. 4.5b). Although it might be expected that the Icelandic samples would fall on a similar array (given that they are generated in the same tectonic setting), it is more compelling that our data from Afar and the disparate USGS standards fall on almost exactly the same trend. Given there is isotopic evidence that crustal assimilation plays a role in the production of the rhyolitic material in the western, continental bounded edge of the Afar rift zone (Barberi et al., 1970) it is even more surprising that the Afar rhyolites fit the igneous trend, and may explain why the lightest rhyolite $\delta^{30}Si$ value in this study (DF28-08) is from this locality.

In the absence of any secondary isotopic alteration, it appears that Si isotopes behave predictably during magma differentiation, such that an ideal magmatic trend can be defined. Empirically, the $\delta^{30}Si$ value and SiO_2 content of a sample in wt.% can be related by the equation:

$$\delta^{30}Si\ (‰) = 0.0056 \times SiO_2 - 0.567\ (\pm\ 0.05\ ‰;\ 2\ \text{s.e. of the regression}).$$

Assuming this relationship is robust then, for igneous rocks, any offset of $\delta^{30}Si$ composition

from this trend could suggest that processes other than partial melting, assimilation and/or fractional crystallisation have been involved in the petrogenesis of such a sample.

4.5.3 Modelling silicon isotope variation during magmatic differentiation

Although we infer that polymerisation is the major physical control over the Si isotope composition of a sample, there still must be a process by which the SiO_2 of the magma is driven to more evolved values. Given the simple, linear, relationship between $\delta^{30}Si$ and SiO_2, we have modelled the evolution of silicon isotopes in a magma chamber as a function of fractional crystallisation. We assume a constant bulk isotopic fractionation factor ($\Delta Si_{solid\text{-}melt}$) between melt and solids, based on the amount of melt remaining in the system and that once removed, the solids do not re-equilibrate with the liquid (Rayleigh fractionation). Sample HEK07-09 is used as the starting composition, as it has the highest MgO content and lightest $\delta^{30}Si$ composition. Figure 4.6 shows liquid isotopic evolution trends for a number of $\Delta Si_{solid\text{-}melt}$ values.

The data from Hekla are plotted on the same graph, using Ba as a proxy for the fraction of melt remaining (assuming Ba is highly incompatible during crystallisation). This estimate suggests that ~45 % crystallisation takes place to form the basaltic andesites from the most primitive basalt – Chekol et al. (2011) obtain a similar value of 42 % using least squares modelling of major elements, adding confidence to the approach adopted. Also, using K_2O concentrations instead of Ba gives comparable results. Our model shows that a bulk $\Delta Si_{solid\text{-}melt}$

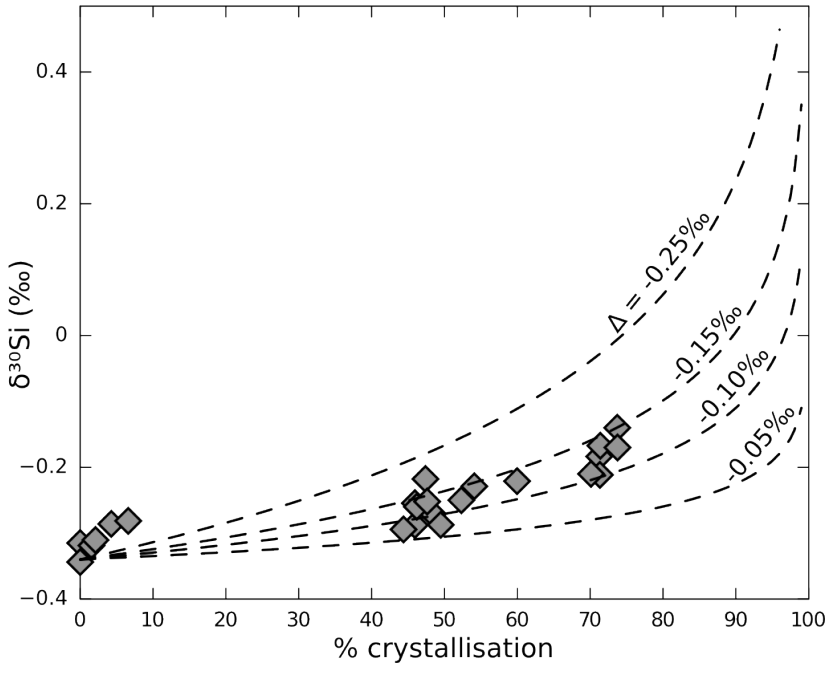


Fig. 4.6 Rayleigh fractionation models of Si isotope evolution in a magma chamber, assuming a constant bulk fractionation factor between solid and melt. Curves are for different bulk fractionation factors (curve labels = $\Delta Si_{solid\text{-}melt} \sim 1000 \cdot \ln\alpha_{solid\text{-}melt}$). Sample HEK07-09 was used as the starting melt composition. The measured data are shown (grey diamonds), using Ba as a proxy for melt fraction and show that a bulk $\Delta Si_{solid\text{-}melt}$ value of ~ −0.125‰ can describe the system at Hekla, and by inference, the igneous Si isotope system. Using K as a proxy for melt fraction yields a similar bulk $\Delta Si_{solid\text{-}melt}$ value.

value of ~ -0.125 ‰ can describe the system at Hekla, and by inference, the igneous Si isotope system.

The relationship between SiO_2 and $\delta^{30}Si$ also suggests that, assuming similar proportions of metasediment, the Si isotope composition of the lower crust will be isotopically light relative to bulk crust due to the presence of restite, mafic and ultramafic cumulates. Thus far, however, no ultramafic rocks have been reported with any resolvable isotopic difference from mafic rocks (e.g. Fitoussi et al., 2009; Chakrabarti and Jacobsen, 2010; Savage et al., 2010).

4.5.4 Modelling silicon isotope fractionation as a result of fractional crystallisation

Using the isotopic analyses of the Skaergaard mineral separates, the effect that fractional crystallisation might have on the Si isotope composition of a magma system can be modelled. Although on Hekla, and in many other systems, partial melting and assimilation are also critical processes during differentiation, for Si isotopes it is here assumed that all these processes will be analogous in the absence of metasediment or altered wall rocks. The model assumes Rayleigh fractionation and constant isotopic fractionation factors between mineral and melt. Fractionation factors were calculated assuming Skaergaard minerals had precipitated from a mafic liquid whose Si isotope composition was that of BSE (Chapter 3; $\delta^{30}Si$ = -0.29 ‰), and are as follows: $\Delta^{30}Si_{olivine\text{-}melt}$ = -0.15 ‰; $\Delta^{30}Si_{clinopyroxene\text{-}melt}$ = -0.21 ‰; $\Delta^{30}Si_{plagioclase\text{-}melt}$ = +0.11 ‰. The starting composition of the melt was set at $\delta^{30}Si$ = -0.34 ‰, the lightest isotopic composition analysed in this study (HEK07-09). Figure 4.7 shows the results of our model for a variety of single phase and multiple phase solid removal, as well as the measured data from Hekla.

From the models we can see that, to reach the Si isotopic composition of the most evolved material, clinopyroxene and olivine are required to be the dominant crystallising phases. Although a very unlikely scenario, formation of all three phases (olivine, plagioclase and clinopyroxene) at a constant rate gives a final melt composition of $\delta^{30}Si$ = -0.25 ‰. This is isotopically too light (curve "all phases" in Fig. 4.7). This is because plagioclase is isotopically heavy when compared to the original liquid composition, and so removal of this phase serves to balance out the removal of lighter isotopes by olivine and clinopyroxene.

It is clearly impossible that the magmas on Hekla have differentiated exclusively with the formation of clinopyroxene ± olivine, and also that all the phases considered in this model formed continuously during differentiation. Plagioclase is present in thin section and, in some

cases, as phenocrysts. It is also unlikely that there is another crystal phase to take into account (magnetite and apatite have subordinate Si concentrations). Therefore, we must reappraise our model.

One possibility is that the isotopic compositions of the mineral separates that we measured are not representative. If either olivine or clinopyroxene were to have a lighter $\delta^{30}Si$, this would help balance out the removal of "heavy" feldspar, and explain the isotopic trend. However, our model suggests that to reach "rhyolitic" $\delta^{30}Si$ values, the olivine or clinopyroxene phase must have an original isotopic value of $\delta^{30}Si \sim -0.7$ ‰, which is extremely light – such light values have not been recorded in igneous rocks by recent studies, and so this scenario is unlikely. The opposite possibility is that the plagioclase value is isotopically too heavy, although the $\Delta^{30}Si_{CPX\text{-}plagioclase}$ value measured in this study agrees well with theoretically calculated fractionation factors (Méheut et al., 2009 – assuming $\Delta^{30}Si_{quartz\text{-}plagioclase} \sim 0$, see above).

In natural systems, all the solid phases of a melt assemblage are not forming constantly during differentiation. Here, mafic phases will dominate at low SiO_2 compositions, and felsic phases at high SiO_2. Two scenarios are modelled in Figure 4.7 (curves "staggered (a)" and "staggered (b)") and are in fairly good agreement with the measured data. In scenario a, olivine is the dominant phase up to 50% SiO_2, and plagioclase starts forming at 60% SiO_2, with clinopyroxene forming constantly, whereas in scenario b, olivine crystallises up to 54% SiO_2, clinopyroxene forms between 54% and 66% SiO_2, thereafter plagioclase and clinopyroxene form in equal amounts.

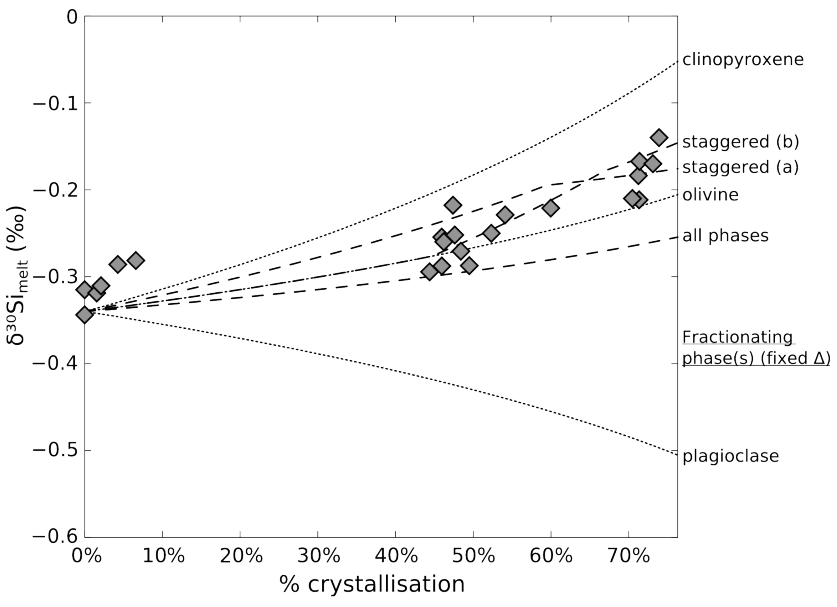


Fig. 4.7 Models of Si isotope evolution of a magma showing the effects of varying fractionating phases (olivine, clinopyroxene and plagioclase feldspar). The models assume Rayleigh fractionation and a constant isotopic fractionation factor between mineral(s) and melt. Fractionation factors were calculated using data from Skaergaard mineral separates (Table 4.2), precipitating from a liquid whose original Si isotope composition was that of BSE (Savage et al., 2010) – each curve describes a different crystallisation trend, see text for discussion. Measured data (grey diamonds) plotted as in Fig. 4.6.

In all of these calculations, we are assuming a constant fractionation factor between solid and liquid. If polymerisation degree is the discriminating factor controlling Si isotope fractionation, then this may not be the case. If the more polymerised phase concentrates the heavier isotopes, then as the liquid evolves to become more polymerised, Si isotopes would not discriminate as highly between a highly polymerised phase and such a melt. It also follows that more mafic minerals forming from that melt would have lighter $\delta^{30}Si$ values than if they have formed from a more primitive melt. Qualitatively, this will drive the liquid composition to heavier isotopic values as long as phases with a lower degree of polymerisation (relative to the melt) are forming throughout the differentiation sequence. Also, the reduction of temperature during cooling of the magma will lead to an increase in the magnitude of fractionation between phases. To test this theory would require more isotopic analyses, and is beyond the scope of this study, but is of clear importance for the further understanding of how Si isotopes fractionate.

4.5.5 The silicon isotopic composition of the continental crust

Assuming the average SiO_2 content of the continental crust is 60.6 wt.% (Rudnick and Gao, 2003), then the average "igneous" $\delta^{30}Si$ composition of the continental crust is ~ -0.23 ± 0.05 ‰, deduced from the "igneous array" equation in Section 4.5.2. This value does not take into account secondary processes such as weathering, which should, if anything, leave residual material that is isotopically light, with heavy dissolved Si being discharged to the oceans (Georg et al., 2006a). Therefore, it is more appropriate to describe this as a maximum value. If we calculate the isotopic effect removal of this "andesitic" material will have on the upper mantle, there is only a minor effect ($\delta^{30}Si_{upper\ mantle}$ reduction of ~0.01 ‰). This is well below analytical uncertainty, and is almost certainly a maximum value as it does not take into account the whole mantle. It is therefore unlikely that removal of material to form continental crust from the mantle will affect the Si isotope signature of BSE.

4.6 CONCLUSIONS

1. Silicon isotope analyses of samples from the volcano of Hekla, Iceland, as well as other localities, show that a strong linear relationship exists between degree of differentiation (SiO_2 content) and $\delta^{30}Si$. Existing studies imply that only igneous processes, that is, assimilation, partial melting and fractional crystallisation, can be the major cause of

fractionation in these samples. The magnitude of isotope fractionation between the basaltic and rhyolitic end members is $\Delta^{30}Si$ ~0.20 ‰.

2. Silicon isotopes behave predictably during magmatic differentiation and an "ideal" igneous trend can be established. Empirically, the $\delta^{30}Si$ value and SiO_2 content of a sample can be related by the equation:

$$\delta^{30}Si\ (‰) = 0.0056 \times SiO_2 - 0.567\ (\pm\ 0.05\ ‰;\ 2\ s.e.)$$

3. A bulk fractionation model suggests that the igneous Si isotope system can be described by a $\Delta^{30}Si_{solid\text{-}melt}$ value of ~ -0.125 ‰. This also suggests that corresponding "light" cumulates should exist in the crust, unless these are recycled back into the mantle, although no direct evidence of this has yet been found.
4. Isotopic analysis of mineral separates and further modelling indicate that removal of isotopically light phases such as olivine and clinopyroxene can go some way to explaining how igneous processes can drive magma composition to heavier, "rhyolitic" isotopic values. However, formation and removal of plagioclase feldspar will counteract this process. We propose that variable fractionation factors between the major partitioning phases and the melt, as a function of temperature and/or relative polymerisation degree between phases can explain the disparity between our model and our measured isotopic data.
5. Despite there being a measurable fractionation of Si isotopes during igneous processes, removal of material from the mantle to form the crust is unlikely to resolvably affect the Si isotope signature of the mantle. The "igneous" estimate of the Si isotopic composition of the continental crust is $\delta^{30}Si$ ~ -0.23 ‰, assuming an "andesitic" crustal composition. This does not take into account the myriad different processes that further the evolution of continental crust, and is therefore not a definitive value.

ACKNOWLEDGEMENTS

The authors thank Dave Ferguson for the Afar samples, and Dave Waters and the Oxford Natural History Museum for the Skaergaard samples that were analysed in this study. We would like to extend our gratitude to all the staff at the Institute of Earth Sciences, University of Iceland and particularly Karl Grönvold, who advised us on sample location and accessibility for the Hekla suite. We thank Ros Armytage and Julie Prytulak for helpful discussion and useful

suggestions along the way. The authors would also like to thank Nick Belshaw, Teodor Krastev, Steve Wyatt and John Watson (Open University) for invaluable technical assistance and support. Comments and suggestions made by Jan Schuessler, two anonymous reviewers and associate editor Clark Johnson greatly honed and improved the manuscript. This work was funded by a NERC CASE studentship supported by Nu Instruments.

Chapter 5: The silicon isotope composition of granitoid rocks

ABSTRACT

Despite their importance in the weathering cycle and ubiquity in the upper continental crust, little information exists on the Si isotopic composition and systematics of granitoid rocks. In principle, granites derived from a sedimentary source should be isotopically light, as weathering enriches sediment in the lighter Si isotopes (e.g. Ziegler et al., 2005a&b), whereas granites derived through igneous processes should be isotopically heavier. Previous work has suggested that relatively large Si isotopic variations exist in granitoid rocks compared to other igneous material, but no systematic differences between granite types have been found (Douthitt, 1982; Ding et al., 1996). Here we revisit this problem with the benefit of more precise techniques and investigate the Si isotopic record of granite petrogenesis, by analysing a representative suite of over 30 Phanerozoic I-, S- and A-type granitoid samples and mineral separates, mainly from Australia, as well as some samples of associated country rocks.

The whole-rock granite data fall between $\delta^{30}Si$ = -0.40 and -0.11 ± 0.04‰ (95% s.e.). This range is more limited than that defined by previous low precision measurements of granitoid material, but is far broader than for more recent, high precision, measurements of high-Si igneous rocks (rhyolites and dacites) from Iceland and Afar (Chapter 4). Although S-type granites are, on average, lighter than I- and A-type granites there is considerable overlap between the groups. Strong negative correlations with alumina saturation index (ASI) values and initial $^{87}Sr/^{86}Sr$ provide evidence that Si isotopic variation in granites can be explained by variable incorporation of an enriched sedimentary component. The average Si isotope value of all granites analysed in this study is $\delta^{30}Si$ = -0.23 ± 0.15 ‰ (2 s.d.), which is entirely consistent with the "igneous" value of continental crust published previously (Chapter 4).

5.1 INTRODUCTION

Granites (and related felsic lithologies) constitute ~50% of the mass of the upper continental crust (Wedepohl, 1995) but are too Si-rich to be in equilibrium with the mantle (Rudnick, 1995) – that is, much of the continental crust cannot have formed through simple mantle melting events. Therefore, there must be some other process or combination of processes such as further differentiation of basaltic igneous material or crustal melting to form evolved melts. The array of likely processes include the following:

i. fractional crystallisation of primitive mantle melts;

ii. partial melting of basaltic crust;
iii. anatexis of crustal sediments;
iv. mixing of magmas of various provenances (derived from processes i-iii).

Processes involving fractional crystallisation ultimately drive the continental crust toward more Si-rich compositions by the subsequent delamination of dense ultramafic cumulate material back into the mantle (e.g. Rudnick, 1995). Anatexis of crustal material that has already experienced supracrustal weathering can also impart a high-Si signature, because weathering enriches the residue in relatively insoluble elements, such as Si and Al, resulting in a fluid phase that is rich in Mg, Ca etc., which eventually enters the ocean (Albarede and Michard, 1986). Therefore, formation of granitoid rocks can involve both primitive, mantle-derived components and/or evolved crustal material. Identifying the provenance of such rock is important, because mantle-derived granites represent new volumes of continental crust.

The Si isotope system has the potential to differentiate between granites of mantle and sedimentary provenance, as follows. Silicon isotopic fractionation is limited in the igneous realm, relative to that generated as a result of low-temperature, secondary or biogenic processes. The $\delta^{30}Si$ value of Bulk Silicate Earth (BSE) is -0.29 ± 0.08 ‰ (Fig. 5.1; Chapter 3) and studies show that mafic and ultramafic igneous rocks show little variation from this value (e.g. Chapter 3; Fitoussi et al, 2009; Zambardi et al., 2009; Armytage et al., 2011). In contrast to many stable isotope systems, which show little resolvable isotopic fractionation as a result of high-temperature igneous processes, i.e. Mg (Teng et al., 2007) or Li (Tomascak et al., 1999), there is resolvable, equilibrium-controlled Si isotopic fractionation during magmatic differentiation, whereby an increase in SiO_2 content is accompanied by a concentration of the heavier Si isotopes (Fig 5.1; Chapter 4). The magnitude of fractionation between the basaltic and rhyolitic end members is $\Delta^{30}Si \sim 0.20$ ‰. Crucially, this enrichment appears to be a fundamental property of the Si isotope system, such that $\delta^{30}Si$ composition varies linearly with SiO_2 content and an ideal "igneous trend" for Si isotopes can be established. This means that, for a given SiO_2 content, an "igneous" $\delta^{30}Si$ composition can be calculated. It is hypothesised, therefore, that granites derived by melting or differentiation of igneous materials should have Si isotopic values that lie on or close to this "igneous trend", comparable to the isotopic compositions of dacites and rhyolites ($\delta^{30}Si \sim -0.21$ to -0.12 ‰).

In contrast, granites derived from anatexis or assimilation of meta-sedimentary rocks

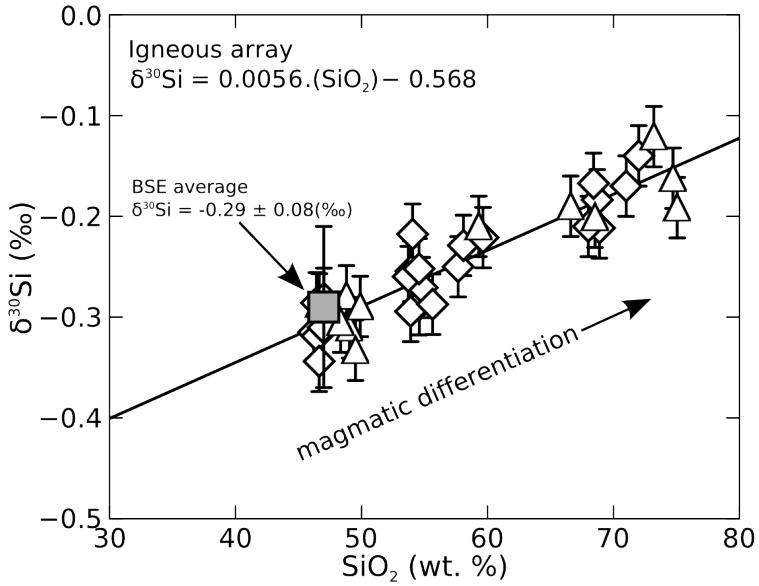


Fig. 5.1 Plot of $\delta^{30}Si$ vs. SiO_2 displaying the "igneous array" for Si isotopes (Chapter 4) defined by analysis of a suite of cogenetic rocks from the volcano of Hekla, Iceland (diamond symbols) and various other volcanic igneous samples (triangle symbols). Magmatic differentiation enriches more silica-rich samples in the heavier isotopes. Also shown is the Si isotope value for Bulk Silicate Earth (BSE, square symbol, Chapter 3).

should not be expected to lie on the igneous trend. The supracrustal Si isotope system is comparatively well-studied and it is established that low temperature equilibrium processes result in relatively large isotopic fractionation; clay minerals and other secondary phases are isotopically light (Ziegler et al., 2005a&b; Georg et al., 2009a). Therefore, sedimentary rocks containing clays formed by weathering will have a lighter Si isotope composition than their unweathered protolith material (Fig. 5.2). This is corroborated by published data for sedimentary rocks, which have an overall lighter and wider range of $\delta^{30}Si$ values than igneous rocks (Fig. 5.2; Douthitt, 1982; Ding et al., 1996). Although the amount of fractionation can be variable, and is predominantly a function of weathering intensity, temperature and fluid composition, we anticipate that granites formed via anatexis of sedimentary material should have lighter and more variable Si isotopic compositions than granites formed by melting or differentiation of mantle derived igneous materials.

The idea that Si isotopes may differentiate between granites of different protoliths is not novel, and has already been tested by Douthitt (1982) by analysing a suite of I- and S-type granites from the Lachlan Fold Belt (LFB), Australia. The results show that both granite types have a large range of $\delta^{30}Si$ values (-0.8 to +0.3 ‰) and that there are no systematic isotopic variations between granites that have igneous or sedimentary affinities (Fig. 5.2). However, the method precision (up to ± 0.6 ‰) is no longer state of the art, so revisiting this problem using much improved and more precise analytical techniques as well as a larger sample set is timely.

Other non-traditional stable isotope systems have also been applied to granitoid rocks,

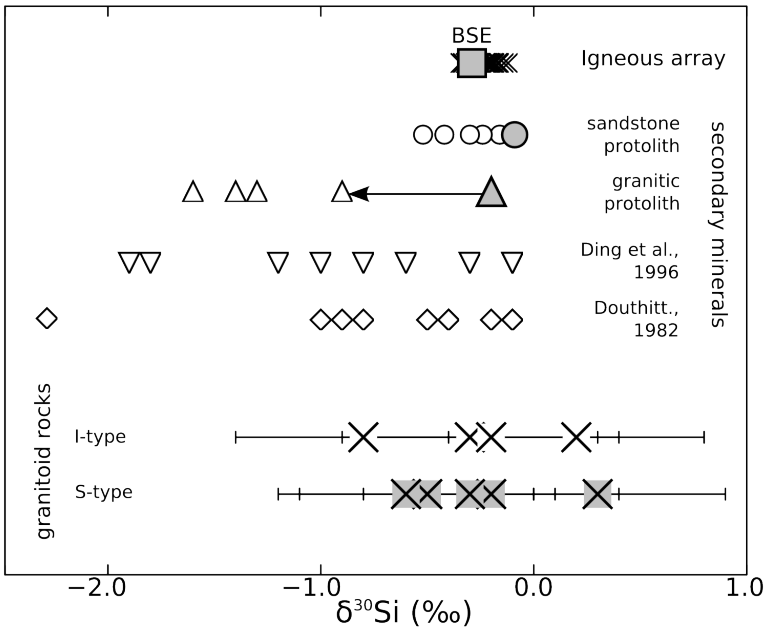


Fig. 5.2 Selection of clay mineral and whole rock data from various sources in the literature, showing that chemical weathering enriches the product in the lighter isotopes of Si. Sandstone protolith data are taken from Georg et al., 2009a; granitic protolith data are taken from Ziegler et al., 2005a&b. Also shown are the I- and S-type granite analyses from Douthitt (1982); this work suggests that, although granites can have a large range of isotopic compositions, Si isotopes do not differentiate between the two types. The data from Figure 1 is given for comparison.

where isotopic variations related to source heterogeneity might be expected, with mixed results. In their study of the Li isotope composition of the upper continental crust, Teng et al. (2004) show a limited range of δ^7Li values in I- and S-type granites from the LFB, with no distinction between granites of different affinities. Heavy Fe isotope compositions, relative to mantle values, have been measured in high-silica granites from various localities (Poitrasson and Freydier, 2005) but this offset is related to isotopic fractionation between melt and an exsolving late magmatic fluid, which preferentially removed the lighter isotopes, rather than source variation. As with the Li study, stable Mg isotopes do not appear to distinguish between I- and S-type granites of the LFB (Li et al., 2010), with both groups showing little variation away from mantle values. However, Mg stable isotopes in granites from China (Li et al., 2010) and California (Shen et al., 2009) appear to reflect, in both cases, mixing between juvenile, mantle-derived material and an evolved (weathered) crustal source. Whether Si isotopes will be useful in this respect is a major question posed by this study.

To investigate the Si isotopic systematics of granitoid rocks, we have analysed a representative suite of samples including I-, S- and A-type granites, pegmatites and aplites from Australia and south-west England. We have also analysed a selection of country rock samples to assess source compositions, as well as a suite of typical granitic mineral phases to investigate isotopic fractionation as a result of fractional crystallisation. Our aims are to examine whether the large range of Si isotopic data seen in granites by Douthitt (1982) is real or an analytical

artifact, assess whether Si isotopes distinguish between granites of various affinities and evaluate how Si isotopes behave during granite formation. As well as providing a framework for Si isotope systematics in granites, we also aim to provide an estimate for the igneous component of the upper continental crust.

5.2 SAMPLES

5.2.1 I- and S-type granites from SE Australia

The Lachlan Fold Belt (LFB) is an area of extensive granitic plutonism located in south-eastern Australian. Granite emplacement is related to the Lachlan orogen, the result of a palaeo-convergent margin along the eastern margin of Gondwanaland present during the early Ordovician to Devonian (Foster and Gray, 2000). The pioneering work of Chappell and White (1974, 2001) noted that, on the basis of mineralogical and major element analysis, most of the granites in the LFB could be split into two constrasting types, which they termed I- and S-type.

I-type granites are metaluminous or weakly peraluminous, hornblende-bearing, and have ASI values < 1.1 (Alumina Saturation Index = molar [Al_2O_3 / (CaO + Na_2O + K_2O)]; Shand, 1927) and high CaO contents and Ca/Na ratios. Some plutons are coeval with basaltic intrustions and/or contain igneous-textured enclaves. On the basis of this evidence, these rocks are inferred to have formed from a predominantly igneous or meta-igneous protolith that has not undergone major continental weathering, hence I-type (Igneous or Infracrustal).

S-type granites, by contrast, are peraluminous (ASI > 1.0), often cordierite-bearing in the LFB, depleted in soluble elements such as Na, Ca and Sr and enriched in Pb relative to I-type rocks. S-type rocks often contain meta-sedimentary enclaves, some of which are of a higher metamorphic grade (often to migmatites) than the country rock (Fleming, 1996; Maas et al., 1997). Therefore, S-type granites have been assigned a Sedimentary, or Supracrustal, source that has a pelitic affinity.

Despite their discrete sources, granites from the LFB often show compositional overlap, which challenges the simplistic I- and S-type classification. Trace element patterns from both groups are very similar (e.g. Collins, 1998) and, most notably, plotted on an εNd vs. initial $^{87}Sr/^{86}Sr$ diagram, I- and S-type granites from the LFB appear to fall on a single hyperbolic array (McCulloch and Chappell, 1982). Many authors have suggested this indicates that, rather than I- and S-type granites forming from discrete protoliths, granite petrogenesis in the LFB is a result

of large scale mixing between two or three isotopically distinct sources (e.g. Gray, 1984; Keay et al., 1997). The models invoke mixing between a primitive depleted mantle component (which is completely absent in the original model) and the ubiquitous Ordovician marine turbidite sequences present as country rock in the LFB (Wyborn and Chappell, 1983). A third component, meta-igneous Cambrian basement (Nelson et al., 1986) which underlies the turbidites, is also sometimes invoked.

This model is particularly useful in explaining why some LFB I-type granites have enriched Sr, Nd and O isotopic compositions, which indicates some component of sedimentary protolith and, likewise, why some S-type granites are relatively primitive. Coupled Hf-O isotopic analysis on zircons from the LFB also indicate that both magmatic and enriched crustal sources are involved in I-type granite petrogenesis (Hawkesworth and Kemp, 2006). However, despite the agreement with isotopic data, simple mixing models cannot adequately replicate the bulk rock compositions of the LFB granites (e.g. Chappell, 1996). Hence, the topic of LFB granite petrogenesis can often be contentious (cf. Collins, 1998, and subsequent replies).

We have analysed a number of I- and S-type granites from across the LFB. All samples were collected away from weathering surfaces and are well characterised for major and trace elements as well as isotopic studies (O'Neil and Chappell. 1977; McCulloch and Chappell, 1982; Chappell et al., 1990; Gray 1990; Chappell et al., 1991; McCullouch and Woodhead, 1993). These samples and localities are described in more detail below.

5.2.1.1 Bega and Moruya batholiths

Six I-type samples were analysed from the Bega (425 – 395 Ma) and Moruya (395 – 389 Ma) batholiths. These batholiths outcrop toward the eastern margin of the LFB, where the meta-sedimentary pile is thought to be thin or absent (Collins, 1998) and, as such, the majority of the granites from these batholiths have I-type affinities. The samples are taken from 6 of the 7 supersuites recognised in this area (Moruya, Cobargo, Glenbog, Tonghi, Candelo and Bemboka; Chappell et al., 1991) and display a range of SiO_2 contents (65 – 73 wt. %; Table 1). The samples also display a range of initial εNd (+3.0 to -6.4) and initial $^{87}Sr/^{86}Sr$ values (0.704 to 0.709), which may indicate the involvement of a non-juvenile source. Within this sample set, the Moruya sample displays the most primitive radiogenic Sr and Nd isotopic signatures analysed from the LFB in this work.

5.2.1.2 Berridale batholith

Eight samples were analysed from the Berridale (428 – 410 Ma) batholith. This batholith is located toward the centre of the LFB, is comprised of approximately equal volumes of I- and S-type granites and straddles the so-called IS-line (White et al., 1976), east of which S-type granites become increasingly rare. As such, one could think of the Berridale granites as transitional, although granites with strong I- and S-type affinities do outcrop in the batholith.

Five S-type granites were chosen for analysis from the Berridale batholith, which are representative of the three identified S-type suites (Cootralantra, Dalgety and Tingaringhy; Chappell et al, 1991). These rocks sample a limited range of SiO_2 contents (67 – 73 wt. %; Table 1) and display an enriched isotopic character (initial εNd = -8.4 to -6.1, initial $^{87}Sr/^{86}Sr$ = 0.710 to 0.712, $\delta^{18}O$ = 9.2 to 10.5 ‰) consistent with derivation from a sedimentary protolith.

The I-type granites from the Berridale batholith form distinct mafic and felsic plutons; as such, one mafic (Tara, 68 wt.% SiO_2) and two felsic (Maffra and Buckley's Lake; 77 and 71 wt. % SiO_2, respectively) samples were chosen for analysis. These samples have much more primitive radiogenic isotope compositions (initial εNd = -3.2 to +0.0, initial $^{87}Sr/^{86}Sr$ = 0.705 to 0.707) than their S-type counterparts, although they do still display elevated $\delta^{18}O$ signatures (+7.9 to +9.3 ‰) relative to mantle values ($\delta^{18}O \sim +5.5$ ‰ , Mattey et al., 1994).

5.2.1.3 Wagga batholith

One S-type sample was analysed from the Wagga batholith (440 – 425 Ma). This batholith is located toward the western margin of the LFB, where the meta-sedimentary pile is thought to be thickest (e.g. Collins, 1998) and S-type granites dominate. The Wagga sample displays a strong S-type affinity, with high ASI (1.3) and radiogenic initial $^{87}Sr/^{86}Sr$ (0.716) values.

5.2.1.4 Ordovician turbidites

Four samples of Ordovician turbidite material from the Snowy Mountains, South-eastern Australia have been analysed. These are described by Wyborn and Chappell (1983) and are cited by many workers as the main sedimentary protolith for S-type granites in the LFB (e.g. Chappell, 1984; Keay et al., 1996). The samples are fresh, having been collected during tunnelling work in the Snowy Mountains, and range from quartz-rich to clay-rich greywackes

and shales, with some marine carbonate and chert bands. High quartz/feldspar ratios suggest that these samples have undergone at least two weathering cycles. The samples we have chosen span the compositional range from silica(detrital quartz)-rich to silica-poor (clay-rich).

5.2.2 New England batholith

Two samples were taken from the New England batholith (NEB), one I-type and one S-type. The New England batholith is located north-east of, and is tectonically distinct from, the LFB, forming during the New England orogen that, like the LFB, was a result of an ocean-continent convergent margin (Devonian to Triassic; Shaw and Flood, 1981). Five granite suites have been identified on the basis of mineralogical and geochemical parameters, two S-type and three I-type (Shaw and Flood, 1981).

The I-type granite is taken from the Moonbi plutonic suite (250 Ma); this suite displays typical I-type characteristics with ASI < 1.0, high Sr and Na concentrations and low initial $^{87}Sr/^{86}Sr$ (0.704 – 0.705).

The S-type sample from the NEB was taken from the Bundarra Plutonic suite (286 Ma); this suite displays many characteristics of S-type granites (high ASI values, cordierite mineralogy, heavy $\delta^{18}O$ values) but does not display the heavy initial $^{87}Sr/^{86}Sr$ ratios and negative initial εNd values that are often associated with such suites. In fact, all of the S-type granites from the NEB have relatively primitive initial $^{87}Sr/^{86}Sr$ ratios (0.706 – 0.708), similar to that of the I-type granites. Many authors have attributed this to a relatively juvenile sedimentary protolith, derived from juvenile volcanogenic sediments generated by arc volcanism associated with orogenic activity (Shaw and Flood, 1977).

5.2.3 A-type granites from SE Australia

A-type granites were first defined by Loiselle and Wones (1979) and display elemental and isotopic characteristics that imply a petrogenetic history distinct to that of I- and S-type granites. They are characterised by high SiO_2, $FeO_{(total)}$ and alkali elements, low MgO, Al_2O_3, CaO and P, high incompatible/compatible trace element ratios, low H_2O, and high F content (e.g. Whalen et al., 1987; Eby, 1990; Frost and Frost, 2011). Isotopically, they typically have low initial $^{87}Sr/^{86}Sr$ and high initial εNd (e.g. Eby, 1990). Such geochemical features tend to preclude the involvement of heavily altered or evolved (meta-igneous or sedimentary) crustal

sources in the parental magma and imply instead that petrogenesis occurred either through extreme fractional crystallisation of a basaltic magma or partial melting of quartz- and feldspar-rich granitoids. Therefore, some A-type granites (the mantle-derived specimens) may be representative of the "igneous" Si-isotopic end-member composition of the upper continental crust, analogous to the rhyolitic samples shown in Figure 5.1.

We have analysed three A-type granites from the Padthaway Ridge suite from south-eastern Australia (Turner et al., 1992). The samples are highly siliceous (SiO_2 > 74 wt.%), have low compatible trace element concentrations (Sr, Sc, Ni, Cr), high incompatible trace element concentrations (Rb, LREE, Nb), negative Eu anomalies as well as mantle-like initial $^{87}Sr/^{86}Sr$ ratios (0.703 – 0.706) and εNd values (-1.7 - -2.3). On the basis of this evidence, Turner et al. (1992) conclude that this suite formed by fractional crystallisation of a basaltic magma, with limited involvement (<10%) of a crustal component.

5.2.4 Aplites and pegmatites from South-west England

Igneous-derived aplites and pegmatites are hypabyssal lithologies, often associated with granitic bodies, that formed from volatile- and incompatible element-rich magma, often inferred to be representative of the residual melt at the final stages of crystallisation (London, 2005). Pegmatites are noted for their megacrystic texture, which is the result of high volatile and/or "flux" element content (e.g. B, Li, P, F). These "fluxes" allow for large crystal size by lowering melt polymerisation (and thus viscosity), crystallisation temperature and nucleation rates and increasing diffusion rates and solubility (Simmons et al., 2003). Aplites are fine grained analogues of pegmatites, formed from similar material which has suddenly lost its volatile and flux content, resulting in a rapid quenching of the melt (London, 2005). Analysis of such lithologies may elucidate whether processes such as volatile enrichment, volatile loss and/or extensive fractional crystallisation can affect the Si isotopic composition of granitoid rocks. As such, a selection of aplitic and pegmatitic samples from south-west England were chosen for analysis.

The Hercynian granitic plutons and associated lithologies from South-west England are all outcrops of a single, 200 km-long, sub-surface granitic body, the Cornubian batholith (Exley and Stone, 1982). This batholith intruded a series of metamorphosed sediments and igneous lithologies of mid-Palaeozoic age at the beginning of the Permian. The Rb-Sr ages from each of

the plutons suggest that the granites formed over a relatively short period of time, between ~290-280 Ma (Darbyshire and Shepherd, 1985; 1987; 1994; Chesley et al., 1993). In contrast to many other granitic terrains, the lithologies present are restricted to coarse-grained, peraluminous leucogranites with a strong S-type affinity (Exley and Stone, 1982). The aplites and pegmatites display strong geochemical similarities to, and have Rb-Sr ages concurrent with, their associated plutons, suggesting that aplite/pegmatite formation was magmatic (Darbyshire and Shepherd, 1985; 1987) and not metasomatic. The samples for this study were taken from the Meldon aplite and the "roof complex" of the Tregonning granite.

The Meldon aplite (279 ± 2 Ma) is geochemically similar to the Dartmoor granite pluton and displays some of the lowest ASI (~1.15) and initial $^{87}Sr/^{86}Sr$ values (0.70976 ± 0.00166) recorded from the Cornubian batholith (Darbyshire and Shepherd, 1985). Three aplite samples from the main body as well as one aplite vein were chosen for analysis. Mineral separates from a pegmatitic zone containing predominantly albite and minor lepidolite and K-feldspar were also picked for Si isotopic analysis.

The Tregonning granite (280 ± 4 Ma) is a non-porphyritic granite which is noted for its abundance of Li-rich micas (Exley and Stone, 1982). In comparison to the Meldon aplite, it has much higher ASI (~1.3) and initial $^{87}Sr/^{86}Sr$ values (0.71498 ± 0.00381), suggesting the involvement of a more evolved sedimentary component during petrogenesis (Darbyshire and Shepherd, 1987). At the upper contact between the granite and the country rock, a "roof complex" of banded aplites and pegmatites has formed. Two aplites and a pegmatite (picked for quartz, albite and tourmaline) were chosen for analysis, as well as a lithionite granite from the Tregonning main intrusion (picked for quartz, albite and lepidolite) for comparison.

5.3 METHODS

All Australian samples were received as powders and required no further processing before alkali fusion. The aplites and pegmatites were collected from the British Geological Survey as whole-rock samples; aplites were crushed and powdered in an agate mill in-house; pegmatites were crushed and mineral separates were picked using a binocular microscope under ethanol, then powdered as with the aplites. The use of agate mills does not affect the Si isotopic composition of samples, as shown from tests made by Zambardi and Poitrasson (2011) and Savage et al. (2011) (Chapter 4).

5.3.1 Alkali fusion

All samples and standards were processed using the HF-free alkali-fusion method as detailed in Georg et al. (2006b). About 10 mg of sample powder was weighed into a silver crucible along with ~ 200 mg of the NaOH flux (analytical grade in pellet form). The crucible was then placed into a muffle furnace, preheated to 720ºC, for 12 minutes. After removal from the furnace, the crucible was allowed to cool slightly before placing it into 20 ml of MQ-e (18.2 MΩ) water. After 24 hours, the fusion cake was agitated in an ultrasonic bath and heated to ~ 60ºC to ensure quantitative removal of the fusion material from the crucible. The solution was then transferred into pre-cleaned PP bottles, diluted further with MQ-e water and acidified with triple-distilled concentrated HNO_3 (to 1% v/v). Sample concentrations and yields were checked after fusion using the "molybdenum-blue" method on a Hach Lange photospectrometer. The average Si yields for all samples processed for this study is 98 ± 1 % (1 s.d.).

All samples and standards were purified before mass spectrometry using a single column pass, using BioRad (Hercules, CA, USA) Poly-prep 10ml columns filled with 1.8 ml DOWEX 50W-X12 (200-400 mesh) cation exchange resin. Because, at low pH, Si exists in the non-ionic or anionic forms $Si(OH)_4$ or $H_3SiO_4^-$, it is not retained by the resin and so was eluted immediately after loading in MQ-e. The samples were then acidified after purification to 1% v/v HNO_3 before analysis. This method ensures quantitative Si recovery and removes all major and trace cations from the eluate (Georg et al., 2006b). The method does not remove anionic species, and the effect that large concentrations of such species in the eluate may have on analysis was tested by Georg et al. (2006b); no difference was recorded in isotope ratios from doped samples analysed against undoped samples. Also, the good reproducibility of external standards using this method suggests that the presence of any anion species in the purified samples does not cause any matrix effects during analysis. Further evidence for the robustness of this method is provided in Chapter 3, Zambardi and Poitrasson (2011) and Armytage et al. (2011).

5.3.2 Mass spectrometry

Silicon isotope analyses were made in-house using a Nu Plasma High-Resolution Multiple-Collector Inductively-Coupled-Plasma Mass Spectrometer (HR-ICP-MS, Nu Instruments, Wrexham, UK). Running conditions for Si isotope analysis are described in detail in Georg et al. (2006b). Samples were ionised using a "dry" plasma; solutions were introduced

using a 6mm PFA concentric microflow nebuliser (Savillex, MN, USA) with an uptake rate of ~ 50 μl min^{-1} and desolvated using an Aridus II (Cetac, NE, USA). The first accelerating potential of the instrument is set at 6 kV.

To avoid polyatomic interferences on the Si beams, isotopic analyses were made at "medium" resolution (resolving power M/ΔM ~ 3300, where ΔM is defined at 5% and 95% for peak height; Weyer and Schwieters, 2003). This requires the ion beam to be physically narrowed by reducing the source slit from 0.3mm to 0.05mm and the closing of "Alpha" slits to correct for beam aberrations, which results in a ~ 85% reduction of instrument sensitivity (at sample Si concentrations of 750 ppb, a total signal of 1×10^{-10}A was typical).

Isotopic analyses were conducted using a standard-sample bracketing protocol to correct for instrumental mass bias. The silica sand standard NBS28 was used as the bracketing standard, and was processed through identical chemistry as for all samples. Each isotope datum consists of an average of ~11 values (5-6 sample analyses) – each analysis comprised 20 cycles and each cycle was integrated for 8 s. Instrumental background was checked before each measurement by deflecting the ESA for 20 s; a typical background signal of 2×10^{-13}A results in a signal to noise ratio of ~ 500.

Variations in Si isotopes are represented by the delta notation as $\delta^{30}Si$ or $\delta^{29}Si$, defined as the deviation in per mil (‰) of a sample's ratio of $^{x}Si/^{28}Si$ from the standard (NBS28), as such:

$$\delta^{30}Si = [(^{30}Si/^{28}Si_{sample})/(^{30}Si/^{28}Si_{standard}) - 1] \times 1000;$$

$$\delta^{29}Si = [(^{29}Si/^{28}Si_{sample})/(^{29}Si/^{28}Si_{standard}) - 1] \times 1000.$$

We discuss our Si isotopic data using $\delta^{30}Si$ values, which are ~ 2x the magnitude of $\delta^{29}Si$ values. This is assuming mass dependence, which, for terrestrial samples, is a valid assumption and indeed, this relationship was used as a test for data quality such that any data that did not display mass dependence were discarded.

5.4 RESULTS

5.4.1 External standards

Sample data accuracy was ensured by the repeat analysis of external standards during each data acquisition session. The standards used were Diatomite and BHVO-2. Diatomite is a natural, pure silica standard (Reynolds et al., 2007; Georg et al., 2009a; Ziegler et al., 2010; Chakrabarti and Jacobsen, 2010; Armytage et al., 2011) and BHVO-2 is a USGS natural basaltic

rock standard (Abraham et al., 2008; van den Boorn et al., 2009; Zambardi and Poitrasson, 2011; Armytage et al., 2011). Both are widely available and have been extensively utilised as external standards for Si isotope studies. As such, a large body of previous analyses are available in the literature for comparison. External standard data is given in Table 5.1. We have also repeatedly analysed two separate dilutions of the USGS granodiorite standard GSP-2 during the course of this study, in an attempt to characterise a natural, Si-rich external standard.

Our values of $\delta^{30}Si$ = -0.30 ± 0.09 ‰ (2 s.d., n = 118) for BHVO-2 and $\delta^{30}Si$ = 1.24 ± 0.11 ‰ (2 s.d., n = 124) for Diatomite agree well with the literature data and exemplify the good levels of precision and reproducibility that can be achieved with our analytical methods and instrumentation. The errors associated with the data are a combination of the "chemical" and "mass spectrometric" reproducibility, as all standards and samples were processed through identical chemistry prior to analysis. Analysis of a replicate dilution of Diatomite gives identical isotopic values, suggesting our sample processing techniques are robust. Repeated analysis gives an isotopic value of $\delta^{30}Si$ = -0.20 ± 0.11 ‰ (2 s.d., n = 44) for GSP-2; the precision and reproducibility are identical to those associated with our other external standards, and isotopic analysis of two separate dilutions shows no sample heterogeneity.

5.4.2 Whole rock sample data

All sample Si isotopic data are given in Tables 5.2 and 5.3. Data precision is represented using both the 2 × standard deviation (2 s.d.) and the standard error of the mean at the 95% confidence level (95%s.e. = t × s.d./$(n)^{1/2}$, where t = inverse survival function of the Student's t-test at the 95% significance level and n-1 degrees of freedom). The average 2 s.d. value for all samples analysed in this study is ± 0.10 ‰, which is very close to the precision given by external standards. At an average population of n =11, this gives an overall 95% s.e. of ± 0.034 ‰, which we take to be our representative precision.

5.4.2.1 Lachlan Fold Belt

Whole rock $\delta^{30}Si$ data for granites from the LFB range from -0.40 to -0.14 ‰ (Fig. 5.3). I-type granites range from $\delta^{30}Si$ = -0.25 to -0.14 ‰ with an average value of $\delta^{30}Si$ = -0.19 ± 0.07 ‰ (2 s.d.), whereas S-types have are larger and lighter isotopic range (viz. $\delta^{30}Si$ = -0.40 to -0.25 ‰) with an average of $\delta^{30}Si$ = -0.28 ± 0.14 ‰ (2 s.d.). There are no strong correlations between

Table 5.1 – External standard data

Standard		SiO_2 (wt.%)	$\delta^{30}Si$ (‰)	2s.d.	95%s.e.	$\delta^{29}Si$ (‰)	2s.d.	95%s.e.	*n*
Diatomite	1	100	1.26	0.11	0.04	0.64	0.06	0.02	11
	2		1.22	0.22	0.07	0.62	0.09	0.03	11
	3		1.27	0.15	0.05	0.69	0.15	0.05	11
	4		1.23	0.08	0.03	0.65	0.07	0.02	11
	5		1.22	0.09	0.03	0.62	0.08	0.03	11
	6		1.26	0.12	0.05	0.63	0.06	0.02	9
	7		1.23	0.10	0.04	0.63	0.07	0.02	11
	8		1.21	0.09	0.06	0.68	0.08	0.05	5
	9		1.27	0.12	0.04	0.68	0.12	0.04	11
Replicate	1		1.22	0.11	0.04	0.61	0.08	0.03	11
	2		1.20	0.10	0.03	0.60	0.06	0.02	11
	3		1.28	0.12	0.04	0.65	0.07	0.02	11
Overall			1.24	0.11	0.01	0.64	0.10	0.01	124
Reynolds et al. (2007)			1.26	0.20		0.64	0.14		
Georg et al. (2009b)			1.23	0.16		0.62	0.11		
Chapter 4			1.23	0.10		0.64	0.08		
BHVO-2	1	49.9	–0.28	0.11	0.04	–0.13	0.06	0.02	9
	2		–0.33	0.16	0.05	–0.18	0.10	0.04	11
	3		–0.28	0.10	0.04	–0.14	0.10	0.03	11
	4		–0.34	0.06	0.02	–0.16	0.11	0.04	11
	5		–0.31	0.08	0.03	–0.17	0.08	0.03	10
	6		–0.29	0.04	0.01	–0.17	0.07	0.02	11
	7		–0.31	0.10	0.03	–0.15	0.09	0.03	11
	8		–0.29	0.07	0.02	–0.16	0.06	0.02	11
	9		–0.31	0.12	0.04	–0.15	0.08	0.03	11
	10		–0.31	0.05	0.02	–0.15	0.05	0.02	11
	11		–0.26	0.12	0.04	–0.13	0.09	0.03	11
Overall			–0.30	0.09	0.01	–0.15	0.09	0.01	118
Abraham et al. (2008)			–0.29	0.11		–0.17	0.04		
Zambardi and Poitrasson (2011)			–0.27	0.08		–0.14	0.05		
Chapter 4			–0.29	0.09		–0.15	0.08		
GSP-2	1	66.6	–0.16	0.11	0.04	–0.06	0.07	0.02	11
	2		–0.23	0.13	0.04	–0.10	0.05	0.02	11
Replicate	1		–0.22	0.11	0.04	–0.11	0.07	0.02	11
	2		–0.21	0.06	0.02	–0.11	0.02	0.01	11
Overall			–0.20	0.11	0.02	–0.10	0.07	0.01	44

Silicon isotope data for external standards, as well as literature values for said standards. Numbers refer to repeat analysis of the same solution, "Replicate" refers to analyses made on a separate dissolution of the standard.

Si isotopic data and proxies for magmatic differentiation (e.g. SiO_2, MgO). The ranges in isotopic composition of both I- and S-type granites from the LFB that we have analysed (~ 0.25 ‰) are more limited than that displayed by the data of Douthitt (>1.0 ‰, Fig 5.2; 1982). The reasons for this are unclear but the lower precision associated with their methods would naturally lead to a statistical increase in spread of the data. Given that we have not analysed the same samples as Douthitt (1982), we cannot unequivocally say that this is the sole explanation.

Even though the range of data is small, the isotopic variations are larger than would be expected from igneous differentiation given the small range of SiO_2 contents (65 to 77 wt.%; see

Table 5.2 – Whole rock Si isotope data for Lachlan Fold Belt and other Australian granites

Sample	Type	Locality	SiO_2 (wt.%)	$\delta^{30}Si$ (‰)	2s.d.	95%s.e.	$\delta^{29}Si$ (‰)	2s.d.	95%s.e.	*n*	ASI	$^{87}Sr/^{86}Sr(i)$	εNd(i)	$\delta^{18}O$ (‰)
Lachlan Fold Belt														
Bega														
AB006	I-type	Glenbog	67.2	−0.18	0.06	0.02	−0.11	0.07	0.03	9	0.95	0.70869	−6.4	8.80
AB082	I-type	Brogo	66.9	−0.21	0.10	0.04	−0.12	0.08	0.03	9	0.96	0.70456	−1.3	
AB102	I-type	Bemboka	72.2	−0.18	0.11	0.03	−0.12	0.08	0.02	22	1.03	0.70790	−6.0	
AB195	I-type	Yurammie	65.3	−0.19	0.07	0.03	−0.12	0.08	0.03	9	0.95	0.70544	−4.6	9.20
AB234	I-type	Tonghi	69.2	−0.24	0.10	0.03	−0.14	0.06	0.02	11	0.98	0.70869	−6.4	
MG58	I-type	Moruya	72.5	−0.14	0.09	0.03	−0.08	0.12	0.04	11	1.10	*0.70410*	3.0	8.10
Berridale														
BB10	I-type	Buckleys Lake	71.2	−0.18	0.04	0.01	−0.10	0.08	0.03	10	1.00	0.70673	−2.6	8.78
BB21	I-type	Maffra	76.6	−0.15	0.14	0.05	−0.08	0.08	0.03	11	1.05	*0.70504*	*0.0*	9.32
				−0.22	0.11	0.04	−0.13	0.04	0.01	11				
				−0.19	0.07	0.03	−0.07	0.07	0.02	11				
				−0.18	0.12	0.02	−0.09	0.08	0.01	33				
BB87	I-type	Tara	67.7	−0.25	0.14	0.05	−0.14	0.08	0.03	10	0.97	0.70628	−3.2	7.86
BB02	S-type	Numbla Vale	73.5	−0.23	0.14	0.05	−0.12	0.10	0.03	11	1.09	0.71076	−8.0	10.23
BB09	S-type	Dalgety	68.2	−0.26	0.04	0.01	−0.12	0.03	0.01	11	1.08	0.70986	−6.1	9.56
BB12	S-type	Dalgety	67.4	−0.25	0.15	0.03	−0.13	0.10	0.02	21	1.06	0.70991	−6.5	9.20
BB53	S-type	Tingaringhy	67.8	−0.33	0.13	0.04	−0.18	0.08	0.02	16	1.13	0.71153	−7.5	10.53
BB83	S-type	Cootralantra	67.4	−0.22	0.07	0.03	−0.14	0.07	0.02	8	1.16	*0.71206*	*−8.4*	10.55
Wagga														
VB140	S-type	Granya	72.5	−0.37	0.16	0.06	−0.20	0.11	0.04	9	1.31	*0.71580*		
				−0.45	0.06	0.02	−0.25	0.05	0.02	11				
				−0.40	0.05	0.02	−0.19	0.06	0.02	11				
				−0.37	0.16	0.06	−0.21	0.13	0.04	10				
				−0.40	0.14	0.02	−0.21	0.10	0.02	43				
Ordovician turbidites														
OS31			63.4	−0.18	0.07	0.02	−0.10	0.04	0.01	11		0.71350	−12	
				−0.26	0.10	0.03	−0.14	0.03	0.01	11				
				−0.27	0.07	0.02	−0.14	0.10	0.03	11				
				−0.24	0.12	0.02	−0.12	0.07	0.01	33				
OS35			56.8	−0.22	0.12	0.04	−0.12	0.04	0.01	11		0.71650	−13	
				−0.14	0.08	0.03	−0.11	0.11	0.04	10				
				−0.18	0.12	0.03	−0.12	0.08	0.02	21				
OS37			89.9	−0.20	0.08	0.03	−0.08	0.03	0.01	11		0.71910	−14	
				−0.18	0.10	0.03	−0.09	0.08	0.03	11				
				−0.19	0.09	0.02	−0.09	0.06	0.01	22				
OS39			80.3	−0.24	0.09	0.03	−0.10	0.04	0.01	11		0.71950	−13	
				−0.18	0.12	0.04	−0.08	0.13	0.05	10				
				−0.21	0.12	0.03	−0.09	0.09	0.02	21				
Other SE Australian														
New England batholith														
NEB247	S-type	Bundarra	72.7	−0.11	0.16	0.04	−0.04	0.08	0.02	20	1.06	*0.70500*	*−0.2*	*12.00*
G38	I-type	Moonbi	68.0	−0.14	0.08	0.01	−0.07	0.07	0.01	33	0.96	*0.70498*	*1.3*	*8.00*
Padthaway														
2001	A-type	Mt. Monster	73.9	−0.13	0.10	0.03	−0.08	0.05	0.02	11	0.99	0.70402	−1.7	
PG-11	A-type	Marcollat	75.1	−0.15	0.06	0.02	−0.07	0.10	0.04	11	0.96	0.70257	−2.7	
2000	A-type	Seismograph	74.6	−0.19	0.09	0.03	−0.11	0.13	0.04	11	0.95	0.70630	−2.3	
				−0.18	0.15	0.07	−0.05	0.06	0.03	7				
				−0.18	0.05	0.02	−0.11	0.18	0.06	10				
				−0.18	0.09	0.02	−0.10	0.14	0.03	28				

Silicon isotope data of whole-rock analyses of Lachlan Fold Belt (and associated sediments), New England Batholith and Padthaway suite granites made during this study. Data in grey boxes are long term averages of repeat analyses of the same sample solution. Other element and isotopic data are taken from the following sources: *LFB*: Chappell and O'Neil, 1977; McCulloch and Chappell, 1982; Wyborn and Chappell, 1983, Gray, 1990; Chappell et al., 1991, McCulloch and Woodhead, 1993, unpub. analyses; *NEB*: O'Neil et al., 1977; Shaw and Flood, 1981; Mensel et al., 1985; Bryant et al., 2004; Shaw and Flood, 2009; *Padthaway*: Turner et al., 1992. Data in italics are taken from a closely related sample from the same pluton or an average made from various analyses from the same locality – these are used only when data is not available for a specific sample. See text for discussion.

Section 5.1). For instance, samples MG58 and VB140 have almost identical SiO_2 contents but, whereas MG58 has a strong I-type affinity and an "igneous" Si isotope composition ($\delta^{30}Si$ = -0.14 ‰), sample VB140 is strongly S-type and has a more negative $\delta^{30}Si$ value (-0.40 ‰). For the most part, there is a lot of overlap between the isotopic compositions of both I and S types (Fig. 5.3), the possible reasons for which will be discussed below.

5.4.2.2 Ordovician turbidites

Silicon isotope data for a selection of Ordovician turbidites from the LFB delineate a limited range ($\delta^{30}Si$ = -0.24 to -0.18 ‰), much smaller than the isotopic ranges for the S-type granites from which these samples are purported to derive. This is surprising, especially given the compositional and mineralogical variation of the samples analysed.

5.4.2.3 New England Batholith

The Si isotopic composition of the I-type granite (G38) from the NEB falls with the range delineated by the I-type granites from the LFB ($\delta^{30}Si$ = -0.14 ‰). The S-type granite (NEB247), interestingly, has an isotopic composition ($\delta^{30}Si$ = -0.11 ‰) that is slightly *heavier* than sample G38 and is resolvably heavier than any of the S-type granites from the LFB (Fig. 5.3).

5.4.2.4 Padthaway (A-type) granites

Three A-type granites from the Padthaway suite show the most limited range of Si isotope data ($\delta^{30}Si$ = -0.18 to -0.13 ‰) and heaviest average ($\delta^{30}Si$ = -0.15 ± 0.05 ‰) of the three granite types analysed in this study. The isotopic range is similar to that seen in rhyolites from Hekla volcano and the Afar region (Chapter 4; Savage et al., 2011), consistent with their derivation from a mantle source.

5.4.3 Aplites and pegmatite mineral separates

Whole rock aplite $\delta^{30}Si$ data range from -0.39 to -0.22 ‰ (Table 5.3, Fig. 5.4). The range of data for the S-type aplites from the Cornubian batholith falls within the range for the S-type granites from the LFB. As with the granites, the aplite data do not show any strong relationship with proxies for magmatic differentiation.

Silicon isotope data for the mineral separates for the Megaliggar pegmatite and host lithionite granite are as follows: pegmatite: $\delta^{30}Si_{quartz}$ = -0.34 ± 0.04‰, $\delta^{30}Si_{albite}$ = -0.48 ± 0.05‰ and $\delta^{30}Si_{tourmaline}$ = -0.22 ± 0.02‰; lithionite granite: $\delta^{30}Si_{quartz}$ = -0.33 ± 0.02‰, $\delta^{30}Si_{albite}$ = -0.43 ± 0.03‰ and $\delta^{30}Si_{lithionite}$ = -0.40 ± 0.04‰ (all errors 95% s.e.; Table 5.3, Fig. 5.4). The similarity between the $\delta^{30}Si$ values for both the quartz and albite samples is striking, as is the magnitude of fractionation between the phases (viz. $\Delta^{30}Si_{qtz\text{-}fspr}$ = ~0.10 – 0.14‰). These fractionation factors agree with those observed in other Si isotope analyses (Georg, 2006) and calculated using Density Functional Theory (Méheut et al., 2009). These data are also consistent with the theory that equilibrium fractionation between mineral phases will be predominantly controlled by degree of polymerisation in the phase, with the heavier isotopes favouring the phase(s) with the higher degree of polymerisation (Grant, 1954), in this case, quartz. However, as noted by Méheut et al. (2009), polymerisation degree is not the only discriminating factor and other network-forming cations, such as Al, could affect bond strength and ultimately the degree of fractionation. This could explain why tourmaline, in which Al and B can both act as network-forming cations, displays a heavier $\delta^{30}Si$ value than quartz.

The Meldon pegmatite data are as follows: $\delta^{30}Si_{K\text{-}feldspar}$ = -0.22 ± 0.03‰, $\delta^{30}Si_{albite}$ = -0.29 ± 0.03‰ and $\delta^{30}Si_{lepidolite}$ = -0.31 ± 0.05‰ (all errors 95% s.e.; Table 5.3, Fig. 5.4). Although the absolute values for the mineral separates are not similar to those from Megaliggar, there are important similarities. In both the Megaliggar and Meldon samples, there is no fractionation between the albite and lepidolite phases. This is in agreement with analyses made by Georg (2006) on granite mineral separates, where feldspar and muscovite are shown to be identical. Also, in both Megaliggar and Meldon, the albite phase seems to concentrate the lighter isotopes. In the Meldon pegmatite (where quartz is not present in appreciable quantities), albite displays a lighter $\delta^{30}Si$ value than the K-feldspar, which is surprising, as it may be expected that both feldspars would have similar isotopic compositions if they formed in equilibrium. However, there is some evidence that albite had already crystallised before pegmatite emplacement (Chaudry, 1971), which may explain this discrepancy. Alternatively, coupled Al-Si substitution in the plagioclase feldspar and lack thereof in the K-feldspar will affect internal bond strengths and so may cause fractionation between the two phases (which will depend on the Ca content).

Modal bulk $\delta^{30}Si$ averages for the pegmatites and lithionite granite have been calculated using the modal abundances (recast to 100%), and weighted by the relative SiO_2 content, of each

Table 5.3 – Silicon isotope data for aplite, pegmatite and host granite samples from SW England

Sample	Type	Description	SiO_2 (wt.%)	$\delta^{30}Si$ (‰)	2s.d.	95%s.e.	$\delta^{29}Si$ (‰)	2s.d.	95%s.e.	*n*	ASI	$^{87}Sr/^{86}Sr(i)$	εNd(i)	$\delta^{18}O$ (‰)
Meldon														
MEL01-10	S-type	Aplite vein	70.3	–0.23	0.14	0.03	–0.14	0.11	0.02	22	*1.15*	*0.70976*	*–4.7*	*10.8*
MEL02-10	K-feldspar	Pegmatitic aplite	69.0	–0.22	0.09	0.03	–0.11	0.07	0.02	11				
	Albite		68.0	–0.29	0.09	0.03	–0.16	0.09	0.03	11				
	Lepidolite		50.0	–0.31	0.16	0.05	–0.16	0.15	0.05	11				
	Modal average (0.12 : 0.76 : 0.12)			–0.28	0.11	0.04	–0.15	0.10	0.03					
MEL03-10	S-type	Aplite	62.0	–0.28	0.07	0.02	–0.16	0.04	0.01	11	*1.15*	*0.70976*	*–4.7*	*10.8*
MEL04-10	S-type	Fine grained aplite	68.9	–0.26	0.13	0.04	–0.13	0.06	0.02	11	*1.15*	*0.70976*	*–4.7*	*10.8*
MEL05-10	S-type	Fine grained aplite	69.3	–0.22	0.12	0.04	–0.11	0.09	0.03	11	*1.15*	*0.70976*	*–4.7*	*10.8*
Megaliggar														
MEG01-10	Quartz	Pegmatite	100.0	–0.34	0.11	0.04	–0.16	0.14	0.05	11				
	Tourmaline		36.0	–0.22	0.07	0.02	–0.09	0.08	0.03	11				
	Albite		65.0	–0.48	0.14	0.05	–0.28	0.10	0.04	10				
	Modal average (0.45 : 0.1 : 0.45)			–0.39	0.11	0.04	–0.21	0.11	0.04					
MEG02-10	S-type	Aplite (top of sill)	69.1	–0.39	0.08	0.03	–0.19	0.04	0.01	11	*1.3*	*0.71498*	*–7.4*	*14*
MEG03-10	S-type	Aplogranite	69.5	–0.35	0.09	0.03	–0.16	0.08	0.03	11	*1.3*	*0.71498*	*–7.4*	*14*
MEG04-10	Quartz	Lithionite granite	100.0	–0.33	0.07	0.02	–0.16	0.08	0.03	11				
		Lepidolite	52.0	–0.40	0.12	0.04	–0.23	0.13	0.04	11				
		Albite	63.0	–0.43	0.08	0.03	–0.23	0.08	0.03	11				
	Modal average (0.45 : 0.1 : 0.45)			–0.38	0.09	0.03	–0.20	0.10	0.03					

Silicon isotope data of the whole-rock aplite and mineral separate pegmatite and granite analyses made during this study. Data in grey boxes represent modal bulk averages calculated from the mineral separate analyses (mineral proportions are given in the brackets). Silica contents were measured spectrophotometrically in-house. Other geochemical data (in italics) were not measured on these samples but are taken from analyses made from the same locality, from Sheppard, 1977 and Darbyshire and Sheppard, 1985 and 1994.

phase (Table 5.3). Bulk Si isotopic estimates fall within the range of data for each locality.

For all the samples analysed in this study, although there are resolvable Si isotopic differences between different granite suites, within each locality there is relatively limited variation (Fig. 5.3 and 5.4). The scale of this provincial control is variable, however, as in the aplites and pegmatites it exists on a pluton-scale, i.e. on a much smaller scale than seen in south-eastern Australia, where variation is limited within each batholith.

5.5 DISCUSSION

5.5.1 Silicon isotope variation in granitoid rocks

A key hypothesis of this study is that granites derived from an igneous source (I- and A-type) should have predictable Si isotope compositions, comparable to that of intraplate rhyolites and dacites, whereas granites with a sedimentary affinity (S-type) should display $\delta^{30}Si$ values that are much more variable and, on average, much lighter. This can be tested by plotting the $\delta^{30}Si$ data against SiO_2 content, along with the "igneous array" for Si isotopes (Fig. 5.5) as defined in Chapter 4. Figure 5.5a shows that the $\delta^{30}Si$ data for I- and A-type granites lie on or very close to the "igneous array" suggesting that the limited isotopic variation displayed by both

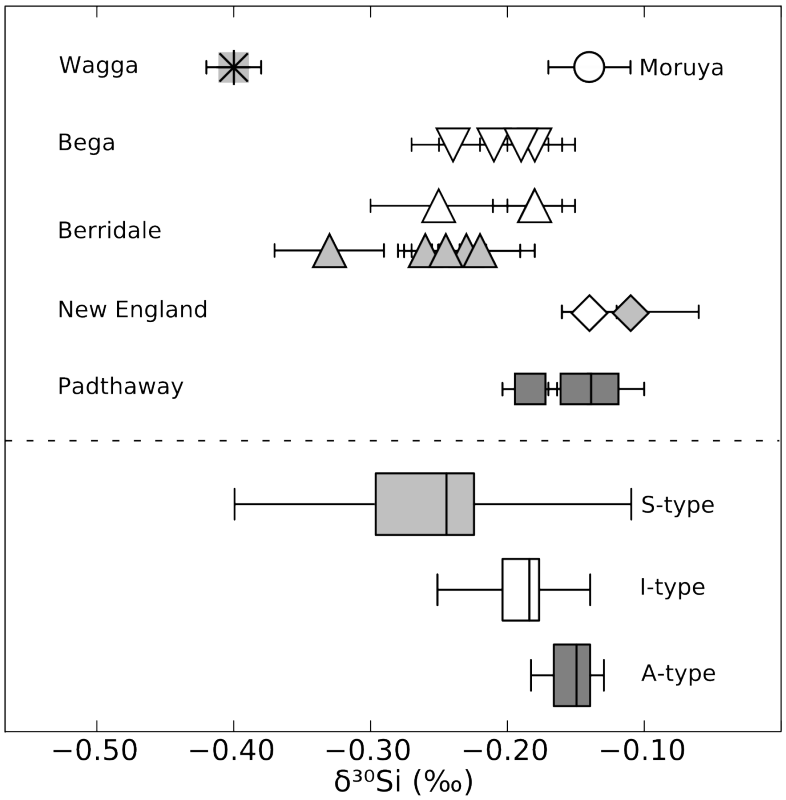


Fig. 5.3 Silicon isotope data for the whole-rock granite samples taken from the Lachlan Fold Belt, New England Batholith and Padthaway suites analysed in this work (error bars are 95% s.e.; see text for sample description and discussion). The box plots in the bottom half of the figure display the sample maxima and minima (the bars), the interquartile range (the box) and the sample median (vertical line in the box), and illustrate the much larger range of data defined by S-type granites.

groups is predominantly a result of magmatic processes, i.e. partial melting and fractional crystallisation, affecting a source magma isotopically similar to the mantle (Chapter 4). Figure 5.5b shows that S-type granites have a much larger range of δ^{30}Si values, many of which, as predicted, do not lie on the "igneous array".

However, there are a number of issues relating to the data, which indicate that the behaviour of Si isotopes in granitoid material is not as simplistic as described in the preceding paragraph. Firstly, there is a significant amount of overlap between the Si isotopic ranges of S-types and other granites. Also, some S-type δ^{30}Si values lie on the igneous array whereas some I-type granites plot below the array. Lastly, both I- and S-type granites from the New England batholith appear to plot *above* (although within error of) the array. Because of this, it is pertinent to investigate what processes may be affecting Si isotopes during petrogenesis and whether source variations are the only control over the Si isotopic composition of granites.

Secondary alteration processes can be ruled out, as all samples were taken from fresh surfaces with no evidence of alteration. The extremely comprehensive body of literature on the samples from the Lachlan Fold Belt and New England Batholith provides ample evidence that these rocks represent pristine granitic material (see Section 5.2 for references and sample

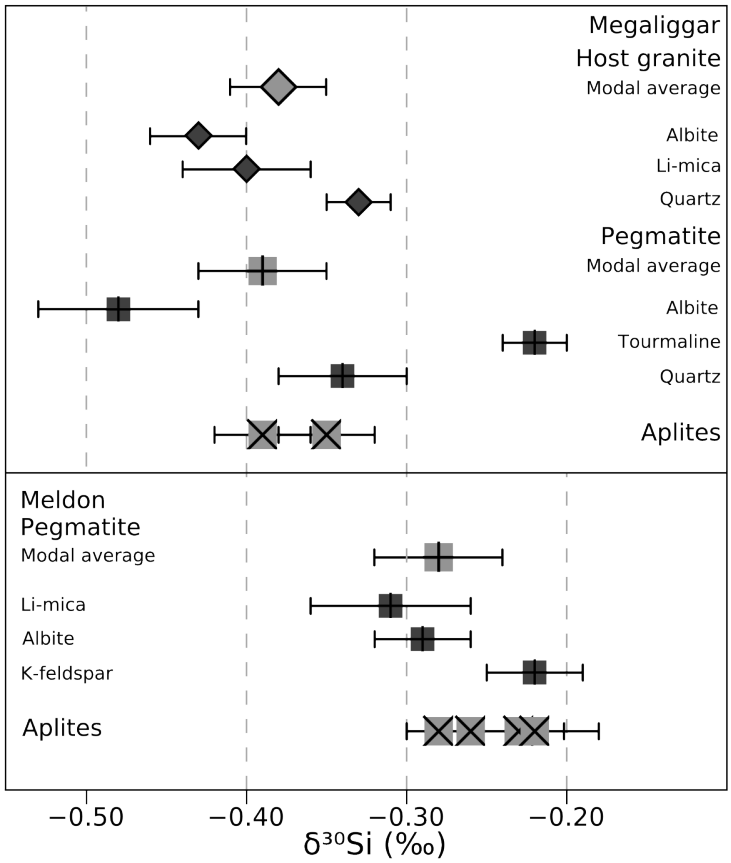


Fig. 5.4 Whole-rock Si isotope data for the aplite samples, and mineral separate data for the pegmatite and granite samples from the Cornubian batholith (error bars are 95% s.e.; see text for sample descriptions and discussion).

descriptions). The limited Mg isotope variation seen by Li et al. (2010) for the LFB also precludes extensive secondary alteration, and as Mg is more fluid-mobile than Si, the affect on Si should be even smaller.

5.5.1.1 Kinetic isotope fractionation

There is increasing evidence that diffusion-related kinetic isotopic fractionation can affect the low-mass non-traditional stable isotopes to a larger degree than equilibrium processes at high temperatures and pressures (see Richter et al., 2009a for a review). Although Si isotopes do not appear to be affected by chemical diffusion (Richter et al., 1999) there is some experimental (Richter et al., 2009b) and theoretical (Lundstrom, 2009) evidence that Soret (thermal) diffusion processes can cause resolvable Si isotopic effects, particularly if a temperature gradient is present for an extensive period, for instance that associated with the cooling of a granite pluton.

The problem is that thermal effects are extremely difficult to test in a natural setting unless a transect across the predicted thermal gradient is available (such as that studied by

Lundstrom, 2009). However, we can use previous stable isotope studies of the LFB to quantify such processes, in particular using Mg. Magnesium isotopes appear to be fractionated readily by thermal diffusion; Richter et al. (2009b) showed, using experimental data, that the magnitude of Mg isotopic fractionation during thermal diffusion is approximately six times that of Si isotopes (see also Huang et al., 2010). Therefore, if Si isotopes had been affected by Soret diffusion during the emplacement of the LFB batholiths, we would expect to see large Mg isotope fractionation in the same system. In fact, the opposite is true: in a recent study, Li et al. (2010) showed that Mg isotopes in LFB granites do not appear to show any variation away from mantle values. Unfortunately, no such data are available for the New England and Cornubian batholiths and so we cannot use this approach to quantify Soret effects, although the relationships between Si isotopes and other geochemical indices of source composition (see later) tend to preclude large kinetic isotope effects in these samples.

5.5.1.2 Volatile phase-related fractionation

Granitic magmas are often volatile-rich and, during crystallisation, the residual melt is enriched in the volatiles, as well as other elements that act as network-modifiers (such as B, P, F, Li) in the melt. The role of network-modifying cations appears to have an important control over

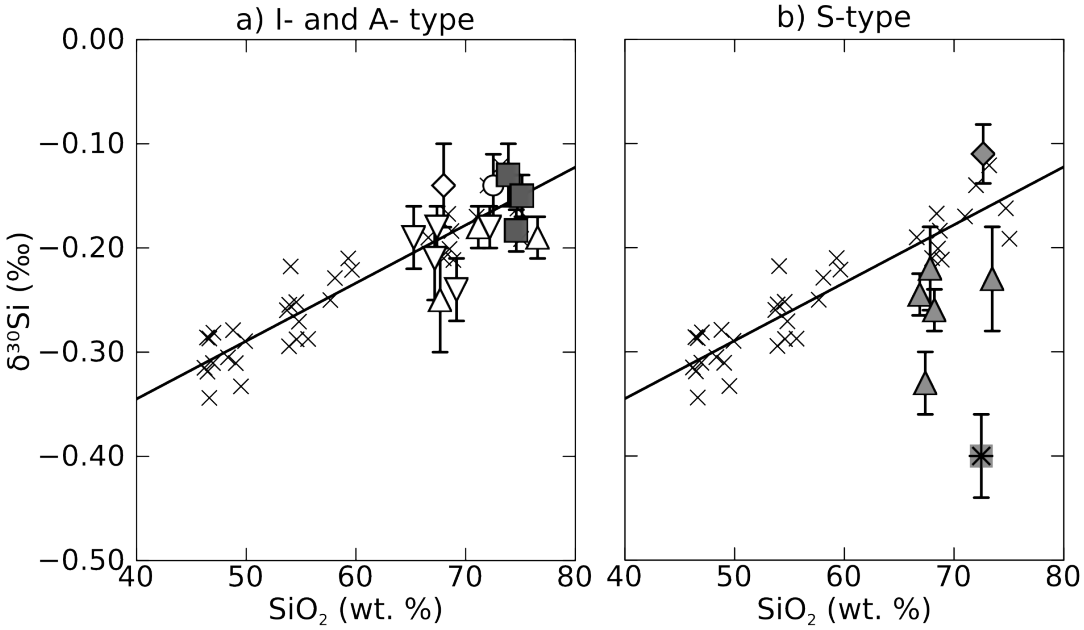


Fig. 5.5 Silicon isotope data for the Lachlan Fold Belt, New England Batholith and Padthaway suite a) I- and A-type and b) S-type granites plotted against SiO_2 (symbols as in Figure 3, error bars are 95% s.e.). Also plotted is the "igneous array" as in Figure 5.1 (Chapter 4). Whereas most of the I- and A-type granites plot on the array, many S-type samples do not.

equilibrium Si isotope fractionation (e.g. Méheut et al., 2009) and so the volatile-rich phase may play a role in the Si isotopic systematics of granitoid rocks, particularly as the residual melt phase will also become extremely Si-rich as crystallisation continues. Therefore, studying the Si isotope composition of zoned aplite and pegmatites, which are both representative of late state, granitic melt and whose petrogenesis has involved variable interaction with volatiles (see Section 5.2) may indicate whether these phases are important in the Si isotope composition of granites.

In both aplite-pegmatite localities analysed in this study, we find no isotopic offset between the bulk δ^{30}Si composition of the pegmatites, aplites and host granite (Fig. 5.4, Table 5.3). This suggests that neither volatile enrichment nor subsequent volatile loss affects the overall Si isotopic composition of the granite or residual phases. What volatile enrichment appears to affect is the Si isotopic composition of individual crystal phases. The magnitudes of offset between the isotopic compositions of crystal phases from the bulk Megaliggar pegmatite are much larger than for the host granite, even though the sense of fractionation of common phases remains the same (Fig. 5.4). We have attributed this to the effect of network-modifying cations (see Section 5.3.).

5.5.1.3 Fractional crystallisation

It is clear that Si isotopes fractionate between coexisting mineral phases in a liquid, which is most likely a result of the difference in polymerisation degree and bond strengths between the phase(s) forming and the melt (e.g. Grant, 1954; Meheut et al., 2009). In an igneous rock that has evolved from a mantle-derived melt, the effect that fractional crystallisation (and/or partial melting) has on the Si isotopic composition of such a rock defines the "igneous array" for Si isotopes (see above; Chapter 4) – which is why we infer that δ^{30}Si values that lie off this trend indicate that such samples have not evolved from a mantle source. However, this does not mean that such samples are not completely igneous, and processes such as cumulate formation could also cause resolvable isotopic fractionation away from the predicted value, particularly if the degree of inter-mineral fractionation is as large as that seen in the Megaliggar pegmatite samples.

However, it is not likely that fractional crystallisation has affected the Si isotopic composition of the Lachlan Fold Belt granites to any large degree. Firstly, fractional

crystallisation has not played an important role in the petrogenesis of the LFB granites; partial melting is inferred to be the major petrogenetic force. Geochemical evidence for fractional crystallisation is scant, and limited to specific plutons, e.g. the Boggy Plain supersuite from the Koscuisko batholith (Chappell, 1999), but these samples have been largely avoided.

Using the pegmatite and granite mineral separate data (Fig. 5.4) we can predict what effect removal of a certain phase would have on the Si isotope composition of a melt. Removal of albite or certain micas (as well as the Li mica analysed here, biotite has also been shown to be isotopically lighter than bulk rock composition; Georg, 2006) will drive the melt to a heavier Si isotopic composition – one could therefore suppose that the S-type granites show overlap with I-type granites because they have experienced removal of such phases.

However, trace element ratios do not support this suggestion: most of the granites we have analysed have Rb/Sr ratios of < 2 (removal of feldspar from a melt will deplete it in Sr relative to Rb; e.g. Halliday et al., 1991) suggesting that feldspar was not residual or removed from the melt. For comparison, Padthaway granites, which have experienced fractional crystallisation of feldspars, have Rb/Sr ratios of between 3 and 9. Of the LFB granites that do have Rb/Sr > 2, VB140 has the largest value (~6) but this sample also displays the *lightest* $\delta^{30}Si$ value.

If mica was a residual or fractionating phase, then it would drive the melt toward high Sr/Ba ratios (e.g. Hanson, 1978) and, possibly, low Li concentrations. However, most Sr/Ba ratios are <0.40 for the granite studied here, and Li concentrations are all much greater than mantle values (Bryant et al., 2004; Teng et al., 2004).

5.5.2 Silicon isotope variations in granites as a function of source heterogeneity

Having ruled out other processes, we conclude that source heterogeneity is the most likely cause of Si isotope variation (away from predicted values) in many of the granites analysed in this study. Using other geochemical proxies for source composition, we can attempt to establish what causes this isotopic heterogeneity to arise. In Figure 5.6, we have plotted Si isotopes against ASI value, $\delta^{18}O$, $^{87}Sr/^{86}Sr_{(initial)}$ and $\varepsilon Nd_{(initial)}$, all of which have been used in the Lachlan Fold Belt to differentiate between granites of igneous or sedimentary affinities. In all the plots, a least-squared linear regression has been performed on the LFB data *only*, this is shown as well as the R^2 value for each regression. These relationships are discussed below.

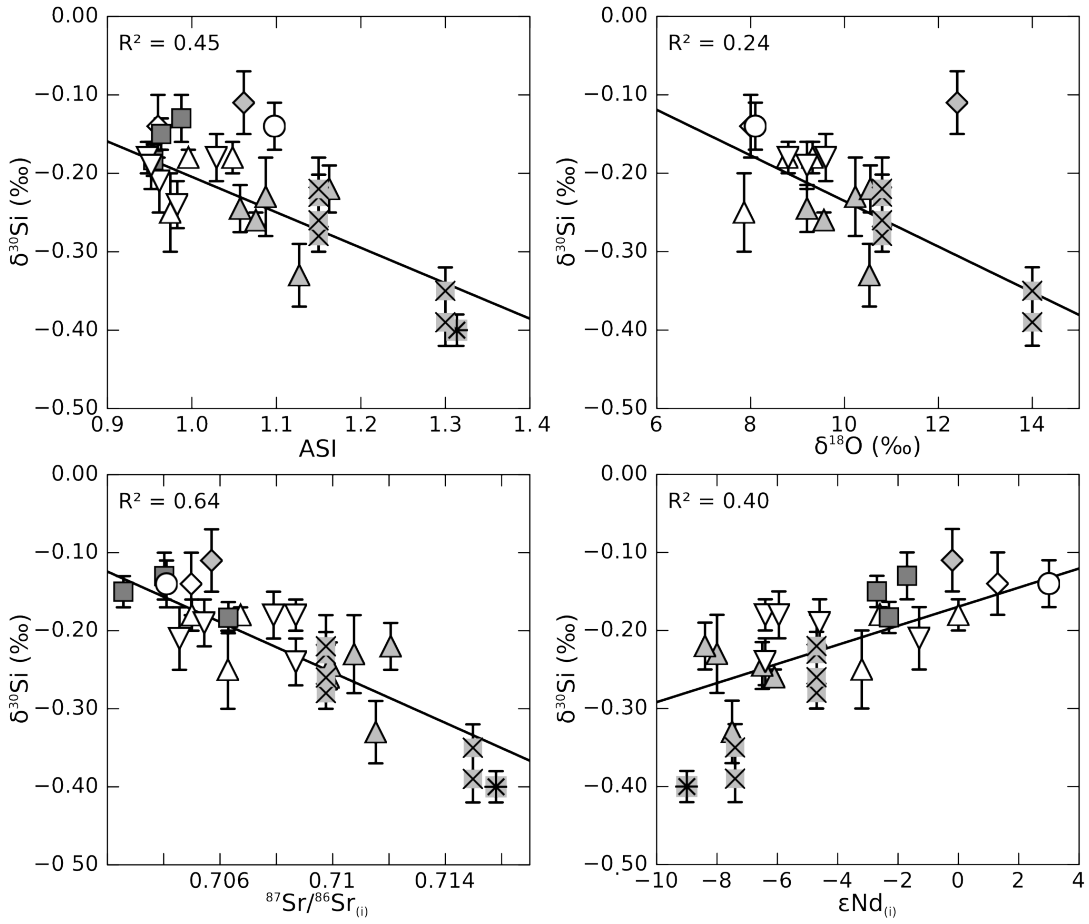


Fig. 5.6 Silicon isotope data for whole-rock granite and aplite samples plotted against a) ASI values, b) $\delta^{18}O$, c) $^{87}Sr/^{86}Sr_{(initial)}$ and d) $\varepsilon Nd_{(initial)}$ where such data was available (error bars are 95% s.e.; symbols as in Figure 3 and 4; data references are given in the text and in Tables 2 and 3). Least-squared linear regressions were performed in Gnumeric (http://projects.gnome.org/gnumeric/) using only the Lachlan Fold Belt data, R^2 values for these are provided. See text for discussion.

Firstly, strong correlations exist between Si isotopes and ASI values, and $^{87}Sr/^{86}Sr_{(initial)}$ (Fig. 5.6a & c). Weaker relationships between $\delta^{18}O$ and $\varepsilon Nd_{(initial)}$ are present, but in all cases, the sense is such that lighter Si isotopic values appear to be related to a more weathered (high ASI and $\delta^{18}O$ values) and less mantle-like (radiogenic Sr, low $\varepsilon Nd_{(initial)}$ values) source.

Secondly, data from the granites not taken from the LFB (i.e. New England Batholith, aplites from the Cornubian batholith) also plot on the arrays delineated by the LFB granites and, in all cases, recalculating the R^2 values using all data results in better correlation statistics. There are some exceptions, for instance the NEB S-type sample in Figure 5.6b, but in general Si isotopic values of granites from unrelated sources display similar systematics, again suggesting that Si isotopic heterogeneity in granites is a result of variations in source components.

However, as has already been noted, the offset between the $\delta^{30}Si$ values of I- and S-type granites is not large and Si isotopes do not appear to clearly differentiate between the two

affinities. Certainly, an inspection of Figure 5.6 indicates that other elemental and isotopic proxies distinguish much more readily between the various affinities. The reason for this, we believe, may be related to the composition of the postulated sedimentary source for many of the LFB granites, the Ordovician turbidites.

5.5.2.1 Isotopic composition of the sedimentary source

An importance caveat of the original hypothesis, that Si isotopes should distinguish between igneous- and sedimentary-derived granites, is that the sedimentary material from which the granites form should be isotopically distinct from the composition of igneous rocks. The large range of very negative $\delta^{30}Si$ data displayed in Figure 5.2 supports this assertion, although it is also evident that some sedimentary material has Si isotope compositions that overlap those of igneous rocks. This is what appears to be the case for the sedimentary source for the Lachlan Fold Belt. The data from these Ordovician turbidites define a remarkably limited Si isotopic range (much smaller than that seen in the granites), with the four samples, which are representative of the range of sedimentary compositions in this suite, having $\delta^{30}Si$ values between -0.24 and -0.18 ‰ (Table 5.2) and an average Ordovician turbidite value of $\delta^{30}Si$ = -0.20 ± 0.05 ‰ (2 s.d.).

If the Ordovician sediment is the enriched source on the LFB granites, as many authors suggest (e.g. Chappell, 1984; Keay et al., 1997; Collins, 1998; Kemp and Hawkesworth, 2003), then any amount of this material in the source of the granites would not result in any isotopic variation away from igneous values. Figure 5.7 shows a simple mixing model (reflecting either mixing of magmas or source rocks during LFB petrogenesis) between various putative end-members for the LFB, in $\delta^{30}Si$ vs. $^{87}Sr/^{86}Sr_{(initial)}$ space. Strontium isotopes were chosen because the correlation between these and Si isotopes is strongest in the LFB and, furthermore, Sr isotopes differentiate well between I- and S-type granites in the LFB with no overlap and the Sr isotope dataset is also the most complete. The solid lines in Fig. 5.7 define a mixing envelope between A: Mantle-derived material of rhyolitic composition; B: Mantle-derived material of basaltic composition, and; C: Average Ordovician turbidite value for the LFB. Silicon isotope data for the LFB granites are also plotted, and it is evident that most granite Si isotope compositions fall within the solid mixing envelope. A line joining end-member A to B is comparable to the "igneous array" (Fig. 5.1). That only one granite sample plots outside of this

range demonstrates that little variation outside of igneous $\delta^{30}Si$ values are predicted for both I- and S-type granites from the Lachlan Fold Belt.

There are two samples (BB53 from the Berridale batholith and VB140 from the Wagga batholith) that clearly plot outside the solid mixing envelope (Fig. 5.7). Both of these samples have strong S-type affinities suggesting that, with VB140 especially, these samples are derived almost completely from sedimentary protoliths. This suggests therefore that there is also present, in the LFB, a sedimentary source that is more negative than, and fractionated with respect to igneous rocks. The dashed lines in Figure 5.7 describe a mixing envelope between the two igneous end-members A and B and a postulated sediment D, which has an identical Sr isotope composition but much more negative Si isotopic composition when compared to end-member C. If a sediment with composition comparable to D exists, then it is not a wide-spread source for S-type granites in the LFB, as only samples BB53 and VB140 plot close to it.

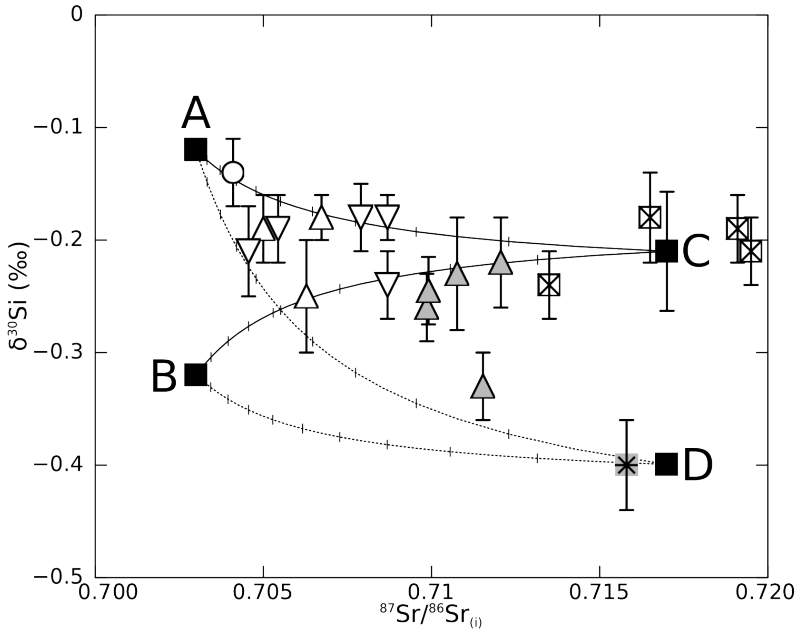


Fig. 5.7 Plot showing $\delta^{30}Si$ vs. $^{87}Sr/^{86}Sr_{(i)}$ isotope mixing curves between two igneous and two sedimentary sources, representative of possible end-member components in the Lachlan Fold Belt. Component "A" represents a rhyolitic mantle-derived melt with SiO_2= 70 wt.%, Sr = 400ppm, $\delta^{30}Si$= -0.12 ‰, $^{87}Sr/^{86}Sr_{(i)}$ = 0.703; component "B" represents a basaltic mantle-derived melt with SiO_2 =48 wt.%, Sr = 300ppm, $\delta^{30}Si$= -0.32‰, $^{87}Sr/^{86}Sr_{(i)}$ = 0.703. A line from component "B" to "A" is analogous to the Si isotope "igneous array" as defined by Savage et al. (2011).
Solid mixing lines define a mixing envelope between the end-members of the igneous array (A and B) and the average Ordovician sedimentary composition (component "C"), as calculated from analyses given in Table 2 and defined as SiO_2= 73 wt.%, Sr = 88ppm, $\delta^{30}Si$= -0.20‰, $^{87}Sr/^{86}Sr_{(i)}$ = 0.717. Dashed mixing lines define a mixing envelope between the igneous array and a sedimentary end member (component "D") with a more negative $\delta^{30}Si$ content ($\delta^{30}Si$= -0.40‰) but otherwise identical to component "C". Tick marks represent 10% mixing graduations. Also plotted are the granite data for the Lachlan Fold Belt samples and the Ordovician sedimentary data (boxed cross symbols are the sediments, otherwise symbols as for Fig. 3, error bars are 95% s.e.). See text for discussion.

Therefore, Si isotopes still have the potential to be used to differentiate between granites derived from igneous or sedimentary material, but this depends wholly on the Si isotopic composition of the sedimentary material itself. It is pertinent to establish that the putative sedimentary component is isotopically distinct from igneous material before attempting to utilise Si isotopes in this way.

5.5.2.2 The New England Batholith

The relatively heavy Si isotope composition of the S-type granite from the New England Batholiths merits comment. This value is the heaviest $\delta^{30}Si$ value measured in this study, heavier than even I- and A-types. The sample is taken from the Bundarra supersuite, which displays many geochemical properties consistent with a sedimentary protolith (high ASI values, heavy $\delta^{18}O$ values, light $\delta^{7}Li$ values; Flood and Shaw., 1977; Bryant et al., 2004) but has, unlike the S-type granites of the LFB, mantle-like Sr and Nd isotopic values (Hensel et al., 1985), suggesting that the sedimentary source was derived from rapid reworking of volcanogenic arc-derived sediment. This rapid weathering may have limited the amount of Si isotope fractionation that occurred in the sedimentary pile, resulting in an unfractionated sediment (relative to igneous rocks) similar in composition to that of the Ordovician turbidites. However, it does not explain why the S-type is heavier than I-type granite. One possibility is that the Si in the sedimentary source derives partially from a biogenic source, which can have much heavier $\delta^{30}Si$ values than igneous rocks (e.g. De la Rocha, 2003; Hendry et al., 2010). Studies have shown that chert bands and other siliceous sediments are common in the sedimentary pile from which the NEB S-type granites are thought to derive (Korsch et al., 1977). Incorporation of this Si-rich material could overwhelm the Si isotope signature of a crustal melt and push it toward heavier isotopic values, but should not affect the Li, Sr and Nd isotopic signatures and would also result in heavy $\delta^{18}O$ values, consistent with an S-type granite affinity. Presence of biogenic material in a granite source will result in a low fO_2 in the granites, and the Bundarra suite is noted for its low Fe_2O_3/FeO ratios (Shaw and Flood, 1981). However, on the basis of one sample, it is difficult to make any firm statements about the petrogenesis of NEB granites.

5.5.3 The silicon isotopic composition of the upper continental crust

Granitoid rocks compose ~ 50% of the upper continental crust, and occur in significant

quantities in the middle and lower crust (Wedepohl, 1995; Rudnick and Fountain, 1995), so providing an average value for granitic crust is an important step to defining the Si isotope composition of the Earth's continental crust. The average value for all the granites (I-, S- and A-type) and the aplites (which we have established are unfractionated from their host granites) analysed in this study is $\delta^{30}Si = -0.23 \pm 0.15$ ‰ (2 s.d.). Although there is a significant amount of isotopic variation, this value is identical to the "igneous" composition of the continental crust that can be calculated using the "igneous array" equation (Fig. 5.1) and Rudnick and Gao's (2003) estimate of the SiO_2 content in the continental crust (60.6 wt.%), which is $\delta^{30}Si = -0.23 \pm 0.05$ ‰ (Chapter 4).

5.6 CONCLUSIONS

1. Analysis of granites from south-eastern Australia and south-west England indicate that significant Si isotopic variations occur in granitoid rocks. This range is greater than that displayed by other high-Si igneous rocks, such as rhyolites and dacites from Hekla and Afar (Chapter 4). We do not replicate the much larger range of Si isotope values that Douthitt (1982) provides for granites from the Lachlan Fold Belt, and we suggest that the large range found in that study is most likely a result of larger analytical uncertainties.
2. On average, Lachlan Fold Belt granites with a sedimentary affinity have lighter Si isotope compositions than igneous-derived granites. Although there is a small amount of fractionation expected from varying degrees of magmatic differentiation, some S-type samples display lighter $\delta^{30}Si$ values than is predicted, had they derived from a purely mantle source. This agrees with the hypothesis that S-type granites should have a lighter Si isotope signature because they derived from sedimentary material, which is typically enriched in the lighter isotopes of Si. However, there is significant overlap between the two affinities.
3. The correlations between Si isotopes and other proxies for source composition in granites (ASI value, $\delta^{18}O$, $^{87}Sr/^{86}Sr_{(initial)}$ and $\varepsilon Nd_{(initial)}$) support the conclusion that Si isotope variation in granitoid material is predominately related to source heterogeneity. It is clear, however, that these geochemical indices distinguish between granites of varying affinities much more conclusively. Silicon isotope analysis of the proposed sedimentary

source for many of the LFB granites reveals why this might be, as these sediments appear to be unfractionated relative to igneous rocks. However, relatively isotopically light S-type granites do exist in the LFB, suggesting that there may be some isotopically lighter sedimentary sources that have not yet been analysed.

4. A volatile-rich melt phase is a common component of granite petrogenesis. However, the aplite and pegmatite data analysed in this study suggest that volatile-related processes do not significantly affect the overall Si isotope composition of granitoid material.
5. The average Si isotope value for granitoid material is $\delta^{30}Si = -0.23 \pm 0.15$ ‰ (2 s.d.). This is entirely consistent with the "igneous" value of continental crust, calculated in Chapter 4, of $\delta^{30}Si = -0.23 \pm 0.05$ ‰.

Chapter 6: The silicon isotope composition of the upper continental crust

6.1 INTRODUCTION

This chapter completes the investigation of the Si isotope composition of the Upper Continental Crust (UCC) and accompanies the study of granites in Chapter 5. Although felsic intrusive rocks are most common, around 20% of the UCC consists of sedimentary or meta-sedimentary material (Wedepohl, 1995). Because of this, and also because there is evidence that sedimentary material exhibits relatively larger degrees of Si isotope fractionation (see Chapter 1), this research focuses on such lithologies in order to form a more comprehensive picture of the Si isotope composition of the UCC.

Silicon is the second most common element in the Earth's crust, and the UCC is the major source of primary silica in the Si cycle – ~ 85% of marine seawater is derived from the continents (Tréguer et al., 1995). The Si cycle is also intrinsically linked with the carbon cycle. For example, Si is a major nutrient for planktonic diatoms and is important for marine primary productivity (e.g. Tréguer et al., 1995; Hendry et al., 2010); this process sequesters atmospheric CO_2 into organic carbon and subsequent burial of this material mediates atmospheric CO_2 (Ragueneau et al., 2000). Also, weathering of fresh silicate minerals by reaction with carbonic acid dissolved in meteoric water is a sink for atmospheric CO_2 (Walker et al., 1981). As stable isotopes can provide information about sources and rates in such cycles, the Si isotope system is an obvious choice for application to the Si cycle.

As such, over the last decade there have been a number of studies that have investigated Si isotopes in both biological and weathering cycles. These have demonstrated that isotopic fractionation is generated as a result of biological utilisation, either by marine organisms (De La Rocha et al., 1998; Hendry et al., 2010) or vegetation (Ding et al., 2005; Opfergelt et al., 2008), low-temperature weathering processes (Ziegler et al., 2005a&b; Georg et al., 2009a; Bern et al., 2010; Opfergelt et al., 2008, 2009, 2010, 2011; Steinhoefel et al., 2011) and precipitation of secondary silica (Basile-Doelsch et al., 2005). All of these processes tend to enrich the product in the lighter isotopes of silica, resulting in a fluid with a relatively heavy Si isotopic signature (De la Rocha et al., 2000; Ding et al., 2004, Georg et al., 2006a, 2009b; Cardinal et al., 2010; Engström et al., 2010). There is, however, a large gap in our knowledge of the Si isotope system; that of the Si isotopic composition of the continental crust. Ultimately, all the Si utilised in the above reactions is sourced from the continents and to further understand the global Si cycle it is key to quantify this source.

The studies of Douthitt (1982) and Ding et al. (1996) were the first to hint at the isotopic composition of the continental crust but, since then, very little progress has been made. In both studies it was demonstrated that evolved igneous rocks were enriched in the heavier isotopes of Si and were more isotopically variable when compared to primitive igneous rocks. Such observations have since been reappraised using more modern analytical techniques, but are still broadly accepted (see Chapters 3, 4 & 5). The former studies also suggest that chemically derived sedimentary material (i.e. siltstone, shale) is, in general, isotopically lighter, whereas the Si isotopic composition of mechanically derived sediment (i.e. sandstone) is comparable to that of igneous rock (again, these observations have been corroborated by more recent weathering studies, see above). However, both of these studies were aimed at cataloguing the natural variation of Si isotopes and so no attempt was made to provide an average isotopic composition.

This research aims to remedy this gap in our knowledge using a set of well-characterised shale and loess samples, as well as the data for granitoid material previously acquired (Chapter 5). Besides providing an average δ^{30}Si value for the UCC, the degree of Si isotopic heterogeneity in the UCC can also be constrained, which may provide information about crust formation and/or long-term weathering. Finally, using shale samples that have deposition ages ranging from >3.3 Ga to 0.2 Ga, the evolution of the Si isotopic signature of the crust through time can be investigated.

6.2 SAMPLES

6.2.1 Loess

Loess is an aeolian sediment, derived predominantly from deserts and/or glacial milling and deposited during cold-dry climatic phases, which covers approximately 10% of the world's land surface (Taylor et al., 1983; Pye, 1995). It is composed mainly of quartz, feldspar, sheet silicates and/or calcite, depending on the regional geology (Taylor et al., 1983). Mechanical sedimentary derivation from glacial milling has limited the amount of chemical weathering that has affected loess, although most loess has experienced at least one cycle of chemical alteration (Gallet et al., 1998). Because loess formation samples large areas of crust, it has been used effectively by many authors to constrain the average elemental composition of the continental crust (e.g. Taylor et al., 1983; Barth et al., 2000; Hu and Gao, 2008). As far as the author is aware, no Si isotopic analyses of loess are available in the literature.

We have analysed 13 Pleistocene loess samples, sourced from China, New Zealand, Germany, Hungary and the USA, which have previously been studied for major and trace elements (Taylor et al., 1983, Gallet et al., 1998, Barth et al., 2000; Hu and Gao, 2008) and Li and Mg stable isotopes (Teng et al., 2004; Li et al., 2010). Major element composition of loess is somewhat variable, with each loess suite reflecting the diverse regional geology of their source region, e.g. Si-rich loess from the Banks Peninsula is derived from Mesozoic greywackes from the Southern Alps, whereas European loess is more carbonate-rich, reflecting its derivation from Alpine terrains. The Iowa and Kansas loess is thought to come from the Rocky mountains. In contrast, much Chinese loess is non-glacial, deriving instead from a desert environment (Taylor et al., 1983).

Degree of chemical weathering of a sediment is often parametrised using the Chemical Index of Alteration (CIA; Nesbitt and Young, 1982) which is defined as CIA = molar Al_2O_3 / [Al_2O_3 + CaO* + Na_2O + K_2O]. In this calculation, CaO* refers to the CaO present only in silicates, not in apatite and carbonate, and is corrected using molar P_2O_5 and Na_2O quantities (see McLennan, 1993). The loess samples analysed in this study have CIA values between 57 and 65, which is slightly elevated when compared to unweathered rocks (CIA ~ 50; Nesbitt and Young, 1982) but lower than shales (see later), which is consistent with the suggestion of Gallet et al. (1998) that most loess has experienced only limited chemical weathering.

6.2.2 Shales

Shales are fine-grained sedimentary rocks composed mainly of clay minerals and detrital quartz, that are deposited in low energy, hot, humid environments. They are derived from erosion over large areas and so, like loess, they are often used as representative samples of the upper continental crust (e.g. Nance and Taylor, 1976; Taylor and McLennan, 1985; Barth et al., 2000). Shale petrogenesis is more complicated than loess, involving both mechanical and chemical weathering as well as variable amounts of diagenesis and metamorphism, resulting in higher CIA values than loess. Despite this, shales show little variation in their insoluble element ratios (Taylor and McLennan, 1985) and so provide good estimates of these in the upper crust. Also, whereas loess is normally confined to the Pleistocene, shales are present in the geological record throughout Earth's history. As far as the authors are aware, no previous Si isotopic analyses of shales are available in the literature, although the Si isotopic systematics of clays

and clay formation have been reasonably well studied (see Section 6.1.).

Thirty eight sedimentary samples, taken from Australia, Canada and the USA were analyed for Si isotopes. Twenty two shales were analysed from the Post-Archaean Australian Shale (PAAS) suite, originally used by Nance and Taylor (1976) to estimate the rare earth element composition of the upper continental crust, and subsequently by Taylor and McLennan (1985), Barth et al. (2000) and Hu and Gao (2008) for further trace element work, and Teng et al. (2004) and Li et al. (2010) for Li and Mg stable isotopes studies respectively. These samples were collected from across Australia (see Figure 1 in Nance and Taylor, 1976) and span a wide range of ages from mid-Protorezoic (1.5 Ga) through to Triassic (200-250 Ma). All samples were taken from well cores to avoid the effects of weathering and/or leaching. CIA values of the PAAS shales are high and variable, ranging from 66 to 80 (c.f. ~50 for unweathered rocks). As well as the PAAS samples, we have analysed two shales from the Pilbara Supergroup, Western Australia (McLennan et al., 1983), which have Archaean deposition ages of around 3.4 Ga (Gorge Creek) and 2.7 Ga (Whim Creek) respectively.

Seven samples were taken from the Huronian Supergroup and Sudbury Basin suites, Canada (McLennan et al., 1979; McDaniel et al., 1994; McLennan et al., 2000). Samples from the Huronian Supergroup are early Protorezoic and composed predominantly of granitoid and volcano-sedimentary material derived from the Archaean-age Superior Province (McLennan et al., 1979). A slightly younger (1.85 Ga) sandstone sample has also been analysed from the nearby Sudbury basin (McDaniel et al., 1994), which is also thought to derive from the Superior Province. Some of these samples resemble tillites or glacial mudstones (i.e. Gowganda, Table 6.3.) that have not experienced high degrees of chemical alteration and have CIA values comparable to those of loess (see above). These samples may therefore be more representative of fresh continental Archaean crust than the more chemically altered shales.

Four metasediment samples were analysed from the Honda Group and Uncomphagre Formation in southwestern North America (McLennan et al., 1995). These samples represent a quartzite-pelite stable-shelf succession, derived from differentiated Protorezoic-age crust with small but variable amounts (10–25%) of Archaean material. Major element systematics indicate that these samples contain minor carbonate and have undergone severe weathering before deposition (McLennan et al., 1995).

Finally, the USGS shale standards SDO-1, SCo-1 and SGR-1b were analysed. All of

these samples are from the USA and contain different amounts of carbonate material, with SCo-1 showing the strongest terrestrial affinity. Sample SGR-1b is from an oil shale – because this sample is not predominately silicate-derived it has an anomalously low SiO_2 content (<30 wt.%) and CIA value (36).

6.3 METHODS

Sample were prepared for MC-ICP-MS analysis following the methods and techniques detailed by Georg et al. (2006b). These procedures are comprehensively described in Chapter 2; only a brief summary and any sample-pertinent information will be given here. All loess and shale samples were received as powders that had been milled in agate. This does not cause isotopic contamination, as described in Chapter 4 and Zambardi and Poitrasson (2011).

Between 5 and 10 mg of sample powder was weighed into a silver crucible along with ~ 200 mg of NaOH flux. The crucible was then placed into a furnace, heated to 720ºC, for 12 minutes, then removed and allowed to cool slightly. After fusion, the crucible was placed into 20 ml of MQ-e water and left to react for 24 hours. The sample was transferred from the crucible via a pipette into pre-cleaned 125 ml PP bottles, diluted with MQ-e water and acidified to 1% v/v with triple-distilled HNO_3. Sample yield was then checked using a photospectrometer; the average yield for all loess and shale samples used in this study is 96 ± 4 % (2 s.d.).

Samples were quantitatively purified before MC-ICP-MS analysis using a single-pass column technique with BioRAD AG50W X12 200-400 mesh cation resin. The samples were acidified after purification to 1% v/v HNO_3. All samples and standards, including the bracketing standard, underwent identical chemical processing before analysis.

Silicon isotope measurements were made in house on a Nu Instruments (Wrexham) Nu Plasma High Resolution Multi-Collector Inductively-Coupled-Plasma Mass Spectrometer (HR-MC-ICP-MS). The machine and running conditions are detailed in Chapter 2 and in Georg et al. (2006b). The machine was operated at "medium" resolution (resolving power $m/\Delta m \sim 3300$, where Δm is defined at 5% and 95% for peak height; Weyer and Schwieters, 2003). Typical sample Si concentrations were between 750 ppb and 1.0 ppm (depending on machine conditions), which gave a total signal of $\sim 1 \times 10^{-10}$A.

Silicon isotope values are calculated with the standard-sample bracketing technique, using NBS28 silica sand as the bracketing standard. Isotopic variations from this standard are

represented in per mil (‰) by the delta notation, defined as:

$$\delta^{30}Si = [(^{30}Si/^{28}Si_{sample})/(^{30}Si/^{28}Si_{standard}) - 1] \times 1000;$$

$$\delta^{29}Si = [(^{29}Si/^{28}Si_{sample})/(^{29}Si/^{28}Si_{standard}) - 1] \times 1000.$$

Data is discussed using the $\delta^{30}Si$ values, which are ~ 2 × the magnitude of the $\delta^{29}Si$ values, assuming mass dependence (which, for terrestrial samples, is a valid assumption).

6.4 RESULTS

6.4.1 External standards

The external standards Diatomite and BHVO-2 were routinely analysed to assess sample data accuracy and precision. Both are widely available and widely utilised by the Si isotope community; as such, well-established "book" values are available for comparison. External standard data are given in Table 6.1 as well as some reference values (see Reynolds et al., 2007; Abraham et al., 2008; Georg et al., 2009a; Savage et al., 2010; Zambardi and Poitrasson, 2011; Armytage et al., 2011; Savage et al., 2011). The data for Diatomite ($\delta^{30}Si$ = 1.22 ± 0.09 ‰; 2 s.d., n = 129) and BHVO-2 ($\delta^{30}Si$ = -0.30 ± 0.09 ‰; 2 s.d., n = 129) illustrate the good levels of accuracy and precision that our methods can attain.

6.4.2 Sample data

Silicon isotope data for the loess and shale samples are given in Tables 6.2 and 6.3. Measurement uncertainties are represented by both 2 s.d. (2 × the standard deviation) and 95% s.e. (95% standard error of the mean = t × s.d./$(n)^{1/2}$, where t = inverse survival function of the Student's t-test at the 95% significance level and n-1 degrees of freedom). The mean 2 s.d. value for all samples analysed in this study is 0.09 ‰, identical to that given by the external standard data. For an average n value of 11 per datum, this gives an average 95% s.e. value of 0.03 ‰, which we consider to be our representative precision.

6.4.2.1 Loess results

Silicon isotope data for the loess samples are given in Table 6.2 and plotted on Figure 6.1. Loess displays limited range of Si isotope compositions, with $\delta^{30}Si$ values ranging from -0.28 to -0.15‰, and an average value of $\delta^{30}Si$ = -0.22 ± 0.07 ‰ (2 s.d., n = 13). There is some minor isotopic variation between localities, with the European (German and Hungarian) loess

Table 6.1 – External standard data

Standard		SiO_2	$\delta^{30}Si$ (‰)	2s.d.	95%s.e.	$\delta^{29}Si$ (‰)	2s.d.	95%s.e.	n
Diatomite	1	100	1.22	0.11	0.04	0.64	0.07	0.02	11
	2		1.23	0.09	0.03	0.62	0.06	0.02	11
	3		1.22	0.07	0.02	0.64	0.07	0.02	11
	4		1.21	0.04	0.02	0.59	0.05	0.02	11
	5		1.20	0.08	0.03	0.61	0.07	0.02	11
	6		1.25	0.08	0.03	0.63	0.07	0.02	11
	7		1.23	0.10	0.04	0.63	0.07	0.02	11
	8		1.20	0.06	0.02	0.63	0.03	0.01	11
	9		1.22	0.09	0.03	0.62	0.08	0.03	11
	10		1.24	0.11	0.04	0.61	0.07	0.02	10
	11		1.23	0.10	0.03	0.65	0.11	0.04	11
	12		1.20	0.10	0.04	0.61	0.05	0.02	9
Average			1.22	0.09	0.01	0.62	0.07	0.01	129
Reynolds et al. (2007)			1.26	0.20		0.64	0.14		
Georg et al. (2009a)			1.23	0.16		0.62	0.11		
Savage et al. (2011)			1.23	0.10		0.64	0.08		
BHVO-2	1	49.9	-0.31	0.05	0.02	-0.14	0.08	0.03	11
	2		-0.34	0.10	0.03	-0.15	0.06	0.02	11
	3		-0.29	0.06	0.02	-0.18	0.04	0.01	11
	4		-0.26	0.05	0.02	-0.13	0.07	0.02	11
	5		-0.29	0.07	0.02	-0.17	0.06	0.02	11
	6		-0.31	0.08	0.03	-0.14	0.03	0.01	11
	7		-0.31	0.10	0.03	-0.15	0.09	0.03	11
	8		-0.29	0.12	0.04	-0.16	0.07	0.02	11
	9		-0.31	0.08	0.03	-0.17	0.08	0.03	10
	10		-0.33	0.10	0.04	-0.16	0.09	0.03	9
	11		-0.28	0.06	0.02	-0.15	0.04	0.01	11
	12		-0.30	0.10	0.03	-0.17	0.06	0.02	11
Average			-0.30	0.09	0.01	-0.15	0.07	0.01	129
Abraham et al (2008)			-0.29	0.11		-0.17	0.04		
Zambardi and Poitrasson (2011)			-0.27	0.08		-0.14	0.05		
Savage et al. (2011)			-0.29	0.09		-0.15	0.08		

Silicon isotope data for external standards analysed during this study. Errors are given as 2 s.d. (2 × standard deviation) and 95% s.e. (95% s.e. = t × s.d./$(n)^{1/2}$, where t = inverse survival function of the Student's t-test at the 95% significance level and n-1 degrees of freedom). Reference values are provided for comparison.

samples having slightly lighter $\delta^{30}Si$. However, these variations are within error and there are no resolvable differences between loess derived from distinct continental provinces. There are also no strong correlations with SiO_2 content, weathering degree (CIA values) or other isotope systems (Figs. 6.2, 6.3b and 6.4). This limited isotopic range is in contrast to the $\delta^{26}Mg$ and $\delta^{7}Li$ compositions of these samples, which display a 3x- and 60x-greater isotopic variability respectively (Teng et al., 2004; Li et al., 2010).

Table 6.2 – Silicon isotope composition of loess

Sample	ID	SiO_2	$\delta^{30}Si$ (‰)	2s.d.	95%s.e.	$\delta^{29}Si$ (‰)	2s.d.	95%s.e.	n	CIA	$\delta^{26}Mg$ (‰)	$\delta^{7}Li$ (‰)
Banks Peninsula, New Zealand	BP-1	72.7	-0.22	0.09	0.03	-0.12	0.06	0.02	11	59	-0.04	-2.6
	BP-2	74.0	-0.26	0.08	0.03	-0.12	0.04	0.02	10	59	0.02	-1.7
	BP-3	72.5	-0.21	0.08	0.03	-0.08	0.06	0.02	9	61	0.05	-3.1
	BP-4	74.0	-0.23	0.06	0.02	-0.12	0.07	0.02	11	57	-0.01	1.4
	BP-5	72.5	-0.28	0.08	0.03	-0.11	0.05	0.02	11	57	-0.07	-0.7
Kansas, USA	CY-4a-A	80.4	-0.23	0.07	0.02	-0.12	0.11	0.04	11	59	-0.23	4.5
	CY-4a-B	80.8	-0.22	0.10	0.04	-0.12	0.07	0.02	11	59	-0.31	4.8
	CY-4a-C	79.9	-0.20	0.07	0.02	-0.10	0.04	0.01	11	58	-0.32	4.2
Muscatine, Iowa, USA	I	79.5	-0.25	0.12	0.04	-0.13	0.07	0.02	11	64	-0.01	-0.3
Kaiserstuhl, Germany	K1	59.9	-0.19	0.09	0.03	-0.09	0.06	0.02	11	65		-0.9
	K2	59.1	-0.15	0.07	0.02	-0.08	0.06	0.02	11	65		-0.7
Hungary	H	52.0	-0.22	0.04	0.01	-0.14	0.04	0.01	11			-0.6
China	CH	56.0	-0.19	0.11	0.04	-0.11	0.07	0.03	10			0.7
	CH-repeat		-0.20	0.08	0.03	-0.08	0.08	0.03	11			

Silicon isotope data for loess samples analysed in this study. Silica contents (in wt.%) and CIA values are taken from Taylor et al. (1983). Magnesium and lithium stable isotope data are taken from Li et al. (2010) and Teng et al. (2004) respectively. See text for discussion.

6.4.2.2 Shales

Silicon isotope data for the shale samples are given in Table 6.3 and are plotted in Figure 6.1. In contrast to the loess data, the PAAS shales define a wide range of $\delta^{30}Si$ values, with samples ranging from $\delta^{30}Si$ = -0.80 to +0.00 ‰ (average $\delta^{30}Si$ = -0.37 ± 0.47 ‰; 2 s.d., n = 22). Compared to igneous rocks, this is a large spread of Si isotope compositions, and is comparable to the range for clays measured by the studies of Douthitt (1982) and Ding et al. (1996) – see Figure 5.2. Although the overall spread of data is large, within each locality there is remarkably limited Si isotope variation – this phenomenon is also apparent in the Mg isotope data of these shales (Li et al., 2010). There are no strong correlations between Si isotopes and SiO_2 (Fig. 6.2) or stable isotopes of Li and Mg (Fig. 6.4), although there is a very vague negative trend (R^2 = 0.14) with CIA values (Fig. 6.3a). The two Archaean Pilbara shales from Australia are both lighter than igneous rocks (sample Pg-7 displays the lightest $\delta^{30}Si$ value analysed in this study, viz. -0.82 ± 0.04 ‰, 95% s.e.), but show similar isotopic values to the younger PAAS shales. The data for the SW USA shales also show a limited range ($\delta^{30}Si$ = -0.51 to -0.40 ‰, average $\delta^{30}Si$ = -0.47 ± 0.10 ‰; 2 s.d., n = 4), again lighter than the range for igneous rocks.

Silicon isotope data for the Canadian samples (Huronian and Sudbury) range from $\delta^{30}Si$ = -0.41 to -0.16 ‰ (average $\delta^{30}Si$ = -0.25 ± 0.20 ‰; 2 s.d., n = 7). Silicon isotopic variation is

Table 6.3 – Silicon isotope composition of shales

Sample	ID	SiO_2	$\delta^{30}Si$ (‰)	2s.d.	95%s.e.	$\delta^{29}Si$ (‰)	2s.d.	95%s.e.	n	CIA	$\delta^{26}Mg$ (‰)	$\delta^{7}Li$ (‰)	Model age (Ga)
Post-Archaean Australian shales													
Perth Basin	PW-4	57.9	-0.69	0.05	0.02	-0.37	0.11	0.04	11	79	0.03		1.87
(200-250Ma)	PW-5	55.3	-0.78	0.10	0.04	-0.41	0.08	0.03	11	80	-0.07	2	
	PW-7	59.6	-0.80	0.12	0.04	-0.41	0.13	0.05	11	75	-0.22		
Caning Basin	PL-1	63.5	-0.45	0.09	0.03	-0.21	0.07	0.02	11	80	-0.13	-0.9	
(250-400Ma)	PL-6	61.1	-0.43	0.08	0.03	-0.25	0.03	0.01	11	76	-0.14		
	PL-7	66.8	-0.47	0.10	0.04	-0.22	0.05	0.02	11	71			1.89
State Circle	SC-1	65.1	-0.19	0.09	0.03	-0.09	0.08	0.03	11	76	-0.05		
(440Ma)	SC-2	65.3	-0.19	0.13	0.05	-0.08	0.10	0.04	11	76	0.04		
	SC-3	67.0	-0.24	0.13	0.05	-0.15	0.07	0.02	11	76	0.03		
	SC-5	65.3	-0.27	0.10	0.04	-0.14	0.12	0.04	11	76	0.07		1.75
	SC-7	65.6	-0.21	0.11	0.04	-0.14	0.04	0.01	11	77	0.02	-0.7	
	SC-8	65.6	-0.19	0.14	0.05	-0.11	0.08	0.03	11	75	0.03	-0.2	
Amadeus Basin	AO-6	61.1	-0.41	0.09	0.03	-0.22	0.07	0.02	11	66	-0.18	-3.1	
(850Ma)	AO-7	61.8	-0.57	0.13	0.05	-0.28	0.10	0.04	11	67		-2.3	2.03
	AO-8	70.0	-0.59	0.08	0.03	-0.31	0.08	0.03	11	71			
	AO-9	65.8	-0.51	0.10	0.04	-0.29	0.08	0.03	11	70	0.05	-2.6	
	AO-10	63.0	-0.47	0.05	0.02	-0.27	0.03	0.01	11	72	0.37	-0.7	
	AO-12	56.6	-0.54	0.12	0.04	-0.28	0.05	0.02	11	66	0.49	3.4	
Mt. Isa	MI-1	71.0	0.00	0.08	0.03	-0.01	0.07	0.02	11	70	0.28		2.47
(1500Ma)	MI-2	56.1	-0.02	0.09	0.03	-0.01	0.06	0.02	11	71	0.23		
	MI-4	69.8	0.00	0.10	0.04	-0.02	0.07	0.02	11	66	0.05		
	MI-5	65.9	-0.21	0.09	0.04	-0.14	0.09	0.04	9	76	0.05		
Pilbara Archaean shales - Australia													
Gorge Creek (3.4 Ga)	Pg-7	57.6	-0.82	0.10	0.04	-0.41	0.08	0.03	11	76			3.78
Whim Creek (2.7 Ga)	WC-3	48.1	-0.48	0.12	0.04	-0.21	0.09	0.03	11	83			3.17
Huronian - Canada (2.5 - 2.2 Ga)													
McKim	M-5	58.5	-0.37	0.13	0.05	-0.21	0.05	0.02	9	75			
Pecors	P-7	56.6	-0.22	0.12	0.04	-0.09	0.11	0.04	11	68			
Gowganga	G-9	59.9	-0.20	0.12	0.04	-0.09	0.04	0.01	11	59			
	G-9-repeat		-0.18	0.09	0.03	-0.07	0.04	0.02	10				
	G-16	57.7	-0.16	0.06	0.02	-0.07	0.05	0.02	11	57			
	G-28	57.6	-0.41	0.11	0.04	-0.21	0.11	0.04	10	71			
Gordon Lake	GL-3		-0.17	0.13	0.05	-0.10	0.07	0.02	11	66			
Sudbury Basin - Canada (1.85 Ga)													
Chelmsford	DKM-6	68.9	-0.20	0.13	0.05	-0.10	0.06	0.02	11	64			
SW USA Proterozoic shales (1.8 - 1.7 Ga)													
Rinconada	R1-1	65.6	-0.51	0.08	0.03	-0.30	0.05	0.02	10	69			
	R4-5	64.8	-0.51	0.06	0.02	-0.27	0.10	0.04	11	78			
Piedra Lumbra	PL-5	68.0	-0.47	0.12	0.04	-0.26	0.13	0.05	11	71			
Uncomphagre	S-4	67.4	-0.40	0.13	0.05	-0.22	0.08	0.03	11	76			
USGS shale standards													
Ohio - Devonian	SDO-1	49.3	-0.24	0.04	0.01	-0.10	0.07	0.02	11	72			
Cody – Cretaceous	SCo-1	62.8	-0.28	0.03	0.01	-0.17	0.04	0.01	11	70			
Green River - Eocene	SGR-1b	28.2	0.01	0.04	0.01	-0.01	0.06	0.02	11	36			

Silicon isotope data for loess samples analysed in this study. Silica contents (in wt.%) and deposition ages are taken from Taylor and McLennan (1976), McLennan et al. (1979), McLennan et al. (1983), McDaniel et al. (1994), McLennan et al., (1995) and the USGS datasheets (http://minerals.cr.usgs.gov/). CIA values are either taken directly from, or calculated using the chemical analyses provided in the above papers. The Nd model ages are taken from Allègre and Rousseau (1984). Magnesium and lithium stable isotope data are taken from Li et al. (2010) and Teng et al. (2004) respectively. See text for discussion.

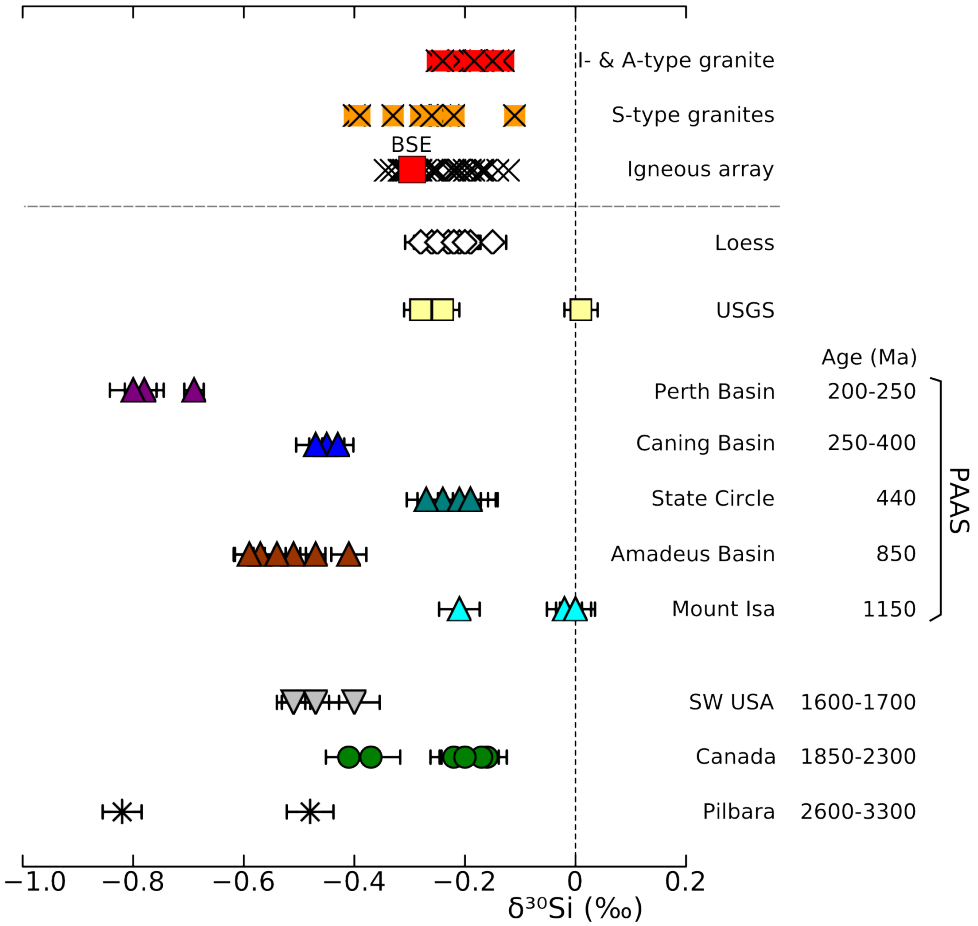


Fig. 6.1 Plot of the $\delta^{30}Si$ values for the loess and shale samples analysed in this study (error bars are 95% s.e.), showing that loess is relatively homogeneous, and that shales define a large range of Si isotopic compositions. Also shown are $\delta^{30}Si$ values for I-, A- and S-type granites (Chapter 5), extrusive igneous rocks (Chapter 4) and Bulk Silicate Earth (Chapter 3) for comparison.

smaller than for the PAAS shales, with the data falling into two populations; one near $\delta^{30}Si$ = -0.39 ‰, the other around $\delta^{30}Si$ = -0.19 ‰, the possible causes of which will be discussed later.

The USGS standards are geologically unrelated, with varied petrogenetic histories and age ranges. The $\delta^{30}Si$ data are within the range defined by PAAS shales. Sample SGR-1b, an organic-rich oil-shale, has a relatively heavy Si isotopic composition ($\delta^{30}Si$ = +0.01 ± 0.03 ‰, 95% s.e.); this could indicate the presence of biogenic silica, which is isotopically heavy compared to terrestrial silicate material (e.g. De la Rocha et al., 1998; Opfergelt et al., 2008; Hendry et al., 2010).

6.5 DISCUSSION

The data described above show that, with respect to Si isotopes, the UCC is heterogeneous relative to igneous rocks (see Chapters 3, 4 and 5). The following discussion concerns how these data can be used to constrain the Si isotopic composition of the modern day UCC, as well as how the UCC has varied through time. These data will then be combined with data from previous chapters to calculate an average Si composition for the UCC.

6.5.1 Loess as a proxy for the composition of the UCC

The differences in isotopic heterogeneity between loess and shales reflect the varying petrogenetic histories of these two lithologies. The consistency of the Si isotopic composition of loess samples taken from all over the globe is remarkable. Not only is the range of loess $\delta^{30}Si$ values limited with respect to shale samples, it is also smaller than the isotopic range displayed by igneous rocks (Fig. 6.1). This is despite loess sampling a wide range of lithologies (Taylor et al., 1983), exhibiting a broad range chemical compositions (SiO_2 content ranging from 52 to 81 wt.%; Fig 6.2), and evidence that most loess samples have experienced at least one cycle of chemical weathering (Gallet et al., 1998). This last point is illustrated in Figure 6.3b, which shows that all the loess samples analysed here have CIA values greater than unweathered igneous material. Finally, these same loess samples show resolvable (and in some cases, quite large) variations in their $\delta^{7}Li$ and $\delta^{26}Mg$ values, which in both cases is related to weathering

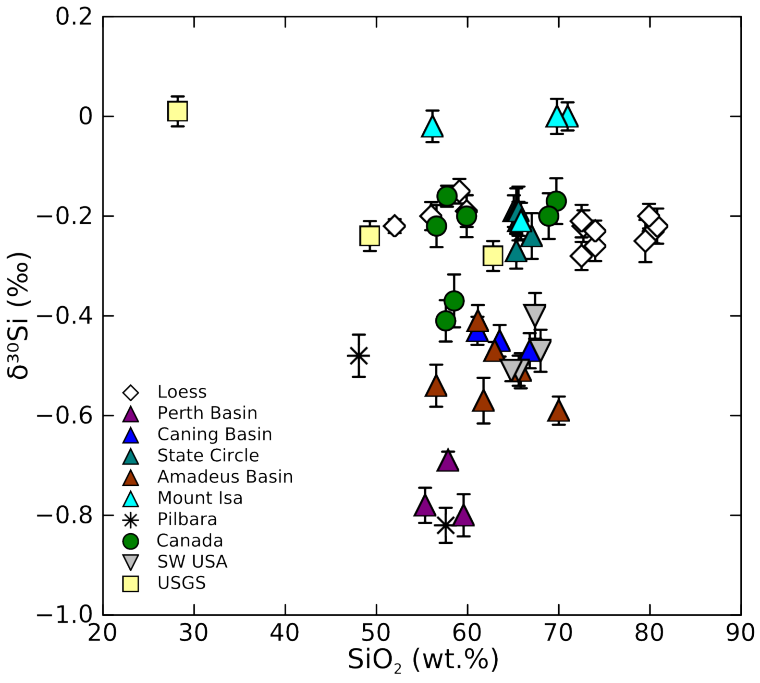


Fig. 6.2 Graph of $\delta^{30}Si$ against SiO_2 for all loess and shale samples (error bars are 95% s.e.) - see text for discussion.

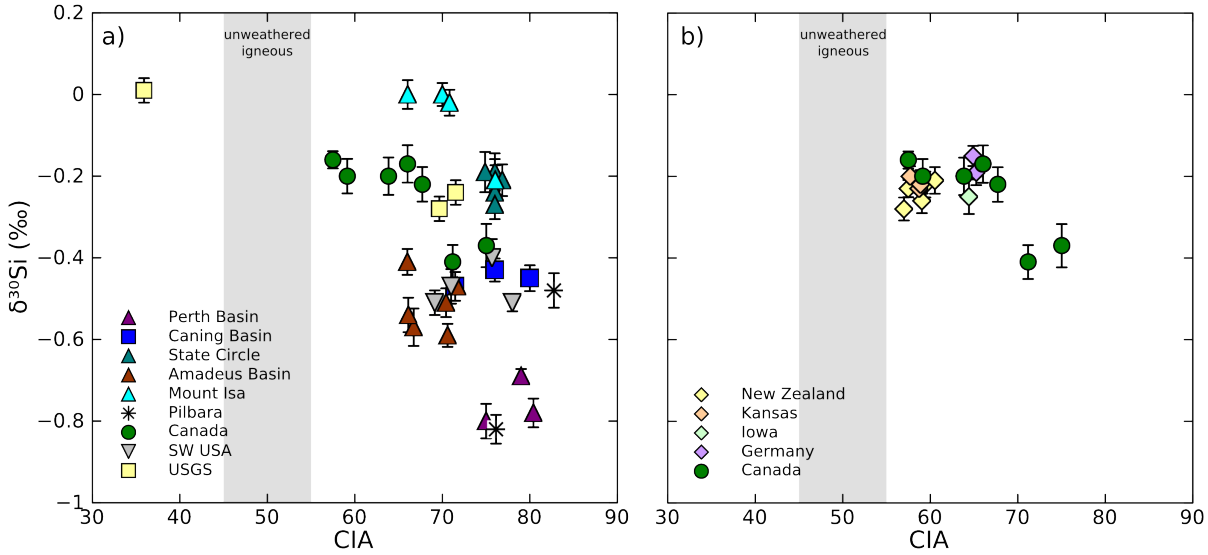


Fig. 6.3 Graph of $\delta^{30}Si$ against CIA value for a) all shale samples and b) all loess samples (error bars are 95% s.e.). The CIA value is defined as CIA = molar Al_2O_3/ [Al_2O_3+ CaO* + Na_2O+ K_2O], where CaO* refers to the CaO present only in silicates (Nesbitt and Young, 1982, McLennan, 1983). The grey bar illustrates the range of CIA values for unweathered igneous material (50 ± 5; Nesbitt and Young, 1982). For the shale samples, a vague negative trend exists between $\delta^{30}Si$ and CIA value, indicating a component of weathering in the Si isotopic compositions of shales. No such relationship exists in loess. The Canadian samples have been plotted in both figures because the sample group contains both loess-like and shale-like samples.

processes (Fig. 6.4; Teng et al., 2004; Li et al., 2010). Why then, are Si isotopes in loess so consistent, when weathering has been shown to have a resolvable Si isotopic effect?

The most likely explanation for this can be found by studying the mineralogy of loess, in which the most common Si-bearing phases are quartz and feldspar, i.e. primary igneous minerals (Pye, 1995). Even though loess may have experienced some weathering, Si isotopes are only affected if there has been formation of secondary mineral phases. Loess is generally poor in these and so the abundance of quartz will dominate the Si budget. This is not so for the CIA value, which is a proxy for loss of fluid-mobile elements (Ca, Na and K) with respect to Al, predominantly due to breakdown of primary feldspar. Even though Si is more water-soluble than Al (at acidic and neutral conditions; $2 < pH < 8$), it is much less so than Ca, Na and K (Turner et al., 1980) and small increases in CIA value recorded by loess should not necessarily imply any significant Si loss from the bulk rock. On the other hand, Mg and Li isotopes are a) both strongly fluid mobile and b) not present in large amounts in either quartz or feldspar, and therefore are more amenable to secondary weathering effects.

Another possibility to explain the large Mg and Li isotopic variations in loess may be the presence (or absence) of carbonate material in the loess source region. Both Mg and Li are

present in significant quantities and display large isotopic ranges in carbonate-derived material (δ^7Li ~ -10 to +30 ‰; Hoefs and Sywall, 1997; δ^{26}Mg ~ -2 to +2 ‰; Galy et al., 2002; Chang et al., 2004) so the presence of carbonate-derived material in loess could cause resolvable isotopic shifts in these isotope systems. This is not true for Si, which is a trace element in carbonates.

The average Si isotope value for loess is δ^{30}Si = -0.22 ± 0.07 ‰ (2 s.d., n = 13). Because the major Si-bearing phases in loess are igneous, it is more likely that loess is a proxy for the Si isotopic composition of "fresh" or "igneous" UCC. Assuming this, it is notable that the average value for loess is similar to the average value for granites, given in Chapter 5 (δ^{30}Si = -0.23 ± 0.15 ‰; 2 s.d.) and also the average "igneous" value for the continental crust, calculated from the "igneous array" in Chapter 4 (δ^{30}Si = -0.23 ± 0.05 ‰; 2 s.e. of the regression statistics).

6.5.2 The composition of Archaean continental crust

The Archaean continental crust is chemically dissimilar to modern continental crust; lower K contents and more fractionated and flatter REE patterns (no Eu anomaly) have all been attributed to a different melting regime at subduction zones before ca. 2.5. Ga (e.g. Martin, 1986; Kemp and Hawkesworth, 2003). It is unclear as to whether this will have had any effect on the Si isotopic composition UCC formed at this time, but we can use the Archaean-derived sedimentary material from Canada (the Huronian and Sudbury samples) to evaluate this possibility.

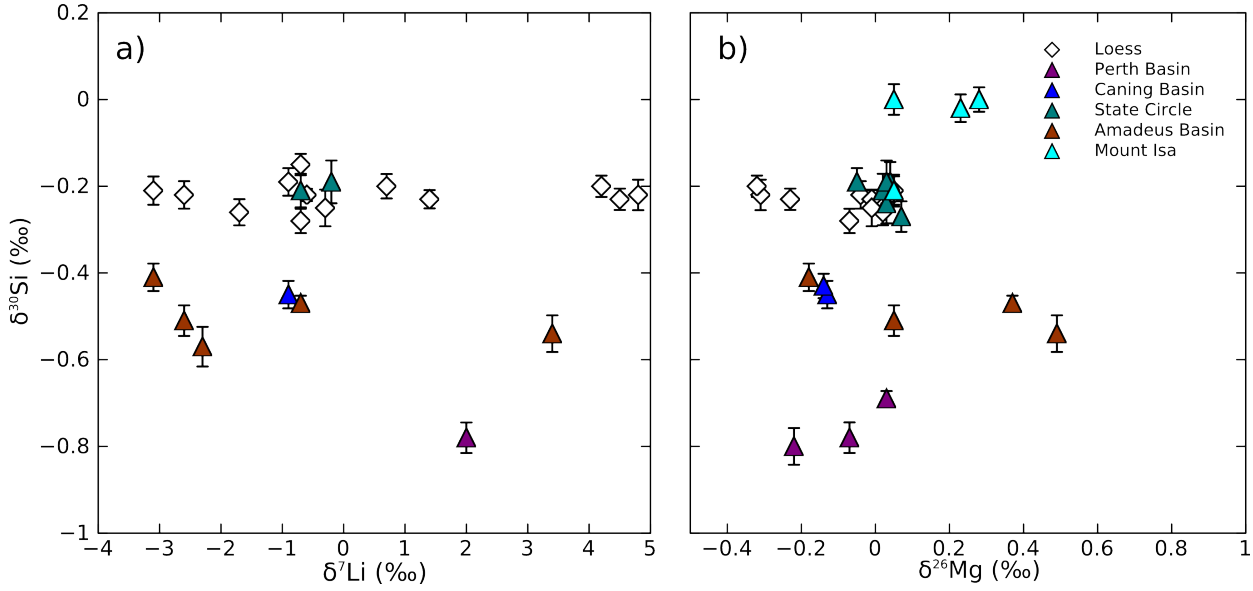


Fig. 6.4 Graph of δ^{30}Si against a) δ^7Li and b) δ^{26}Mg for the loess and shale samples, where available (error bars are 95% s.e.), which illustrates the large range of δ^{26}Mg and δ^7Li and small range of δ^{30}Si for the loess. Even though all three isotope systems are affected by weathering processes, there are no relationships displayed.

The Canadian sediments define two Si isotope populations (Fig. 6.1), which appear to be related to weathering degree, with the more isotopically negative group displaying higher CIA values (Fig. 6.3). The samples with heavier Si isotopic compositions also have CIA values comparable to loess (Fig 6.3b) and are thought to be glaciogenic (Gowganda formation, McLennan et al., 1979), i.e. they formed via predominantly mechanical processes, similar to loess. If we accept that the Si isotopic composition of loess represents the igneous composition of the modern day continental crust, then the low-CIA samples from the Huronian and Sudbury basin should record the same reservoir at the time given by their Nd model ages, in this case between 2.7 and 3.0 Ga (McLennan et al., 2000). The average Si isotope composition for these samples is $\delta^{30}Si = -0.19 \pm 0.05$ ‰ (2 s.d.), very close to that given by modern day loess ($\delta^{30}Si = -0.22 \pm 0.07$ ‰). This indicates that the Si isotopic composition of new (i.e. igneous) continental crust has remained constant since at least 3.0 Ga, and was not affected by the predicted change in melting regime since the Archaean.

The more isotopically negative shale samples from the Canadian suite, as well as the Pilbara suite and SW USA shales, are all derived from Archaean or Palaeo-protorezoic terranes, implying that the UCC was as heterogeneous then, with respect to Si isotopes, as it is today (see later).

6.5.3 The formation of shales

If loess represents the primary igneous Si isotopic composition of the UCC, then the more variable isotopic compositions in shales illustrate the effect that geological processes at the Earth's surface have on Si isotopes, in particular, weathering and the sedimentary cycle. The effect of weathering on Si isotopes is now well established in studies of natural soil and clay formation (Ziegler et al., 2005a&b; Georg et al., 2009a; Bern et al., 2010; Opfergelt et al., 2008, 2009, 2010, 2011; Steinhoefel et al., 2011) as well as studies of riverine Si and associated bedrock (De la Rocha et al., 2000; Ding et al., 2004, Georg et al., 2006a, 2009b; Cardinal et al., 2010; Engström et al., 2010) and experimental work (Ziegler et al, 2005a; Delstanche et al., 2009). These studies show that precipitation of Si from solution enriches the product (e.g. secondary mineral phases) in the lighter isotopes of Si, leaving an isotopically heavy fluid.

Given that shales are composed of significant quantities of clay minerals, do the Si isotopic systematics of shales reflect their mineralogy? Certainly, some samples do display very

light $\delta^{30}Si$ values (i.e. Perth Basin, Pilbara) and the mean $\delta^{30}Si$ value for shales is lighter than for loess. However, there are some shales that have $\delta^{30}Si$ values that are unfractionated relative to igneous material and, also, some samples that display Si isotopic compositions that are *heavier* than unweathered continental crust (i.e. the Mt. Isa group), which is contrary to what is predicted for clay minerals (see above). Therefore, it appears that the presence of secondary phases does not always cause a shift towards light Si isotope compositions in shales.

As well as, and possibly because of this, there are also no simple relationships between Si isotope composition and weathering proxies in shales. This is illustrated by the poor correlation between $\delta^{30}Si$ and CIA values (Fig. 6.3a) and Li and Mg isotopic compositions (Fig. 6.4). For example, the State Circle shales have elevated CIA values of ~ 76 (Table 6.3), indicating significant amounts of alteration, while having $\delta^{30}Si$ values unfractionated from igneous material. Conversely, the Perth Basin shales have the similarly elevated CIA values but are, isotopically, much lighter (Fig. 6.3a).

At this point, a discussion on weathering degree is useful. Typically, weathering of upper crustal material is divided into three stages (Chesworth, 1977; Kronberg et al., 1979). "Early stage" weathered material is dominated by primary minerals (that is, minerals that constitute fresh igneous or metamorphic lithologies) with a clay fraction consisting of chlorite, vermiculite, smectite and illite. Loess is a perfect example of "early stage" weathering. "Intermediate stage" material has detrital quartz and a clay fraction predominately composed of smectite and illite (accompanied by loss of feldspar). "Late stage" is dominated by the quartz-kaolinite-gibbsite-goethite system.

Most shales have "intermediate stage" mineralogies, where the feldspar has been completely replaced by clay minerals. As mentioned above, clay mineral formation enriches the product in the lighter isotopes, so such phases should be isotopically lighter than their source feldspars. However, the quartz in these shales will be unaltered, and should have a primary Si isotopic composition. As such, the Si isotopic composition of shales is a function of the abundance of detrital quartz as well as the abundance and isotopic composition of the secondary phases. However, unless a shale is almost completely composed of quartz (very unlikely), the Si isotopic composition of shales is still predicted to be lighter than loess, which is not the case.

Georg et al. (2009a) suggest that formation of kaolinite (a 1:1 clay) is accompanied by much larger degrees of Si isotopic fractionation than smectite (a 2:1 clay), with kaolinite

displaying more negative $\delta^{30}Si$. Because kaolinite tends to form during "late-stage" weathering, it should not be present in large quantities in shales. As a result, the Si isotopic composition of the clay fraction of many shales may not be as negative as first predicted because of the predominance of 2:1 clays. Furthermore, during "late stage" alteration, a light isotopic shift associated with kaolinite formation may be compounded by the associated formation of Fe oxides, as sorbtion of Si on to Fe-oxides also results in a light enrichment in Si isotopes (Delstanche et al., 2009).

Therefore, more intense or prolonged weathering (kaolinite and Fe-oxide formation) is a likely cause for the very negative Si isotopic compositions seen in some shales, but this is not strongly reflected by CIA values. However, this parameter does not reflect the remaining amount of primary Si in a shale. Silicon in feldspar is subject to alteration, but the Si present in quartz is relatively insoluble (although dissolution of quartz during weathering does occur; Taylor and McLennan, 1985). Quantifying the amount of primary Si remaining in the quartz phase (Si_{qtz}) may be a more useful parameter for quantifying the Si isotopic composition of shales.

One way to assess this is may be to study the relationship between Si isotopes and insoluble elements, such as the Rare Earth Elements (REEs), Nb, Ti, Fe, Al, etc. (Taylor and McLennan, 1985). Because these elements are unaffected by fluid flux, chemical denudation of a sample during weathering will gradually increase the concentration of these elements (Duddy, 1980) and will also gradually reduce the amount of Si_{qtz}. Laterite formation for example, which involves intense degrees of weathering, can significantly concentrate the REEs (Kronberg et al., 1979) and would be predicted to result in light Si isotope compositions, due to large proportions of kaolinite and Fe-oxides. It is interesting, therefore, that negative correlations do exist between Si isotope composition and insoluble element concentration in sediments, for instance TiO_2 (R^2 = 0.41), Al_2O_3 (R^2 = 0.43), Ho (R^2 = 0.45), Hf (R^2 = 0.55 – not including loess, which shows evidence of zircon accumulation). The example for Nb is shown in Figure 6.5; also shown is the average Nb composition of the UCC (~12 ppm; Rudnick and Gao, 2003), which is coincident with the average Si isotopic composition of fresh (igneous) continental crust, as defined by loess and granites.

As with all of the negative relationships described above, the shales that display the largest enrichment in insoluble elements (i.e. have the lowest Si_{qtz} contents) tend to have the

lightest Si isotope compositions compared to fresh igneous crust (e.g. Pilbara, Perth Basin). Those shales with insoluble element compositions close to average upper crust also have Si isotope compositions unfractionated from igneous upper crust (e.g. State Circle). All shales show similar depletions of fluid-mobile elements as a result of feldspar breakdown (recorded by their CIA values), but in samples enriched in the insoluble elements, alteration has been more intense or involved reworking of already-weathered sediment – enough to induce negative shifts in Si isotope composition.

Another outcome of the relationship between Si isotopes and insoluble element concentrations is that it offers a possible explanation for the relatively heavy Si isotopic compositions in some shales. Taylor and McLennan (1995) noted shales with low REE abundances contain a significant quantity of marine-derived material. Because REEs are so insoluble, their concentration in seawater is very low, and this is reflected in the REE abundances of carbonates and other marine lithologies, including cherts and siliceous ooze. Seawater also has a heavy Si isotope composition (De La Rocha et al., 2000) and so seawater derived sedimentary material is also relatively heavy, compared to igneous rocks (De la Rocha, 2006; Hendry et al., 2010; cf. Diatomite standard). Therefore, if a sediment is predominantly marine, then it will have both low insoluble element concentrations and heavy Si isotope compositions, which can explain the deviation toward heavier Si isotopes in Figure 6.5. In this

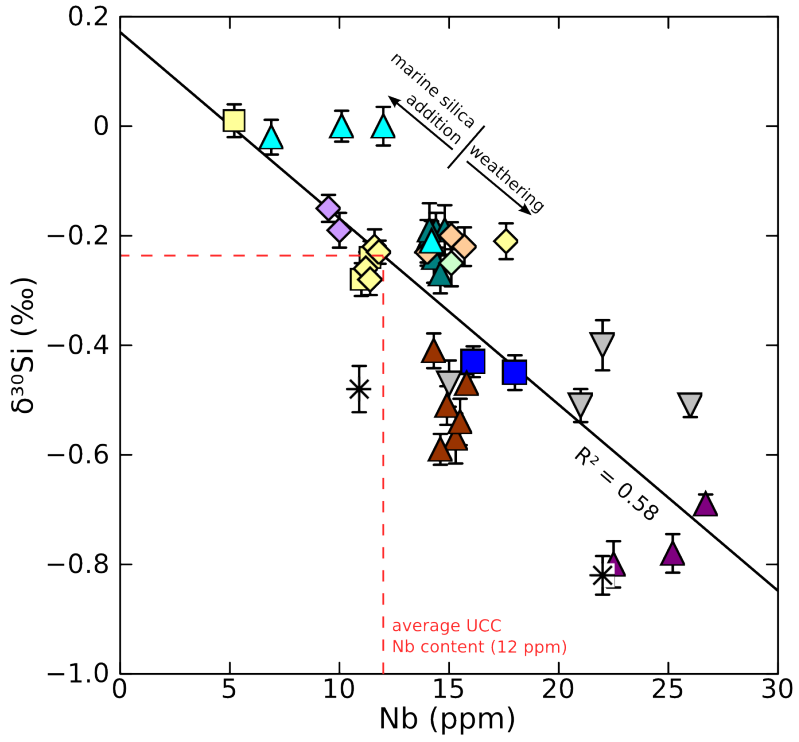


Fig. 6.5 Graph of $\delta^{30}Si$ against Nb contents for loess and shales (symbols as in Figure 6.3, error bars are 95% s.e.), which illustrates the good negative relationship between the two (regressions statistics calculated in Gnumeric (http://projects.gnome.org/gnumeric/). Similarly good relationship exist with $\delta^{30}Si$ and other insoluble elements; see text for discussion.

figure, two sample groups that plot towards heavier values have marine affinities: the Mt. Isa group has chert, dolomite and carbonate horizons and contains stromatolites and halite pseudomorphs (Geoscience Australia; http://dbforms.ga.gov.au); the loess from Germany is sourced from Alpine terrains, which have abundant carbonate lithologies (Taylor et al., 1983). A third sample, the isotopically heavy USGS standard SGR-1b, is an organic-rich oil shale, of lacustrine origin. The Si in this sample is most likely biogenic in origin, which can also concentrate the heavier isotopes (Opfergelt et al., 2008).

A final point to make is that the processes that appear to be controlling the Si isotopic composition of shales, namely weathering and addition of marine-derived silica, are not mutually exclusive. Mixing between these two end-members could result in a Si isotopic composition that is unfractionated with respect to igneous rocks, masking the various isotopically fractionated components of such a sample. However, this homogenisation (of various and varied crustal sources) is the reason why shales have been so useful in constraining the average composition of the UCC, and should hopefully provide a more representative upper crustal Si isotopic composition.

6.5.4 Evolution of shale Si isotope composition with time

Despite the apparent robust behaviour of Si isotopes in shales, there are resolvable isotopic variations between shales of different ages and localities. Do these variations reflect what is known about the crustal growth and evolution of the continents they have formed from? The PAAS and Pilbara shale samples are all sourced from the same continental mass (Australia and, before, Gondwanaland) and have deposition ages ranging from >3 Ga to 0.2 Ga, and so provide an appropriate set of samples with which to investigate this possibility.

The Sm-Nd isotope system has been successfully applied to the problem of how long the continental crust has been subject to weathering (McCulloch and Wasserburg, 1978; Goldstein et al., 1984). Weathering does not fractionate these elements, so shales record the Nd isotopic composition of the continental crust which they sample, which in turn records the time of mantle extraction. Calculating a Nd "model age" from this gives the average age of the crust that the shale has sampled. Comparing this value to the shale deposition ages indicates the amount of time that such material has been resident in the crust. A longer residence time gives more opportunity for alteration and reworking of sediment.

Allègre and Rousseau (1984) made a Nd isotope study of the PAAS and Pilbara shales and their calculated Nd model ages for each unit are given in Table 6.3. These model ages decrease steadily over time, but plateau at around 1.8 Ga in shales with deposition ages younger than 0.5 Ga. They concluded that this reflects a reduction in the addition of new continental crust to the Gondwanan continent around this time. Figure 6.6 plots the δ^{30}Si values of PAAS and Pilbara shales against deposition ages. From this diagram, it appears that there has been a steady trend toward more negative Si isotope compositions since 0.5 Ga (i.e. since their model ages plateaued). This suggests then, that lack of fresh igneous continental material has meant that the sedimentary source for these shales was constantly recycled and became steadily more weathered, with a concomitant enrichment in the lighter Si isotopes (as well as insoluble element concentrations, see above).

Also shown in Figure 6.6 is the "recycling coefficient" (R_c) for Gondwanan crust, as calculated by Allègre and Rousseau (1984). This describes the amount of recycling of older crustal sources into creation of new crust during a specific time interval: an R_c value of 1 indicates no addition of mantle-derived material to the crust; an R_c value of 0 indicates that new crust was completely mantle-derived. Since 1.0 Ga, the growth of continental crust is dominated by recycled material, coinciding with a shift to relatively light shale isotope compositions, as described above. The isotopically heavy Mt. Isa shales were deposited ~ 1.5 Ga, when new crust was completely mantle-derived. Although these shales have a strong marine affinity (see above), this also suggests that any terrestrial silica in these shales would be relatively unweathered, and any silica addition from this source would have relatively heavy, igneous-like (or loess-like) Si isotopic compositions.

The extremely light Si isotopic composition of the Archaean shales is less easy to explain using this hypothesis. The continental sources during this time would be relatively young, providing less time for weathering to generate a light Si isotope signature. Also, the R_c value during time of deposition indicates that mantle-derived continental crust dominated the budget (Allègre and Rousseau , 1984). Therefore, long-term reworking of sediment is unlikely to be the cause of isotopically light shales in the Archaean.

Another way to generate the lighter isotopic composition is to invoke an increase in weathering intensity, caused by a more aggressive climatic regime. It has been hypothesised by a number of studies (e.g. Fedo et al., 1986; Sugitani et al., 1996; Lowe and Tice, 2004) that such

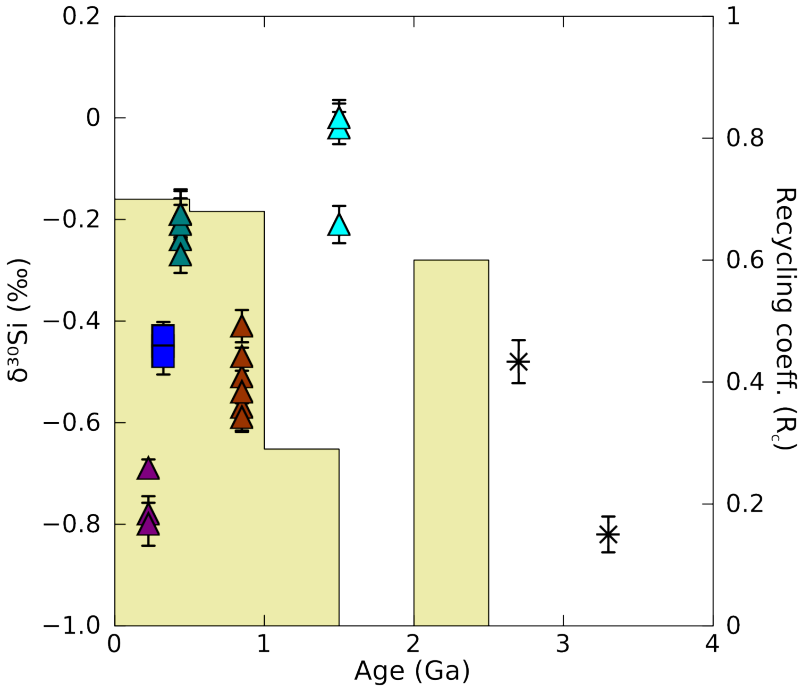


Fig. 6.6 Graph of $\delta^{30}Si$ against deposition age for the PAAS and Pilbara shales, Australia (symbols as in Figure 6.3, error bars are 95% s.e.). Also shown is the "Recycling coefficient", as defined by Allègre and Rousseau (1984) for Gondwanaland. See text for discussion.

conditions existed during the Archaean. High atmospheric CO_2 and CH_4 contents maintained high surface temperatures before ~ 3.2 Ga, after which new formation of large blocks of continental crust caused CO_2 draw-down from the atmosphere. This could explain the Si isotopic compositions of the Archaean shales. The oldest sample (Pg-7) formed when surface temperatures and atmospheric CO_2 composition was high, resulting in an intense weathering environment which could create very light Si isotopic compositions. The more recent Archaean shale (WC-3) formed after CO_2 draw-down had occurred. Weathering conditions were therefore more moderate during this time and the Si isotopic composition would remain relatively unperturbed.

Therefore, it appears that the Si isotopic signature of shales can reflect the long term weathering history of continents, as long as the average weathering intensity and climatic conditions remain relatively constant. The aggressive climatic regime in the early Archaean appears to be the cause of significant negative Si isotope fractionation in the shales deposited at this time. Similarly fractionated sedimentary material may also be detectable at other points in Earth history when conditions were similar (e.g. Palaeo-protorezoic, Cretaceous).

6.5.5 The silicon isotope composition of the upper continental crust

The upper continental crust consists predominantly of sedimentary and felsic igneous lithologies (or their metamorphosed analogues; Wedepohl, 1995) and so by combining the data

acquired during this study with that for granitoid material (Chapter 5), an attempt can be made to characterise the Si isotopic composition of the UCC. This data is shown in histogram form in Figure 6.7, which illustrates that these data cluster about one peak. This fairly sharp peak is centred around $\delta^{30}Si \sim -0.25$ to -0.20 ‰ and is defined primarily by the granite and loess data, with the shale data defining much larger and relatively even spread of Si isotope compositions.

The UCC is much more isotopically heterogeneous than the mantle or oceanic crust, with respect to Si isotopes. This heterogeneity is displayed by the shale samples, which reflect long-term weathering processes, and also, the presence of marine-derived sedimentary material that is now part of the continental crust. The granites define a more reduced range, but do show more variability than their extrusive counterparts (rhyolites and dacites; Chapter 4); a result of sediment anatexis during granite petrogenesis. The loess samples define the most narrow range of Si isotopic compositions. This is likely due to the fact that loess mineralogy is dominated by primary minerals (see Section 6.5.1.). The overriding "igneous" affinity of loess is demonstrated by the fact that the average value for loess ($\delta^{30}Si = -0.22 \pm 0.07$ ‰) is almost identical to that of granites ($\delta^{30}Si = -0.23 \pm 0.15$ ‰).

Calculating an average isotopic value for the upper continental crust requires an estimate of the average proportions and SiO_2 compositions of the various lithologies that comprise the UCC. Using the study of Wedepohl (1995), 4 major units were defined along with their average SiO_2 contents (Table 6.4), as follows: sedimentary lithologies (14%; SiO_2 = 52.4 wt.%); felsic

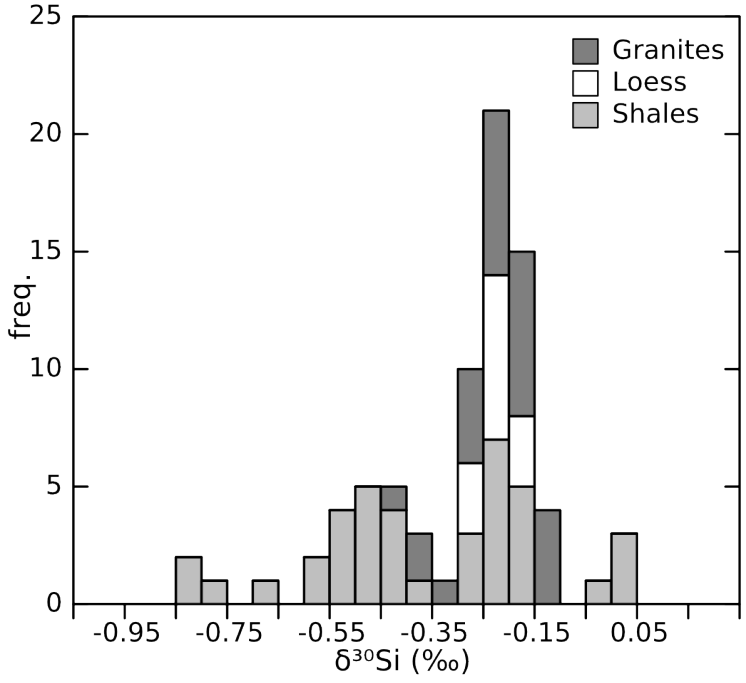


Fig. 6.7 Histogram of the $\delta^{30}Si$ values of the upper crustal lithologies analysed in this study and Chapter 5. The data peak, around $\delta^{30}Si = -0.25$ to -0.20 ‰, is defined mainly by the granites and loess samples. This peak also coincides with the weighted average $\delta^{30}Si$ value for the upper continental crust.

instrusive lithologies (50%; SiO_2 = 69.2 wt.%); gabbros (6%; SiO_2 = 50.1 wt.%); metamorphic lithologies (30%; SiO_2 = 63.7 wt.%). Then, the average $\delta^{30}Si$ value for each of these units was calculated and used to derive a weighted UCC Si isotopic composition. Note that the estimates of Wedepohl (1995) give a UCC SiO_2 content of 64.1 wt.%; this value has been superceded by a slightly higher value of 66.6 wt.% (Rudnick and Gao, 2003), but recasting the data using this estimate does not affect the final outcome of the calculation. In the following discussion, all errors will be quoted to 2 s.d.

Using data from previous chapters, the granite average of $\delta^{30}Si$ = -0.23 ± 0.15 ‰ was used as an estimate for felsic volcanic rocks, and, because there is insignificant Si isotopic variation in primitive igneous rocks (Chapter 3), the BSE value of $\delta^{30}Si$ = -0.29 ± 0.08 ‰ was used to represent the gabbros.

Because of the greater amount of isotopic heterogeneity, calculating the average $\delta^{30}Si$ value for the sedimentary unit is more complicated. Firstly, 4 sub-units were defined (shales and siltstones, sandstones, mafic volcanic material and carbonates; Table 6.4), again following the study of Wedepohl (1995). SiO_2 contents of the sub-units were calculated using the SiO_2 averages of the samples analysed in this study, or in the case of the mafic volcanic and carbonate sub-units, estimated from other studies. This approach yielded an average unit composition of SiO_2 = 52.6 wt.%, which is almost identical to that given by Wedepohl (1995). The average shale $\delta^{30}Si$ value of -0.36 ± 0.44 ‰ was used to represent the shale and siltstone sub-unit. Because they are both petrogenetically similar, the average loess $\delta^{30}Si$ value of -0.22 ± 0.07 ‰ was used for the sandstone sub-unit. As with the gabbro unit, the BSE average was used to represent mafic volcanic sedimentary material. The carbonates were assumed to contain negligible amounts of Si, and so are disregarded in the calculation (the final sedimentary $\delta^{30}Si$ value does not change significantly even if the carbonate unit were to contain 10 wt.% SiO_2 with a $\delta^{30}Si$ value of +1.00 ‰, due to the small relative proportion of this unit). The above approach yields a $\delta^{30}Si$ value of -0.31 ± 0.26 ‰ for the sedimentary unit.

To calculate an average $\delta^{30}Si$ value for the metamorphic unit, it is first assumed that this unit contains lithologies that have protoliths present in similar proportions to those in the unmetamorphosed portion of the upper continental crust, because the average SiO_2 composition of this unit is very similar to that of the UCC (Table 6.4). As there is evidence that metamorphism does not affect the bulk Si isotopic composition of a sample (see Chapter 7, also

Table 6.4 – Silicon isotopic composition of the upper continental crust

Rock unit	Proportion in upper crust (%)	Avg. SiO_2 (wt.%)	$\delta^{30}Si$ (‰)	2 s.d.
Sedimentary	14	52.4	-0.31	0.26
Sub-units	of which			
Shales, siltstones	6	61.7	-0.36	0.44
Sandstones	3	73.2	-0.22	0.07
Mafic volcanic	3	50.1	-0.29	0.08
Carbonates	2	0	-	-
Felsic intrusive	50	69.2	-0.23	0.15
Gabbro	6	50.1	-0.29	0.08
Metamorphic	30	63.7	-0.25	0.16
Upper continental crust		64.1	-0.25	0.16

Estimate of the weighted average Si isotopic composition of the upper continental crust, as well as the calculated $\delta^{30}Si$ averages for the component lithologies. Lithological units, proportions and SiO_2 contents are taken from Wedepohl (1995) except for the sedimentary sub-unit SiO_2 contents, which were estimated using the samples analysed in this study. The sedimentary $\delta^{30}Si$ was calculated using data form this research; the felsic intrusive unit was constrained using data from Chapter 5; the $\delta^{30}Si$ value of the gabbroic unit is the BSE value (Chapter 3). See text for discussion on calculations.

André et al., 2006), the $\delta^{30}Si$ composition of this unit should therefore be simply the weighted average of the sedimentary, felsic and gabbroic units. Alternatively, removing the metamorphic unit from the equation will not affect the final UCC $\delta^{30}Si$ value.

Using the above approach, the average Si isotopic value of the upper continental crust is calculated to be $\delta^{30}Si = -0.25 \pm 0.16$ ‰. This value coincides with the peak illustrated in Figure 6.7. It is slightly heavier than, but within error of, the value for BSE. The enrichment in the heavier Si isotopes reflects the predominance of felsic lithologies in the upper crust, which have relatively heavier Si isotopic signatures. However, the Si isotopic composition of the UCC is not as heavy as that of granites due to the effect of weathering, which results in an enrichment in the light isotopes. Because the UCC continental crust is slightly heavier than the BSE value, it can be surmised that the lower portion of the crust will be enriched in the lighter isotopes relative to BSE. This will be investigated in the next chapter.

6.6 CONCLUSIONS

1. Pleistocene loess samples define a narrow range of Si isotopic compositions ($\delta^{30}Si$ = -0.28 to -0.15 ‰), a result of their primary igneous mineralogy and predominantly mechanical weathering history. The average Si isotopic composition of loess is $\delta^{30}Si$ =

-0.22 ± 0.07 ‰ (2 s.d.), which is similar to the average Si isotope composition of granites (Chapter 5), and also the δ^{30}Si value calculated for continental crust using the "igneous array" (Chapter 4). This suggests that loess represents the Si isotopic composition of fresh (or "new") continental crust. Glaciogenic samples sourced from Archaean continental crust display a similar isotopic composition to Pleistocene loess, implying that the Si isotopic composition of fresh continental crust has remained constant over geological time.

2. Compared to loess, the Si isotopic composition of shale is much more variable (δ^{30}Si = -0.82 to +0.00 ‰) which is a result of a more complicated petrogenesis that can involve, for instance, chemical and physical weathering, diagenesis, etc.. The average Si isotopic composition of shale (δ^{30}Si = -0.36 ± 0.44 ‰ ; 2 s.d.) is lighter than loess, due to increased secondary (clay) mineral content. Despite this, shales are not always isotopically light compared to unweathered igneous material. In the absence of marine-derived silica, the δ^{30}Si of a shale sample is a function of the abundance of detrital quartz and the abundance and Si isotopic composition of the secondary phases in that sample. Heavy Si isotopic compositions in shales relative to igneous rocks cannot be a result of terrestrial weathering and most likely indicate the presence of marine-derived silica, either by reworking of marine lithologies or deposition in a marine environment.
3. Because of the relatively low solubility of Si, the Si isotope system is much more robust than Mg or Li isotopes during weathering. Because of this, Si isotopes in shales do not correlate with the canonical proxies for weathering, such as CIA values. Instead, good negative correlations between δ^{30}Si values and insoluble element concentrations indicate that more intensive or prolonged chemical weathering of a sedimentary source is required before resolvable negative Si isotopic fractionation occurs. This is evident in the PAAS shale samples from Australia, which show a gradual enrichment in the light Si isotopes with time, as a result of increasing relative source age (Nd model age minus deposition age). These isotopically lighter shales were also deposited during a time when crustal formation was dominated by recycling of older crustal lithologies.
4. Negative Si isotopic compositions in Archaean shales cannot be explained by long-term continental weathering, and may be a result of more intense weathering, due to more aggressive climatic conditions, during early Earth history.

The upper continental crust is heterogeneous with respect to Si isotopes ($\delta^{30}Si$ = -0.82 to +0.00 ‰) and has a weighted average composition of $\delta^{30}Si$ = -0.25 ± 0.16 ‰ (2 s.d.), which is slightly heavier than the Bulk Silicate Earth. This suggests that the lower continental crust may have a lighter Si isotopic composition than the mantle.

Chapter 7: The silicon isotope composition of the deep continental crust

7.1 INTRODUCTION

In this chapter we present the first silicon (Si) isotopic measurements of granulite facies xenoliths, with the aim of constraining the Si isotopic composition of the middle and lower continental crust. Silicon is the 2nd-most abundant element in the Earth's continental crust (Si ~28 wt.%) and is an important element in many geo- and biochemical cycles. Therefore, knowledge of the Si isotope composition and systematics in the lower continental crust is key to understanding the Si isotope system as a whole.

The continental crust can be split into three layers, the upper, middle and lower crust, on the basis of seismological profiles (e.g. Holbrook et al., 1992; Rudnick and Fountain, 1995) and examination of exhumed crustal profiles (e.g. Fountain and Salisbury, 1981; Bohlen and Mezger, 1989). For an average crust thickness of ~40 km, the base of the upper crust is at around 10 – 15 km depth and is composed predominantly of felsic granitoid material with significant sedimentary and metamorphic components (see Chapters 5 and 6). Below the upper crust, between 10-15 km and 20-25 km depth, the middle crust is composed of amphibolite and lower-granulite facies, intermediate (andesitic) meta-igneous and meta-sedimentary rocks. At more than 20-25 km depth, the lower crust is more primitive, consisting predominantly of granulite facies mafic meta-igneous rocks, with a minor but significant proportion of meta-sedimentary material (see Rudnick and Gao, 2003, and references therein).

In the main, two sample types have been utilised to investigate the composition of the deep crust. These are tectonically-exhumed high-grade metamorphic terranes (e.g. Bohlen and Mezger, 1989) and granulite facies xenoliths erupted through volcanic conduits (e.g. Dawson, 1977; Rudnick et al., 1986; Rudnick and Taylor, 1987; Condie and Selverstone, 1999; Villaseca et al., 1999; Liu et al., 2001). Because of their higher metamorphic grade, most granulite facies xenoliths are thought to be derived from the lower crust, whereas terranes, typically of amphibolite and lower granulite facies, are more representative of the middle crust. In this study we have analysed a set of 16 granulite facies xenoliths, taken from the McBride and Chudleigh volcanic provinces, north Queensland, Australia – these are described in the next section. We have chosen to limit our analysis to granulite facies xenolith samples, for reasons given below.

7.2 SAMPLE DESCRIPTION

We have chosen to analyse xenolith material as opposed to granulite terrane samples

because xenoliths are erupted relatively instantaneously from the deep crust, whereas terranes are exhumed over millions of years. This reduces the effect of retrograde metamorphism to negligible levels (only garnets appear to have undergone decompression reactions in the xenoliths; Rudnick et al., 1986; Rudnick and Taylor, 1987) and also limits the scope for any metasomatic processes that could affect Si elemental and isotopic composition of the primary crust.

There are some questions as to how representative granulite facies xenoliths are and this could bias estimates of the bulk Si isotopic composition of the deep crust. Specifically, felsic xenoliths may not survive transport in a magma hotter than their solidus. However, Rudnick and Fountain (1995) conclude that this should only happen if the lower crust was already partially molten before eruption. Even if the risk of bias is small, we have taken this into account in our calculations of crustal composition (Section 7.5.6).

7.2.1 McBride xenolith suite, Queensland, Australia

Eight granulite xenolith samples from the McBride volcanic province, northern Queensland, were analysed for Si isotopes. These samples are taken from a suite already well-characterised for major and trace elements, as well as radiogenic (Sr, Nd, U, Pb) and stable (Li, O) isotopes (Rudnick and Taylor, 1987; Rudnick and Williams, 1987; Rudnick, 1990; Kempton and Harmon, 1992; Teng et al., 2008).

The McBride xenoliths used in this study were first described by Rudnick and Taylor (1987). The xenoliths are hosted in a single basaltic cinder cone of late Cenozoic age, are small (< 11 cm in diameter) and display a wide range of chemical and mineralogical contents, with SiO_2 ranging from 41 to 67 wt.%. Thermobarometric techniques indicate that most of the xenoliths equilibrated in the lower crust (between 26 and 40 km), with only one sample, 85-107, displaying cooler temperatures indicative of a shallower (~18 km) origin. Equilibrium mineral assemblages suggest that minimal temperature and/or pressure variations have affected the samples since peak granulite metamorphism, and post-eruptive alteration is also limited. Strontium-neodymium isotope systematics suggests that the samples formed by mixing of a mantle-derived basaltic melt with pre-existing lower crust (represented by the meta-sedimentary and felsic meta-igneous xenoliths, see below) and subsequent fractional crystallisation (Rudnick, 1990).

The McBride xenoliths represent a wide range of protoliths, providing clear evidence for a chemically heterogeneous lower crust. Of the five mafic granulites analysed in this study, two are representative of basaltic melts (85-100 and 85-120), two are melt-depleted restites (83-159 and 85-114) and one is a mafic cumulate (85-107). As well as mafic material, two felsic xenoliths were analysed that have protoliths similar to the Phanerozoic calc-alkaline granitoid rocks present at the surface in the McBride volcanic province (83-160 and 83-162). Intermediate-composition granulites from this suite are interpreted to have a sedimentary protolith; sample 83-157 is a metapelite (all protolith information taken from Rudnick and Taylor, 1987).

7.2.2 Chudleigh xenolith suite, Queensland, Australia

To complement the McBride suite, eight granulite facies xenoliths were analysed from the Chudleigh volcanic province, north Queensland, Australia. As with the above samples, the Chudleigh xenoliths were taken from a suite already well-characterised for major and trace elements as well as radiogenic (Sr, Nd, Pb, Os) and stable (O, Li) isotopes (Rudnick et al., 1986; Rudnick and Goldstein., 1990; Kempton and Harmon., 1992; Saal et al., 1998; Teng et al., 2008).

The Chudleigh xenoliths used in this study are described in detail by Rudnick et al. (1986). They were hosted in Plio-pleistocene alkali basaltic vents, are large (between 5 and 50 cm), blocky and coarse-grained. Unlike the McBride xenoliths, these samples show little variation in silica, ranging from 49 to 51 wt.%, and all the samples are derived from mafic igneous protoliths. All samples display limited post-eruptive alteration.

Three types of xenolith are recognised in the Chudleigh suite (of which we have analysed a representative selection): plagioclase-rich granulites (samples 83-107, 83-112, 83-125, 83-127 and 83-131); pyroxene-rich granulites (samples 83-110 and 83-115) and transitional granulites (which show chemical properties that lie between the other two types; sample BC). Despite little variation in major element compositions, there are large mineralogical differences, which indicate a wide range of equilibration depths, of between 20 and 40 km, and also large temperature differences of between 600 and 1000ºC (Rudnick et al., 1986). High Si/Na ratios in the samples suggest that the xenoliths are unlikely to be melt-derived. Instead, they are inferred to be igneous cumulates, formed in a system where plagioclase was subordinate to

ferromagnesian phases. Sr-Nd systematics suggest that the cumulates and coexisting melt phase (which is not represented in the Chudleigh xenoliths) evolved through AFC processes (Assimilation and Fractional Crystallisation; DePaolo, 1981), with the mantle-derived basaltic melt assimilating a pre-existing felsic crustal source (Rudnick et al., 1986).

7.3 METHODS

Xenolith samples were provided in powder form from R. Rudnick. Although the samples were powdered in an agate mill, this method has no significant effect on the Si isotope composition of a sample (Zambardi and Poitrasson., 2011; Chapter 2 and 4). All samples and standards were processed for MC-ICP-MS analysis following the HF-free alkali fusion technique as detailed by Georg et al. (2006b) and described in detail in Chapter 2.

In brief: ~10 mg of sample powder was added to a silver crucible with ~200 mg of analytical grade NaOH (Merck) in pellet form. The crucible was heated to 720ºC for 12 minutes, removed and left to cool, then placed in ~20 ml of MQ-e (18.2 MΩ) water. After 24 hours, the fusion cake was transferred into solution, again in MQ-e water, and acidified to 1% v/v with HNO_3. Silicon concentrations were analysed using a spectrophotometer and fusion yields were assessed. Average yield for this study was 100 ± 3 % (2 s.d.) for 16 fusions; no Si aliquot with a yield less than 97% was measured.

Ion chromatography purification and MC-ICP-MS analysis techniques are all detailed in Georg et al. (2006b) and Chapter 2. Sample solutions were purified before mass spectrometry using a single-pass column technique using BioRAD AG50W X12 200-400 mesh cation resin, and acidified to 1% v/v HNO_3 before analysis. There is no evidence for matrix effects from other anionic species on the measured Si isotopic ratios (Georg et al., 2006b), and the external standards BHVO-2 and Diatomite were routinely analysed to assess method accuracy and precision.

Isotopic measurements were made using a Nu Instruments Nu Plasma HR High Resolution Multi-Collector Inductively-Coupled-Plasma Mass Spectrometer (HR-MC-ICP-MS). Samples were taken up using a 6 mm PFA concentric microflow nebuliser and desolvated using an Aridus II (Cetac, NE, USA). Isotopic analyses were made at “medium” resolution (resolving power $M/\Delta M \sim 3300$, where ΔM is defined at 5% and 95% for peak height; Weyer and Schwieters, 2003) to avoid poly-atomic interferences, which resulted in a ~ 85% reduction of

instrument sensitivity (at sample Si concentrations of 750 ppb, a total signal of 1×10^{-10}A was typical).

Isotopic analyses were calculated via the standard-sample bracketing protocol, using NBS28 (silica sand) as the bracketing standard. Variations in Si isotopes are represented by the delta notation as $\delta^{30}Si$ or $\delta^{29}Si$, defined as the deviation in per mil (‰) of a sample's ratio of $^{x}Si/^{28}Si$ from the standard (NBS28), as such:

$$\delta^{30}Si = [(^{30}Si/^{28}Si_{sample})/(^{30}Si/^{28}Si_{standard}) - 1] \times 1000;$$

$$\delta^{29}Si = [(^{29}Si/^{28}Si_{sample})/(^{29}Si/^{28}Si_{standard}) - 1] \times 1000.$$

We discuss our Si isotopic data using $\delta^{30}Si$ values, which are roughly twice the magnitude of $\delta^{29}Si$ values. Assuming mass dependence, which, for terrestrial samples, is a valid assumption, this relationship was used as a further test for data quality. Any data that did not display mass dependence were discarded.

7.4 RESULTS

7.4.1 External Standards

Sample data accuracy and precision were assessed using routine and repeated analysis of the external standards Diatomite and BHVO-2 during data acquisition. Diatomite is natural pure silica standard (Reynolds et al., 2007; Georg et al., 2009a; Ziegler et al., 2010; Chakrabarti and Jacobsen, 2010; Armytage et al., 2011) and BHVO-2 is a USGS natural basaltic rock standard (Abraham et al., 2008; van den Boorn et al., 2009; Zambardi and Poitrasson, 2011; Armytage et al., 2011) that are both now widely utilised and well established in Si isotope studies.

The Si isotopic data for 4 repeat runs of each standard (each on a different day) as well as the long term average, are given in Table 7.1. Our data for Diatomite ($\delta^{30}Si = 1.24 \pm 0.12$ ‰; 2 s.d., n = 44) and BHVO-2 ($\delta^{30}Si = -0.29 \pm 0.10$ ‰; 2 s.d., n = 44) agree well with other published values for the standards, and illustrate the good precision that is currently attainable using our methods.

7.4.2 Granulite facies xenoliths

Silicon isotope data for the granulite facies xenoliths are given in Table 7.1. Measurement uncertainty is represented using both the 2 × standard deviation (2 s.d.) and 95% standard error of the mean (95% s.e. = t × s.d./$(n)^{1/2}$, where t = inverse survival function of the

Table 7.1 – Silicon isotope data for external standards and granulite facies xenoliths

Sample	ID	Description	SiO_2 (wt.%)	$\delta^{30}Si$ (‰)	2s.d.	95%s.e.	$\delta^{29}Si$ (‰)	2s.d.	95%s.e.	*n*	$\delta^{30}Si$(m) (‰)	off.
BHVO-2	1			–0.31	0.12	0.04	–0.15	0.08	0.03	11		
	2			–0.29	0.07	0.02	–0.13	0.06	0.02	11		
	3			–0.31	0.05	0.02	–0.15	0.05	0.02	11		
	4			–0.26	0.12	0.04	–0.13	0.09	0.03	11		
	Overall		49.9	–0.29	0.10		–0.14	0.07		44		
Diatomite	1			1.22	0.11	0.04	0.61	0.08	0.03	11		
	2			1.25	0.11	0.04	0.66	0.12	0.04	11		
	3			1.20	0.10	0.03	0.60	0.06	0.02	11		
	4			1.28	0.12	0.04	0.65	0.07	0.02	11		
	Overall		100.0	1.24	0.12		0.63	0.10		44		
McBride	83-157	Metasediment	54.6	–0.31	0.13	0.04	–0.15	0.11	0.04	11		
	83-159	Mafic restite	43.4	–0.35	0.12	0.04	–0.17	0.08	0.03	10		
	83-160	Felsic melt	64.0	–0.15	0.13	0.04	–0.07	0.07	0.02	11		
	83-162	Felsic melt	66.9	–0.22	0.06	0.02	–0.14	0.06	0.02	9		
	85-100	Mafic melt	51.7	–0.28	0.09	0.03	–0.13	0.08	0.03	11		
	85-107	Mafic cumulate	52.8	–0.26	0.08	0.03	–0.14	0.08	0.03	11		
	85-114	Mafic restite	41.2	–0.40	0.11	0.04	–0.22	0.04	0.01	11		
	85-120	Mafic melt	52.4	–0.32	0.09	0.03	–0.14	0.05	0.02	11		
Chudleigh	83-107	Plag-rich	49.6	–0.26	0.10	0.03	–0.11	0.05	0.02	11	*–0.25*	5%
	83-110	Pyroxene-rich	50.8	–0.29	0.09	0.03	–0.13	0.07	0.02	11	*–0.39*	33%
	83-112 (WR)	Plag-rich	51.0	–0.29	0.11	0.05	–0.13	0.09	0.04	8	*–0.24*	17%
	83-115 (WR)	Pyroxene-rich	50.9	–0.43	0.12	0.04	–0.21	0.09	0.03	11	*–0.39*	9%
	83-125	Plag-rich	50.7	–0.25	0.06	0.02	–0.12	0.09	0.03	11	*–0.28*	11%
	83-127 (WR)	Plag-rich	50.1	–0.20	0.08	0.03	–0.11	0.08	0.03	11	*–0.26*	32%
	83-131	Plag-rich	50.5	–0.23	0.14	0.05	–0.11	0.09	0.03	11	*–0.26*	15%
	BC (WR)	Transitional	49.7	–0.40	0.13	0.04	–0.21	0.13	0.04	11	*–0.28*	30%

Silicon isotope data for external standards and whole-rock xenoliths from McBride and Chudleigh volcanic provinces, Australia. Errors are given as 2 s.d. (2 × standard deviation) and 95% s.e. (95% s.e. = t × s.d./$(n)^{1/2}$, where t = inverse survival function of the Student's t-test at the 95% significance level and n-1degrees of freedom). Silica contents are taken from Rudnick et al. (1986) and Rudnick and Taylor (1987). The $\delta^{30}Si$(m) values are the predicted Si isotopic compositions of the Chudleigh xenoliths, based on their CIPW normative mineralogy. Also shown are the percentage offsets of the model values from their actual isotopic compositions. See text for discussion.

Student's t-test at the 95% significance level and n-1degrees of freedom). The average of all the 2 s.d. values in this study is ± 0.10 ‰, which is close to the precision for both external standards. At an average n value of 11 per datum, this gives an overall 95% s.e. value of ± 0.03 ‰.

The $\delta^{30}Si$ values for the xenoliths range from -0.43 to -0.15 ‰, with both suites displaying similar isotopic ranges (McBride $\delta^{30}Si$ = -0.40 to -0.15 ‰; Chudleigh $\delta^{30}Si$ = -0.43 to -0.20 ‰). These xenoliths record some of the lightest "high temperature" terrestrial Si isotope compositions so far measured with moden high precison techniques (i.e. Chapter 3; Fitoussi et

al., 2010; Armytage et al., 2011). The range of data for the McBride suite (~0.25 ‰) is similar to that seen in other igneous settings where there is also a wide range of SiO_2 concentrations (i.e. Hekla; Chapter 4). There is also a good correlation between $\delta^{30}Si$ and SiO_2 ($R^2 = 0.81$) for the McBride samples (Fig. 7.1). The Chudleigh samples do not show a similar correlation, and the range of SiO_2 is much more limited (Fig. 7.1). However, the isotopic range is similar.

7.5 DISCUSSION

7.5.1 Silicon behaviour during high-grade metamorphism

Before we can use the xenolith $\delta^{30}Si$ data to assess the Si isotope composition of the deep crust, we must first assess any effect that syn- and post-eruptive alteration and/or high-grade metamorphism may have had on the primary Si concentration and isotopic signatures of the samples.

Low-temperature processes such as weathering and secondary mineral formation result in relatively large degrees of Si isotopic fractionation compared to that seen during igneous processes (e.g. Ziegler et al., 2005a&b; Georg et al., 2009b; Opfergelt et al., 2011), which enrich the product in the lighter isotopes. It is unlikely that such processes have not altered the primary Si isotopic compositions of the samples, as all weathered surfaces were removed before analysis, and no clay minerals have been identified (Rudnick et al., 1986; Rudnick and Taylor, 1987; Teng et al., 2008). Also, Li and O isotopes, which are both much more fluid-mobile than Si, show no evidence for weathering having affected the xenoliths (Kempton and Harmon, 1992;

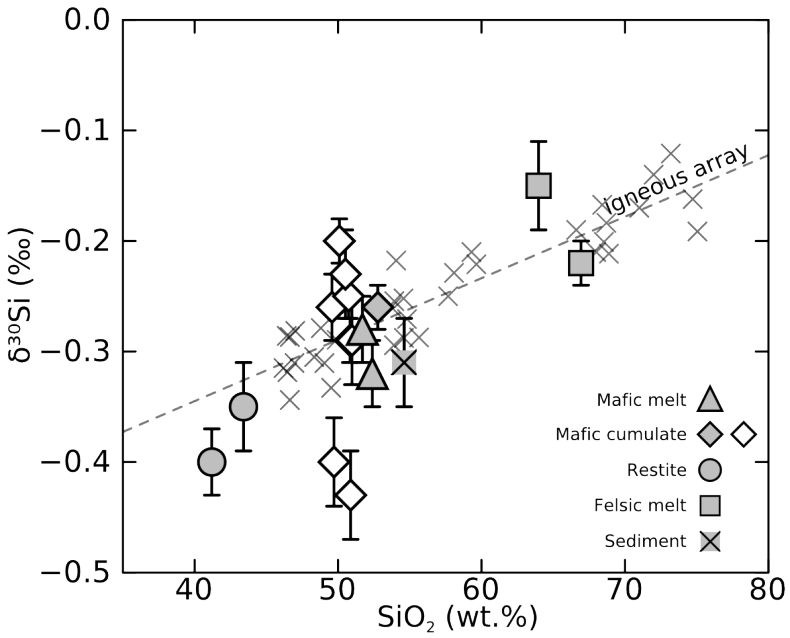


Fig. 7.1 Graph of $\delta^{30}Si$ against SiO_2 for the Chudleigh (white symbols) and McBride (grey symbols) xenolith data (error bars are 95% s.e.). Also plotted for comparison is the "igneous array" (crosses and trend line), as defined in Chapter 4.

Teng et al., 2008). The rapid exhumation of the xenolith material will limit any alteration during eruption and, also, minimise retrograde metamorphism (see above). Lastly, there is no evidence for magmatic infiltration into the samples (Rudnick et al., 1986; Rudnick and Taylor, 1987).

Xenolith material in a basaltic magma is not at equilibrium, so diffusion of material between xenolith and melt could modify the primary chemical composition recorded by the sample. Large variations measured in Li isotopes in the Chudleigh and McBride xenolith samples are attributed to kinetic isotope fractionation as a result of diffusion between xenolith and magma (Teng et al., 2008). This work identified two samples whose mineral δ^7Li values are equal to their bulk δ^7Li composition and are, therefore, in isotopic equilibrium. These samples (BC and 83-131 from Chudleigh) have δ^{30}Si values that bracket the Si isotopic range for the xenoliths ($\delta^{30}Si_{BC}$ = -0.40 ± 0.04 ‰, $\delta^{30}Si_{83\text{-}131}$ = -0.23 ± 0.04 ‰; Table 7.1). Given that Li isotopes are much more susceptible to kinetic isotope effects than Si (Richter et al., 2003, 2009a; Huang et al., 2010), we are confident that kinetic processes have not affected the Si isotopic composition of the xenoliths.

Finally, we assess the effect that granulite facies metamorphism has had on the bulk Si isotopic compositions of the xenolith. In the presence of a volatile phase, Si mobility increases with increasing temperature and, under such conditions, is mobile during metamorphism. Prograde metamorphism to granulite facies often involves dehydration (e.g. Stahle et al., 1987), which will reduce concentrations of fluid-mobile elements (such as Cs, U, B etc; Rudnick et al., 1985; Leeman et al., 1992) and could affect Si, although it is much less soluble. There are some granulite terranes where metasomatism via high temperature CO_2-rich fluids has mobilised Si (Stahle et al., 1987; Newton, 1989) but in many of these cases this is related to retrograde metamorphism, which is avoided by studying xenoliths. Nevertheless, a major metasomatic event that significantly alters the silica content of a xenolith may also alter primary δ^{30}Si. In the original studies of both xenoliths suites, no evidence of metasomatism has been noted (Rudnick et al., 1986; Rudnick and Taylor, 1987); comparing the silica contents of the xenoliths to the average of their protoliths, there is no evidence that Si has been lost or gained to any great degree during metamorphism and residence in the lower crust (i.e. Rudnick and Taylor, 1987, point out the similarities between major element composition of the mafic and felsic melts, and their upper crust counterparts). This is strongly endorsed by the Si isotopic compositions themselves; the δ^{30}Si values for the xenoliths correspond to the average isotopic composition of

their inferred protoliths. Mafic melts have δ^{30}Si of -0.32 to -0.28 ‰, identical within error to the δ^{30}Si BSE value and MORB/IAB averages (Chapter 3) and the felsic xenoliths have δ^{30}Si values of -0.22 to -0.15 ‰, which are within the range measured for dacites and rhyolites from Hekla and other localities (see Chapter 4). This is strong evidence that the Si isotopic compositions of these xenoliths record the primary isotopic composition of the deep continental crust.

7.5.2 Silicon isotope heterogeneity in the deep crust

Given that the xenoliths from Chudleigh and McBride record their primary Si isotopic compositions, it is evident that significant Si isotopic heterogeneity exists in the lower continental crust. Although not as variable as the upper crust (which also records the effects of low-temperature weathering and biogenic processes), this range of δ^{30}Si is comparable to that displayed by igneous rocks of the oceanic and upper continental crust and the mantle (i.e. Chapters 3 and 4; also: Georg et al., 2007; Fitoussi et al., 2009; Zambardi et al., 2009; Armytage et al, 2011). This is perhaps not surprising, as field, geochemical and seismological studies all indicate that a variety of lithologies, from mafic to felsic meta-igneous to meta-sedimentary, are present in significant quantities in the lower crust (e.g Fountain and Salisbury, 1981; Rudnick and Fountain, 1995) and, although predominantly mafic, the lower continental crust is chemically heterogeneous on a number of scales (see Rudnick and Gao, 2003, for a review of the literature).

7.5.3 Silicon isotopic variation in the McBride xenolith suite

In many ways, the McBride xenolith suite is the ideal set of samples to study how Si isotopes behave in the lower crust. The suite consists of samples that are genetically unrelated (there are no obvious correlations with major or trace elements so there is no risk of a cogenetic bias; Rudnick and Taylor, 1987). Also, the samples yield a wide spread of zircon ages, sampling lower crust that has formation ages spanning millions of years (between Protorezoic and Permo-triassic; Rudnick and Williams, 1987). Lastly, the wide range of protolith lithologies represented by the McBride xenoliths contain most (if not all) of the rock types that are thought to comprise the lower crust (e.g. Rudnick and Fountain, 1995).

There are striking similarities between the Si isotopic composition of the xenoliths and those of their protoliths (as noted above). This is clearly demonstrated by the strong positive

correlation between $\delta^{30}Si$ and SiO_2 (Fig. 7.1, $R^2 = 0.81$) which is collinear with the same relationship observed for many volcanic rocks that have not been contaminated by (meta)sedimentary continental crust. This relationship appears to be a fundamental property of the Si isotope system (at least for mantle-derived igneous material), is recorded in numerous magmatic systems and describes the so-called "igneous array" (Chapter 4) which is also plotted on Figure 7.1 for comparison. The fact that all of the xenolith data plot on or near to the array is evidence that the processes that control the Si isotopic composition of igneous rocks erupted at the surface are common to those controlling the composition of the lower crust. Such controls are not completely understood, but the major factor is thought to be the relative Si-O bond strengths (controlled predominantly by polymerisation degree and chemical composition) between either a partial melt and restite, or a melt and crystallising phase that drives more silica-rich samples to heavier Si isotopic compositions (e.g. Grant, 1954; Méheut et al., 2009; Chapter 4).

Samples 85-100 and 85-120, which are thought to have crystallised from basaltic magmas, have $\delta^{30}Si$ (-0.32 to -0.28 ‰) identical within error to those of MORB, IAB and mantle samples (Chapter 3). These samples probably represent basaltic material added to the lower crust by underplating (Rudnick, 1990). Simplistically, the Si isotope composition of the rest of the McBride samples could be explained by partial melting or further crystallisation of this basaltic material to create a felsic melt with a heavy $\delta^{30}Si$ signature (samples 83-160 and 83-162) which would leave restite enriched in the lighter isotopes (samples 83-159 and 85-114). Further fractional crystallisation of the felsic magma would then create a mafic cumulate (sample 85-107) with a Si isotope composition intermediate between the mafic and felsic magmas. That the meta-sedimentary sample also plots on the "igneous array" is likely to be a coincidence, as the $\delta^{30}Si$ compositions of sediments are controlled by completely separate processes (Chapter 6).

Although this simple framework adequately explains the Si isotopic variation, the petrogenesis of these xenoliths is thought to be far more complicated. The Sr, Nd and O isotope compositions of the xenolith suite provide evidence that a significant amount of assimilation of an evolved crustal source was involved in the petrogenesis (Rudnick, 1990; Kempton and Harmon, 1992). This has the potential to alter Si isotopes. A plot of $\delta^{30}Si$ against initial $^{87}Sr/^{86}Sr$ and εNd, and $\delta^{18}O$ for the same samples (Fig. 7.2, εNd plot not shown) reveals an excellent

correlation with O isotopes, but no relationship with radiogenic isotopes. The inferred crustal assimilant in the McBride suite has more radiogenic $^{87}Sr/^{86}Sr$ ratios, lower εNd values and higher $\delta^{18}O$ values, so any affect of crustal assimilation on Si isotopes should be indicated by all these plots. Yet the lack of correlation between $\delta^{30}Si$ and initial $^{87}Sr/^{86}Sr$ and εNd contrasts with the strong positive correlation with $\delta^{18}O$ ($R^2 = 0.77$). The felsic meta-igneous samples have the heaviest $\delta^{18}O$ values. Because igneous differentiation cannot fractionate O isotopes to this degree, the felsic material is thought to have been derived from melting of an enriched source, most likely meta-sedimentary. This felsic melt could then mix with mantle-derived material to create the $\delta^{30}Si$-$\delta^{18}O$ array.

Why the radiogenic compositions are decoupled is unclear. However, it does require that there were more than two components. As such the data provide evidence that, in the deep crust, O and Si isotopes and silica contents can follow surprisingly simple relationships, regardless of the ages of crustal units being assimilated. Contrary to expectation, the assimilated sedimentary component does not drive the silicon isotopic composition of the magmas to light values, as with granitoid material (Chapter 5).

7.5.4 Silicon isotopic variation in the Chudleigh xenolith suite

In comparison to the variety of lithologies represented by the McBride suite, the

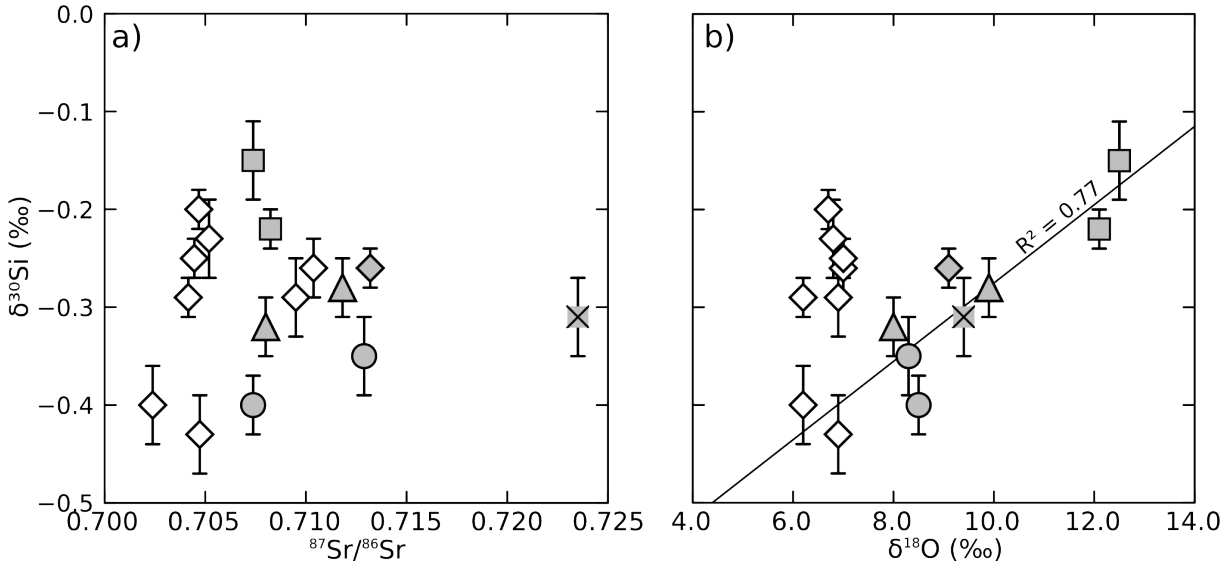


Fig. 7.2 Graph of $\delta^{30}Si$ against a) $^{87}Sr/^{86}Sr$ and b) $\delta^{18}O$ for the Chudleigh and McBride xenoliths (symbols and error bars as for Figure 7.1). Strontium isotopic data for the McBride samples are age corrected; this correction has not been made for the Chudleigh suite but makes no differece, as Rb/Sr ratios are extremely low; as such, there has been insubstantial ^{87}Sr ingrowth. Trend line in b) is for the McBride data only.

Chudleigh xenoliths are all mafic cumulates (with SiO_2 between and 49.6 and 51.0 wt %). They display much more mantle-like $\delta^{18}O$, $^{87}Sr/^{86}Sr$ and εNd (Fig. 7.2), indicating that crustal assimilation was either more limited than for the McBride samples, or that the crustal end-member was much less evolved. Despite this, the range of Si isotopic compositions for the Chudleigh xenoliths is comparable to that of the McBride suite (Fig. 7.1). This is a much larger range than would be predicted if the Chudleigh xenolith protoliths represented mafic melts, and so it seems likely that this large variation is a result of the cumulate-derived mineralogy and composition of the xenoliths.

This mineralogical control is demonstrated by a negative correlation between $\delta^{30}Si$ and Mg# (Mg# = molar $MgO/[MgO + 0.85 \times FeO_{total}]$; Fig. 7.3; $R^2 = 0.63$, excluding sample 83-112 whose Mg# is much lower due to cumulate oxide phases, Rudnick et al., 1986). Furthemore, there is a positive correlation between $\delta^{30}Si$ and Eu/Eu* (Fig. 7.3, $R^2 = 0.52$). High Mg# can be an indication of large original proportions of olivine and pyroxene (Mg-rich phases), and higher Eu/Eu* (defined as $2 \times Eu_N/[Sm_N \times Gd_N]^{0.5}$ where subscript N denotes that the concentrations are normalised to chondritic values) most likely indicates the presence of cumulate plagioclase in a sample. Therefore, the Si isotopic composition of the Chudleigh xenoliths appear to be controlled by the ratio of olivine and pyroxene to plagioclase in the cumulate, with the most negative $\delta^{30}Si$ values corresponding to the largest proportions of Mg-rich phases. There is also a strong negative correlation between $\delta^{30}Si$ and CIPW normative diopside (not shown, $R^2 = 0.78$).

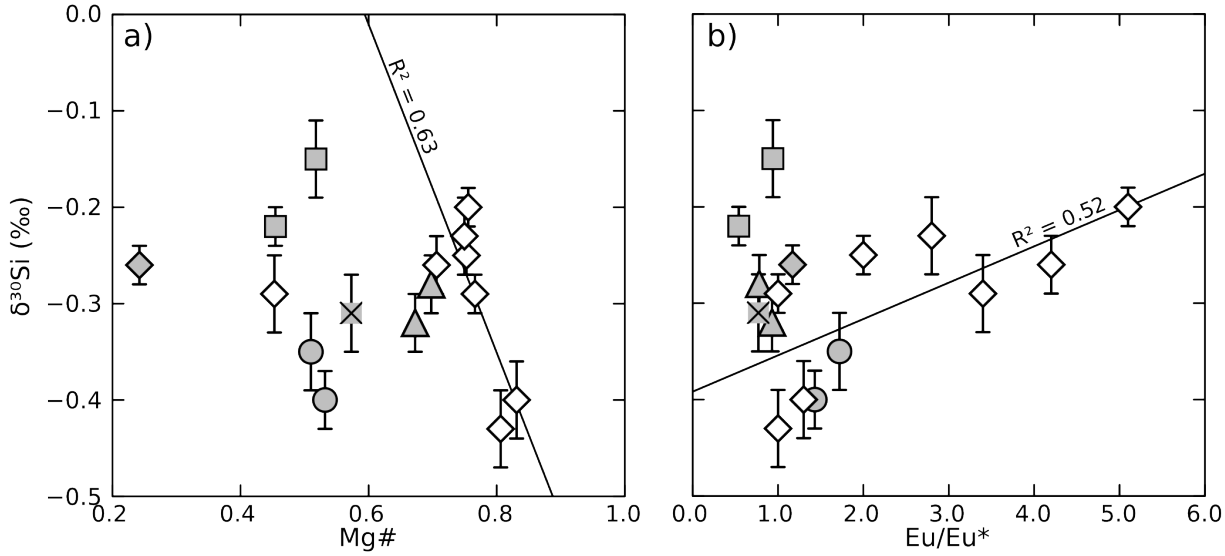


Fig. 7.3 Graph of $\delta^{30}Si$ against a) Mg# and b) Eu/Eu* for the Chudleigh and McBride xenoliths (symbols and error bars as for Figure 7.1). Trend lines in both plots are for the Chudleigh data only. See text for discussion.

Taken with the better correlation for Mg# than Eu/Eu*, this provides evidence that the abundance of ferromagnesian phases, more specifically pyroxene, is the dominant control over Si isotopes in this cumulate system.

Using samples from the Skaergaard layered igneous intrusion (Wager, 1960), it has already been shown that there is significant Si isotopic fractionation between different mineral phases crystallising from a mafic melt (Chapter 4). Specifically, olivine and clinopyroxene are isotopically lighter, and plagioclase heavier than the bulk rock. This is consistent with the data from the Chudleigh xenoliths. Using these mineral separate data and the CIPW normative mineral compositions given in Rudnick et al. (1986), the predicted δ^{30}Si value of the xenoliths can be calculated assuming that the cumulates formed from a mafic melt (Table 7.1). While the range of predicted values (δ^{30}Si = -0.39 to -0.24 ‰) is close to the measured range there is little correspondence between the predicted and actual isotopic composition for each xenolith sample. Either the fractionation factors deduced from the Skaergaard samples are not universally applicable, or another process, other than cumulate formation, may be affecting the Si composition of these xenoliths. Although the former cannot be discounted, the major element characteristics provide evidence for the latter.

Rudnick et al. (1986) state that the variation in Mg# displayed by the Chudleigh xenoliths is too large to be solely affected by the proportions of ferromagnesian phases in the sample. They suggest that these data also reflect variations in the composition of the coexisting melt. Specifically, those xenoliths with low Mg# have equilibrated with a more evolved (Si-rich) melt. Assuming a more Si-rich melt will have a heavier Si isotopic composition, then cumulate phases deriving from this phase should be correspondingly enriched in the heavier isotopes. This may be too simplistic a statement, however, as the Si isotopic composition of a mineral phase is likely to be controlled by the *relative* bonding environments of Si between the phase and the melt (Méheut et al., 2009; Chapter 4) and an increase in the polymerisation degree of a melt will result in variations in the mineral-melt fractionation factors. Nevertheless, the data suggest that the Si isotopic compositions of the Chudleigh xenoliths are controlled predominantly by mineralogy, with subtle isotopic variations introduced by compositional changes in the coexisting melt phase.

7.5.5 Silicon isotopic composition of the lower and middle crust

There are a number of ways that the xenolith data can be used to calculate a Si isotope composition for the lower crust. The first is to take a simple arithmetic mean, which gives a value of $\delta^{30}Si = -0.29 \pm 0.15$ ‰ (2 s.d.; Table 7.2); this value is identical to the $\delta^{30}Si$ BSE value (Chapter 3) and reflects the overall mafic composition of the lower crust. The relatively large errors on the mean reflect the range of isotopic compositions that are displayed in the lower crust.

The second is to take a weighted mean, using the ratio of a sample's SiO_2 content against that of the lower crust (53.4 wt.%, Rudnick and Gao, 2003) as the weighting parameter. This gives an extremely similar value, of $\delta^{30}Si = -0.28 \pm 0.15$ ‰ (2 s.d.; Table 7.2), most likely because most of the xenoliths analysed are also mafic.

The final way is more involved, and uses the average lithological compositions of the lower crust, as estimated by Rudnick and Fountain (1995), and our average Si isotope compositions for each lithology, to calculate a bulk estimate. This method is arguably the most robust, as bulk xenolith composition and the lithologies represented vary considerably between continents (e.g. Condie and Selverstone, 1999; Villaseca et al., 1999; Liu et al., 2001) and so using the first two methods, rather than calculating a global lower crustal average, could bias the calculation toward the Australian lower crust.

This method starts by providing average values for the mafic, intermediate (andesitic), felsic and sedimentary components of the crust. The felsic average was taken from the two xenoliths that represent felsic melts from McBride, and the sedimentary average was taken from Chapter 6. This estimate of $\delta^{30}Si = -0.32 \pm 0.40$ ‰ (2 s.d.) has large error bars, reflecting the large range of data for sediments compared to igneous rocks, although the mean value is very close to the one meta-sediment analysed in this study (83-157). The mafic average is more complicated, because, as is shown above, mafic cumulates have a much larger range of $\delta^{30}Si$ values than mafic melts – therefore it is important to calculate a value that reflects the ratio of cumulate-derived to melt-derived material in the lower crust. To estimate this, the global compilation of granulite facies xenolith data of Kempton and Harmon (1992) was used to infer cumulate:melt:restite populations; from this estimate, of the mafic xenoliths, 52% are melt-, 41% are cumulate-, and 6% are restite-derived. This results in a mafic average of $\delta^{30}Si = -0.30 \pm 0.07$ ‰ (2 s.d.). Finally, the intermediate average is taken as the mean of the mafic and felsic

Table 7.2 – Silicon isotope composition of the deep continental crust

	Mafic	Felsic	Int.	Sed	δ^{30}Si (‰)	2s.d.
	proportions (%)					
Lower crust						
Simple average[a]					–0.29	0.15
Weighted average[b]					–0.28	0.10
Igneous array[c]					–0.27	0.05
Lithological averages[d]						
Archaean	65	15	15	5	–0.28	0.10
Post-Archaean	70	10	10	10	–0.29	0.11
Extensional regions	40	25	25	10	–0.26	0.13
Shield/platforms	90	0	0	10	–0.30	0.10
Middle crust						
Weighted average[b]					–0.23	0.15
Igneous array[c]					–0.21	0.05
Lithological average[d]	22.5	22.5	45	10	–0.25	0.15

Estimates of the Si isotopic composition of the lower and middle continental crust, calculated via various methods:
[a]simple arithmetic mean.
[b]weighted mean, using the ratio of a sample's SiO_2 content against the average SiO_2 content of the lower or middle crust (53.4 wt.% and 63.5 wt.%; Rudnick and Gao, 2003) and as the weighting parameter.
[c]calculated using the "igneous array" equation: [$\delta^{30}Si = 0.0056 \times SiO_2 - 0.567$] (see Chapter 4) and the average SiO_2 contents of the lower and middle crust.
[d]calculated by, first, assigning δ^{30}Si values to crustal lithologies, based on the xenolith data, then combining these values using the range of lithological proportions as inferred by Rudnick and Fountain (1995) – see text for details. A range of isotopic compositions for various crustal composites are given.

averages, viz. $\delta^{30}Si = -0.24 \pm 0.16$ ‰ (2 s.d.).

Table 7.2 shows the results for a number of different lower crustal types, with different lithological proportions. There is very little variation between the calculated lower crustal compositions, with all values (δ^{30}Si ranging from -0.30 to -0.26 ‰) close to the simple and weighted means. For comparison, in Table 7.2, we also give the "igneous" lower crustal composition as calculated by the "igneous array" (Chapter 4), which gives a value of $\delta^{30}Si = -0.27 \pm 0.05$ ‰ (2 s.e. of the regression). The consistency of all of these values gives confidence that our original, simple mean value of $\delta^{30}Si = -0.29 \pm 0.15$ ‰ (2 s.d.) is a good estimate of the Si isotope composition of the lower crust. The precision on this estimate reflects the Si isotope variability in the lower crust; however, the consistency of the average δ^{30}Si calculated using various methods suggests that this value is better constrained than the precision indicates. Using a 95% standard error reflects the precision of this mean at the 95% confidence level, and gives a more precise estimate of $\delta^{30}Si = -0.29 \pm 0.04$ ‰ (95% s.e.). As an aside, the 2 s.d. calculated

using the various average δ^{30}Si lower crust compositions given in Table 7.2 is even smaller (viz. ± 0.03 ‰).

The composition of the middle crust can also be estimated using the weighted mean method, igneous array calculation, and also the lithological method as described above; these estimates are also presented in Table 7.2, and also give remarkably similar values. Given that the median value is the weighted mean, we choose to take this value (δ^{30}Si = -0.23 ± 0.15 ‰; 2 s.d.; ± 0.04 ‰; 95% s.e.) as the Si isotope composition of the middle crust. This is slightly heavier than both the lower and upper crust and reflects the predominantly andesitic composition, and paucity of weathered sedimentary material, of this region.

7.6 CONCLUSIONS

Granulite xenolith samples from the Chudleigh and McBride volcanic provinces, Australia, record the Si isotopic composition of the lower crust. We measured sixteen samples, which display a range of isotopic data (δ^{30}Si = -0.43 to -0.15 ‰) comparable to that measured elsewhere in igneous rocks, from the upper crust, oceanic crust and mantle. This variation lends further support to the suggestion that the lower crust, although dominated by mafic lithologies, contains significant proportions of felsic meta-igneous and meta-sedimentary material.

The Si isotopic variation in the lower crust is controlled via two mechanisms. For melt-derived material, magmatic differentiation appears to be the major factor, whereby increasing SiO_2 content is accompanied by a concomitant increase in the heavier isotopes. This phenomenon is observed globally, in many other magmatic systems (see Chapter 4) and appears to be a fundamental property of the Si isotope system.

The Si isotopic composition of cumulate-derived material, which comprise a large proportion of the lower crust, is predominantly controlled by the mineralogy of individual cumulates. In particular, phases that have higher Mg# tend to concentrate the lighter isotopes, therefore a cumulate that is olivine or pyroxene-rich will have a lighter isotopic composition. Although these cumulates formed via magmatic processes, they do not fall on the "igneous array" because these samples are not representative of equilibrium melt assemblages, i.e. they are not of melt compositions. It also means that, for a given SiO_2 content, cumulate material can have a relatively large range of Si isotopic values.

The average Si isotopic compositions for the lower and middle crust have been

calculated using the xenolith data, combined with a number of weighting methods. The methods all give estimates that agree with one another, so we are confident that our compositions are representative. We calculate a Si isotopic composition of $\delta^{30}Si = -0.29 \pm 0.04$ ‰ (95% s.e.) for the lower crust, and $\delta^{30}Si = -0.23 \pm 0.04$ ‰ (95% s.e.) for the middle crust.

Chapter 8: Summary and outlook

The objective of this research was to reappraise the silicon isotope behaviour and composition of the silicate Earth, with the benefit of more precise analytical techniques as described by Georg et al. (2006b). This was achieved by analysing a broad range of igneous, metamorphic and sedimentary lithologies, sourced from many and varied tectonic settings. The major conclusions from this research are summarised below.

The significant result of Georg et al. (2007), that the Si isotopic composition of chondritic meteorites were lighter than that of Bulk Silicate Earth (BSE), required a robust estimate of $\delta^{30}Si_{BSE}$. The previous estimates of Douthitt (1982) and Ding et al. (1996) were made at lower analytical precisions and, since then, there had been no attempt to reassess these values. To rectify this omission, thirty five well-characterised terrestrial mafic and ultramafic samples were analysed for their Si isotope compositions. BSE was characterised as essentially homogeneous with respect to Si isotopes, with an average $\delta^{30}Si$ composition of -0.29 ± 0.08 ‰ (2 s.d.). Other studies have replicated this value (albeit on the basis of fewer samples) and most agree that the canonical Si isotopic composition of BSE is $\delta^{30}Si \sim -0.30$ ‰ (e.g. Fitoussi et al., 2009; Zambardi et al., 2009; Armytage et al., 2011). The exception is the study of Chakrabarti and Jacobsen (2010) who quote a resolvably lighter $\delta^{30}Si_{BSE}$ value; however, apart from analytical differences, there is no explanation as to why this study returns such light BSE values.

Within the data analysed in this study, small Si isotopic variations were noted. Although these were too small to confidently resolve outside of analytical uncertainty, it was suggested that this could be related to increase of the heavier isotopes of Si as a function of melt polymerisation (Grant, 1954; Méheut et al., 2009), a process that would be investigated further as part of this thesis.

Early Si isotope studies identified a trend whereby more evolved, Si-rich igneous rocks had heavier Si isotope compositions than their primitive counterparts (Douthitt, 1982; Ding et al., 1996). Theoretical studies also suggested such an effect should exist (Grant, 1954; Méheut et al., 2009). To investigate this phenomenon, the Si isotope composition of a set of samples from the volcano of Hekla, Iceland, as well as other localities were analysed. The results show that a strong linear relationship exists between degree of differentiation (SiO_2 content) and $\delta^{30}Si$. Only igneous processes (e.g. assimilation, partial melting and fractional crystallisation) were involved in the petrogenesis of these samples, therefore, these must also be the major cause of isotopic

fractionation. Mineral separate analysis and modelling indicated that removal of isotopically light phases goes some way to explain this effect, and also implied that corresponding isotopically "light" cumulates might exist in the crust. This was investigated using a set of lower crustal xenoliths (see later).

Because Si isotopes appeared to behave so predictably during magmatic differentiation, an "ideal" igneous trend was established, which empirically related the $\delta^{30}Si$ value to the SiO_2 content of a sample as such:

$$\delta^{30}Si\ (‰) = 0.0056 \times SiO_2 - 0.57\ (\pm\ 0.05\ ‰;\ 2\ s.e.)$$

This equation was used to calculate an "igneous" estimate for the Si isotopic composition of the continental crust, assuming an "andesitic" crustal composition, of $\delta^{30}Si \sim -0.23 \pm 0.05$ ‰. It was shown that, despite there being a measurable fractionation of Si isotopes during igneous processes, removal of material of this composition from the mantle to form the crust is unlikely to have resolvably affected the Si isotope signature of the mantle.

To establish this relationship as a truly global effect, future work might involve Si isotope analysis of another well-characterised differentiation sequence; e.g. Kilauea Iki lava lake (Tomascak et al., 1999; Teng et al., 2007). Also, analysis of more extreme end-members of the differentiation sequence, for instance high-silica rhyolites (Halliday et al., 1991) or komatiites (Huppert et al., 1984) should define a wider range of Si isotopic values if the "igneous array" is a robust relationship.

To further investigate the Si isotope composition of the continental crust, and because Si isotopes have the potential to discriminate between granites of different crustal affinities, a selection of granitoid samples from south-eastern Australia and south-west England were analysed. The results showed that significant Si isotopic variations occur in granitoid rocks, greater than that displayed by the high-silica samples (rhyolites and dacites) analysed in the previous chapter (Chapter 4). On average, granites with a sedimentary affinity have lighter Si isotope compositions than igneous-derived granites. This agrees with the hypothesis that S-type granites should be isotopically lighter because they derived from sedimentary material, which typically has a light $\delta^{30}Si$ signature. However, the data display a lot of overlap. Correlations between Si isotopes and other indices for source composition in granites (ASI value, $\delta^{18}O$,

$^{87}Sr/^{86}Sr_{(initial)}$ and $\varepsilon Nd_{(initial)}$) support the conclusion that Si isotope variation is largely related to source heterogeneity, but that other geochemical indices distinguish much more conclusively between granites "types". Analysis of aplite and pegmatite data suggest that volatile-related processes do not affect the bulk Si isotope composition of granitoid material in a closed system. The average Si isotope value for granitoid material was calculated as $\delta^{30}Si$ = -0.23 ± 0.15 ‰ (2 s.d.), which is remarkably close to the "igneous" value of continental crust (see above; Chapter 4) of $\delta^{30}Si$ = -0.23 ± 0.05 ‰.

To complete the study of the Si isotopic composition of the upper continental crust (UCC), a selection of well-characterised loess and shale samples, sourced globally, were analysed. Loess defines a narrow range of Si isotopic compositions ($\delta^{30}Si$ = -0.28 to -0.15 ‰), a result of their primary igneous mineralogy and predominantly mechanical weathering history. The average $\delta^{30}Si$ loess value was calculated as -0.22 ± 0.07 ‰ (2 s.d.), very similar to the average granite $\delta^{30}Si$ (Chapter 5), and "igneous" $\delta^{30}Si$ values (Chapter 4), which suggests that loess represents the Si isotopic composition of fresh, igneous, continental crust. Loess-like Archaean samples have a similar isotopic composition to Pleistocene loess; as such, it appears that the Si isotopic composition of igneous continental crust has remained constant over geological time.

Compared to loess, the Si isotopic composition of shales is shown to be much more variable ($\delta^{30}Si$ = -0.82 to +0.00 ‰), a result of their more complicated petrogenesis. Shale Si isotope composition do not correlate with canonical proxies for weathering, such as CIA values, but do correlate negatively with insoluble element concentrations, which indicates that more intensive or prolonged chemical weathering of a sedimentary source is required before resolvable negative Si isotopic fractionation occurs. From this, it was suggested that the $\delta^{30}Si$ of a shale is a function of the abundance of detrital quartz versus the abundance and composition of the secondary phases in that sample. Shale $\delta^{30}Si$ values heavier than igneous rocks cannot be a result of terrestrial weathering and most likely indicates the presence of marine-derived silica. Extremely negative Si isotopic compositions in Archaean shales may be due to them having experienced more intense weathering, as a result of more aggressive climatic conditions at that time. A weighted average composition of $\delta^{30}Si$ = -0.25 ± 0.16 ‰ (2 s.d.) for the UCC was calculated, which is only slightly heavier than the Bulk Silicate Earth.

In future research, the apparently contrasting behaviour of Si isotopes under either physical or chemical weathering regimes could be used to indicate the presence of fluid in past environments. This may be particularly useful in the debate about the presence of liquid water on the early Martian surface.

The Si isotopic composition of the deep crust was investigated, using a set of granulite xenolith samples from the Chudleigh and McBride volcanic provinces, Australia. These display a range of isotopic data ($\delta^{30}Si$ = -0.43 to -0.15 ‰) comparable to that displayed by igneous rocks from the upper crust, oceanic crust and mantle. The data indicate that Si isotopic variation in the lower crust is controlled via two mechanisms. For melt-derived material, magmatic differentiation appears to be the major factor, as investigated in Chapter 4. For cumulate-derived material, mineralogy of individual cumulates is the major control. The average Si isotopic compositions for the lower and middle crust were calculated using the xenolith data, using a number of weighting methods. The methods all give similar estimates of $\delta^{30}Si = -0.29 \pm 0.15$ ‰ (2 s.d.) for the lower crust, and $\delta^{30}Si = -0.23 \pm 0.15$ ‰ (2 s.d.) for the middle crust.

Before this study began, it was already known that the range of Si isotopic variations in endogenous rocks was small, relative to variations recorded elsewhere in the isotope system (see Fig. 1.1). The most striking result of this study is just *how* limited this system appears to be, when analysed using high precision analytical techniques; this is illustrated in Figure 8.1. For instance, the range for igneous rocks given in Douthitt (1982) is $\delta^{30}Si$ = -0.80 to +0.30 ‰; igneous rocks analysed in this study define a range that is more than three times smaller ($\delta^{30}Si$ = -0.43 to -0.11 ‰). This difference is most likely to be due to a significant increase in analytical precision; the errors quoted in these early papers were as large as ± 0.6 ‰, whereas errors of less than ± 0.10 ‰ (2 s.d.) are common using current techniques. Interestingly, the conclusion of Douthitt (1982), that BSE has a Si isotopic composition of $\delta^{30}Si = -0.40 \pm 0.20$ ‰, is identical, within error, to our current estimate of $\delta^{30}Si = -0.29 \pm 0.08$ ‰ (2 s.d.).

One area that has not been investigated during this thesis, but should be the subject of subsequent research, is that of Si isotope fractionation as a result of metasomatic processes. Silicon solubility increases with increasing fluid temperature, which is why quartz veins are common in areas that have undergone hydrothermal alteration, and chemically precipitated Si can record very extreme $\delta^{30}Si$ values (e.g. Basile-Doelsch et al., 2005). There is also some

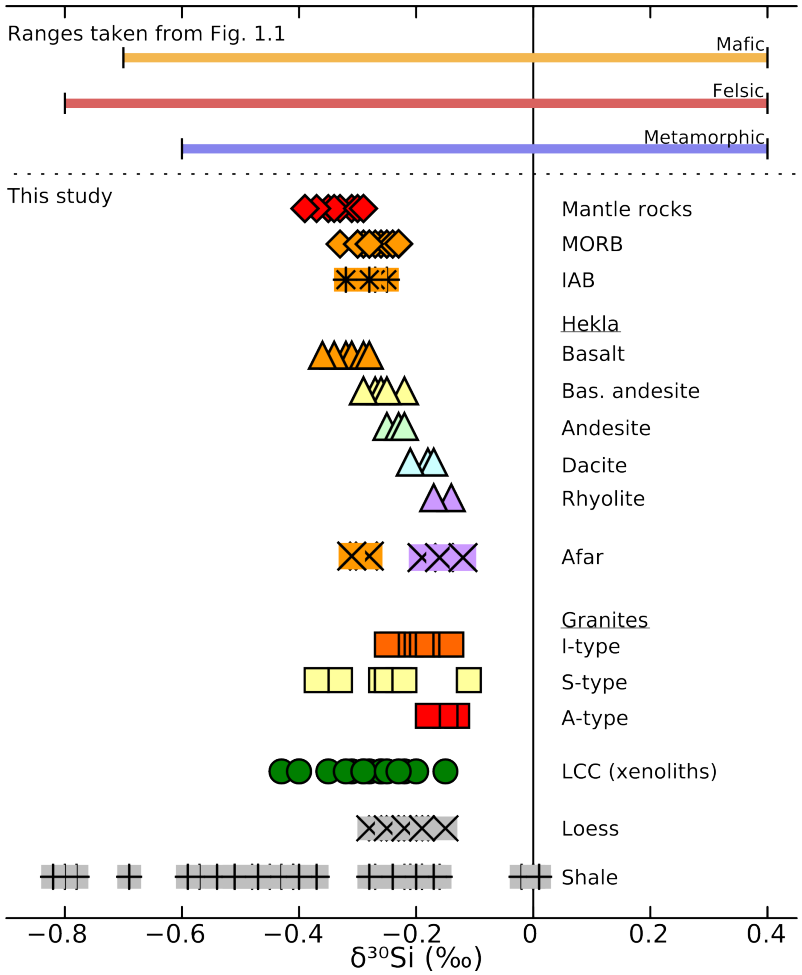


Fig. 8.1 Graph of the range of $\delta^{30}Si$ values analysed in this thesis, illustrating the small range of data recorded by the Si isotope system. This is compared to that of less recent studies, where much larger ranges were presented; this disparity is most likely the result of the significant increase in analytical precision between our methods and those of prior studies. The range for clays, published by the earlier studies, is not provided, as this would compress the data ranges further (vis. $\delta^{30}Si$ = -2.5 to +0.1 ‰; see Fig. 1.1).

evidence that the degree and sense of fractionation during silica precipitation is temperature-dependent, suggesting there is a kinetic, Rayleigh-type fractionation occurring at the precipitation site (Ding et al., 1996). Because of these effects, samples that may have undergone Si alteration as a result of metasomatism have been avoided during this research. However, the oceanic crust is typically heavily metasomatised, so that the material returning to the mantle at subduction zones may not have a BSE-like Si isotopic composition. Therefore, to accurately constrain this tectonic setting as regards Si isotopes, such lithologies should be analysed.

Finally, even though the supracrustal Si cycle can induce much larger isotopic variations than those seen in igneous rocks (see Chapter 6), these do not significantly affect the bulk compositions of many of the silicate reservoirs on Earth, even when supracrustal materials are intrinsically involved (such as sediment anatexis; see Chapter 5). The similarity of the $\delta^{30}Si$ values for BSE, UCC and the deep crust are testament to this observation and are a result of the ubiquity of Si – even though sediments are highly fractionated, they are a mere epidermis to the body of the Earth.

References

Abraham K., Opfergelt S., Fripiat F., Cavagna A., de Jong J. T. M., Foley S. F., André L. and Cardinal D. (2008) $\delta^{30}Si$ and $\delta^{29}Si$ determinations on USGS BHVO-1 and BHVO-2 reference materials with a new configuration on a Nu Plasma Multi-Collector ICP-MS. *Geostand. Geoanal. Res.* **32,** 193-202.

Albarede F. and Michard A. (1986) Transfer of continental Mg, S, O and U to the mantle through hydrothermal alteration of the oceanic crust. *Chem. Geol.* **57,** 1-15.

Alexandre A., Meunier J., Colin F. and Koud J. (1997) Plant impact on the biogeochemical cycle of silicon and related weathering processes. *Geochim. Cosmochim. Acta* **61,** 677-682.

Allègre C. J. and Rousseau D. (1984) The growth of the continent through geological time studied by Nd isotope analysis of shales. *Earth Planet. Sci. Lett.* **67,** 19-34.

Allègre C. J., Poirier J., Humler E. and Hofmann A. W. (1995) The chemical composition of the Earth. *Earth Planet. Sci. Lett.* **134,** 515-526.

Allenby R. J. (1954) Determination of the isotopic ratios of silicon in rocks. *Geochim. Cosmochim. Acta* **5,** 40-48.

André L., Cardinal D., Alleman L. Y. and Moorbath S. (2006) Silicon isotopes in ~3.8 Ga West Greenland rocks as clues to the Eoarchaean supracrustal Si cycle. *Earth Planet. Sci. Lett.* **245**, 162-173.

Armytage R. M. G., Georg R. B. and Halliday A. N. (2009) Silicon isotopes in achondrites and the light element in Earth's core. *Geochim. Cosmochim. Acta* **73**, A53.

Armytage R. M. G., Georg R. B., Savage P. S., Williams H. M. and Halliday A. N. (2011) Silicon isotopes in meteorites and planetary core formation. *Geochim. Cosmochim. Acta* **75,** 3662-3676.

Barberi F., Borsi S., Ferrara G., Marinelli G. and Varet J. (1970) Relationships between tectonics and magmatology of the northern Afar (or Danakil depression), Symp. Roy. Soc. London, mars 1969. *Philos. Trans. R. Soc. London* **267,** 292-311.

Barth M. G., McDonough W. F. and Rudnick R. L. (2000) Tracking the budget of Nb and Ta in the continental crust. *Chem. Geol.* **165,** 197-213.

Basile-Doelsch I. (2006) Si stable isotopes in the Earth's surface: A review. *J. Geochem. Explor.* **88,** 252-256.

Basile-Doelsch I., Meunier J. D. and Parron C. (2005) Another continental pool in the terrestrial silicon cycle. *Nature* **433,** 399-402.

Batiza R. and Yaoling Niu (1992) Petrology and magma chamber processes at the East Pacific Rise ~ 9°30′N. *J. Geophys. Res.* **97,** 6779-6797.

Belshaw N. S., Freedman P. A., O'Nions R. K., Frank M. and Guo Y. (1998) A new variable dispersion double-focusing plasma mass spectrometer with performance illustrated for Pb isotopes. *Int. J. Mass Spectrom.* **181,** 51-58.

Bergquist B. A. and Blum J. D. (2007) Mass-dependent and -independent fractionation of Hg isotopes by photoreduction in aquatic systems. *Science* **318,** 417-420.

Bern C. R., Brzezinski M. A., Beucher C., Ziegler K. and Chadwick O. A. (2010) Weathering, dust, and biocycling effects on soil silicon isotope ratios. *Geochim. Cosmochim. Acta* **74,** 876-889.

Berner R. A. (1997) The rise of plants and their effect on weathering and atmospheric CO_2. *Science* **276,** 544-546.

Bohlen S. R. and Mezger K. (1989) Origin of granulite terranes and the formation of the lowermost continental crust. *Science* **244,** 326-329.

Bryant C. J., Chappell B. W., Bennett V. C. and McCulloch M. T. (2004) Lithium isotopic compositions of the New England Batholith: Correlations with inferred source rock compositions. *T. Royal Soc. Edinburgh Earth Sci.* **95,** 199-214.

Cardinal D., Alleman L. Y., De Jong J., Ziegler K. and André L. (2003) Isotopic composition of silicon measured by multicollector plasma source mass spectrometry in dry plasma mode. *J. Anal. Atom. Spectrom.* **18,** 213-218.

Cardinal D., Gaillardet J., Hughes H. J., Opfergelt S. and André L. (2010) Contrasting silicon isotope signatures in rivers from the congo basin and the specific behaviour of organic-rich waters. *Geophys. Res. Lett.* **37,** L12403

Chakrabarti R. and Jacobsen S. B. (2010) Silicon isotopes in the inner Solar System: Implications for core formation, solar nebular processes and partial melting. *Geochim. Cosmochim. Acta* **74,** 6921-6933.

Chan L., Alt J. C. and Teagle D. A. H. (2002) Lithium and lithium isotope profiles through the upper oceanic crust: A study of seawater-basalt exchange at ODP Sites 504B and 896A. *Earth Planet. Sci. Lett.* **201,** 187-201.

Chang V. T., Williams R. J. P., Makishima A., Belshaw N. S. and O'Nions R. K. (2004) Mg and Ca isotope fractionation during $CaCO_3$ biomineralisation. *Biochem. Biophys. Res. Comm.* **323,** 79-85.

Chappell B. W. (1984) Source rocks of I- and S-type granites in the Lachlan fold belt, southeastern Australia. *Phil. Trans. Royal Soc. London* **A310**, 693-707.

Chappell B. W. (1996) Magma mixing and the production of compositional variation within granite suites: Evidence from the granites of southeastern Australia. *J. Petrol.* **37,** 449-470.

Chappell B. W. (1999) Aluminium saturation in I- and S-type granites and the characterization of fractionated haplogranites. *Lithos* **46,** 535-551.

Chappell B. W. and White A. J. R. (1974) Two contrasting granite types. *Pacific Geology* **8,** 173-174.

Chappell B. W. and White A. J. R. (2001) Two contrasting granite types: 25 years later. *Aust. J. Earth Sci.* **48,** 489-500.

Chappell B. W., Williams I. S., White A. J. R. and McCulloch M. T. (1990) Granites of the Lachlan Fold Belt. *ICOG 7 Conference Field Guide. Bureau of Mineral Resources, Geology and Geophysics, Australia.*

Chappell B. W., White A. J. R. and Williams L. S. (1991) A transverse section through granites of the Lachlan Fold Belt. *Second Hutton Symposium on Granites and Related Rocks.*

Chaudry, M.N. (1971) Feldspars from the Meldon aplite, Devonshire, England. *Min. Mag.,* **38***,* 179-185.

Chekol T. A., Kobayashi K., Yokoyama T., Sakaguchi C. and Nakamura E. (2010) Timescales of magma differentiation from basalt to andesite beneath Hekla Volcano, Iceland: Constraints from U-series disequilibria in lavas from the last quarter-millennium flows. *Geochim. Cosmochim. Acta* **75**, 256-283.

Chesley J. T., Halliday A. N., Snee L. W., Mezger K., Shepherd T. J. and Scrivener R. C. (1993) Thermochronology of the Cornubian batholith in southwest England: Implications for pluton emplacement and protracted hydrothermal mineralization. *Geochim. Cosmochim. Acta* **57,** 1817-1835.

Chesworth W. (1977) Weathering stages of the common igneous rocks, index minerals and mineral assemblages at the surface of the earth. *J. Soil Sci.* **28,** 490-497.

Chmeleff J., Horn I., Steinhoefel G. and von Blanckenburg F. (2008) In situ determination of precise stable Si isotope ratios by UV-femtosecond laser ablation high-resolution multi-collector ICP-MS. *Chem. Geol.* **249,** 155-166.

Collins W. J. (1998) Evaluation of petrogenetic models for Lachlan Fold Belt granitoids: implications for crustal architecture and tectonic models. *Aust. J. Earth Sci.* **45,** 483-500.

Condie K. C. and Selverstone J. (1999) The crust of the Colorado Plateau: New views of an old arc. *J. Geol.* **107,** 387-397.

Courtillot V. (1982) Propagating rifts and continental breakup. *Tectonics* **1,** 239-250.

Darbyshire D. P. F. and Shepherd T. J. (1985) Chronology of granite magmatism and associated mineralization, SW England. *J. Geol. Soc.* **142,** 1159-1177.

Darbyshire D. P. F. and Shepherd T. J. (1987) Chronology of magmatism in southwest England: The minor intrusions. *Proc. Ussher Soc.* **6,** 431-438.

Darbyshire D. P. F. and Shepherd T. J. (1994) Nd and Sr isotope constraints on the origin of the Cornubian batholith, SW England. *J. Geol. Soc.* **151,** 795-802.

Dawson J. B. (1977) Sub-cratonic crust and upper mantle models based on xenolith suites in kimberlite and nephelinitic diatremes. *J. Geol. Soc.* **134,** 173-184.

Dawson J. B., Powell D. G. and Reid A. M. (1970) Ultrabasic xenoliths and lava from the Lashaine Volcano, Northern Tanzania. *J. Petrology* **11,** 519-548.

de Hoog J. C. M., van Bergen M. J. and Jacobs M. H. G. (2005) Vapour-phase crystallisation of silica from SiF_4-bearing volcanic gases. *Ann. Geophys.* **48,** 775-785.

De La Rocha C. L. (2002) Measurement of silicon stable isotope natural abundances via multicollector inductively coupled plasma mass spectrometry (MC-ICP-MS). *Geochem. Geophys. Geosyst.* **3,** 1045.

De la Rocha C. L. (2003) Silicon isotope fractionation by marine sponges and the reconstruction of the silicon isotope composition of ancient deep water. *Geology* **31,** 423-426.

De La Rocha C. L. (2006) Opal-based isotopic proxies of paleoenvironmental conditions. *Global Biogeochem. Cycles* **20,** GB4S09

De La Rocha C. L. and Bickle M. J. (2005) Sensitivity of silicon isotopes to whole-ocean changes in the silica cycle. *Marine Geology* **217,** 267-282.

De La Rocha C. L., Brzezinski M. A., DeNiro M. J. and Shemesh A. (1998) Silicon-isotope composition of diatoms as an indicator of past oceanic change. *Nature* **395,** 680-683.

De La Rocha C. L., Brzezinski M. A. and Deniro M. J. (2000) A first look at the distribution of the stable isotopes of silicon in natural waters. *Geochim. Cosmochim. Acta* **64,** 2467-2477.

Delstanche S., Opfergelt S., Cardinal D., Elsass F., André L. and Delvaux B. (2009) Silicon isotopic fractionation during adsorption of aqueous monosilicic acid onto iron oxide. *Geochim. Cosmochim. Acta* **73,** 923-934.

DePaolo D. J. (1981) Trace element and isotopic effects of combined wallrock assimilation and fractional crystallization. *Earth Planet. Sci. Lett.* **53,** 189-202.

Ding T., Jiang S., Wan D., Li Y., Li J., Song H., Liu Z. and Yao X. (1996) *Silicon Isotope Geochemistry.* Geological Publishing House, Beijing, China.

Ding T., Wan D., Wang C. and Zhang F. (2004) Silicon isotope compositions of dissolved silicon and suspended matter in the Yangtze River, China. *Geochim. Cosmochim. Acta* **68,** 205-216.

Ding T. P., Ma G. R., Shui M. X., Wan D. F. and Li R. H. (2005) Silicon isotope study on rice plants from the Zhejiang province, China. *Chem. Geol.* **218,** 41-50.

Dobson D. P. and Brodholt J. P. (2005) Subducted banded iron formations as a source of ultralow-velocity zones at the core-mantle boundary. *Nature* **434,** 371-374.

Douthitt C. B. (1982) The geochemistry of the stable isotopes of silicon. *Geochim. Cosmochim. Acta* **46,** 1449-1458.

Duddy L. R. (1980) Redistribution and fractionation of rare-earth and other elements in a weathering profile. *Chem. Geol.* **30,** 363-381.

Eby G. N. (1990) The A-type granitoids: A review of their occurrence and chemical characteristics and speculations on their petrogenesis. *Lithos* **26,** 115-134.

Elderfield H. and Greaves M. J. (1981) Strontium isotope geochemistry of Icelandic geothermal systems and implications for sea water chemistry. *Geochim. Cosmochim. Acta,* **45,** 2201-2212.

Elliott T., Plank T., Zindler A., White W. and Bourdon B. (1997) Element transport from slab to volcanic front at the Mariana arc. *J. Geophys. Res. B: Solid Earth* **102,** 14991-15019.

Engström E., Rodushkin I., Ingri J., Baxter D. C., Ecke F., Österlund H. and Öhlander B. (2010) Temporal isotopic variations of dissolved silicon in a pristine boreal river. *Chem. Geol.* **271,** 142-152.

Epstein S. and Taylor Jr. H. P. (1970) $^{18}O/^{16}O$, $^{30}Si/^{28}Si$, D/H, and $^{13}C/^{12}C$ studies of lunar rocks and minerals. *Science* **167,** 533-535.

Epstein S. and Taylor H. P. (1973) $^{18}O/^{16}O$, $^{30}Si/^{28}Si$, $^{13}C/^{12}C$, D/H and Hydrogen and Carbon Concentration Data on Apollo-17 Soils. *Trans. Amer. Geophys. Union* **54,** 585-586.

Exley C. S. and Stone M. (1982) Hercynian intrusive rocks *in Igneous Rocks of the British Isles,* John Wiley & Sons, United Kingdom.

Fedo C. M., Eriksson K. A. and Krogstad E. J. (1996) Geochemistry of shales from the Archean (~3.0 Ga) Buhwa Greenstone Belt, Zimbabwe: Implications for provenance and source-area weathering. *Geochim. Cosmochim. Acta* **60,** 1751-1763.

Ferguson D. J., Barnie T. D., Pyle D. M., Oppenheimer C., Yirgu G., Lewi E., Kidane T., Carn S. and Hamling I. (2010) Recent rift-related volcanism in Afar, Ethiopia. *Earth Planet. Sci. Lett.* **292,** 409-418.

Fitoussi C., Bourdon B., Kleine T., Oberli F. and Reynolds B. C. (2009) Si isotope systematics of meteorites and terrestrial peridotites: implications for Mg/Si fractionation in the solar nebula and for Si in the Earth's core. *Earth Planet. Sci. Lett.* **287,** 77-85.

Fleming P. D. (1996) Inherited deformation structures in metasedimentary enclaves in granites as "windows" into deeper levels of the crust. *Tectonophysics* **267,** 177-185.

Flood R. H. and Shaw S. E. (1977) Two "S-type" granite suites with low initial $^{87}Sr/^{86}Sr$ ratios from the New England Batholith, Australia. *Contrib. Min. Pet.* **61,** 163-173.

Foster D. A. and Gray D. R. (2000) Evolution and structure of the Lachlan Fold Belt (Orogen) of eastern Australia. *Ann. Rev. Earth Planet. Sci.* **28,** 47-80.

Fountain D. M. and Salisbury M. H. (1981) Exposed cross-sections through the continental crust: implications for crustal structure, petrology, and evolution. *Earth Planet. Sci. Lett.* **56,** 263-277.

Francis P., Chaffin C., Maciejewski A. and Oppenheimer C. (1996) Remote determination of SiF_4 in volcanic plumes: A new tool for volcano monitoring. *Geophys. Res. Lett.* **23,** 249-252.

Frost C. D. and Frost R. R. (2011) On ferroan (A-type) granitoids: Their compositional variability and modes of origin. *J. Petrol.* **52 (1)**, 39-53.

Gallet S., Jahn B., Van Vliet Lanoë B., Dia A. and Rossello E. (1998) Loess geochemistry and its implications for particle origin and composition of the upper continental crust. *Earth Planet. Sci. Lett.* **156,** 157-172.

Galy A., Bar-Matthews M., Halicz L. and O'Nions R. K. (2002) Mg isotopic composition of carbonate: Insight from speleothem formation. *Earth Planet. Sci. Lett.* **201,** 105-115.

Garlick G. D. (1966) Oxygen isotope fractionation in igneous rocks. *Earth Planet. Sci. Lett.* **1,** 361-368.

Georg R. B. (2006) Geochemistry of Stable Silicon Isotopes measured by High-Resolution Multi-Collector Inductively-Coupled Plasma Mass Spectrometry (HR-MC-ICP-MS). PhD Thesis, ETH Zurich, Switzerland.

Georg R. B., Reynolds B. C., Frank M. and Halliday A. N. (2006a) Mechanisms controlling the silicon isotopic compositions of river waters. *Earth Planet. Sci. Lett.* **249,** 290-306.

Georg R. B., Reynolds B. C., Frank M. and Halliday A. N. (2006b) New sample preparation techniques for the determination of Si isotopic compositions using MC-ICPMS. *Chem. Geol.* **235,** 95-104.

Georg R. B., Halliday A. N., Schauble E. A. and Reynolds B. C. (2007) Silicon in the Earth's core. *Nature* **447,** 1102-1106.

Georg R. B., Zhu C., Reynolds B. C. and Halliday A. N. (2009a) Stable silicon isotopes of groundwater, feldspars, and clay coatings in the Navajo Sandstone aquifer, Black Mesa, Arizona, USA. *Geochim. Cosmochim. Acta* **73,** 2229-2241.

Georg R. B., West A. J., Basu A. R. and Halliday A. N. (2009b) Silicon fluxes and isotope composition of direct groundwater discharge into the Bay of Bengal and the effect on the global ocean silicon isotope budget. *Earth Planet. Sci. Lett.* **283,** 67-74.

Goldstein S. L., O'Nions R. K. and Hamilton P. J. (1984) A Sm Nd isotopic study of atmospheric dusts and particulates from major river systems. *Earth Planet. Sci. Lett.* **70,** 221-236.

Grant F. S. (1954) The geological significance of variations in the abundances of the isotopes of silicon in rocks. *Geochim. Cosmochim. Acta* **5,** 225-242.

Gray C. M. (1984) An isotopic mixing model for the origin of granitic rocks in southeastern Australia. *Earth Planet. Sci. Lett.* **70,** 47-60.

Gray C. M. (1990) A strontium isotopic traverse across the granitic rocks of southeastern Australia: petrogenetic and tectonic implications. *Aust. J. Earth Sci.* **37,** 331-349.

Halliday A. N., Davidson J. P., Hildreth W. and Holden P. (1991) Modelling the petrogenesis of high Rb/Sr silicic magmas. *Chem. Geol.* **92,** 107-114.

Hamelin B. and Allègre C. J. (1985) Large-scale regional units in the depleted upper mantle revealed by an isotope study of the South-West Indian Ridge. *Nature* **315,** 196-199.

Hanson G. N. (1978) The application of trace elements to the petrogenesis of igneous rocks of granitic composition. *Earth Planet. Sci. Lett.* **38,** 26-43.

Harley S. L. (1989) The origins of granulites: a metamorphic perspective. *Geol. Mag.* **126,** 215-247.

Hawkesworth C. J. and Kemp A. I. S. (2006) Using hafnium and oxygen isotopes in zircons to unravel the record of crustal evolution. *Chem. Geol.* **226,** 144-162.

Heck P. R., Huberty J. M., Kita N. T., Ushikubo T., Kozdon R. and Valley J. W. (2011) SIMS analyses of silicon and oxygen isotope ratios for quartz from Archean and Paleoproterozoic banded iron formations. *Geochim. Cosmochim. Acta* **75,** 5879-5891.

Heimann A., Beard B. L. and Johnson C. M. (2008) The role of volatile exsolution and sub-solidus fluid/rock interactions in producing high $^{56}Fe/^{54}Fe$ ratios in siliceous igneous rocks. *Geochim. Cosmochim. Acta* **72,** 4379-4396.

Hemond C., Arndt N.T., U. Lichtenstein U. and Hofmann A. W. (1993) The heterogeneous Iceland plume: Nd-Sr-O isotopes and trace elements constraints. *J. Geophys. Res.,* **98**, 15833–15850.

Hendry K. R., Georg R. B., Rickaby R. E. M., Robinson L. F. and Halliday A. N. (2010) Deep ocean nutrients during the Last Glacial Maximum deduced from sponge silicon isotopic compositions. *Earth Planet. Sci. Lett.* **292,** 290-300.

Hensel, H. D., McCulloch, M. T., and Chappell, B. W., (1985) The New England Batholith: constraints on its derivation from Nd and Sr isotopic studies of granitoids and country rocks, *Geochim. Cosmochim. Acta*, **49**, 369-384.

Hoefs J. and Sywall M. (1997) Lithium isotope composition of Quaternary and Tertiary biogene carbonates and a global lithium isotope balance. *Geochim. Cosmochim. Acta* **61,** 2679-2690.

Hofmann A. W. (1988) Chemical differentiation of the Earth: the relationship between mantle, continental crust, and oceanic crust. *Earth Planet. Sci. Lett.* **90,** 297-314.

Holbrook W. S., Mooney W. D. and Christensen N. I. (1992) The seismic velocity structure of the deep continental crust. *Continental Lower Crust,* 1-43.

Höskuldsson, A., Vogfjord K., Oskarsson N., Petersen R. and Grönvold K. (2007) The millennium eruption of Hekla in February 2000. *Bull. Volcanol.* **70**, 169–182.

Hu Z. and Gao S. (2008) Upper crustal abundances of trace elements: A revision and update. *Chem. Geol.* **253,** 205-221.

Huang F., Chakraborty P., Lundstrom C. C., Holmden C., Glessner J. J. G., Kieffer S. W. and Lesher C. E. (2010) Isotope fractionation in silicate melts by thermal diffusion. *Nature* **464,** 396-400.

Huppert, H. E., Sparks, R. S. J , Turner, J. S., & Arndt, N. T., (1984). The emplacement and cooling of komatiite lavas. *Nature*, **309**, 19-23.

Jagoutz, E., Palme, H., Baddenhausen, H. et al., 1979. The abundances of major, minor and trace elements in the Earth's mantle as derived from primitive ultramafic nodules. Proc. Lunar Planet. Sci. Conf. 10th. 2031-2050

Jeffcoate A. B., Elliott T., Kasemann S. A., Ionov D., Cooper K. and Brooker R. (2007) Li isotope fractionation in peridotites and mafic melts. *Geochim. Cosmochim. Acta* **71,** 202-218.

Keay S., Collins W. J. and McCulloch M. T. (1997) A three-component Sr-Nd isotopic mixing model for granitoid genesis, Lachlan fold belt, eastern Australia. *Geology* **25,** 307-310.

Kemp A. I. S. and Hawkesworth C. J. (2003) Granitic perspectives on the generation and secular evolution of the continental crust. *Treatise on Geochemistry* **3,** 349-410.

Kempton P. D. and Harmon R. S. (1992) Oxygen isotope evidence for large-scale hybridization of the lower crust during magmatic underplating. *Geochim. Cosmochim. Acta* **56,** 971-986.

Klein E. M., Langmuir C. H. and Staudigel H. (1991) Geochemistry of basalts from the Southeast Indian Ridge, 115°E- 138°E. *J. Geophys. Res.* **96,** 2089-2107.

Korsch R. J. (1977) A framework for the Palaeozoic geology of the southern part of the New England Geosyncline. *J. Geol. Soc. Australia* **25,** 339-355.

Kronberg B. I., Fyfe W. S., Leonardos Jr. O. H. and Santos A. M. (1979) The chemistry of some Brazilian soils: Element mobility during intense weathering. *Chem. Geol.* **24,** 211-229.

Lahitte P., Gillot P. and Courtillot V. (2003) Silicic central volcanoes as precursors to rift propagation: The Afar case. *Earth Planet. Sci. Lett.* **207,** 103-116.

Langmuir C. H. (1993) Intensive rock sampling of 16 ridge segments between 32 and 41°N: Preliminary results from shipboard analyses. *Eos* **74,** 380.

Le Bas M. J., Le Maitre R. W., Streckeisen A. and Zanettin B. (1986) A chemical classification of volcanic rocks based on the total alkali-silica system. *J. Petrol.* **27,** 247-257.

Lee D., Halliday A. N., Davies G. R., Essene E. J., Fitton J. G. and Temdjim R. (1996) Melt enrichment of shallow depleted mantle: A detailed petrological, trace element and isotopic study of mantle-derived xenoliths and megacrysts from the Cameroon line. *J. Petrol.* **37,** 415-441.

Leeman W. P., Sisson V. B. and Reid M. R. (1992) Boron geochemistry of the lower crust: Evidence from granulite terranes and deep crustal xenoliths. *Geochim. Cosmochim. Acta* **56,** 775-788.

Li W., Teng F-Z., Ke S., Rudnick R. L., Gao S., Wu F. and Chappell B. W. (2010) Heterogeneous magnesium isotopic composition of the upper continental crust. *Geochim. Cosmochim. Acta* **74,** 6867-6884.

Liu Y., Gao S., Jin S., Hu S., Sun M., Zhao Z. and Feng J. (2001) Geochemistry of lower crustal xenoliths from Neogene Hannuoba Basalt, North China Craton: Implications for petrogenesis and lower crustal composition. *Geochim. Cosmochim. Acta* **65,** 2589-2604.

Loiselle M. C. and Wones D. R. (1979) Characteristics and origin of anorogenic granites. *Geological Society of America Abstracts with Programs* **11,** 468.

London D. (2005) Granitic pegmatites: An assessment of current concepts and directions for the future. *Lithos* **80,** 281-303.

Lowe D. R. and Tice M. M. (2004) Geologic evidence for Archean atmospheric and climatic evolution: Fluctuating levels of CO2, CH4, and O2 with an overriding tectonic control. *Geology* **32,** 493-496.

Lundstrom C. C. (2009) Hypothesis for the origin of convergent margin granitoids and Earth's continental crust by thermal migration zone refining. *Geochim. Cosmochim. Acta* **73,** 5709-5729.

Lundstrom C. C., Chaussidon M., Hsui A. T., Kelemen P. and Zimmerman M. (2005) Observations of Li isotopic variations in the Trinity Ophiolite: Evidence for isotopic fractionation by diffusion during mantle melting. *Geochim. Cosmochim. Acta* **69,** 735-751.

Maas R., Nicholls I. A. and Legg C. (1997) Igneous and metamorphic enclaves in the S-type Deddick Granodiorite, Lachlan fold Belt, SE Australia: Petrographic, geochemical and Nd-Sr isotopic evidence for crustal melting and magma mixing. *J. Petrol.* **38,** 815-841.

Martin H. (1986) Effect of steeper Archean geothermal gradient on geochemistry of subduction-zone magmas. *Geology* **14,** 753-756.

Mattey D., Lowry D. and Macpherson C. (1994) Oxygen isotope composition of mantle peridotite. *Earth Planet. Sci. Lett.* **128,** 231-241.

McBirney A. R. (1996) The Skaergaard Intrusion. *Layered intrusions,* 147-180.

McBirney A. R. and Creaser R. A. (2003) The Skaergaard Layered Series, part VII: Sr and Nd isotopes. *J. Petrol.* **44,** 757-771.

McCulloch M. T. and Chappell B. W. (1982) Nd isotopic characteristics of S- and I-type granites. *Earth Planet. Sci. Lett.* **58,** 51-64.

McCulloch M. T. and Wasserburg G. J. (1978) Sm-Nd and Rb-Sr chronology of continental crust formation. *Science* **200,** 1003-1011.

McCulloch M. T. and Woodhead J. D. (1993) Lead isotopic evidence for deep crustal-scale fluid transport during granite petrogenesis. *Geochim. Cosmochim. Acta* **57,** 659-674.

McDaniel D. K., Hemming S. R., McLennan S. M. and Hanson G. N. (1994) Petrographic, geochemical, and isotopic constraints on the provenance of the early Proterozoic Chelmsford Formation, Sudbury Basin, Ontario. *J. Sed. Res. A* **64 A,** 362-372.

McLennan S. M. (1993) Weathering and global denudation. *J. Geol.* **101,** 295-303.

McLennan S. M., Fryer B. J. and Young G. M. (1979) Rare earth elements in Huronian (Lower Proterozoic) sedimentary rocks: Composition and evolution of the post-Kenoran upper crust. *Geochim. Cosmochim. Acta* **43,** 375-388.

McLennan S. M., Taylor S. R. and Eriksson K. A. (1983) Geochemistry of Archean shales from the Pilbara Supergroup, Western Australia. *Geochim. Cosmochim. Acta* **47,** 1211-1222.

McLennan S. M., Hemming S. R., Taylor S. R. and Eriksson K. A. (1995) Early Proterozoic crustal evolution: Geochemical and NdPb isotopic evidence from metasedimentary rocks, southwestern North America. *Geochim. Cosmochim. Acta* **59,** 1153-1177.

McLennan S. M., Simonetti A. and Goldstein S. L. (2000) Nd and Pb isotopic evidence for provenance and post-depositional alteration of the Paleoproterozoic Huronian Supergroup, Canada. *Precambrian Res.* **102,** 263-278.

Méheut M., Lazzeri M., Balan E. and Mauri F. (2007) Equilibrium isotopic fractionation in the kaolinite, quartz, water system: Prediction from first-principles density-functional theory. *Geochimica et Cosmochimica Acta* **71,** 3170-3181.

Méheut M., Lazzeri M., Balan E. and Mauri F. (2009) Structural control over equilibrium silicon and oxygen isotopic fractionation: A first-principles density-functional theory study. *Chem. Geol.* **258,** 28-37.

Molini-Velsko C., Mayeda T. K. and Clayton R. N. (1986) Isotopic composition of silicon in meteorites. *Geochim. Cosmochim. Acta* **50,** 2719-2726.

Moune S., Sigmarsson O., Thordarson T. and Gauthier P. (2007) Recent volatile evolution in the magmatic system of Hekla volcano, Iceland. *Earth Planet. Sci. Lett.* **255,** 373-389.

Mysen B. O. (1983) The structure of silicate melts. *Ann. Rev. Earth Planet. Sci.,* **11,** 75-97.

Nance W. B. and Taylor S. R. (1976) Rare earth element patterns and crustal evolution-I. Australian post-Archean sedimentary rocks. *Geochim. Cosmochim. Acta* **40,** 1539-1551.

Nelson D. R., McCulloch M. T. and Sun S. (1986) The origins of ultrapotassic rocks as inferred from Sr, Nd and Pb isotopes. *Geochim. Cosmochim. Acta* **50,** 231-245.

Nesbitt H. W. and Young G. M. (1982) Early proterozoic climates and plate motions inferred from major element chemistry of lutites. *Nature* **299,** 715-717.

Newton R. C. (1989) Metamorphic fluids in the deep crust. *Ann. Rev. Earth Planet. Sci.,* **17,** 385-412.

O'Neil J. R. (1986) Theoretical and experimental aspects of isotopic fractionation. *Stable Isotopes in High Temperature Geological Processes. Rev Mineral.* **16,** 1-40.

O'Neil J. R. and Chappell B. W. (1977) Oxygen and hydrogen isotope relations in the Berridale batholith. *J. Geol. Soc.* **133,** 559-571.

Opfergelt S., Delvaux B., André L. and Cardinal D. (2008) Plant silicon isotopic signature might reflect soil weathering degree. *Biogeochemistry* **91,** 163-175.

Opfergelt S., de Bournonville G., Cardinal D., André L., Delstanche S. and Delvaux B. (2009) Impact of soil weathering degree on silicon isotopic fractionation during adsorption onto iron oxides in basaltic ash soils, Cameroon. *Geochim. Cosmochim. Acta* **73,** 7226-7240.

Opfergelt S., Cardinal D., André L., Delvigne C., Bremond L. and Delvaux B. (2010) Variations of δ^{30}Si and Ge/Si with weathering and biogenic input in tropical basaltic ash soils under monoculture. *Geochim. Cosmochim. Acta* **74,** 225-240.

Opfergelt S., Georg R. B., Burton K. W., Guicharnaud R., Siebert C., Gislason S. R. and Halliday A. N. (2011) Silicon isotopes in allophane as a proxy for mineral formation in volcanic soils. *Appl. Geochem.* **26,** S115-S118.

Palme H. and Jones A. (2003) Solar system abundances of the elements. *Treatise on Geochemistry* **1,** 41-61.

Paslick C., Halliday A., James D. and Dawson J. B. (1995) Enrichment of the continental lithosphere by OIB melts: Isotopic evidence from the volcanic province of northern Tanzania. *Earth Planet. Sci. Lett.* **130,** 109-126.

Plank T. and Langmuir C. H. (1998) The chemical composition of subducting sediment and its consequences for the crust and mantle. *Chem. Geol.* **145,** 325-394.

Poitrasson F. and Freydier R. (2005) Heavy iron isotope composition of granites determined by high resolution MC-ICP-MS. *Chem. Geol.* **222,** 132-147.

Potts P. J. (1987) *A Handbook of Silicate Rock Analysi*s. Blackie Academics and Professional.

Pye K. (1995) The nature, origin and accumulation of loess. *Quat. Science Rev.* **14,** 653-667.

Ragueneau O., Tréguer P., Leynaert A., Anderson R. F., Brzezinski M. A., DeMaster D. J., Dugdale R. C., Dymond J., Fischer G., François R., Heinze C., Maier-Reimer E., Martin-Jézéquel V., Nelson D. M. and Quéguiner B. (2000) A review of the Si cycle in the modern ocean: Recent progress and missing gaps in the application of biogenic opal as a paleoproductivity proxy. *Global Planet. Change* **26,** 317-365.

Ramsey M. H., Potts P. J., Webb P. C., Watkins P., Watson J. S. and Coles B. J. (1995) An objective assessment of analytical method precision: comparison of ICP-AES and XRF for the analysis of silicate rocks. *Chem. Geol.* **124,** 1-19.

Reynolds J. H. and Verhoogen J. (1953) Natural variations in the isotopic constitution of silicon. *Geochim. Cosmochim. Acta* **3,** 224-234.

Reynolds J. R., Langmuir C. H., Bender J. F., Kastens K. A. and Ryan W. B. F. (1992) Spatial and temporal variability in the geochemistry of basalts from the East Pacific Rise. *Nature* **359,** 493-499.

Reynolds B. C., Aggarwal J., André L., Baxter D., Beucher C., Brzezinski M. A., Engström E., Georg R. B., Land M., Leng M. J., Opfergelt S., Rodushkin I., Sloane H. J., Van Den Boorn S. H. J. M., Vroon P. Z. and Cardinal D. (2007) An inter-laboratory comparison of Si isotope reference materials. *J. Anal. Atom. Spectrom.* **22,** 561-568.

Richter F. M., Liang Y. and Davis A. M. (1999) Isotope fractionation by diffusion in molten oxides. *Geochim. Cosmochim. Acta* **63,** 2853-2861.

Richter F. M., Davis A. M., DePaolo D. J. and Watson E. B. (2003) Isotope fractionation by chemical diffusion between molten basalt and rhyolite. *Geochim. Cosmochim. Acta* **67,** 3905-3923.

Richter F. M., Dauphas N. and Teng F. (2009a) Non-traditional fractionation of non-traditional isotopes: Evaporation, chemical diffusion and Soret diffusion. *Chem. Geol.* **258,** 92-103.

Richter F. M., Watson E. B., Mendybaev R., Dauphas N., Georg B., Watkins J. and Valley J. (2009b) Isotopic fractionation of the major elements of molten basalt by chemical and thermal diffusion. *Geochim. Cosmochim. Acta* **73,** 4250-4263.

Ringwood A. E. (1989) Significance of the terrestrial Mg/Si ratio. *Earth & Planetary Science Letters* **95,** 1-7.

Robert F. and Chaussidon M. (2006) A palaeotemperature curve for the Precambrian oceans based on silicon isotopes in cherts. *Nature* **443,** 969-972.

Roe J. E., Anbar A. D. and Barling J. (2003) Nonbiological fractionation of Fe isotopes: Evidence of an equilibrium isotope effect. *Chem. Geol.* **195,** 69-85.

Rosenberg P. E. (1973) HF-SiF_4 ratios in volcanic and magmatic gases. *Geochim. Cosmochim. Acta* **37,** 109-112.

Rudnick R. L. (1990) Nd and Sr isotopic compositions of lower-crustal xenoliths from north Queensland, Australia: Implications for Nd model ages and crustal growth processes. *Chem. Geol.* **83,** 195-208.

Rudnick R. L. (1995) Making continental crust. *Nature* **378,** 571-578.

Rudnick R. L. and Fountain D. M. (1995) Nature and composition of the continental crust: A lower crustal perspective. *Rev. Geophys.* **33,** 267-309.

Rudnick R. L. and Gao S. (2003) Composition of the continental crust. *Treatise on Geochemistry* **3,** 1-64.

Rudnick R. L. and Goldstein S. L. (1990) The Pb isotopic compositions of lower crustal xenoliths and the evolution of lower crustal Pb. *Earth Planet. Sci. Lett.* **98,** 192-207.

Rudnick R. L. and Ionov D. A. (2007) Lithium elemental and isotopic disequilibrium in minerals from peridotite xenoliths from far-east Russia: Product of recent melt/fluid-rock reaction. *Earth Planet. Sci. Lett.* **256,** 278-293.

Rudnick R. L. and Taylor S. R. (1987) The composition and petrogenesis of the lower crust: A xenolith study. *J. Geophys. Res.* **92,** 13981-14005.

Rudnick R. L. and Williams I. S. (1987) Dating the lower crust by ion microprobe. *Earth Planet. Sci. Lett.* **85,** 145-161.

Rudnick R. L., McDonough W. F., McCulloch M. T. and Taylor S. R. (1986) Lower crustal xenoliths from Queensland, Australia: Evidence for deep crustal assimilation and fractionation of continental basalts. *Geochim. Cosmochim. Acta* **50,** 1099-1115.

Saal A. E., Rudnick R. L., Ravizza G. E. and Hart S. R. (1998) Re-Os isotope evidence for the composition, formation and age of the lower continental crust. *Nature* **393,** 58-61.

Savage P. S., Georg R. B., Armytage R. M. G., Williams H. M. and Halliday A. N. (2010) Silicon isotope homogeneity in the mantle. *Earth Planet. Sci. Lett.* **295,** 139-146.

Savage P. S., Georg R. B., Williams H. M., Burton K. W. and Halliday A. N. (2011) Silicon isotope fractionation during magmatic differentiation. *Geochim. Cosmochim. Acta* **75,** 6124-6139.

Schauble E. A. (2004) Applying stable isotope fractionation theory to new systems. *Reviews in Mineralogy and Geochemistry* **55,** 65-111.

Schiano P., Birck J. and Allègre C. J. (1997) Osmium-strontium-neodymium-lead isotopic covariations in mid-ocean ridge basalt glasses and the heterogeneity of the upper mantle. *Earth Planet. Sci. Lett.* **150,** 363-379.

Schoenberg R. and von Blanckenburg F. (2006) Modes of planetary-scale Fe isotope fractionation. *Earth Planet. Sci. Lett.* **252,** 342-359.

Schuessler J. A. and von Blanckenburg F. (2011) Exploring micro-scale stable isotope variations using femtosecond laser ablation MC-ICP-MS. *Min. Mag.*, **75 (3)**, 1826.

Schuessler J. A., Schoenberg R. and Sigmarsson O. (2009) Iron and lithium isotope systematics of the Hekla volcano, Iceland - Evidence for Fe isotope fractionation during magma differentiation. *Chem. Geol.* **258,** 78-91.

Shahar A. and Young E. D. (2007) Astrophysics of CAI formation as revealed by silicon isotope LA-MC-ICPMS of an igneous CAI. *Earth Planet. Sci. Lett.* **257,** 497-510.

Shahar, A., Ziegler, K., Young, E.D., Ricolleau, A., Schauble, E.A. and Fei, Y. (2009) Experimentally determined Si isotope fractionation between silicate and Fe metal and implications for Earth's core formation. *Earth Planet. Sci. Lett.* **288,** 228-234.

Shand S.J. (1927) On the Relations between Silica, Alumina, and the Bases in Eruptive Rocks, considered as a Means of Classification. *Geol. Mag.*, **64**, 446-449

Shaw D. M. (1956) Geochemistry of pelitic rocks. Part III: Major elements and general geochemistry. *Geological Society of America Bulletin* **67,** 919-934.

Shaw S. E. and Flood R. H. (1981) The New England batholith, eastern Australia: geochemical variations in time and space. *J. Geophys. Res.* **86,** 10530-10544.

Shen B., Jacobsen B., Lee C. -. A., Yin Q. -. and Morton D. M. (2009) The Mg isotopic systematics of granitoids in continental arcs and implications for the role of chemical weathering in crust formation. *Proc. Natl. Acad. Sci. U. S. A.* **106,** 20652-20657.

Sigmarsson O., Condomines M. and Fourcade S. (1992) A detailed Th, Sr and O isotope study of Hekla: differentiation processes in an Icelandic Volcano. *Contrib. Min. Pet.* **112,** 20-34.

Simmons W. B., Webber K. L., Falster A. U. and Nizamoff J. W. (2003) *Pegmatology: Pegmatite Mineralogy, Petrology and Petrogenesis* 176.

Soosalu H. and Einarsson P. (2004) Seismic constraints on magma chambers at Hekla and Torfajökull volcanoes, Iceland. *Bull. Volc.* **66,** 276-286.

Stähle H. J., Raith M., Hoernes S. and Delfs A. (1987) Element mobility during incipient granulite formation at Kabbaldurga, Southern India. *J. Petrol.* **28,** 803-834.

Steinhoefel G., Horn I. and von Blanckenburg F. (2009) Micro-scale tracing of Fe and Si isotope signatures in banded iron formation using femtosecond laser ablation. *Geochim. Cosmochim. Acta* **73,** 5343-5360.

Steinhoefel G., Breuer J., von Blanckenburg F., Horn I., Kaczorek D. and Sommer M. (2011) Micrometer silicon isotope diagnostics of soils by UV femtosecond laser ablation. *Chem. Geol.* **286,** 280-289.

Stewart B. W. and DePaolo D. J. (1990) Isotopic studies of processes in mafic magma chambers: II. The Skaergaard Intrusion, East Greenland. *Contrib. Min. Pet.* **104,** 125-141.

Stone J., Hutcheon I. D., Epstein S. and Wasserburg G. J. (1991) Correlated Si isotope anomalies and large 13C enrichments in a family of exotic SiC grains. *Earth Planet. Sci. Lett.* **107,** 570-581.

Sugitani K., Horiuchi Y., Adachi M. and Sugisaki R. (1996) Anomalously low Al_2O_3/TiO_2 values for Archean cherts from the Pilbara Block, Western Australia - Possible evidence for extensive chemical weathering on the early earth. *Precambrian Res.* **80,** 49-76.

Taylor H. P. and Epstein S. (1970) Oxygen and Silicon Isotope Ratios of Lunar-Rock-12013. *Earth Planet. Sci. Lett.* **9,** 208-210.

Taylor H. P. and Epstein S. (1973) Oxygen and Silicon Isotope Ratios of Luna-20 Soil. *Geochim. Cosmochim. Acta* **37,** 1107-1109.

Taylor H. P. and Forester R. W. (1979) An oxygen and hydrogen isotope study of the Skaergaard intrusion and its country rocks: A description of a 55 M.Y. old fossil hydrothermal system. *J. Petrol.* **20,** 355-419.

Taylor S. R. and McLennan S. M. (1985) *The Continental Crust: Its Composition and Evolution.* Blackwell Scientific Publications.

Taylor S. R., McLennan S. M. and McCulloch M. T. (1983) Geochemistry of loess, continental crustal composition and crustal model ages. *Geochim. Cosmochim. Acta* **47,** 1897-1905.

Teng F. Z., McDonough W. F., Rudnick R. L., Dalpé C., Tomascak P. B., Chappell B. W. and Gao S. (2004) Lithium isotopic composition and concentration of the upper continental crust. *Geochim. Cosmochim. Acta* **68,** 4167-4178.

Teng F. Z., McDonough W. F., Rudnick R. L. and Walker R. J. (2006) Diffusion-driven extreme lithium isotopic fractionation in country rocks of the Tin Mountain pegmatite. *Earth Planet. Sci. Lett.* **243,** 701-710.

Teng F. Z., Wadhwa M. and Helz R. T. (2007) Investigation of magnesium isotope fractionation during basalt differentiation: Implications for a chondritic composition of the terrestrial mantle. *Earth Planet. Sci. Lett.* **261,** 84-92.

Teng F. Z., Rudnick R. L., McDonough W. F., Gao S., Tomascak P. B. and Liu Y. (2008) Lithium isotopic composition and concentration of the deep continental crust. *Chem. Geol.* **255,** 47-59.

Thiemens M. H. (2006) History and applications of mass-independent isotope effects. *Ann. Rev. Earth Planet. Sci.* **34,** 217-262.

Thirlwall M. F., Gee M. A. M., Lowry D., Mattey D. P., Murton B. J. and Taylor R. N. (2006) Low $\delta^{18}O$ in the Icelandic mantle and its origins: Evidence from Reykjanes Ridge and Icelandic lavas. *Geochim. Cosmochim. Acta* **70,** 993-1019.

Thorarinsson S. (1967) The eruption of Hekla 1947-48. 1-The eruptions of Hekla in historical times. *Soc Scientiarum Islandica* **1** 170.

Tilles D. (1961a) Natural Variations in Isotopic Abundances of Silicon. *J. Geophys. Res.* **66,** 3003-3014.

Tilles D. (1961b) Variations of Silicon Isotope Ratios in a Zoned Pegmatite. *J. Geophys. Res.* **66,** 3015-3020.

Tomascak P. B., Tera F., Helz R. T. and Walker R. J. (1999) The absence of lithium isotope fractionation during basalt differentiation: New measurements by multicollector sector ICP-MS. *Geochim. Cosmochim. Acta* **63,** 907-910.

Tomascak P. B., Langmuir C. H., le Roux P. J. and Shirey S. B. (2008) Lithium isotopes in global mid-ocean ridge basalts. *Geochim. Cosmochim. Acta* **72,** 1626-1637.

Tréguer P., Nelson D. M., Van Bennekom A. J., DeMaster D. J., Leynaert A. and Quéguiner B. (1995) The silica balance in the world ocean: A reestimate. *Science* **268,** 375-379.

Turner D. R., Dickson A. G. and Whitfield M. (1980) Water-rock partition coefficients and the composition of natural waters - A reassessment. *Mar. Chem.* **9,** 211-218.

Turner S. P., Foden J. D. and Morrison R. S. (1992) Derivation of some A-type magmas by fractionation of basaltic magma: An example from the Padthaway Ridge, South Australia. *Lithos* **28,** 151-179.

van den Boorn S. H. J. M., Vroon P. Z., Van Belle C. C., Van Der Wagt B., Schwieters J. and Van Bergen M. J. (2006) Determination of silicon isotope ratios in silicate materials by high-resolution MC-ICP-MS using a sodium hydroxide sample digestion method. *J. Anal. Atom. Spectrom.* **21,** 734-742.

van den Boorn S. H. J. M., van Bergen M. J., Nijman W. and Vroon P. Z. (2007) Dual role of seawater and hydrothermal fluids in Early Archean chert formation: Evidence from silicon isotopes. *Geology* **35,** 939-942.

van den Boorn S. H. J. M., Vroon P. Z. and Van Bergen M. J. (2009) Sulfur-induced offsets in MC-ICP-MS silicon-isotope measurements. *J. Anal. At. Spectrom.* **24,** 1111-1114.

Varela D. E., Pride C. J. and Brzezinski M. A. (2004) Biological fractionation of silicon isotopes in Southern Ocean surface waters. *Global Biogeochemical Cycles* **18,** GB1047 1-8.

Villaseca C., Downes H., Pin C. and Barbero L. (1999) Nature and composition of the lower continental crust in Central Spain and the granulite-granite linkage: Inferences from granulitic xenoliths. *J. Petrol.* **40,** 1465-1496.

Wade J. and Wood B. J. (2005) Core formation and the oxidation state of the Earth. *Earth Planet. Sci. Lett.* **236,** 78-95.

Wager L. R. (1960) The major element variation of the layered series of the skaergaard intrusion and a re-estimation of the average composition of the hidden layered series and of the successive residual magmas. *J. Petrol.* **1,** 364-398.

Walker J. C. G., Hays P. B. and Kasting J. F. (1981) A negative feedback mechanism for the long-term stabilization of Earth's surface temperature. *J. Geophys. Res.* **86,** 9776-9782.

Watkins J. M., DePaolo D. J., Ryerson F. J. and Peterson B. T. (2011) Influence of liquid structure on diffusive isotope separation in molten silicates and aqueous solutions. *Geochim. Cosmochim. Acta* **75,** 3103-3118.

Watson J. S., (1996) Fast, simple method of powder pellet preparation for X-ray fluorescence analysis. *X-ray Spectrom.*, **25**, 173–174.

Wedepohl K.H. (1995) The composition of the continental crust. *Geochim. Cosmochim. Acta* **59,** 1217-1232.

Whalen J. B., Currie K. L. and Chappell B. W. (1987) A-type granites: geochemical characteristics, discrimination and petrogenesis. *Contrib. Min. Pet.* **95,** 407-419.

White A. J. R., Williams I. S. and Chappell B. W. (1976) The Jindabyne thrust and its tectonic, physiographic and petrogenetic significance. *J. Geol. Soc. Australia* **23,** 105-112.

Weyer, S. and Schwieters, J. (2003) High precision Fe isotope measurements with high mass resolution MC-ICPMS. *Int. J. Mass Spectrom*. **226**, 355-368.

Wille M., Sutton J., Ellwood M. J., Sambridge M., Maher W., Eggins S. and Kelly M. (2010) Silicon isotopic fractionation in marine sponges: A new model for understanding silicon isotopic variations in sponges. *Earth Planet. Sci. Lett.* **292,** 281-289.

Williams H. M., Peslier A. H., McCammon C., Halliday A. N., Levasseur S., Teutsch N. and Burg J. -. (2005) Systematic iron isotope variations in mantle rocks and minerals: The effects of partial melting and oxygen fugacity. *Earth Planet. Sci. Lett.* **235,** 435-452.

Wunder B., Meixner A., Romer R. L. and Heinrich W. (2006) Temperature-dependent isotopic fractionation of lithium between clinopyroxene and high-pressure hydrous fluids. *Contrib. Min. Pet.* **151,** 112-120.

Wunder B., Meixner A., Romer R. L., Feenstra A., Schettler G. and Heinrich W. (2007) Lithium isotope fractionation between Li-bearing staurolite, Li-mica and aqueous fluids: An experimental study. *Chem. Geol.* **238,** 277-290.

Wyborn L. A. I. and Chappell B. W. (1983) Chemistry of the Ordovician and Silurian greywackes of the Snowy Mountains, southeastern Australia: An example of chemical evolution of sediments with time. *Chem. Geol.* **39,** 81-92.

Young E. D., Galy A. and Nagahara H. (2002) Kinetic and equilibrium mass-dependent isotope fractionation laws in nature and their geochemical and cosmochemical significance. *Geochim. Cosmochim. Acta* **66,** 1095-1104.

Zambardi T. and Poitrasson F. (2011) Precise Determination of Silicon Isotopes in Silicate Rock Reference Materials by MC-ICP-MS. *Geostand. Geoanal. Res.* **35,** 89-99.

Zambardi T., Poitrasson F., Quitté G. and Anand M. (2009) Silicon isotope variations in the Earth and meteorites. *Geochim. Cosmochim. Acta* **73,** A1497.

Ziegler K., Chadwick O. A., Brzezinski M. A. and Kelly E. F. (2005a) Natural variations of $\delta^{30}Si$ ratios during progressive basalt weathering, Hawaiian Islands. *Geochim. Cosmochim. Acta* **69,** 4597-4610.

Ziegler K., Chadwick O. A., White A. F. and Brzezinski M. A. (2005b) $\delta^{30}Si$ systematics in a granitic saprolite, Puerto Rico. *Geology* **33,** 817-820.

Ziegler K., Young E. D., Schauble E. A. and Wasson J. T. (2010) Metal-silicate silicon isotope fractionation in enstatite meteorites and constraints on Earth's core formation. *Earth Planet. Sci. Lett.* **295,** 487-496.

Appendix 1: Hekla samples - major and trace elements

	HEKLA BASALTS							Relative precision (%)
Sample	HEK06-09	HEK05-09	HEK04-09	HEK07-09	HEK12-09	HEK09-09		
Age	1913 A.D.	1913 A.D.	1878 A.D.	1878 A.D.	1913 A.D.	1878 A.D.		
SiO2	46.20	46.47	46.97	46.64	46.42	47.01		0.21
TiO2	4.51	4.49	4.42	4.31	4.47	4.53		0.41
Al2O3	13.73	13.85	13.83	13.77	13.59	13.67		0.18
Fe2O3	17.28	17.28	17.23	16.97	17.18	17.41		0.21
MnO	0.25	0.25	0.26	0.25	0.26	0.26		0.85
MgO	5.40	5.48	5.53	5.57	5.23	5.30		0.49
CaO	9.45	9.53	9.57	9.62	9.22	9.29		0.31
Na2O	2.74	2.76	2.81	2.74	2.81	2.87		0.54
K2O	0.64	0.63	0.65	0.64	0.67	0.69		0.20
P2O5	0.54	0.53	0.55	0.54	0.57	0.59		0.73
LOI	-0.40	-0.38	-0.39	-0.42	-0.29	-0.46		
Total	100.34	100.90	101.42	100.64	100.14	101.17		
ppm							Approx. Det.Lt.	
Rb	12	12	12	13	14	12	2	0.24
Sr	366	364	364	362	371	361	2	0.5
Y	45.7	44.6	45.2	44.9	49.2	47.7	2	1.58
Zr	260	254	263	259	275	275	2	0.55
Nb	39	38	39	39	41	41	1.5	2.13
Ba	169	180	181	177	185	190	12	1.03
Pb	6	5	8	8	9	6	5	3.96
Th	5	5	1	3	3	3	4	10.57
U	1	2	1	1	0	0	3	16.83
Sc	32	32	34	32	34	34	5	9.61
V	314	323	319	309	304	317	5	2.85
Cr	7	12	9	10	2	2	4	1.43
Co	32	35	31	34	31	33	2	1.57
Ni	11	17	13	18	7	3	3	0.42
Cu	38	47	40	47	26	25	3	2.43
Zn	134	136	136	135	139	144	3	0.97
Ga	26	24	24	25	25	24	3	3.51
Mo	1	0	0	0	2	0	2	
As	1	0	1	4	0	2	5	
S	172	151	123	124	104	122	50	9.61

Notes
Ages in italics are approximations only
Relative precision taken from method paper - Ramsey et al., 1995, Chem Geol. 124, 1-19

	HEKLA BASALTIC ANDESITES							HEKLA ANDESITES				Relative precision (%)	
Sample	HEK02-09	HEK03-09	HEK08-09	HEK13-09	HEK16-09	HEK14-09	HEK17-09	HEK21-09	HEK11-09	HEK10-09	HEK15-09		
Age	1970 A.D.	1970 A.D.	1970 A.D.	1991 A.D	1980 A.D.	1991 A.D.	1980 A.D.	1390 A.D.	1947 A.D	1947 A.D	1980 A.D.		
SiO2	53.92	54.05	54.59	53.90	54.81	53.71	54.57	55.64	58.09	57.67	59.64		0.21
TiO2	2.01	2.04	1.90	2.12	1.96	2.12	2.06	1.77	1.47	1.48	1.16		0.41
Al2O3	14.76	14.96	14.80	14.83	14.90	14.80	14.75	15.14	15.31	15.20	15.22		0.18
Fe2O3	13.01	13.17	12.62	13.22	12.71	13.26	13.05	12.56	11.02	11.06	10.27		0.21
MnO	0.27	0.28	0.27	0.28	0.27	0.27	0.28	0.27	0.24	0.24	0.25		0.85
MgO	2.86	2.92	2.68	2.98	2.74	2.97	2.86	2.58	2.16	2.17	1.57		0.49
CaO	6.74	6.83	6.58	6.92	6.67	6.98	6.80	6.34	5.76	5.77	5.07		0.31
Na2O	3.88	3.97	4.04	3.92	4.02	3.95	3.94	4.12	4.22	4.21	4.55		0.54
K2O	1.25	1.25	1.33	1.23	1.28	1.23	1.26	1.35	1.47	1.47	1.66		0.20
P2O5	0.98	1.01	0.86	1.06	0.93	1.07	1.01	0.87	0.65	0.65	0.42		0.73
LOI	-0.14	-0.20	-0.10	-0.10	-0.11	-0.15	-0.13	-0.09	-0.11	-0.09	0.03		
Total	99.55	100.28	99.57	100.34	100.19	100.21	100.45	100.55	100.27	99.84	99.85		
ppm												Approx. Det.Lt.	
Rb	25	25	27	24	26	25	26	29	31	31	35	2	0.24
Sr	389	390	386	384	381	392	378	389	365	362	361	2	0.5
Y	73.5	75.8	74.6	73.5	74.3	74.5	73.2	75.9	70.8	69.8	80.2	2	1.58
Zr	459	458	478	443	465	453	456	488	485	483	595	2	0.55
Nb	59	59	60	57	60	57	57	60	58	56	70	1.5	2.13
Ba	328	337	328	319	343	329	338	351	386	372	443	12	1.03
Pb	5	8	4	6	5	4	4	7	5	6	5	5	3.96
Th	4	6	6	5	4	4	8	7	5	3	5	4	10.57
U	1	1	3	0	2	0	2	3	1	3	4	3	16.83
Sc	21	23	22	22	24	22	23	22	18	20	20	5	9.61
V	50	49	49	66	53	64	57	34	30	32	13	5	2.85
Cr	9	12	15	12	9	12	7	8	2	11	8	4	1.43
Co	10	9	7	5	7	10	7	6	7	4	0	2	1.57
Ni	3	3	3	3	3	4	3	1	2	3	5	3	0.42
Cu	15	16	15	16	16	17	15	18	18	19	13	3	2.43
Zn	163	164	167	161	163	163	168	162	150	149	163	3	0.97
Ga	27	26	27	25	26	28	26	27	26	25	27	3	3.51
Mo	2	3	2	3	3	1	1	2	4	3	4	2	-0
As	0	0	2	0	0	2	2	1	1	0	4	5	-0
S	31	40	49	57	42	39	58	26	6	15	14	50	9.61

Notes

Ages in italics are approximations only

Relative precision taken from method paper - Ramsey et al., 1995, Chem Geol. 124, 1-19

	HEKLA DACITES				HEKLA RHYOLITES		OTHER ICELANDIC			Relative precision (%)	
Sample	HEK01-09	HEK18-09	HEK19-09	HEK02-10	HEK01-10	HEK03-10	BUR20-09	SIB	RHY01-09		
Age	2800 B.P.	2800 B.P.	2800 B.P.	2800 B.P.	6600 B.P.	4000 B.P.	~ 1700 A.D.		Postglacial		
SiO2	68.71	68.41	68.88	68.31	71.89	72.07	49.05	49.52	68.53		0.21
TiO2	0.33	0.31	0.32	0.35	0.17	0.16	1.47	2.52	0.43		0.41
Al2O3	14.30	14.24	14.18	14.47	13.14	13.16	15.05	13.67	14.76		0.18
Fe2O3	4.54	4.55	4.34	4.73	2.56	2.54	11.84	14.54	3.79		0.21
MnO	0.13	0.13	0.12	0.13	0.09	0.08	0.19	0.23	0.09		0.85
MgO	0.26	0.25	0.25	0.30	0.08	0.08	7.57	5.52	0.54		0.49
CaO	2.55	2.55	2.46	2.63	1.51	1.52	12.82	10.02	1.57		0.31
Na2O	4.85	4.84	4.82	4.81	4.78	4.76	2.02	2.80	5.40		0.54
K2O	2.31	2.31	2.35	2.29	2.79	2.79	0.14	0.52	4.23		0.20
P2O5	0.06	0.06	0.06	0.07	0.03	0.02	0.13	0.29	0.07		0.73
LOI	1.76	1.86	1.85	1.64	2.45	2.23	-0.08	1.07	0.23		
Total	99.80	99.51	99.64	99.73	99.47	99.42	100.21	100.71	99.64		
ppm										Approx. Det.Lt.	
Rb	54	53	56	52	63	64	3	11	111	2	0.24
Sr	214	211	203	212	120	122	162	247	102	2	0.5
Y	84.7	85.2	86.2	84.9	93.1	94.3	24	39.8	67	2	1.58
Zr	598	597	585	602	340	341	81	187	654	2	0.55
Nb	67	66	66	67	80	80	9	21	103	1.5	2.13
Ba	616	619	618	593	674	675	40	115	463	12	1.03
Pb	7	6	8	6	7	8	3	5	11	5	3.96
Th	13	10	11	11	11	12	0	2	18	4	10.57
U	2	5	4	3	4	4	0	0	6	3	16.83
Sc	5	8	6	9	4	4	41	41	4	5	9.61
V	5	2	4	7	7	4	300	407	16	5	2.85
Cr	2	3	4	5	3	4	166	38	4	4	1.43
Co	0	0	0	1	2	2	36	34	3	2	1.57
Ni	4	5	4	3	4	8	80	39	5	3	0.42
Cu	19	21	20	18	12	13	126	150	10	3	2.43
Zn	115	118	114	122	126	126	76	108	96	3	0.97
Ga	26	25	25	25	23	23	19	21	27	3	3.51
Mo	5	5	5	6	5	5	0	0	8	2	
As	3	1	2	0	4	1	0	1	3	5	
S	0	2	0	38	25	24	39	0	6	50	9.61

Notes

Ages in italics are approximations only

Relative precision taken from method paper - Ramsey et al., 1995, Chem Geol. 124, 1-19